University of London
Imperial College of Science, Technology and Medicine
Department of Life Sciences

In vivo function of the immunoreceptor NKG2D in intestinal inflammation and tumorigenesis

Sophie Curio

A thesis submitted for the degree of
Doctor of Philosophy
November 2020

Declaration of Originality

I hereby declare that I conducted or supervised all scientific work described in this thesis, with the following exceptions: where indicated, macroscopic data of DSS-treated mice and data relating to disease endpoint of $Apc^{min/+}$ mice were performed by two previous lab members, Jenny McGovern and Chiara Triulzi. Data relating to Figures 3.42 and 3.41 were collected by UROP student Harry Baird. Figure 2.1 and data relating to Figure 3.50c-f were generated by B.Sc. student Alexander Steemers. Figure 3.52 was created by Eve Hopkins and Izabela Glegola-Madejska. 16S rRNA sequencing was performed by LC Sciences. RNAseq data in Figure 3.30 and 3.31 was provided by the Department of Surgery at the University of Otago, Christchurch. Wax embedding was performed by Lorraine Lawrence (Imperial College Research Histology Facility). Flow cytometry experiments using the Cytek Aurora were performed with assistance from Jane Srivastava and Jessica Rowley. Images were created using BioRender.

Copyright

Acknowledgements

Firstly, I would like to thank my supervisor Dr Nadia Guerra for the opportunity to carry out this project in her lab. Her guidance, discussions and mentorship have truly made me a better scientist.

A huge thank you to my all my colleagues, especially Gustav Jonsson, Helena Dodd, Jehanne Hassan, Chrysi Christodoulidou, Daniela Prinz and Lauren Russell for the great times we had together in the lab. Thanks to Dr Rachel Purcell for giving me the opportunity to work in her lab for three months and Will Taylor for answering all my questions about R. Thank you to our collaborators, especially Dr Jia Li and Dr Seth Coffelt for the useful and exciting discussions.

I am grateful that I had to opportunity to undertake a PhD program funded by the Wellcome Trust, which allowed me to do research in various labs - thank you Dr Brian Robertson, Dr Sandra Newton, Dr Robert Snelgrove and Prof Clare Lloyd for giving me the opportunity to work in your labs. Thank you also to all staff at Imperial College London, in particular the Flow Cytometry Facility.

Thank you to my friends from all over the world, especially my gliding friends, who encouraged me to go flying on weekends instead of working and my science friends, who supported me through difficult times and kept me sane. Thank you to Michael and Sheila for proof-reading my thesis.

Thank you to my family - Mama, Papa, Clemens, Johannes, Beatrice, Dorothee and Claudia for your endless support and for always believing in me. I could not have asked for better parents and siblings.

Last but not least, I would like to thank Matthew Scutter for his unconditional support. Thank you for challenging me and making me learn how to program, being my technical support, believing in me even when I didn't, putting up with all my complaining and taking me to so many fantastic places all over the world.

Abstract

NKG2D is an activating receptor expressed on various immune cells. Engagement of NKG2D through its ligands, which are expressed mainly on transformed or stressed cells, typically leads to target cell death, thereby making it a potent player in anti-tumor immunity.

We recently identified a pro-tumor role for NKG2D in the context of inflammation-driven cancer, where sustained expression of NKG2D and its ligands resulted in exacerbated disease in a model of hepatocellular carcinoma.

NKG2D has been implicated in various inflammatory disorders, where aberrant expression and activation of NKG2D-expressing effector cells can lead to tissue damage and autoinflammation. The intestine is of particular interest, as NKG2D ligands have been shown to be constitutively expressed on healthy epithelial cells. Further, NKG2D has been implicated in human inflammatory bowel disease. The role of NKG2D in colorectal cancer is unclear, but being an inflammation-driven cancer, we hypothesized that NKG2D would contribute and exacerbate intestinal tumorigenesis.

In this thesis, we show that NKG2D expression is elevated on various immune cells in the healthy murine intestine and confirm that germline deletion of NKG2D does not impact intestinal health at steady state. We further demonstrate that NKG2D exacerbates inflammation-driven intestinal cancer and identify $CD8^+$ T cells and γδT cells as the main drivers of disease. We confirm that IFN-γ-producing $CD8^+$ T cells preferentially accumulate in intestinal tumors in an NKG2D-dependent manner and reveal a novel role for PD-1^+ γδT cells in driving disease. We show that disease progression is associated with mild changes in the microbiota, but is independent of NKG2D expression. Lastly, we investigate the function of NKG2D in two models of intestinal inflammation and show that NKG2D is dispensable for the immune response in sterile colitis. Using a model of infectious-induced colitis, we show that NKG2D deficiency delays colonization of pathogenic bacteria, but does not influence the severity of inflammation.

Together, we provide valuable insight into NKG2D-mediated immunity in the setting of intestinal homeostasis, tumorigenesis and inflammation.

Contents

List of Tables

List of Figures

Introduction

1.1 The intestine and its immune system

The intestine fulfills the important task of absorbing nutrients and water from the food consumed and comprises a surface area of approximately 200m^2 in humans (Hooper *et al.* 2010), making it one of the largest organs in the mammalian body. Enabling the uptake of nutrients requires mucosal surfaces to be thin and permeable, making them particularly vulnerable and easy to breach. Further, the intestine is constantly exposed to foreign antigens, such as food particles and the commensal microbiota. The intestinal epithelium requires tight regulation to maintain gut homeostasis, but at the same time react to potential pathogens or other detrimental substances. The abundance and heterogeneity of immune cells within the gut epithelium and underlying lamina propria (LP) signify the complexity of this system that keeps the intestine healthy. The following section describes the role of the intestinal epithelium, summarizes the function of immune cells in the healthy intestine, outlines differences in mouse and human immunity and provides an introduction to the importance and function of the intestinal microbiota.

1.1.1 Barrier function of the epithelial layer

The protective function of the epithelial layer is threefold: it acts as a physical, chemical and immunological barrier. Intestinal epithelial cells (IEC), the cells lining the inside of the intestine, are in direct contact with the luminal content and are hence the first cells that sense any foreign antigens. They form a tight physical barrier preventing the passage of intestinal

content and only allowing tightly regulated transfer of material (Figure 1.1). IEC can produce chemicals, such as anti-microbial peptides (AMP)s, which form a chemical barrier and prevent the translocation of potentially pathogenic bacteria. Additionally, intestinal immune cells, which can be found within the epithelium and are termed intraepithelial cells (IEL), are highly specialized and trained to tolerate non-pathogenic bacteria and luminal content, while at the same time are able to react to potentially pathogenic material, thereby forming an immunological barrier (Figure 1.1, Vancamelbeke *et al.* 2017). IEL consist of a variety of T cell subsets, including conventional T cells expressing cluster of differentiation (CD)4^+ or $CD8^+$, as well as γδT cells (Cheroutre *et al.* 2011). Beneath the epithelium lies a layer of connective tissue, which comprises further immune cells, termed lamina propria lymphocytes (LPL) (Figure 1.1). These include T cells, B cells, myeloid cells and innate lymphoid cells (ILC)s, which have both regulatory and effector functions (Levy *et al.* 2017).

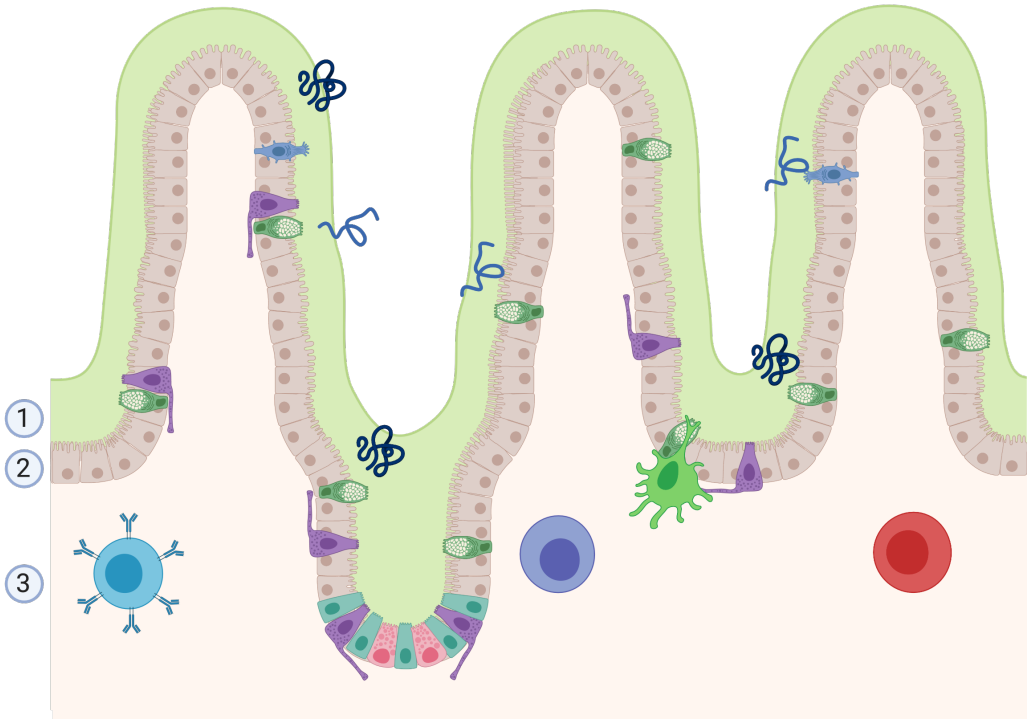

Figure 1.1: Simplified representation of the gastrointestinal wall. The gastrointestinal wall consists of a chemical barrier containing mucus and AMPs (1) secreted by IEC (2). The epithelial layer consists of IEC and IEL, specialized immune cells residing within IECs (2). The connective tissue below the epithelial layer, the LP, contains lymphocytes, termed LPL (3). AMP = antimicrobial peptide, IEC = intestinal epithelial cells, IEL = intraepithelial lymphocytes, LP = lamina propria, LPL = lamina propria lymphocytes. Image was created using BioRender.

1.1.2 The intestinal innate immune system

Myeloid cells, which include dendritic cells (DC)s and macrophages, are among the most abundant immune cells in the healthy intestine. Intestinal macrophages, typically residing in the LP, contribute to the maintenance of tissue homeostasis by clearance of apoptotic cells, antibacterial effector functions against invading pathogens (Nagashima *et al.* 1996) and tissue remodelling and regeneration (Pull *et al.* 2004). In humans, macrophages express human leukocyte antigen (HLA)-DR, CD14 and CD64 and can further be divided into tolerogenic, tissue-resident CD11c$^-$ CCR2$^-$ CX$_3$CR1$^-$ and pro-inflammatory, 'monocyte-like' CD11c^{high} CCR2$^+$ CX$_3$CR1$^+$ macrophages (Bernardo *et al.* 2018). Despite the phagocytic function and their phenotypic similarities to circulating monocytes, intestinal macrophages do not usually trigger a typical pro-inflammatory responses, which is characterized by high production of IL-1, IL-6 and tumor necrosis factor (TNF)-α, suggesting some level of anergy (Smythies *et al.* 2005). While these macrophages do in fact express toll-like receptors (TLR) and other pattern recognition receptors (PRR), the expression of adapter proteins, such as Myeloid differentiation primary response 88 (MyD88) and TIR-domain-containing adapter-inducing interferon-β (TRIF) is significantly reduced, explaining the lack of a typical pro-inflammatory macrophage response. Cytokine production is not completely abrogated, with intestinal macrophages producing low levels of TNF-α as well as interleukin (IL)-10 under steady-state conditions (Smythies *et al.* 2010). While IL-10, a typical anti-inflammatory cytokine, is involved in inhibiting excessive immune activation by acting on regulatory T cells (T_{reg}) cells to express Forkhead box P3 (Foxp3) (Murai *et al.* 2009) and maintaining epithelial integrity (Morhardt *et al.* 2019), the function of TNF-α is less well understood. TNF-α is often associated with an inflammatory response, however, the constitutive expression of low levels of TNF-α by intestinal macrophages seems to have a more regulatory effect. While this is not well studied under homeostatic conditions, one study showed that TNF-α can positively regulate epithelial cells and intestinal stem cell (ISC), thereby contributing to the maintenance of the epithelial barrier (Bradford *et al.* 2017).

DCs are classical antigen presenting cells (APC) and are therefore not only found in the LP, but also at sites of T cell priming, such as the Peyer's patch (PP) and mesenteric lymph nodes (MLN). Generally, mouse intestinal DCs can be distinguished using the surface markers CD103

and CD11b, with $CD103^{+}CD11b^{-}$ cells primarily inducing a T_H1 response, $CD103^{+}CD11b^{+}$ DCs leading to T_H17 and T_H2 responses and the activation of ILC3s and $CD103^{-}CD11b^{+}$ DCs priming all three T_H cell subsets (Joeris *et al.* 2017). In humans, DC subsets highly similar to the mouse subsets have been identified, indicating high similarities among species (Watchmaker *et al.* 2013).

In addition to myeloid cells, ILCs are an important part of the immune system. These cells lack adaptive antigen receptors, but are functionally similar to T cells. ILCs can be divided into five groups - natural killer (NK) cells, ILC1, ILC2, ILC3 and lymphoid tissue-inducer (LTi) cells. ILC1 and 2 are functionally similar to T_H1 and 2 cells, reacting to intracellular pathogens and extracellular parasites or allergens, respectively. ILC3s are the counterpart to T_H17 cells and are involved in the immune response to extracellular bacteria and fungi. NK cells are classic cytotoxic cells and therefore functionally similar to $CD8^{+}$ cytotoxic T lymphocytes (CTL), which are important in an anti-viral and anti-tumor response. LTi, as the name suggests, are functionally different from the other ILCs and are involved in tissue development and maintenance, in particular that of secondary lymphoid structures (Vivier *et al.* 2018). ILC3s are the most abundant subtype of ILCs in the intestine and play a critical role in the maintenance of gut homeostasis, as demonstrated by Sonnenberg and colleagues, who showed that depletion of IL-22 producing ILCs results in bacterial dissemination and systemic inflammation (Sonnenberg *et al.* 2012). ILC3s can be subdivided into two groups, both of which express the transcription factor RAR-related orphan receptor gamma ($ROR\gamma T$) and have the ability to produce IL-22, but show some functional differences. The two groups are distinguished by the expression of natural cytotoxicity receptors (NCR) and the transcription factors T-box transcription factor (T-bet) and Aryl hydrocarbon receptor (AhR). NCR^{+} ILC3s express T-bet and have the ability to produce interferon (IFN)-γ, while NCR^{-} ILC3s are AhR^{+} and produce IL-17 in addition to IL-22. ILC3s contribute to intestinal homeostasis through a range of mechanisms, many of which are not yet fully understood. Being the main producers of IL-22 in the intestine (Sawa *et al.* 2011), it is not surprising that ILCs play a crucial role in barrier protection and stem cell regeneration. IL-22 acts directly on ISC to initiate their DNA damage response (DDR) machinery, protecting their genome integrity and preventing malignant transformation (Gronke

et al. 2019). Studies reporting that lack of IL-22 leads to changes in the microbiota, making it more transmissible and colitogenic (Zenewicz *et al.* 2013, Sonnenberg *et al.* 2012), suggest that IL-22 plays an important role in regulating the interactions between the host and the microbiota, for example through the production of AMPs, which highly depend on IL-22 (Wolk *et al.* 2004). Another way in which ILC3s have been shown to contribute to intestinal homeostasis is by regulating $CD4^+$ T cells to prevent reactivity towards the commensal microbiota. A surprising role of ILC3s as APCs was identified by Hepworth and colleagues, who showed that a subtype of ILC3s in the MLN express Major histocompatibility complex (MHC)-II and that ILC3-specific deletion of MHC-II results in a $CD4^+$ T cell response against the commensal microbiota, leading to dysregulation and intestinal inflammation (Hepworth *et al.* 2013). These cells can further modulate the adaptive immune response by presenting antigen to T follicular helper (Tfh) cells, inducing antigen-specific immunoglobulin (Ig)A responses (Melo-Gonzalez *et al.* 2019).

While these studies investigated ILC3s residing in the MLN, data shows that ILC3s can also regulate tissue-resident T cells within the LP. A mechanism proposed by Mortha *et al.* involves IL-1β release by intestinal myeloid cells in response to microbiota-derived stimuli, which acts on ILC3s to release Granulocyte-macrophage colony-stimulating factor (GM-CSF). GM-CSF stimulates DCs and macrophages to release anti-inflammatory and immune regulatory molecules, such as IL-10 and retinoic acid (RA), which modulate the T cell response and induce T_{reg} cells (Mortha *et al.* 2014). Not only do these studies demonstrate the importance of this relatively small population of ILCs, they also underline the complexity of the system and the importance of cellular crosstalk.

Intestinal ILC1 and 2 have not been studied in detail and their role in homeostatic conditions is unclear. ILC2s have recently been shown to be a source of IL-10 in the healthy mouse intestine, suggesting that they contribute to tissue homeostasis (Bando *et al.* 2020). While there is a lack of studies investigating the function of ILC1s in intestinal homeostasis directly, deficiency of T-bet, the transcription factor driving ILC1 development, in Recombination Activating Gene 2 $(RAG2)^{-/-}$ mice which lack adaptive immune cells, leads to a spontaneous colitis. It can therefore be concluded that T-bet-expressing innate cells play a regulatory role in intestinal

immunity (Garrett *et al.* 2007). However, due to the lack of NCR^+ ILC3s in T-bet-deficient mice (Klose *et al.* 2014), the possibility that ILC3s and not ILC1s are responsible for this phenotype cannot be excluded.

Similarly, little is known about the function of NK cells in the healthy intestine. A study investigating changes in the innate cell compartment of human infants showed that NK cells are more abundant in infants compared to adults and that throughout the first year of life, the frequency of these cells decreases (Sagebiel *et al.* 2019). A possible explanation for this could be that cytotoxic NK cells are crucial in host defense at early stages of life before the onset of an appropriate T cell response. In healthy adult mice, NK cells have basal levels IFN-γ, Granzyme B and perforin expression (Sanos *et al.* 2009) which points towards a patrolling, rather than regulatory function (Figure 1.2).

1.1.3 The intestinal adaptive immune system

The adaptive arm of the intestinal immune system consists of T and B cells. T cells can either reside within the epithelium (IEL) or the lamina propria (LPL), while B cells are found only in the lamina propria or PP, which are lymphoid follicles and the main site of immune cell induction (Mowat *et al.* 2014).

The intestine harbors a range of T cell subsets, including tissue-resident $CD4^+$ and $CD8^+$ T cells, as well as γδT cells, T_{reg} cells and Mucosal associated invariant T cell (MAIT)s. IEL consist mainly of $CD4^+$ and $CD8^+$, as well as γδT cells, while the majority of T cells residing in the lamina propria are either $CD4^+$ or γδT cells (Lutter *et al.* 2018). The differences in location might be due to distinct functions of the various cell types - IELs patrol the epithelium and react quickly to any potential pathogens, while T cells in the lamina propria fulfill more regulatory functions. IELs are tissue-resident (Jarry *et al.* 1990, Sugahara *et al.* 1999) and their functions are diverse. Due to their role as sentinels, they need to be able to react quickly and are equipped with a range of additional activating receptors typically found on NK cells, including Natural killer group 2D (NKG2D), CD160 and CD94 (Vandereyken *et al.* 2020). They can be cytotoxic (Hongo *et al.* 2000) and express effector cytokines, such as IFN-γ (Jarry *et al.* 1990), inducing an immune response to foreign antigens and/or pathogens.

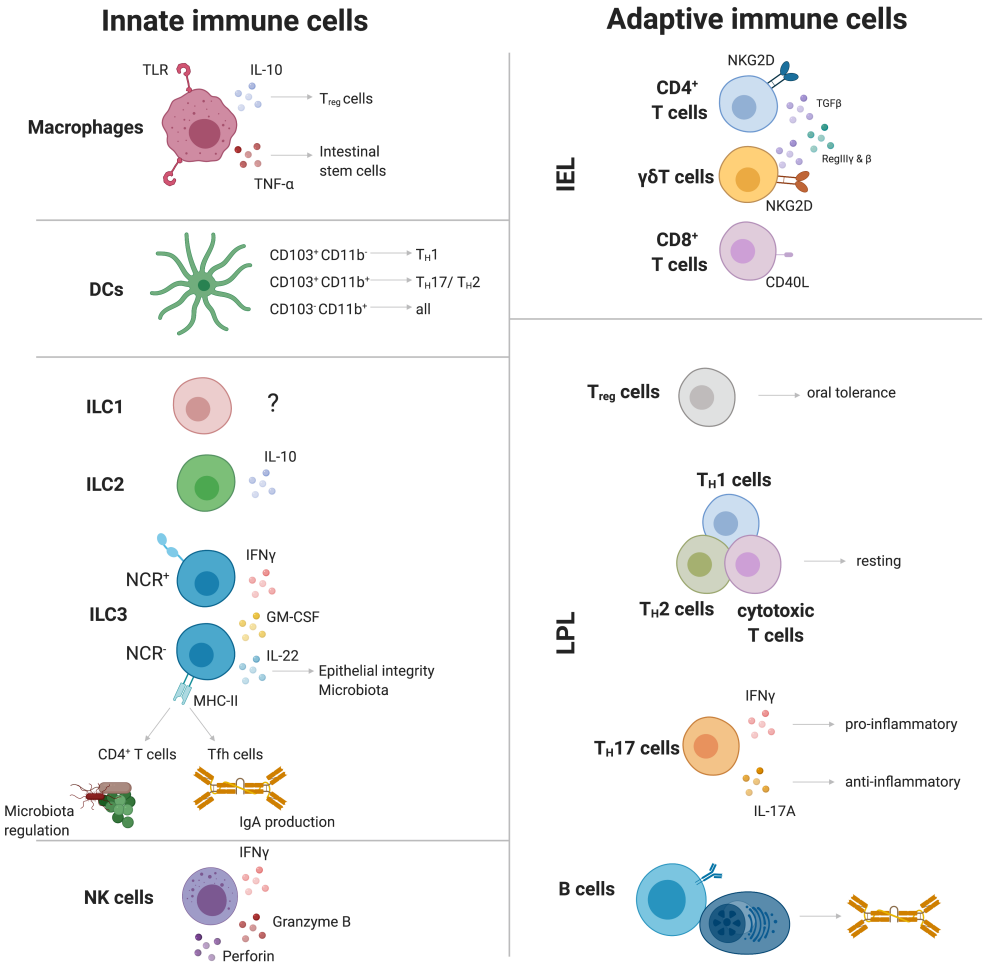

Figure 1.2: Simplified representation of immune cells and their function in intestinal homeostasis. The innate immune cell compartment consists of macrophages, which express PRR but regulate regulatory T cells and intestinal stem cells through the secretion of IL-10 and low levels of TNF-α in the absence of foreign stimuli. DCs are the main antigen-presenting cells in the lamina propria and induce different T_H cell responses depending on their subtype. ILCs comprise of ILC1-3 and NK cells; the function or ILC1s is unclear under homeostatic conditions, whereas ILC2s have been shown to produce IL-10. ILC3s can be NCR^+ or NCR^- and produce IFN-γ and IL-22, respectively. NCR^- express MHC-II and can act as antigen-presenting cells, thereby regulating $CD4^+$ T cells and Tfh cells. The adaptive arm consists of IEL, residing within the epithelium and containing NKG2D-expressing $CD4^+$ and γδT cells that secrete regulatory factors, such as TGF-β and RegIIIγ and β. $CD8^+$ T cells are present in the healthy IEL, but require additional stimulation through CD40L. LPL contain T_{reg} cells, which induce oral tolerance, as well as various subtypes of resting T cells. T_H17 cells produce low levels of pro-inflammatory IFN-γ and anti-inflammatory IL-17A at steady-state. B cells are present in the lamina propria and produce antibodies, mainly IgA, that act as a first line of defense. PRR = pattern recognition receptors, DC = dendritic cell, T_H = T helper, ILC = innate lymphoid cell, NCR = natural cytotoxicity receptor, Tfh = T follicular helper, IEL = intraepithelial lymphocytes, TGF = transforming growth factor, RegIII = Regenerating islet-derived protein III, LPL = lamina propria lymphocytes, T_{reg} cells = regulatory T cells, IgA = immunoglobulin A. Image was created using BioRender.

Further, IEL have important functions in regulating homeostasis; specifically γδT cells have been shown to be important in limiting bacterial dissemination by the production of anti-microbial molecules such as Regenerating islet-derived protein 3 (RegIII)γ and β (Ismail *et al.* 2011). Additionally, they have the capability of producing Transforming growth factor (TGF)-β (Bhagat *et al.* 2008, Shires *et al.* 2001), suggesting that they play a regulatory role in maintaining homeostasis and tolerating the intestinal microbiota. This interplay between IEL and the microbiota was further supported by the observation that while γδT cells are present in germ-free (GF) mice (Bandeira *et al.* 1990), their location and movement pattern, most likely linked to their functionality, is dependent on the microbiota (Konijnenburg *et al.* 2017). αβT cells can either express CD4, CD8 or be double-negative (DN). Their T cell receptor (TCR) repertoire is polyclonal *in utero* and shortly after birth, before clonal expansion reduces the diversity. This reduction in TCR diversity appears to be influenced by the microbiota, indicating that after colonization of the intestine, the T cell clones that tolerate the microbiota are selected (Probert *et al.* 2007). While their primary task is to recognize and eliminate antigens, they further have immunoregulatory functions which include, but are not limited to the secretion of TGF-β and the expression of Lymphocyte-activation gene 3 (LAG3) (Denning *et al.* 2007). As opposed to splenic T cells, $CD8^+$ IELs require co-stimulation through CD40L, indicating that these cells require additional signals for activation to prevent an overreaction (Masopust *et al.* 2001).

The LP contains mostly $CD4^+$ T helper cells as well as T_{reg} cells, which can either arise from the thymus with a broad antigen repertoire that recognizes both foreign as well as self antigen (Sakaguchi 2004) or be induced in the periphery, a process crucial for oral tolerance (Hadis *et al.* 2011). T_H17 cells can have either pro- or anti-inflammatory functions and studies have demonstrated that their function is largely dependent on the bacteria present in the intestine: while commensal bacteria, such as segmented filamentous bacteria (SFB) induced a 'regulatory' T_H17 subtype, producing IL-17A but no IFN-γ, pathogenic bacteria result in a highly pro-inflammatory subtype (Omenetti *et al.* 2019). The remaining subsets, which include T_H1 and T_H2 cells, as well as a few cytotoxic T cells, are tissue-resident memory cells, which are typically in a resting state and only become activated during viral, bacterial or parasitic infections (Ma

et al. 2019).

B cells, due to their ability to produce and secrete antibodies, play a crucial role in maintaining gut homeostasis. The humoral immune response plays a particularly important role in the gastrointestinal tract due to the abundance of foreign antigens. B cells, which are primed in lymphoid structures, such as PP, MLN or lymphoid follicles, migrate to the lamina propria as IgM^+ cells, where local stimuli induce switching to IgA^+ plasma cell (PC)s (Fagarasan *et al.* 2001). IgA, which is the classical antibody found at mucosal sites, has a range of functions. Pathogenic bacteria have been shown to be preferentially coated in IgA, suggesting that this reduces their pathogenicity (Palm *et al.* 2014). Indeed, binding of IgA inhibits the motility or pathogenicity of certain pathogens, such as *Salmonella enterica serovar Typhimurium* (Forbes *et al.* 2008) or Reovirus type 1 Lang (Hutchings *et al.* 2004). Through a process called 'immune exclusion', IgA is able to cross-link microorganisms in the intestinal lumen, thereby preventing them from penetrating the epithelium (Mantis *et al.* 2010). Mice lacking an appropriate IgA response have been shown to have an altered microbiota (Fagarasan *et al.* 2002), suggesting that IgA plays an important role in tolerating the microbiota. Further supporting the importance of the humoral immune response is the fact that a large proportion of commensal bacteria are coated in IgA (Waaij *et al.* 1996). B cells, and their antibodies can therefore be seen as a first line of defense at the very interface between the intestinal content and the host (Figure 1.2).

1.1.4 Impact of the microbiota on health and disease

The human intestine harbors more than 30 trillion bacteria, making up roughly 200 grams (g) of the total body weight (Sender *et al.* 2016). In recent years, the microbiota has been implicated in a variety of diseases, ranging from diseases of the intestinal tract, such as inflammatory bowel disease (IBD) (Zuo *et al.* 2018) to cardiovascular diseases (Brown *et al.* 2018), obesity (Maruvada *et al.* 2017), neurological disorders (Sharon *et al.* 2016) and last, but not least, cancer and cancer therapy (Helmink *et al.* 2019). It is therefore of great importance to understand the relationship between the microbiota and pathogenesis and to dissect the molecular mechanisms leading or contributing to disease development. Trying to understand what a 'healthy' microbiota entails has been subject of research for many years, but is complicated

by the fact that the microbiota is highly variable between individuals (Turnbaugh *et al.* 2007). Further, some bacterial species have still not been identified due to the inability to culture them outside of the intestine (Walker *et al.* 2014). Lastly, while early studies investigated the composition of the microbiota, it has become evident that functional differences, i.e. the production of metabolites, might be a better predictor of mechanisms contributing to dysfunction (Rooks *et al.* 2016). Due to the complexity of the subject and the availability of extensive review papers (Clemente *et al.* 2012, Rooks *et al.* 2016, Lee *et al.* 2014), the relevant findings will be discussed in the specific subsections describing changes in the microbiota assocaited with IBD (1.2.2) and colorectal cancer (CRC) (1.3.4).

1.2 Inflammatory Bowel Disease

Inflammatory bowel diseases (IBD) may develop when mechanisms regulating the intestinal immune system fail. In humans, IBDs include Crohn's disease (CD) and ulcerative colitis (UC) and are characterized by an excessive inflammatory response in the intestinal mucosa. The incidence of IBD is increasing, with more than 3.5 million individuals affected across Europe and North America (Ng *et al.* 2018), thereby posing a global health burden. A variety of risk factors have been identified, including environmental factors and genetic pre-dispositions that lead to disease development, making it a multi-factorial disease (Uhlig *et al.* 2018). Several genetic mutations have been linked to the onset of childhood IBD and have helped to understand mechanisms leading to disease. Common mutations among pediatric IBD patients affect IL-10 signaling, suggesting that IL-10 plays a crucial role in gut homeostasis (Glocker *et al.* 2009). Other genetic mutations are not causative, but predispose individuals to the development of IBD as adults. Nucleotide-binding oligomerization domain-containing protein 2 (NOD2), an intracellular PRR upstream of nuclear factor kappa-light-chain-enhancer of activated B cells (NF-$\varkappa$B), is commonly altered in CD patients (Hugot *et al.* 2001, Ogura *et al.* 2001) and has been recognized as a CD risk factor. Environmental risk factors include, but are not limited to, diet, smoking, stress, air pollution and infection (Abegunde *et al.* 2016). A selection of treatments is available, most of which aim to dampen the immune response by inhibiting certain

effector molecules (anti-TNFα-antibody therapy) or by systemic immune suppression (steroids). However, these therapies do not target the underlying cause of disease and often require life-long medication with sometimes severe side effects (Carter *et al.* 2004). Additionally, many patients develop drug-resistance or loss of response and have to switch to different medications (Baumgart *et al.* 2012).

Nonetheless, the success of anti-TNFα-antibody therapy, a treatment with few side effects and stable remission in a group of patients has demonstrated the benefits of targeted therapy (Colombel *et al.* 2007). It is crucial to understand molecular and cellular mechanisms in the context of health and disease, as existing treatments are unsatisfactory and new treatment cannot be developed without a deeper understanding of the immune response leading to IBD. This section describes the immune response and microbial changes associated with IBD, introduces and describes the two mouse models of colitis used in this study and outlines current gaps in knowledge.

1.2.1 The immune response in inflammatory bowel disease

The immune response leading to exacerbated inflammation and tissue damage proves to be complex and diverse with both innate and adaptive immune cells contributing to the pathology of IBD. Generally, CD is characterized by the expression of cytokines associated with T_H1/T_H17 response, whereas UC shows features of a T_H2 response. The signature cytokines of these responses are IFN-γ, IL-17 and IL-22 for a T_H1/T_H17 response and IL-5 and IL-13 for a T_H2 response with increased levels of cytokines in CD and UC patients, respectively (Strober *et al.* 2011). However, the mechanisms leading to aberrant cytokine production as well as downstream effects need to be understood to treat and prevent pathology.

1.2.1.1 Pro- and anti-inflammatory properties of myeloid cells in inflammatory bowel disease

IBD has been shown to be associated with an expansion of pro-inflammatory $CD11c^{high}CCR2^{+}CX_3CR1^{+}$ macrophages (Bernardo *et al.* 2018). Inflammation is associated with an increased infiltration of these pro-inflammatory macrophages to the mucosa in a

CCR2-dependent manner and a lack of differentiation into tolerogenic $CD11c^{-}CCR2^{-}CX_3CR1^{-}$ macrophages. As opposed to other studies, which have demonstrated the importance of TNF-α production by macrophages (Atreya *et al.* 2011), Bernado *et al.* showed low levels of TNF-α in the pro-inflammatory subset, and instead argue that IL-1β is the main driver of disease.

Further, IL-23 production by macrophages has been implicated in mediating intestinal inflammation. IL-23, a heterodimer consisting of IL-12p40 and IL-23p19, is secreted preferentially by $CD14^{+}$ macrophages. Macrophages isolated from human IBD patients show increased expression of the genes encoding the two subunits compared to healthy controls, as well as better responsiveness, measured as IL-23 secretion upon stimulation with heat-killed bacteria (Kamada *et al.* 2008). IL-23 has been shown to contribute to intestinal inflammation in numerous ways by promoting the release of pro-inflammatory cytokines by T cells (Ahern *et al.* 2010, Yen *et al.* 2006).

Similar to macrophages, DCs can either be tolerogenic and have regulatory functions, or drive inflammation through the secretion of pro-inflammatory cytokines and activation of adaptive immune cells. Longman *et al.* showed that a certain subset of DCs, namely CX_3CR1^{+} DCs are crucial regulators of IL-22 production and demonstrated that lack of this subset of DCs results in a more severe colitis due to a lack of IL-22 production by colonic ILC3s (Longman *et al.* 2014). Contrary to this regulatory subset, Hart *et al.* observed an upregulation of PRRs such as TLRs 4 and 6, increased expression of the activation marker CD40 and increased secretion of the pro-inflammatory cytokines IL-6 and IL-12 in CD patient-derived DCs, leading them to suggest a pro-inflammatory and pro-pathogenic role of DCs (Hart *et al.* 2005).

1.2.1.2 The multifaceted role of innate lymphoid cells in intestinal inflammation

The first characterization of ILC1s in IBD came from Bernink *et al.*, who showed a potential role of IFN-γ-producing ILC1s in CD patients. They observed a significant increase in ILC1s frequencies, which express transcripts for IFN-γ but not cytotoxic molecules such as perforin and Granzyme B (GzB), as well as a decrease of RORγT-expressing ILC3s. They further showed that RORγT-expressing ILC3s can in fact differentiate into IFN-γ-expressing ILC1s, indicating a high plasticity among ILCs (Bernink *et al.* 2013). Just after the discovery of these

potentially disease-promoting ILC1s in the colonic LP of CD patients, Fuchs and colleagues published their findings on the presence of ILC1s within the intestinal epithelium. They differ from LP ILC1s in that they lack the expression of CD127 (IL-7 receptor α) and respond to IL-12 and IL-15, rather than IL-12 and IL-18 (Fuchs *et al.* 2013). It remains to be determined how these subsets differ functionally, but both authors suggest that ILC1s contribute to the aberrant IFN-γ production in CD patients.

Despite studies from as early as 1983 showing a potential role of NK cells in IBD pathogenesis (Ginsburg *et al.* 1983), surprisingly little is understood regarding their function in intestinal health and disease to this day. A study by Steel *et al.* dissected phenotypical and functional properties of NK cells in patients with IBD compared to healthy individuals before and after treatment with the immunosuppressive agent azathioprine. NK cells in the colonic lamina propria and peripheral blood were distinguished using the CD16 and CD56 markers (Steel *et al.* 2011). Typically, human peripheral blood (PB) $CD56^{bright}$ $CD16^{low}$ NK cells are the main cytokine producers, secreting cytokines such as IFN-γ, while $CD56^{dim}CD16^{high}$ NK cells, which are the predominant subtype in human PB, are cytotoxic and express perforins and granzymes at high levels (Marcenaro *et al.* 2017). Steel *et al.* showed a slight increase in CD16-expressing NK cells in the colonic LP of patients with CD and UC, with the increase being abrogated upon treatment with azathioprine. The authors argued that the increase of cytotoxic NK cells might contribute to the overall inflammation and tissue damage (Steel *et al.* 2011), but fail to address functionality of the tissue-resident NK cells.

Several studies addressing the role of NK cells in mouse models of colitis have demonstrated that lack of NK cells leads to increased disease severity and imply the importance of NK cells in maintaining gut homeostasis. Fort *et al.* utilized a model of adoptive T cell transfer, where $CD4^+$ T cells isolated from IL-$10^{-/-}$ mice that were transferred to RAG2-deficient recipients caused colitis. To test the role of NK cells in this model, anti-NK1.1 and anti-asialo-GM1 antibodies were used to deplete NK cells. Both antibody treatments resulted in a significantly increased disease score compared to control mice, which led the authors to suggest that NK cells regulate colitogenic T cells and that lack of NK cells leads to increased disease severity (Fort *et al.* 1998). Another study illustrates the importance of NK cells in a chemically-

induced colitis model, the dextran sodium sulfate (DSS) model. Again, using the anti-asialo-GM1 antibody to deplete NK cells, as well as transgenic mice lacking NK1.1^{+}CD3^{-} cells, the authors demonstrated a significantly worse outcome for NK cell-deficient mice (Hall *et al.* 2013a). Despite being convincing as such, all three studies fail to address the possibility of the shown effects being mediated by ILC1s rather than NK cells. While NK1.1 has been shown to be expressed on ILC1s (Jiao *et al.* 2016), no data is available on the specificity of the anti-asialo-GM1 antibody in depleting NK cells and not ILC1s. It is therefore possible that the observed phenotypes are in fact mediated by ILC1s rather than NK cells. In addition to the above mentioned studies, various other studies addressed the importance of a certain subset of NK cells, namely IL-22-secreting NK cells, in maintaining intestinal homeostasis (Takayama *et al.* 2010, Cella *et al.* 2009, Satoh-Takayama *et al.* 2009). These cells were termed NK22 cells, but were later discovered to be in fact distinct from the NK cell lineage and instead resemble ILC3s (Vonarbourg *et al.* 2010).

However, the shortcoming of all these studies is that they study general effects of IL-22 and IL-17A and fail to investigate an ILC-specific role. The first evidence for a disease-promoting role of ILCs specifically was revealed by Buonocore *et al.*, who showed that bacteria-driven innate colitis is dependent on IL-23, which acts on IL-23R-expressing ILCs to promote IL-17 and IFN-γ production, thereby promoting inflammation. This was shown to be dependent on the transcription factor RORγT, indicating that this is an ILC3-specific pathway (Buonocore *et al.* 2010). These findings were later confirmed in human patients, where IL-23-responsive ILCs accumulate in the inflamed intestine of CD patients (Geremia *et al.* 2011). Another study by the Powrie group examined the role of ILCs specifically using, among other methods, *in vivo* microscopy (Pearson *et al.* 2016). They revealed a crucial role for GM-CSF and showed that ILC3s exit cryptopatches during intestinal inflammation in a GM-CSF-dependent manner, while at the same time being main producers of GM-CSF themselves. The authors showed that this ILC3-dependent production of GM-CSF leads to the recruitment of pro-inflammatory immune cells, in particular monocytes. The production of GM-CSF by ILC3s appeared to be dependent on IL-23, but not IL-22. The study revealed a novel pathway, which, if shown to be translatable to human disease, can be a new target for therapeutic interventions. A recent study further

investigated the relationship between GM-CSF-producing ILCs and monocytes and found that GM-CSF drives polarization to pro-inflammatory macrophages with enhanced anti-bacterial, but decreased wound-healing properties (Castro-Dopico *et al.* 2020). Similar to the previous study, the authors showed that GM-CSF acts on ILC3s in an autocrine manner and induces a T_H17 response. Together, they demonstrated that GM-CSF produced by ILC3s is a critical regulator of intestinal macrophages and that heightened production favors a pro-inflammatory response, potentially contributing to intestinal inflammation and IBD.

In summary, these studies suggest a pro-inflammatory role for IFN-γ-producing ILC1s and an increase of cytotoxic NK cells in IBD patients. The function of ILC3s is complex, due to the potential to produce anti-inflammatory IL-22 and pro-inflammatory IL-17A. Both lack of IL-22 and aberrant production of IL-17A has been linked to intestinal inflammation, but further research is needed to understand stimuli leading to this imbalance.

1.2.1.3 T_H1, T_H2 and T_H17 cells can contribute to intestinal inflammation

As previously mentioned, CD and UC patients display a T_H1/T_H17 and T_H2-like inflammation, respectively. Though it has become increasingly clear that these phenotypes are not solely mediated by T cells, they play a crucial role in both maintenance of gut homeostasis as well as IBD pathology.

IFN-γ-producing $CD4^+$ T cells accumulate in the LP of CD patients, where they are thought to contribute to the detrimental inflammation (Fais *et al.* 1994). However, targeting IFN-γ through the administration of IFN-γ-blocking antibodies (fontolizumab) has proven unsuccessful (Reinisch *et al.* 2006), suggesting that, though contributing to disease, IFN-γ is not a crucial mediator in the acute phase. Yet, sustained IFN-γ production can have deleterious effects on barrier integrity and can potentially be a driver of early disease. ISC have been shown to be sensitive to IFN-γ-induced toxicity and apoptosis, which, if sustained, results in reduced epithelial integrity and fosters further inflammation (Takashima *et al.* 2019). Anti-TNF-α antibodies have been proven to be more successful (Dullemen *et al.* 1995), however, it is not clear to what extent T cells contribute to the aberrant production of TNF-α.

A subset of T_H1 cells that expresses NKG2D has been implicated in CD pathology: Allez *et al.*

showed an increase in NKG2D$^+$CD4$^+$ T cells in the inflamed mucosa of CD patients and demonstrate that, in addition to secreting T_H1-associated cytokines, such as IFN-γ and TNF-α, those cells also display cytotoxic functions, as indicated by the intracellular expression of perforin (Allez *et al.* 2007). The authors argued that this cytotoxicity is most likely directed towards epithelial cells that express MHC class I chain-related protein (MIC)A, a ligand to NKG2D, that is upregulated upon stress. A follow-up study further characterizing the NKG2D$^+$CD4$^+$ cells in CD revealed that they are a major source of IL-17 and, to a lesser extent, IL-22 and that they respond strongly to T_H17-promoting cytokines, such as IL-23 (Pariente *et al.* 2011). IL-17 is the signature cytokine of a T_H17 response and can be secreted by T_H17 (Kurts 2008) as well as γδT cells (Papotto *et al.* 2017). Under steady-state conditions, T_H17 cells preferentially reside in the LP of the small intestine and are scarce in the colon (Esplugues *et al.* 2011), but infiltrate the mucosa all throughout the intestinal tract during inflammatory responses (Gálvez 2014).

T_H2 cytokines include IL-4, IL-5 and IL-13 and have been implicated in development of UC. While the inflamed mucosa of UC patients shows increased expression levels of classical pro-inflammatory cytokines such as IL-1 and TNF-α, it is also accompanied by an increase of IL-5 and IL-13 expression (Chen *et al.* 2016). IL-5 is associated with an IL-23-dependent infiltration of eosinophils and eosinophil-dependent tissue damage (Griseri *et al.* 2015), whereas IL-13 seems to have a direct effect on epithelial cells, leading to decreased barrier functions (Heller *et al.* 2005). However, it has been shown that not only CD4$^+$ T cells contribute to the secretion of T_H2-associated cytokines and that other cells, such as IL-13-secreting Natural killer T (NKT) cells (Fuss *et al.* 2004) or ILC2s might also play a role in pathology.

1.2.1.4 Inflammatory bowel disease is associated with aberrant IgA production

B cells and their production of Igs play a crucial role in maintaining gut homeostasis. IgA has been accepted as a crucial immune component that keeps the intestinal microbiota in check (Pabst 2012) and aberrant production of IgA has been shown to be a hallmark of both human (Kett *et al.* 1987) and mouse (Palm *et al.* 2014) colitis. The later study shows that colitogenic

bacteria tend to be preferentially coated in IgA and that transfer of an intestinal microbiota with a high frequency of IgA-coated bacteria exacerbates colitis. However, it is unclear whether the high IgA coating is just a result of the presence of colitogenic bacteria or whether the high levels of IgA actively promote inflammation. The authors hypothesize that high levels of IgA induce an inflammatory response in the host, insufficient for bacterial clearance, yet contributing to and exacerbating the existing inflammation. In addition to producing antibodies which bind to colitogenic bacteria, IBD patients have been shown to produce autoantibodies, in particular IgA, but not IgG (Kazemi-Shirazi *et al.* 2002). Another study suggests that, possibly in addition to aberrant antibody production, B cells isolated from IBD patients display an activated phenotype. B cells were found to express TLR2 and, in CD patients, IL-8 at increased levels, suggesting that B cells potentially contribute to the inflammatory response by mechanisms other than antibody production (Noronha *et al.* 2009). While antibody production appears to be dysfunctional and contribute to IBD to some extent, it is not yet clear whether the aberrant IgA production is merely a consequence of the presence of colitogenic bacteria or whether it precedes changes in the microbiota.

1.2.2 Chronic intestinal inflammation and the microbiota

The role of the microbiota in human IBD has been a subject of research for many years, but only recent advances in sequencing technology have allowed researchers to gain a better insight into what changes occur in the composition of the microbiota and how they contribute to pathogenesis. Early studies suggested that the absolute number of bacteria found in the mucosa of IBD patients is higher (Schultsz *et al.* 1999), but that the diversity is reduced (Manichanh *et al.* 2006). Both studies relied on extremely low samples sizes, however, follow-up studies confirmed a reduction in diversity in both CD and UC and show that IBD is often associated with an increase in *Bacteroidetes* and *Enterobacteriaceae*, in particular in CD patients, as well as a decrease in *Firmicutes* (Walker *et al.* 2011, Wright *et al.* 2015). A study comparing the microbiota of CD patients with their healthy siblings revealed that they are in fact very similar (Hedin *et al.* 2014), suggesting that the altered microbiota is not the sole driver of disease.

In an attempt to gain insight into functional consequences following intestinal dysbiosis, Morgan and colleagues performed metagenomic analysis and identified several metabolic pathways that were disturbed in IBD patients. One significant change was an increase in cysteine metabolism and N-acetylgalactosamine transporters in patient samples, suggesting that the abundance of bacteria using mucins as their primary energy source is increased in patients, potentially leading to barrier dysfunction (Morgan *et al.* 2012). Another mechanism by which the microbiota can contribute to disease is by the production, or the absence, of certain metabolites. Short-chain fatty acid (SCFA), typically thought to contribute to intestinal health, were indeed reduced in UC patients (Vermeiren *et al.* 2011). Some bacteria that have been shown to be enriched in IBD patients, such as a certain subtype of *Escherichia coli* (*E. coli*), can have direct cytotoxic functions (Martin *et al.* 2004), while others can induce inflammation through the high abundance of lipopolysaccharide (LPS) (Stephens *et al.* 2019). Conversely, the lack of certain commensals with regulatory functions can contribute to the inflammatory process (Round *et al.* 2010). Yet, the question whether microbial dysbiosis is a cause or consequence remains to be answered.

Studying human tissue has greatly improved our understanding of IBD pathology and advanced drug development, yet, many questions remain and molecular mechanisms are not fully understood. Studying tissue derived from patients is often limited to phenotypic characterization of changes in immune cell function or the microbiota and functional analyses or targeted deletion of certain immune mediators or microbes is impossible. Due to the similarities between the human and mouse immune system, mouse models provide a valuable tool to study intestinal inflammation.

1.2.3 Mouse model of inflammatory bowel disease

To study IBD without having to rely on human tissue, several mouse models have been developed. Generally, they can be divided into germ-line encoded, such as IL-10$^{-/-}$ mice (Kühn *et al.* 1993), chemically induced, such as DSS (Okayasu *et al.* 1990a) or 2,4,6-trinitrobenzene sulfonic acid (TNBS) (Morris *et al.* 1989) or infection-induced, such as *C. rodentium* (Bhinder *et al.* 2013) and *Helicobacter hepaticus* (*H. hepaticus*) (Fox *et al.* 2011). Due to the complexity of

human IBD, various mouse models are needed to study different aspects of the disease. In the following sections, the two mouse models used in this study will be reviewed and compared.

1.2.3.1 DSS-induced colitis

DSS is a chemical which is administered in the drinking water and routinely used to induce colitis in mice. It acts by damaging the intestinal epithelium, leading to increased barrier permeability and translocation of bacteria and resulting in the initiation of an immune response. DSS treatment leads to weight loss and diarrhea and, when administered over a longer period of time, structural changes of the epithelium, including mucin and goblet cell depletion and epithelial disruption (Eichele *et al.* 2017). DSS can be used to study acute or chronic colitis, with a short-term treatment of typically seven days or repeated cycles of DSS treatment serving as models for acute and chronic inflammation, respectively (Eichele *et al.* 2017). Several studies dissecting the role of the diverse parts of the immune system have helped understand the complex system mediating immune homeostasis and pathology by using DSS-induced colitis. Here, I am reviewing several studies using the DSS model of colitis to summarize current knowledge and understanding of the immune response evoked by administration of DSS.

The response to DSS treatment varies according to the strain of mice used, with C57Bl/6 mice presententing with severe gut pathology upon DSS treatment compared to Balb/c mice, which are more resistant to disease development. While C57Bl/6 mice show a strong T_H1 response, mediated by IFN-γ and TNF-α, the response in Balb/c mice is skewed towards a T_H17 response, associated with higher levels of IL-17F and IL-22, as well as IL-10, indicating the involvement of regulatory T_{reg} cells (Yang *et al.* 2017). The authors concluded that a T_H17/T_{reg} cell response is beneficial, while a T_H1 response leads to detrimental intestinal pathology. The fact that a T_H1 response is associated with pathology was supported by studies showing that IFN-γ-deficient mice do not develop DSS-induced colitis (Ito *et al.* 2006). Similarly, blocking of TNF-α ameliorated disease, but did not prevent it (Xiao *et al.* 2016). Studies investigating DSS susceptibility in IL-17F$^{-/-}$ and IL-22$^{-/-}$ mice on a C57Bl/6 background also supported the findings by Yang *et al.*, and showed that both IL-17F and IL-22 are protective cytokines and that lack of either leads to enhanced pathology (Yang *et al.* 2008, Zenewicz *et al.* 2008). IL-17A

on the other hand promotes disease and IL-17A$^{-/-}$ mice display with less severe inflammation and pathology (Ito *et al.* 2008). Together, these studies suggest a detrimental role of IFN-γ, TNF-α and IL-17 and beneficial roles of IL-17F and IL-22 in DSS-induced colitis.

In the mouse intestine, macrophages and DCs are the most abundant myeloid cells and have been shown to be important in mediating gut homeostasis (Bain *et al.* 2014, Qualls *et al.* 2009). It is therefore not surprising that depletion of macrophages and DCs leads to enhanced susceptibility to DSS-induced colitis (Qualls *et al.* 2006). This depletion was associated with an increase in neutrophils and the phenotype was reversible by additionally depleting neutrophils, suggesting a protective role for macrophages and DCs and a pathogenic role for neutrophils. Interestingly, in a study published by the same group a few years later, the authors specifically depleted DCs, leading to a similar increase in disease susceptibility as observed previously. However, in this setting, it appeared to be independent of neutrophils with no increase in neutrophil numbers in the more inflamed intestine (Qualls *et al.* 2009). It can be concluded that while both cell types are important in mediating gut homeostasis, the mechanisms are distinct. Additionally, a major drawback of the studies is that in the first study, all cells expressing the Colony stimulating factor 1 receptor (CSF1R) were depleted compared to the second study, where cells expressing CD11c were targeted. It has become increasingly evident that different subsets of macrophages and DCs have very different functions (Jones *et al.* 2018) and it would therefore be of great interest to investigate their functions further. However, when studying the different cell types without the distinction of specific subtypes, it can be concluded that macrophages and DCs are important regulators of the DSS-induced immune response, while neutrophils contribute to the inflammation and pathological response.

Two main studies dissected the role of NK cells in DSS-mediated colitis. In a study by Hall *et al.*, the injection of the NK cell-depleting anti-asialo-GM1 antibody led to significantly reduced survival and severe inflammation. This was associated with an accumulation of neutrophils and an increase in IL-17A production by neutrophils, indicating that in this case, neutrophils significantly contribute to gut pathology. The authors demonstrate that NK cells directly interact with neutrophils and inhibit their activity through the inhibitory NK cell receptor Natural killer group 2A (NKG2A), leading to a reduction of IL-6, IL-17 and reactive oxygen species (ROS)

production by the neutrophils. Further, reversing this NKG2A-mediated inhibition led to accelerated disease (Hall *et al.* 2013a). Another study investigated changes in NKG2D expression during DSS-induced colitis and showed that while there was no difference in frequencies of NK cells, the percentage of NKG2D-expressing NK cells was significantly reduced at acute phases of colitis compared to healthy controls (Wang *et al.* 2017).

ILC1s typically elicit an immune response similar to a T_H1 response, characterized by the secretion of mostly IFN-γ and have been shown to be involved in human IBD. In addition to showing an accumulation of ILC1s in the inflamed tissue of CD patients, Bernink *et al.* demonstrated that ILC1s are expanded in DSS-induced colitis (Bernink *et al.* 2013). However, this study used mice with a humanized immune system and the results are therefore not directly translatable to the model used in other studies. The exact role of ILC1s in DSS-mediated colitis remains unclear due to the difficulty of performing functional analysis on ILCs.

Similar to T_H17 cells, ILC3s mainly produce IL-17 and IL-22. They are thought to have mostly protective functions and are reduced in the inflamed human intestine (Forkel *et al.* 2016). The function of ILC3s in DSS-mediated colitis has not been studied, but Mielke *et al.* showed that enhanced production of IL-22 by ILC3s, induced by retinoic acid, reduced disease severity (Mielke *et al.* 2013).

Together, these studies underline the complexity of the immune response following DSS treatment (Table 1.1). DSS-induced colitis serves as a good model for human IBD and studying the immune response in DSS-treated mice can help understand human disease. However, the acute and extensive damage to the intestinal epithelium leading to sudden translocation of the intestinal microbiota does not reflect human IBD, where disease develops over years or decades. Nonetheless, understanding immune cell function in DSS-induced colitis can greatly advance understanding of human disease.

The advantage of DSS-induced colitis over other chemically-induced models of IBD is the fact that DSS is administered in the drinking water whereas TNBS is injected directly to the rectum and requires anesthesia (Morris *et al.* 1989). Transgenic mouse models often develop slowly and depleting certain cell types or blocking pathways can be difficult due to the length of the experiment. Transgenic models further require complex breeding setups and the intensity of

disease cannot be controlled. Using DSS to induce colitis allows testing the response to different intensities and lengths and is therefore a suitable model to study both acute and chronic intestinal inflammation.

1.2.3.2 The *Citrobacter rodenium* model of infectious-induced colitis

C. rodentium is a mouse pathogen that is commonly used to study mucosal immune responses and serves as a mouse model for IBD. Together with the human Enterohemorrhagic *Escherichia coli* (EHEC) and Enteropathogenic *Escherichia coli* (EPEC), *C. rodentium* belongs to the group of attaching and effacing (A/E) pathogens. These are equipped with a Type III secretion system (T3SS) allowing the bacteria to inject their effector proteins into host cells, thereby modulating signaling pathways involved in, amongst others, apoptosis, tight junction integrity and innate immune responses (Collins *et al.* 2014). Infection with *C. rodentium* leads to a T_H1 response, characterized by an increase in $CD4^+$ T cells and increased production of T_H1 cytokines, such as IFN-γ, TNF-α and IL-12. It was therefore proposed to be used as a model for IBD (Higgins *et al.* 1999). Since then, the role of various immune components in *C. rodentium*-induced colitis has been studied.

To dissect the role of the adaptive immune system using the *C. rodentium* mouse model, Bry *et al.* compared several mouse strains lacking part of the T cell compartment, B cells or both (Bry *et al.* 2004). Interestingly, deficiencies in $CD8^+$ or $\gamma\delta$T cells did not result in changes in disease susceptibility, whereas CD4-deficient mice showed significantly decreased survival. All $RAG2^{-/-}$ mice, lacking both T and B cells, succumbed to infection, similar to mice deficient in B cells only, suggesting an indispensable role for B cells and equally underlining the importance of $CD4^+$ T cells. The authors went on to show that the increased disease susceptibility observed in mice lacking $CD4^+$ T cells was due to failure in mounting appropriate T cell-dependent IgG and IgM responses. While this study demonstrated the importance of B cells and antibodies in the protection against disease, a study by Koroleva *et al.* suggested that mediating Ig production was not the only function of $CD4^+$ T cells in *C. rodentium*-induced colitis. Using the same B cell-deficient mouse strain, the authors showed 100% mortality, but at much later stages than Bry *et al.* (Koroleva *et al.* 2015). In the first study, all B cell-deficient mice succumbed to

infection by day 20 post infection, whereas mice survive as long as 70 days post infection (dpi) in the experiments performed by Koroleva at al.

Using elegant mouse models, Shiomi *et al.* demonstrated that IFN-γ-production by $CD4^+$ T cells is indeed of importance in clearance of infection and that lack thereof leads to increased bacterial burden and pathology (Shiomi *et al.* 2010). The authors showed that IFN-γ is important in initiating an appropriate T cell response by enhancing the ability of APCs to stimulate the proliferation of antigen-specific T cells. Additionally, they showed that IFN-γ has a beneficial effect on macrophages, leading to an increased phagocytic capacity.

The innate immune system, acting as a first line of defense, plays a crucial role in the recognition and elimination of bacteria. Activation of MyD88, a downstream signaling molecule of the majority of TLRs, leads to the recruitment of immune cells, as well as inducible nitric oxide synthase (iNOS), IL-6 and TNF-α production by colonic macrophages. Lack thereof leads to increased bacterial burden and severe mucosal injury, suggesting that MyD88 is a key molecule involved in recognition of *C. rodentium* and the induction of an appropriate immune response (Gibson *et al.* 2008). Both NK cells and ILC1s have been shown to play a crucial role in host defense (Spits *et al.* 2016), but only NK cells have been studied in the context of infection with *C. rodentium*. Two studies have dissected the role of NK cells in the host response to *C. rodentium*: Hall *et al.* depleted NK cells using the anti-asialo-GM1 antibody and showed increased pathology and bacterial burden in NK cell-depleted mice compared wild-type controls (Hall *et al.* 2013b). Reid-Yu on the other hand used the NK1.1-depleting PK136 antibody and showed no difference in bacterial burden, but a delay in the T_H1 response, measured by secretion of IFN-γ, IL-12 and TNF-α (Reid-Yu *et al.* 2013). The authors argued that while NK cells play no direct role in the elimination of the pathogen, they are important in the recruitment of T cells and the initiation of a T_H1 response. Differences between the two studies are likely due to different targets of the depleting antibodies – while PK136 depletes all cells expressing NK1.1, which can include certain subsets of ILC1s, NKT cells and LTi cells (Vivier *et al.* 2018), anti-asialo-GM1 has been shown to also deplete a subset of macrophages (Wiltrout *et al.* 1985). ILC3s, in particular in the context of IL-22 production, have been extensively studied. Deficiencies in IL-22 lead to a severe colitis and high mortality (Zheng *et al.* 2008), with innate cells,

later identified as ILC3s, being the main producers of IL-22 (Zheng *et al.* 2008, Satoh-Takayama *et al.* 2008). Zheng *et al.* showed that IL-22, induced by IL-23, enhances the production of anti-microbial proteins, in particular RegIII-β and RegIII-γ (Zheng *et al.* 2008). Another indication that IL-22 produced by ILC3s and not $CD4^+$ T cells are crucial for defense against *C. rodentium* comes from a recent study investigating the role of Signal transducer and activator of transcription (STAT)5. As opposed to $CD4^+$ T cells, ILC3s rely on STAT5 for IL-23-mediated IL-22 secretion and lack of STAT5 leads to significantly increased pathology and morbidity, suggesting non-redundant roles of IL-22 produced by ILC3s and $CD4^+$ T cells (Bauché *et al.* 2020). STAT5 suppresses IL-17 production in T cells (Yang *et al.* 2011), so it is plausible that increased pathology in STAT5 mice is not only caused by the lack of IL-22, but also an overproduction of IL-17.

Another molecule of interest is osteopontin (OPN), which is upregulated in human IBD and therefore of interest in gut pathology. By using OPN-deficient mice, Wine *et al.* showed that lack of OPN leads to decreased bacterial burden and reduced gut inflammation, associated with lower levels of IFN-γ and TNF-α, suggesting that these cytokines are not only involved in bacterial clearance, but also gut pathology (Wine *et al.* 2010).

While IL-17 is clearly important in bacterial clearance and deficiencies in IL-17A, IL-17F or both lead to increased bacterial burden (Ishigame *et al.* 2009), members of the IL-17 family can also have pro-inflammatory and disease-progressing effects. Deficiency in Resistin-Like Molecule (RELM)-α, which regulates IL-17, has no effect on bacterial burden or weight loss, but ameliorates inflammation and reduces levels of IL-17 (Chen *et al.* 2014). This suggests that IL-17 has pleiotropic functions – while IL-17 is important for bacterial clearance, high levels can have pro-inflammatory effects leading to a more severe colitis.

Overall these studies suggest that clearance of *C. rodentium* requires an extremely tightly regulated immune response. Both lack of an appropriate immune response and an overreaction can have detrimental effects (Table 1.1).

While *C. rodentium* is not an ideal model for human IBD due to the introduction of a pathogenic bacteria in an otherwise healthy mouse, it helps understand the role of the different immune components in gut homeostasis and pathology. In addition to being used as a model of colitis,

administration of *C. rodentium* can be used to study the host response to intestinal infection. We chose to infect mice with *C. rodentium* and not *H. hepaticus*, as *H. hepaticus* only induce inflammation in immunodeficient hosts, whereas wild-type C56BL/6 mice develop colitis following infection with *C. rodentium*. *C. rodentium*-induced colitis it therefore an easier and more appropriate model to study both the innate and adaptive immune response to infection.

Table 1.1: Table summarizing function of different immune cells in different models.

Cell type	**human IBD**	**DSS model**	***C. rodentium* model**
Macrophages (Mφ)	- pro-inflammatory Mφ ↑ - tolerogenic Mφ ↓ - IL-23 ↑ - potential role of TNF-α and IL-1β	- protective, mechanism unclear	- phagocytic (clear infection)
DCs	- IL-22$^+$ DCs ↓ - activating receptors↑	- protective, mechanism unclear	- unknown
ILC1	- IFN-γ$^+$ ILC1s ↑ - ILC3s → ILC1s ↑	- expanded, mechanism unclear	- unknown
ILC3	- decreased, mechanism unclear	- IL-22 ↑ (protective)	- IL-22 ↑ (protective)
NK cells	- CD16$^+$ NK cells ↑ (role unclear)	- inhibition of neutrophil function via NKG2A (protective) → IL-6, IL-17, ROS ↓	- protective, recruitment of T cells and initiation of T_H1 response
T cells	- IFN-γ$^+$ T cells ↑ - cytotoxic and pro-inflammatory function of NKG2D$^+$CD4$^+$ T cells - IL-1, TNF-α and (in UC patients), IL-5 and IL-13 ↑	- disease-promoting T_H1 response (IFN-γ, TNF-α)	- disease-promoting T_H1 response (IFN-γ, TNF-α, IL-12) - IFN-γ important for clearance of infection

B cells	- IgA-coated pathogenic bacteria↑ - TLR2 ↑	- unclear	- protective, mechanism unclear

1.3 Colorectal cancer

It has been well-established that inflammation can lead to tumorigenesis and chronic inflammation has now been added to Weinberg's hallmarks of cancer (Hanahan *et al.* 2011). It is therefore not surprising that IBD patients are at much greater risk of developing CRC (Triantafillidis *et al.* 2009). CRC is now the third most common cancer and one of the leading causes of death due to malignancies, with roughly 1.2 million new cases and 600,000 deaths per year across the world (Brenner *et al.* 2014). Tumor development is a multi-step process and Fearon and colleagues proposed the adenoma-carcinoma sequence model for colorectal tumorigenesis in 1990, where they hypothesized that tumorigenesis arises due to multiple mutations in oncogenes or tumor suppressor genes (Fearon *et al.* 1990). Early mutations can lead to hyperproliferation of the epithelium and early, benign adenomas, whereas late adenomas and carcinomas only arise when further mutations accumulate. One key tumor suppressor is the *adenomatous polyposis coli* (*Apc*) gene, which is mutated in the vast majority of CRC patients. In fact, germline mutations in the *Apc* gene leads to a hereditary form of CRC, familial adenomatous polyposis (FAP) (Fodde *et al.* 2001). Disruption of the *Apc* suppressor gene results in the activation of the Wnt pathway, which is disrupted in the majority of CRC cases, leading to aberrant self-renewal (Schepers *et al.* 2012). Despite this commonality in most patients, CRC is a heterogeneous disease with many different molecular characteristics. Here, we summarize what is known about the heterogeneity of the disease, review treatment options, outline immunological networks in CRC and summarize the importance of the microbiota in cancer progression. Lastly, we introduce the model of CRC used in this model, the $Apc^{min/+}$ mouse model.

1.3.1 Subtypes of colorectal cancer

To improve diagnostics and treatment options, it is important to understand and classify different subtypes of the disease. Several classifications based on the gene expression profile of the tumors have been proposed, which has helped establish prognostic and therapeutic markers. Microsatellites, which are a class of repetitive deoxyribonucleic acid (DNA) consisting of certain DNA motifs present in the human genome, have been found to be hypermutated in a subset of patients and correlated with increased patient survival (Thibodeau *et al.* 1993). A study using The Cancer Genome Atlas (TCGA) datasets revealed 16% of colorectal carcinomas to be hypermutated, either due to microsatellite instability high (MSI-H) tumors or deficient mismatch-repair (dMMR) (Muzny *et al.* 2012). However, the remaining 84% of cases, which are associated with a worse outcome, remain poorly understood.

A study from 2015 identified four different subtypes of CRC, called consensus molecular subtype (CMS), which are based on biological and genetic characteristics and allow more targeted interventions and better understanding of 'non-MSI' tumors. Four different subtypes have been defined: CMS1, also defined as 'MSI immune', encompasses the hypermutated tumors and is associated with high immune infiltration and activation. CMS2, the 'canonical subtype' is characterized by Wnt and Myc activation and is, with a frequency of 37%, the most common subtype. Metabolically dysregulated tumors (CMS3) are the scarcest subtype with only 13%, are often associated with KRAS mutations and can be MSI-H or low. CMS4, the 'mesenchymal subtype' is characterized by stromal infiltration, TGF-β activation and strong angiogenesis. 23% of all patients fall into this category, which is also associated with the worst relapse-free and overall survival outcome (Guinney *et al.* 2015).

1.3.2 Treatment options for colorectal cancer

Depending on the cancer stage, which ranges from localized (Stage I) to metastasized (Stage IV), different therapeutic approaches can be taken. In early stages of the disease, surgical resection is the most desirable approach, as it often allows complete resection of the tumor and therefore a curative treatment. Surgery can be combined with radiotherapy with preoperative

radiotherapy reducing the risk of local recurrence (Dekker *et al.* 2019). However, this is often not sufficient and more systemic therapies are often needed, in particular in metastatic cancer. Chemotherapy has been the first line of treatment for patients with metastatic CRC for many decades, with the most common therapy being a combination of two cytotoxic drugs, Fluorouracil (5-FU) and either oxaliplatin or irinotecan or a combination of all three (Falcone *et al.* 2007). However, chemotherapy is non-specific and often has severe side-effects, which is why targeted therapy is favored.

Targeted therapies that are approved as treatment for CRC include three antibodies that target specific pathways - cetuximab, bevacizumab and panitumumab. Cetuximab and panitumumab target the Epidermal growth factor receptor (EGFR), while bevacizumab is a monoclonal antibody (mAb) against Vascular endothelial growth factor (VEGF) (Noguchi *et al.* 2013). Both pathways are upregulated in many CRC patients, with VEGF inducing angiogenesis and EGFR being associated with increased proliferation and thereby accelerating tumor growth (Tabernero 2007).

The CMS classification has helped better understand and evaluate treatment options based on each specific subtype. As previously described, CMS1 is associated with immune cell infiltration and activation and is therefore a potential target for Immune Checkpoint Inhibitors (ICI). ICI, which target immune receptors associated with immune cell exhaustion, such as Programmed cell death protein 1 (PD-1), cytotoxic T-lymphocyte-associated protein 4 (CTLA-4) and Programmed death-ligand 1 (PD-L1), reactivate tumor-specific immune cells and elicit a specific immune response, which will be further discussed in section 1.3.3. (Pardoll 2012). dMMR and MSI-H have been proposed as biomarkers to predict the response to ICI with one study associating dMMR tumors with a good response to pembrolizumab, an anti-PD-1 antibody (Le *et al.* 2017) and another study showing clinical benefit of dMMR and MSI-H with nivolumab (anti-PD-1) and ipilimumab (anti-CTLA-4) (Overman *et al.* 2018). Patients classified as CMS2, a subtype often associated with an activated EGFR pathway, have been shown to have an increased overall survival when receiving chemotherapy in combination with cetuximab compared to the other subtypes (Lenz *et al.* 2019).

While these studies only offer limited guidance, in particular in subtypes other than CMS1 and

2, future clinical studies and/or therapies targeting specific pathways unique to certain subtypes are promising approaches. One of these approaches is turning a 'cold', immune-excluded tumor into a 'hot' tumor that can be targeted by ICI. For this, CMS4 tumors are particularly interesting candidates, as they are characterized by a high expression of the immunosuppressive TGF-β. This 'remodelling' could potentially be achieved by using a combination therapy of chemotherapy and ICI therapy, leading to the elimination of pro-tumorigenic cells, such as Myeloid-derived suppressor cell (MDSC), while at the same time promoting the infiltration of T cells and ensuring immune cell activation (Vincent *et al.* 2010). This combination therapy consisting of chemotherapy and the administration of anti-PD-1 therapy has been tested in mouse models, where it showed promising results (Dosset *et al.* 2018).

A recent study demonstrates that, if treated at early stages, patients with tumors that are MMR-proficient can benefit from a combination of ipilimumab and nivolumab. The response rate was only 27%, but the authors demonstrate that even in non-responders, the TCR clonality, frequency of $CD8^+$ T cells and CXCL3 expression was increased (Chalabi *et al.* 2020). This suggests that it is indeed possible to increase the immunogenicity of immune 'cold' tumors with a combination of immune-activating therapies.

Another attractive target is the Wnt pathway, which is dysregulated in the majority of CRC patients. Small-molecule inhibitors can interfere with the hyperactivated Wnt pathway and have been shown to be successful in pre-clinical models (Lau *et al.* 2013, Menon *et al.* 2019). Understanding the underlying molecular mechanisms leading to the development and molecular mechanisms specific to different subtypes of CRC will allow more targeted therapy with fewer side-effects and better patient outcomes.

1.3.3 Immunological networks in colorectal cancer

Being both a malignancy, as well as an inflammatory disorder, the role of the immune system is particularly complex in CRC. While the immune system is indispensable for recognizing and eliminating nascent tumor cells, a dysregulated and chronic immune response can promote intestinal tumorigenesis. The interactions between the immune system and the tumor microenvironment are therefore complex and highly context-dependent.

T cells, in particular CTL, as well as NK cells are often the first cells to recognize and eliminate nascent tumor cells. Galon and colleagues first proposed to characterize the type, density and location of tumor-infiltrating lymphocyte (TIL)s, rather than just quantifying T cell numbers. He showed that a T_H1 response, as well as the presence of cytotoxic and memory T cells is a good predictor of tumor rejection by the host immune system (Galon *et al.* 2006). An extensive meta-analysis of 43 studies confirmed these results and identified high TIL counts and $CD3^+$ T cell density as the best predictors of survival (Idos *et al.* 2020). Further, they found that Foxp3, which identifies T_{reg} cells and is often associated with decreased survival in solid tumors (Bates *et al.* 2006, Petersen *et al.* 2006), serves as a good prognostic marker in CRC patients.
Immune cell exhaustion is defined as a state of hyporesponsiveness that immune cells enter upon persistent and chronic activation. It is characterized by a decrease or absence of the production of effector cytokines and cytotoxic molecules, and is often associated with an upregulation of inhibitory receptors, such as PD-1 and CTLA-4. Due to the chronicity of the disease, T cell exhaustion is a hallmark of many tumors (Jiang *et al.* 2015) and the frequencies of both PD-1 expressing $CD4^+$ and $CD8^+$ T cells appears to be increased in the tumor of CRC patients compared to surrounding tissue (Dunne *et al.* 2016). Further, a high ratio of PD-1 expressing TILs among all $CD8^+$ T cells has been shown to be bad prognostic marker for CRC patients (Shibutani *et al.* 2017), suggesting that T cell exhaustion does indeed take place in the tumor microenvironment (TME) of CRC patients.
In addition to immune exhaustion, overreacting immune cells and chronic inflammation can contribute to CRC development. In particular IL-17 has been implicated in promoting inflammation and tumorigenesis in the intestine. Indeed, a follow-up study by Galon and colleagues revealed that patients with high expression of genes associated with a T_H17 response, such as *IL17A* and *RORC*, encoding the transcription factor RORγT, as well as high infiltration of IL-17 expressing cells showed reduced disease-free survival compared to those with a weak T_H17 and strong T_H1 response (Tosolini *et al.* 2011). While this study does not specifically identify T cells as the source of IL-17, it points towards a disease-promoting role of IL-17. However, a study which further investigated the source of IL-17 found that indeed most of the IL-17^+ cells were $CD4^+$ T cells (Amicarella *et al.* 2015). They were unable to confirm the reduced disease-

free survival in patients with high IL-17, as observed by Galon *et al.*, and instead propose an anti-tumor function for IL-17 producing cells residing in the epithelium. They argue that IL-17 is correlated with an increase in CTL and neutrophils and suggest that intraepithelial T_H17 cells contribute to the recruitment of these cells to the tumor bed.

Yet another study suggests that not T_H17, but instead γδT cells are the primary source of IL-17 in tumors from CRC patients. They showed that in addition to IL-17, these cells produce IL-8, GM-CSF and TNF-α, which act together to promote the recruitment of tumor-promoting MDSCs to the tumor, leading to an immunosuppressive and tumor-promoting environment (Wu *et al.* 2014). Indeed, the frequencies of MDSC were increased in tumor samples and peripheral blood of CRC patients and correlated with disease stage and lymph node metastasis (OuYang *et al.* 2015). Several studies have unveiled the immunosuppressive functions of mouse MDSC, which include inhibiting TCR recognition (Nagaraj *et al.* 2007), increased expression of arginase, depriving T cells of L-Arginine (Raber *et al.* 2012), upregulation of PD-L1 and inhibition of T cells by engagement of PD-1 (Noman *et al.* 2014), the secretion of angiogenesis- and metastasis-promoting factors, such as Matrix metalloproteinase (MMP)s (Qu *et al.* 2011) and the production of the T cell suppressive ROS (Kusmartsev *et al.* 2004).

The function of other myeloid cells, which include macrophages, DCs and neutrophils is more complex, as they can have both pro- and anti-tumorigenic functions. Different subtypes of DCs have been shown to be correlated with good or poor survival, with $CD1a^+$ DCs that reside in the tumor epithelium and can be regarded as immature, being correlated with a higher infiltration of $CD4^+$ T cells and better survival, while $CD208^+$ mature DCs, which mostly reside in the tumor stroma and not the epithelium, were associated with worse survival (Sandel *et al.* 2005). While these are just correlations and the function of the different subtypes is not well understood, this study demonstrates that functional differences in DCs can impact disease outcome.

High infiltration of macrophages has initially been associated with an increased infiltration of T cells and better survival, suggesting that they are involved in lymphocyte recruitment (Forssell *et al.* 2007). Macrophages are plastic cells that can polarize towards a more pro- or anti-inflammatory phenotype depending on the microenvironment. Despite being an oversim-

plification, tumor-associated macrophage (TAM)s are often divided into 'M1', pro-inflammatory and anti-tumorigenic and 'M2', anti-inflammatory and pro-tumorigenic subsets (Mantovani *et al.* 2002). A study further investigating the role of macrophages in the TME suggested that high numbers of Nitric oxide synthase 2 $(NOS2)^+$ 'M1' cells were associated with a good prognosis. However, rather than being inversely correlated with the $CD163^+$ 'M2' macrophages, the authors not only found a significant correlation between $NOS2^+$ and $CD163^+$ cells, but also a decrease of both cell types with increasing cancer stage (Edin *et al.* 2012). The decrease of $CD163^+$ 'M2' macrophages with increasing cancer stage was confirmed by a later study, which additionally investigated the impact on lymph node metastasis and found that high numbers of $CD163^+$ cells were associated with fewer metastasis (Koelzer *et al.* 2015). Opposing conclusions were drawn by another study, correlating high macrophage infiltration with worse survival (Kang *et al.* 2010), however sample numbers of this study were small and results not conclusive. Neutrophils can kill disseminated tumor cells directly via the production of ROS and thereby limit metastatic spread and contribute to anti-tumor activity (Gershkovitz *et al.* 2018). However, similar to macrophages, they can additionally display pro-tumor functions, which include, but are not limited to the production of MMPs (Ardi *et al.* 2007), the release of Neutrophil extracellular traps (NET)s (Park *et al.* 2016, Yang *et al.* 2020) and production of pro-angiogenic factors, such as VEGF (Kuang *et al.* 2010). Similar to macrophages, a 'N1' and 'N2' nomenclature has been suggested to distinguish pro- and anti-inflammatory neutrophils (Park *et al.* 2016). In the context of CRC, the number of neutrophils were significantly lower in Stage IV patients compared to stage I-III and a higher number of neutrophils was associated with better survival. Further, a high number of neutrophils was linked to a better response to 5-FU chemotherapy (Galdiero *et al.* 2016). This was confirmed by an independent study, which suggested that low neutrophil infiltration at early stages is a strong predictor of worse survival (Wikberg *et al.* 2017). Yet, the role of neutrophils in CRC is controversial, and a study by Rao *et al.* suggested that high neutrophil numbers are a predictor of worse survival (Rao *et al.* 2012). Again, low sample numbers, in particular at later cancer stages, could explain the discrepancies, but these studies make it clear that quantifying neutrophil and macrophage numbers by immunohistochemistry (IHC) is not sufficient, and that their functional characteristics might

be of better prognostic value.

NK cells, which are classically involved in the recognition of tumor cells by recognizing both the expression of ligands, typically expressed by malignant cells, as well as the absence of ligands expressed on all healthy cells, such as MHC-I. CRC is often associated with a loss of MHC-I, making it a good target for NK cell recognition (Momburg *et al.* 1986). Due to their potent anti-tumor function, NK cells have often been associated with good survival in a range of cancers, including CRC (Sconocchia *et al.* 2014, Coca *et al.* 1997). However, the frequency of patients with high NK cell infiltration was low and only 25 out of the 157 patients from the second study were classified to have 'extensive' NK cell infiltration. Additionally, the cells that do infiltrate the tumor were shown to have a distinct phenotype compared to PB NK cells. Specifically, the frequencies of NK cells expressing activating receptors or receptors associated with cell activation, including CD16, NKG2D, NKp46 or DNAX Accessory Molecule-1 (DNAM1) were reduced in both the healthy surrounding mucosa as well as tumor-infiltrating NK cells compared to PB (Rocca *et al.* 2012). While this may indicate that the changes in NK cell functionality are gut-specific rather than a consequence of tumorigenesis, some differences point towards tumor-specific changes. The frequency of NK1.1-expressing NK cells was significantly reduced within the tumor compared to surrounding tissue, and other receptors, specifically NKG2D, NKp30, NKp46 and DNAM1 showed a similar trend, though the differences were not statistically significant. This was supported by the observation that the expression of NKG2D, DNAM1 and NKp30 was significantly reduced on PB NK cells isolated from CRC patients compared to healthy controls. A novel role for NK cells in the context of tumorigenesis was suggested by Bruno *et al.*, who further characterized both PB as well as tumor-infiltrating NK cells from CRC patients and showed that they release proangiogenic factors and MMPs, suggesting that they acquire a pro-tumorigenic phenotype throughout disease development (Bruno *et al.* 2018). Together, these studies demonstrate that I. NK cells are often unable to efficiently infiltrate the tumor and II. when they do infiltrate the tumor, they are not necessarily anti-tumorigenic and can acquire pro-tumorigenic functions.

Due to the relative recent discovery and the scarcity of ILCs within the tissue, data investigating the role of ILCs in the context of CRC is limited. However, extensive analysis of samples from

35 CRC patients, including mass cytometry and RNA sequencing (RNAseq) was performed by de Vries *et al.*, who, for the first time, demonstrated the importance of ILCs in CRC. They showed that ILCs with a cytotoxic gene expression profile were indeed enriched in tumor tissue, in particular in patients with dMMR (Vries *et al.* 2019). They further correlated ILC infiltration with presence and activity of γδT cells and showed that, in dMMR tumors, presence of ILCs was strongly correlated with infiltration of PD-1-expressing γδT cells, indicating that they are indeed involved in the anti-tumor response. Due to their cytotoxic gene expression profile, the ILCs identified in this study most likely fall into the category of ILC1s. ILC3s, that mainly produce IL-17 and IL-22, and are abundant in the intestine (see section 1.1.2) and have been implicated in contributing to mouse models of intestinal inflammation (see section 1.2.3), but have not been studied in the context of human CRC.

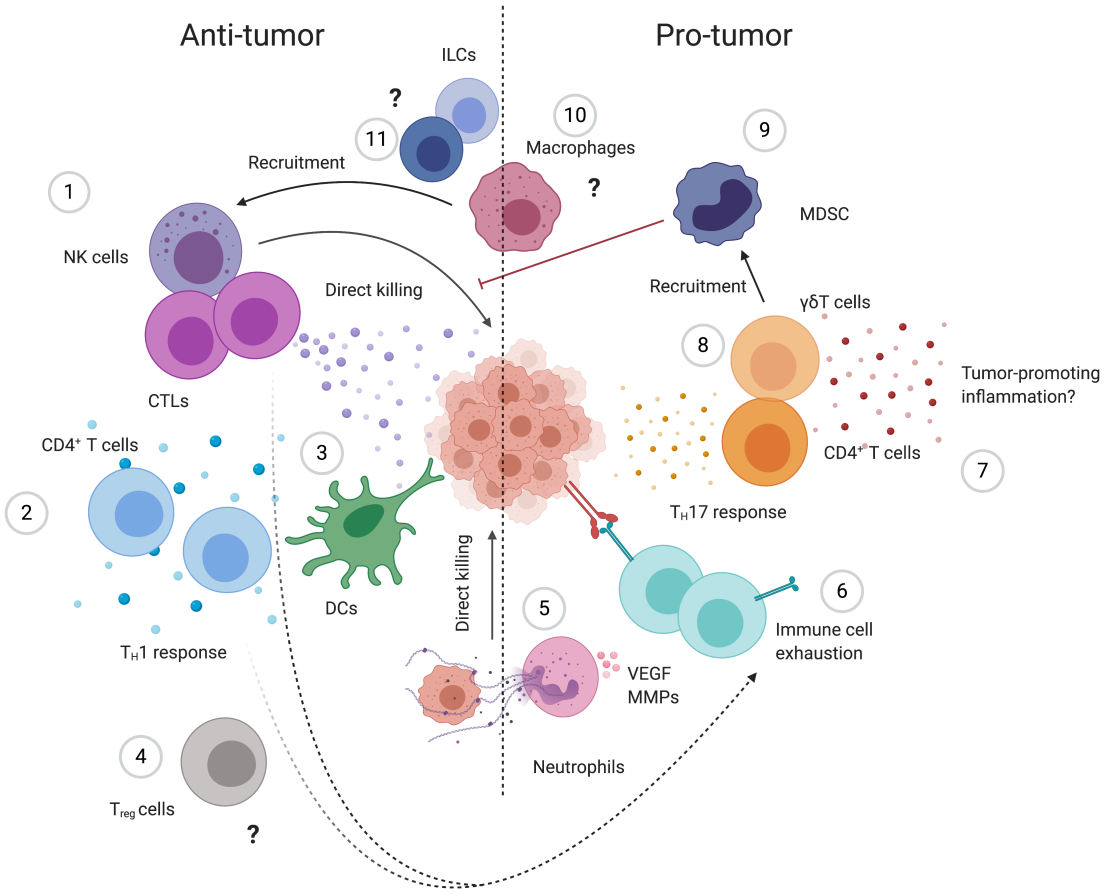

Figure 1.3: Simplified representation of immunological networks in CRC. Function of anti- (left) and pro-tumor (right) immune cells in CRC. NK cells and CTLs (1) typically exhibit strong anti-tumor functions by killing tumor cells directly, but sustained activation can lead to tumor-promoting immune cell exhaustion (6). $CD4^+$ T cells (2) can contribute to anti-tumor activity by secreting T_H1 cytokines. DCs (3) can have a dual function but are typically involved in T cell recruitment and activation and therefore anti-tumorigenic. The function of T_{reg} cells (4) is unclear, but has been shown to be a good prognostic marker in CRC. Neutrophils (5) can trap and kill tumor cells in circulation and prevent dissemination, but can equally contribute to metastasis and angiogenesis by the release of MMPs and VEGF. Exhausted immune cells (6) upregulate inhibitory receptors and their presence is associated with worse survival. IL-17 produced by T_H cells (7) and γδT cells (8) is thought to promote inflammation and tumorigenesis in CRC patients. γδT cells (8) produce, in addition to IL-17, TNF-α, IL-8 and GM-CSF, which leads to the recruitment of MDSCs (9). MDSCs suppress anti-tumor immune responses by a variety of mechanism. The role of macrophages (10) is not fully understood and their presence can be both a good and a bad predictor of disease outcome. Similarly, the role of ILCs (11) is not fully understood, but ILC1s producing T_H1 cytokines are generally thought to be anti-tumorigenic, while the role of ILC3s is less clear. CRC = colorectal cancer, CTL = cytotoxic lymphocytes, DC = dendritic cell, T_{reg} = regulatory T cell, MMP = matrix metalloproteinase, VEGF = Vascular endothelial growth factor, TNF = tumor necrosis factor, GM-CSF = Granulocyte-macrophage colony-stimulating factor, MDSC = myeloid-derived suppressor cell, ILC = innate lymphoid cell. Image was created using BioRender.

1.3.4 Colorectal cancer is associated with changes in the microbiota

Considering the direct interactions between the intestinal microbiota and the epithelium, it is not surprising that the role of the microbiota in CRC has been a subject of great interest for many years. The observation that the microbiota plays a role in tumorigenesis goes back to 1967, where a study showed that GF rats were less susceptible to chemically-induced carcinogenesis (Laqueur *et al.* 1967). Further studies have identified a variety of bacteria that are more abundant in CRC patients, some of which have been shown to be cytotoxic or pro-inflammatory, as well as groups of metabolites that can have pro-tumorigenic functions. While it is difficult to pinpoint specific changes in the microbiota to disease development, it is accepted that tumorigenesis is generally associated with a change in the microbial composition (Hale *et al.* 2016). Some bacteria have been directly associated with tumor development due to their ability to cause DNA damage or inflammation, while other bacteria preferentially proliferate in an already disturbed environment (Tjalsma *et al.* 2012).

A study by Dai *et al.* identified a set of seven bacteria preferentially enriched in CRC patients, namely *Bacteroides fragilis* (*B. fragilis*), *Fusobacterium nucleatum* (*F. nucleatum*), *Porphyromonas asaccharolytica* (*P. asaccharolytica*), *Parvimonas micra* (*P. micra*), *Prevotella intermedia* (*P. intermedia*), *Alistipes finegoldii* (*A. finegoldii*) and *Thermanaerovibrio acidaminovorans* (*T. acidaminovorans*) (Dai *et al.* 2018). Interestingly, several of these are oral commensals and not typically found in the intestinal tract. In the setting of CRC, *F. nucleatum*, one of the best studied bacteria associated with CRC, can directly induce oncogenes by binding of its adhesin FadA, which activates β-catenin signaling and induces Wnt expression (Rubinstein *et al.* 2013). Simultaneously, it activates pro-inflammatory pathways, which, if left uncontrolled, lead to DNA damage and epigenetic changes, eventually leading to tumor progression. Conversely, *F. nucleatum* has been shown to have immunomodulating properties, which can specifically dampen the anti-tumor response. A protein found on the surface of *F. nucleatum*, Fusobacterial apoptosis protein 2 (Fap2), can bind to the inhibitory NK cell receptor TIGIT and suppress the anti-tumor function of NK cells in the tumor microenviroenment (Gur *et al.* 2015). Further, studies using a mouse model have demonstrated that *F. nucleatum* specifically recruits tumor-infiltrating, pro-tumorigenic myeloid cells (Kostic *et al.* 2013). An immunomodulatory

role of certain bacteria was supported by a recent study comparing immune cell infiltration in patients with 'high' versus 'low/absent' levels of *F. nucleatum*. Patients with 'high' levels had a higher $CD163^+$ to $CD68^+$ ratio, suggesting preferential infiltration and/or polarization to M2 macrophages (Qi *et al.* 2020). *F. nucleatum* is one of the best understood bacteria infiltrating intestinal tumors, yet the origin is not clear. It is typically absent in the intestine and is instead found in the oral cavity of healthy individuals (Griffen *et al.* 2011). Recent evidence suggests that *F. nucleatum* reaches intestinal tissue via the blood circulation rather than the digestive tract in a pre-clinical mouse model of CRC (Abed *et al.* 2020). This means that *F. nucleatum* avoids having to compete with the commensal microbiota and allows infiltration directly into the tumor via tumor-associated blood vasculature.

Interestingly, other species typically found in the oral cavity, including *Porphyromonas gingivalis* (*P. gingivalis*) and *P. micra* are associated specifically with CMS1, the 'immune' subtype, further pointing towards a relationship between the microbiota and immune activation (Purcell *et al.* 2017). Another bacteria of interest is *B. fragilis*, which, like *F. nucleatum*, secretes a toxin that leads to the cleavage of E-cadherin and subsequent activation of the β-catenin pathway (Wu *et al.* 2003). Further, a study using a mouse model suggests that IL-17 is involved in the pro-tumorigenic process by showing that mice with deficient IL-17 signaling in colonic epithelial cells are less susceptible to *B. fragilis*-induced tumor development (Chung *et al.* 2018).

While these are all examples of bacteria with pro-carcinogenic features, potentially driving the disease ('driver' bacteria), other bacteria associated with intestinal dysbiosis have no known mechanisms contributing to disease. These bacteria, often termed 'passenger' bacteria, typically sparsely colonize the healthy intestine, but have a competitive advantage over other microbes in a pro-inflammatory and -tumorigenic environment (Tjalsma *et al.* 2012). Evidence for 'passenger' bacteria comes from studies comparing the microbiota of healthy individuals to CRC patients. One example is *Streptococcus bovis* (*S. bovis*), which has been shown to be a strong predictor of intestinal disease, with 10.5% of healthy patients testing positive for *S. bovis* and 55.6% of patients with CRC (Klein *et al.* 1977). While passenger bacteria are unlikely to directly contribute to disease, they can potentially serve as diagnostic markers, in particular if they arise in early stages of disease, such as *S. bovis* (Boleij *et al.* 2011).

The fact that changes in the microbiota often precede disease onset has fuelled research into further characterizing these changes and using them as diagnostic markers. A study examining TCGA datasets for microbial reads determined cancer-specific microbial profiles in both blood and tissue samples, allowing the discrimination of healthy and diseased patients based on plasma-derived microbial DNA (Poore *et al.* 2020). While there are limitations to the study, it underlines not only the potential of better understanding changes in the microbiota, but also the complexity of the system, which can only be resolved using computational approaches.

Further evidence of the importance of the microbiota has come from studies investigating response to treatments, in particular treatment to ICI. A series of studies published in Science demonstrated a relationship between the microbiota and response to therapy. In a mouse model of transplanted tumors, mice showed a weakened response to immunotherapy, in this case anti-IL-10R antibodies and CpG-oligodeoxynucleotides, when treated with antibiotics compared to control mice, suggesting a role for the microbiota in the success of cancer therapy (Iida *et al.* 2013). This was supported by a study published two years later showing that commensal bacteria, more specifically *Bifidobacterium*, promote anti-tumor activity after treatment with anti-PD-L1 antibodies, again in a mouse model of transplanted tumors (Vétizou *et al.* 2015). In 2017, two studies were published back to back, demonstrating for the first time that this is relevant in human patients. Both studies investigated the success of anti-PD-1 therapy by comparing the microbiota of responders versus non-responders. Melanoma patients who responded to ICI displayed significantly higher alpha-diversity as well as increased relative abundance of *Ruminococcaceae*. Further, the relative abundance of *Faecalibacterium* was increased and that of *Bacteroidales* decreased. The presence of *Faecalibacterium* and *Bacteroidales* correlated with high versus low $CD8^+$ T cell density, respectively, suggesting interactions between the microbiota and the immune system (Gopalakrishnan *et al.* 2017). The idea that the response to ICI depends on the composition of the patient's microbiota was supported by a study published only a few weeks later, which divided patients, in this case Non-small-cell lung carcinoma (NSCLC), Renal cell carcinoma (RCC) and urothelial carcinoma patients, into responders and non-responders and showed that only Fecal microbiota transplant (FMT) of responders and not non-responders to mice resulted in ICI-dependent tumor rejection. In their responder cohort,

Akkermansia muciniphila (*A. muciniphila*) was highly enriched and its importance was demonstrated by monocolonization of mice, which was sufficient to induce an anti-tumor response to PD-1 blockade. The authors further studied changes in the immune response upon colonization with *A. muciniphila* and treatment with ICI and showed an increase in $CCR9^+$ central memory $CD4^+$ T cells in the tumor bed and draining lymph nodes, a higher $CD4^+/Foxp3^+$ ratio and a higher IL-12 secretion by DCs (Gopalakrishnan *et al.* 2017). However, the exact mechanisms by which certain bacteria contribute to the response to ICI remain unclear. To study this further, Coutzac and colleagues not only assessed differences in relative abundance of different bacteria, but also measured microbial metabolites in melanoma patients treated with ipilimumab. Interestingly, and contrary to the hypothesis that high abundance of *Firmicutes* phylum is associated with higher concentration of SCFA, the authors found an inverse correlation between the frequency of *Firmicutes* phylum and butyrate in the serum. They further confirmed low serum butyrate and proprionate to be a predictor of longer survival and showed that in a mouse model, supplementation with butyrate during anti-CTLA-4 therapy, at least partially, abrogated the anti-tumor response by inhibiting DC priming and T cell maturation (Coutzac *et al.* 2020).

In a recent study, McCoy and colleagues identified another metabolite as a strong predictor of ICI treatment response in a mouse model of CRC (Mager *et al.* 2020). Inosine was shown to enhance the anti-tumor T cell response by engaging the adenosine A_{2A} receptor. Importantly, oral administration of inosine resulted in enhanced tumor regression upon treatment with ICI therapy, underlining the potential of combining ICI therapy with the administration of bacterial metabolites to improve patient response and disease outcome.

These studies underline the significance of the microbiota in response to ICI, as well as the importance of studying the mechanisms involved in microbiota-related immune suppression or enhancement to target these pathways and improve patient response to ICI.

1.3.5 Using the *Apc*$^{min/+}$ mouse model to study the immune system in colorectal cancer

The fact that *Apc* is an important tumor suppressor gene and that loss of heterozygosity leads to human disease was exploited in the development of a mouse model for CRC. *Apc*$^{min/+}$ mice, which carry the multiple intestinal neoplasia (Min) allele, a mutant allele of the mouse *Apc* locus, spontaneously develop multiple polyps throughout the intestinal tract. While CRC manifests in a large number of tumors in the colon, *Apc*$^{min/+}$ mice present with more polyps in the small intestine and only very few in the colon (Moser *et al.* 1995). Additionally, tumors are typically benign and show no signs of invasion or metastasis (Yamada *et al.* 2007). Yet, it is a very popular model that has been used in many studies investigating tumorigenesis and the role and influence of the immune system.

One key study by Zhang *et al.* showed that CD11b-expressing cells contribute to tumorigenesis by recruiting pro-tumorigenic Ly6G$^+$Ly6C^{low} MDSCs to the tumor environment, which inhibit IFN-γ secretion by antigen-specific CD8$^+$ T cells (Zhang *et al.* 2015). Additionally, they showed that lack of CD11b is accompanied by a reduced production of TNF-α, supporting the idea that the pro-inflammatory cytokine contributes to tumor progression.

Several reports study the involvement of T_{reg} cells in the development of intestinal tumors, but showed conflicting results. While Erdman *et al.* showed that T_{reg} cells, in their study defined as CD4$^+$CD25$^+$ cells, can directly induce regression of intestinal polyps in an IL-10-dependent manner (Erdman 2005), Akeus *et al.* demonstrated that mice lacking T_{reg} cells do not show changes in tumor incidence or survival, but an increase of CXCL9 and CXCL10 within the tumor. The authors suggest that the depletion of T_{reg} cells might lead to an accumulation of T cells with anti-tumor activity within the tumor *milieu* (Akeus *et al.* 2018). A more recent study supported this observation and showed the involvement of Invariant Natural Killer (iNKT) cells in regulating T_{reg} cells (Wang *et al.* 2018). Lack of iNKT cells leads to decreased tumor burden, accompanied by a lower number of T_{reg} cells, an increase of pro-inflammatory macrophages and higher expression of transcripts associated with a pro-inflammatory T_H1 response, such as IFN-γ and iNOS. One explanation for the discrepancies might be that while Wang and Akeus

utilized knock-out mice, meaning that iNKT and T_{reg} cells were absent from the earliest stages of disease, Erdman adoptively transferred T_{reg} cells into $Apc^{min/+}$ mice at timepoints at which the mice had already developed tumors. These studies indicate that T_{reg} cells can have both pro- and anti-tumorigenic properties, dependent on timing and the stage of disease.

Tumorigenesis in the $Apc^{min/+}$ mouse model is associated with an increased expression of pro-inflammatory cytokines, such as IFN-γ, IL-17, cyclooxygenase (COX)-2 and TNF-α (Wang *et al.* 2015b) and several studies have tried to dissect the contribution of each of these cytokines to disease development: while ablation of IL-17A (Chae *et al.* 2010) and COX-2 (Chulada *et al.* 2000) significantly reduces tumor burden, defects in IFN-γ or the IFN-γ receptor lead to significantly enhanced disease and worse outcomes (Wang *et al.* 2015a). Surprisingly, mice lacking TNF-α show no difference in tumor burden or survival compared to TNF-α-sufficient mice (Sakai *et al.* 2010). While germline deletion of genes of interest can provide valuable information, many genes and inflammatory mediators have distinct functions at different time-points of the disease. Nontheless, these studies demonstrate the importance of understanding the interplay of cell types and cytokines in the course of disease development.

1.4 NKG2D

NKG2D is a potent immunoreceptor that is expressed on a variety of innate and adaptive immune cells, which in mice, include activated $CD8^+$ T cells, γδT cells, iNKT cells, $CD4^+$ T cells under certain conditions, NK cells and, to some extent, ILC1 and ILC3s (Stojanovic *et al.* 2018). Expression patterns on human immune cells is similar with the exception that $CD8^+$ T cells express NKG2D constitutively (Bauer *et al.* 1999). This section provides an overview of the molecular and cellular function of NKG2D and its ligands. I review current knowledge on the role of NKG2D in disease, ranging from cancer to autoimmunity and summarize studies specifically relating to the intestine.

1.4.1 NKG2D signaling in humans and mice

Upon binding to one of its ligands, NKG2D, which itself does not contain any intracellular signaling domains, associates with an adaptor molecule to initiate the signaling cascade. In mice, these adapter molecules are either DAP10 or DAP12, while human NKG2D exclusively signals through DAP10 (Wensveen *et al.* 2018). DAP12 contains a single Immunoreceptor tyrosine-based activation motif (ITAM), which is phosphorylated upon receptor activation and recruits the Tyrosine-protein kinases Syk and ZAP70. Activation of these result in the production of cytokines and degranulation of cytotoxic cells, such as NK and $CD8^+$ T cells. DAP10 on the other hand contains a YINM sequence which, upon activation and phosphorylation, recruits Phosphoinositide 3-kinase (PI3K) and Son of sevenless homolog 1 (SOS1). It is much less efficient at inducing a cytokine/cytotoxic response, which is why it is thought to act more as a costimulatory signal with a certain level of pre-activation needed to mediate effector functions (Lanier 2009). The discrepancies of NKG2D signaling in mice and humans can be explained by two isoforms in mice, which differ in that the longer NKG2D isoform contains an additional 13 amino acids. While the short isoform can associate with DAP10 and DAP12, the long isoform, which is the only one present in humans, can only signal through DAP10 (Rosen *et al.* 2004).

1.4.2 NKG2D ligand diversity and function

Ligands recognized by NKG2D are diverse and comprise several different classes of molecules. Structurally, they resemble MHC-I molecules and are clustered on chromosome 10 in mice and and 6 in humans. Typically, they are absent from healthy tissue and only expressed on stressed, infected or transformed cells and therefore act as a 'danger signal' (Raulet 2003).

In humans, there are two main families of ligands, the MIC family, encoded on the MHC locus, and the ULBP family. The MIC family contains two ligands, MICA and MICB, which show high polymorphism, while the ULBP family contains six genes (*ULBP1-6*) and is less polymorphic. None of the mouse NKG2D ligands (NKG2DL) are encoded on the MHC locus, but there is a mouse orthologue to the ULBP family, which encodes three classes of ligands, including the Retinoic acid early inducible 1 (RAE-1)α-ε, Histocompatibility 60 (H60) and Murine

UL16 binding protein-like transcript (MULT1). The diversity of ligands for one receptor is remarkable, but the biological function of the diversity is not yet fully understood. From an evolutionary perspective, a high diversity of ligands that act as 'danger signals' is beneficial, as it decreases the chance of pathogens developing immune evasion strategies. An example of this is Human Cytomegalovirus (HCMV), which encodes UL16, a protein that prevents trafficking of MICB, ULBP1 and ULBP2 to the cell surface. This is thought to be an evasion strategy by the virus, yet the sustained expression of MICA and ULBP3, which are unaffected by UL16, allows host recognition (Dunn *et al.* 2003). Evidence further suggests functional diversity among ligands, including one study showing that MICA induces stronger downregulation of NKG2D on the surface of effector cells compared to ULBP2 (Molfetta *et al.* 2014). Receptor affinity in mice has been shown to vary greatly (O'Callaghan *et al.* 2001), potentially leading to differences in signal transduction and effector cell responses. Further, different ligands have been detected in different tissues at protein or transcriptional level. MICA protein has been shown to be constitutively expressed on intestinal epithelial tissue (Groh *et al.* 1996) and transcript for H60c has been detected in, among others, skin, tongue and eye tissue (Yoshida *et al.* 2012). NKG2DL expression is tightly regulated and aberrant expression can lead to damaging immune responses, including autoimmunity. Regulation can occur at different stages, including transcriptional regulation, ribonucleic acid (RNA) and DNA stabilization, trafficking to the cell surface and shedding from the cell surface (Raulet *et al.* 2013). NKG2DL shedding has been studied extensively in the context of tumorigenesis, where it has been shown that NKG2DL can be cleaved from the surface of tumor cells by MMPs. Binding of soluble ligand to NKG2D on effector cells can lead to the downregulation of NKG2D and an impairment of the immune response (Groh *et al.* 2002). A high level of soluble NKG2DL in the serum of cancer patients is therefore often associated with poor prognosis, including in hepatocellular carcinoma (HCC) (Easom *et al.* 2020), melanoma (Paschen *et al.* 2009) and pancreatic ductal adenocarcinoma (PDA) (Chen *et al.* 2015).

Recently, a role for NKG2DL-expressing immune cells, in particular myeloid cells, has been demonstrated. Macrophages can upregulate NKG2DL upon stimuli via TLR (Hamerman *et al.* 2004) or infection (Rausch *et al.* 2006), indicating that NKG2DL play an important role in

cross-talk between myeloid cells and lymphoid cells in a setting of infection. Additionally, it has been shown that MDSCs infiltrating tumors can express NKG2DL, leading to NKG2D-dependent lysis of ligand-expressing myeloid cells (Nausch *et al.* 2008). In addition to myeloid cells, NK cells have been shown to express NKG2DL in human peripheral blood. Specifically, ULBP2 was found on $CD57^+$ NK cells that had recently been activated or stimulated with IL-2, suggesting a particular role for NKG2DL on terminally differentiated NK cells (Brennan *et al.* 2016). Consequences of ligand engagement and the physiological function of NKG2DL expression on NK cells remains to be determined.

1.4.3 Anti-tumor function of NKG2D in the context of tumor immunity

The fact that NKG2DL are upregulated on a vast number of tumors indicates its importance in tumor surveillance (Ghadially *et al.* 2017). In fact, several studies have demonstrated the importance of NKG2D in tumor elimination *in vitro* and *in vivo*. Diefenbach *et al.* showed that NKG2DL-expressing cells are susceptible to NK cell-mediated killing *in vitro* (Diefenbach *et al.* 2000) and later demonstrated NKG2D-mediated rejection of ligand-expressing tumor cells *in vivo* (Diefenbach *et al.* 2001). In addition to NK cells, NKG2D-expressing $CD8^+$ T cells have been implicated in anti-tumor immunity. $CD8^+$ T cells that lack NKG2D were unable to mount a tumor-specific immune response against tumor cell lines *in vitro* and tumor transplant mouse models, suggesting that $CD8^+$ T cells contribute to NKG2D-mediated anti-tumor activity (Gilfillan *et al.* 2002). Further, engagement of NKG2D on $CD4^+$ T cells was shown to result in an increased proliferation of $CD4^+$ T cells secreting Fas ligand (FasL), resulting in enhanced tumor cell death *in vitro* (Groh *et al.* 2006). These observations for a crucial role of NKG2D in anti-tumor immunity was supported by studies of mouse models of malignancies, where NKG2D-deficient mice were shown to be more susceptible to cancer models, such as B cell lymphoma and prostate adenocarcinoma (Guerra *et al.* 2008).

These findings have fuelled research into harnessing NKG2D in cancer therapy and several approaches have been developed, with clinical testing underway. The most advanced therapy is CYAD-01 (also known as NKR-2) by Celyad Oncology, a therapy utilizing autologous chimeric

antigen receptor (CAR) T cells consisting of NKG2D fused with the human CD3ζ cytoplasmic signaling domain (Murad *et al.* 2018). Phase I clinical trials in acute myeloid leukemia (AML)-myelodysplastic syndrome (MDS) and multiple myeloma (MM) patients have been completed without raising safety concerns (clinical trial NCT02203825, Baumeister *et al.* 2018). A second trial assessing safety and clinical activity of a combination therapy of CYAD-01 and FOLFOX (leucovorin calcium (folinic acid), fluorouracil and oxaliplatin), a standard chemotherapy regimen, in metastatic colorectal cancer (mCRC) patients is currently running (clinical trial NCT03310008). In parallel, a therapy using allogeneic CAR T cells to treat mCRC patients will be conducted (clinical trial NCT03692429). Further, CYAD-02, a second-generation NKG2D-CAR T cell therapy, has been developed and clinical trials in AML-MDS patients have started (clinical trial NCT04167696). In addition to this, CytoMed Therapeutics Pte Ltd developed an approach using γδ CAR T cells expressing NKG2D and targeting NKG2DL in breast cancer, CRC, sarcoma, nasopharyngeal cancer, prostate cancer or gastric cancer (clinical trial NCT04107142).

A variety of other approaches have shown promising results in pre-clinical studies. One popular approach is the development of fusion proteins targeting the NKG2D/NKG2DL axis. Fusion proteins can be seen as a 'bridge' between the target and effector cells, with the idea being that one part binds to a protein highly expressed on target cells, while the other induces an immune response by activating effector cells. In the example of NKG2D-Fc fusion proteins, NKG2DL-expressing tumor cells bind to NKG2D, while the Fc region binds to CD16 on NK cells, where it induces antibody-dependent cellular cytotoxicity (ADCC), leading to target cell death (Raab *et al.* 2014, Steinbacher *et al.* 2014). A recent study suggests that in addition to targeting tumor cells, the NKG2D-Fc protein might induce cell death in NKG2DL-expressing tumor-promoting immune cells, such as MDSC and T_{reg} cells (Feng *et al.* 2020). Other approaches, such as fusion of NKG2D or NKG2DL with IL-2 or IL-12, is based on a similar principle in that the cytokine is delivered to a specific place where it has the potential to unleash anti-tumor activity (Kang *et al.* 2012, Tietje *et al.* 2017).

Efficacy of fusion proteins can be enhanced by combining the drug with nanoparticles that help specifically deliver the protein or the plasmid encoding the protein to the target site. Chitosin

nanoparticles are a promising drug-delivery system due to their enhanced permeability and retention in tumor tissue. Nanoparticles loaded with DNA encoding an NKG2D-IL-21 fusion protein have been shown to suppress tumor growth in a mouse model by increasing the frequency of tumor-infiltrating $CD8^+$ T cells and NK cells (Tan *et al.* 2017). However, changes in survival and tumor growth were subtle, questioning the efficacy and viability in human trials. A major drawback of these therapeutic approaches is that they rely on expression of NKG2D and/or NKG2DL in the tumor microenvironment. Tumors often evolve immune evasion strategies, resulting in an insufficient immune response and subsequent tumor growth.

Shedding of NKG2DL from the cell surface of cancer cells and secretion of soluble NKG2DL is one way in which tumors can escape NKG2D-mediated recognition. Due to the ability of soluble NKG2DL to downregulate NKG2D on the surface of effector cells and thereby inhibiting the immune response. To target NKG2DL shedding therapeutically, a neutralizing antibody against soluble MIC has been developed (Lu *et al.* 2015). In particular the combination with an IL-15 agonist (Basher *et al.* 2016) or PD-1/ PD-L1 blocking antibodies (Zhang *et al.* 2019, Basher *et al.* 2020) to ensure sufficient NK and T cell responses, respectively, has shown promising results in pre-clinical testing. Preventing shedding from the cell surface using a blocking antibody has the advantage that it does not only prevent ligand-induced downregulation of NKG2D, but at the same time increases the ability of NKG2D-expressing effector cells to recognize and eliminate tumor cells (Andrade *et al.* 2018, Wu *et al.* 2020).

Not only soluble NKG2DL can induce downregulation of NKG2D from the surface of effector cells. Indeed, sustained expression of NKG2DL has been shown to impair NK cell and $CD8^+$ T cell-mediated cancer surveillance (Oppenheim *et al.* 2005), suggesting that prolonged expression can ultimately favor tumor growth by impairing immune cell function.

Other immune evasion strategies include TGF-β-mediated downregulation of NKG2D and impairment of NK cell function. TGF-β, an immunosuppressive cytokine, is often highly expressed in the TME and associated with disease progression (Yang *et al.* 2010). TGF-β has been shown to downregulate NKG2D surface expression, thereby inhibiting NK and CTL cell-mediated anti-tumor responses (Castriconi *et al.* 2003, Friese *et al.* 2004). Further evidence suggests that not only NKG2D, but also NKG2DL expression is affected by TGF-β in the TME, further im-

pairing the NKG2D-mediated response (Eisele *et al.* 2006). Recent evidence suggests a level of plasticity between ILCs and NK cells and TGF-β has been implicated in driving conversion from anti-tumorigenic NK cells to pro-tumorigenic ILC1s (Gao *et al.* 2017). Additionally, TGF-β can inhibit ICI (Mariathasan *et al.* 2018), hence blocking antibodies in combination with ICI therapy are a promising approach to restore immune cell functionality (Bai *et al.* 2019). Another mechanism by which tumor cells can downregulate NKG2DL is via Poly [ADP-ribose] polymerase 1 (PARP1), which leads to loss of ligand expression on chemotherapy-resistant leukemic stem cells (LSC) in AML patients (Paczulla *et al.* 2019). Whether this is restricted to AML or can be translated to other cancers is yet to be determined, but pharmacologic inhibition of PARP1 has shown promising results in patient-derived xenotransplant models.
These studies not only underline the importance of the NKG2D/NKG2DL axis in tumorigenesis, but also demonstrate the great potential of harnessing the system for therapeutic approaches.

1.4.4 Aberrant expression of NKG2D or NKG2DL can drive autoimmunity

Aberrant expression of NKG2DL has not only been observed in tumorigenesis, but also in settings of autoinflammation and upregulation of NKG2DL and/or NKG2D has been shown to promote disease progression in a variety of autoimmune diseases (Table 1.2). Several cell types have been implicated in driving disease, yet exact mechanisms leading to the activation of these cells are not fully understood.
NKG2D-expressing $CD8^+$ T cells appear to be the autoreactive cells driving disease in a mouse model of diabetes (Ogasawara *et al.* 2004), the Experimental Autoimmune Encephalomyelitis (EAE) mouse model of Multiple Sclerosis (MS) (Legroux *et al.* 2019) and human Celiac Disease (CeD) (Meresse *et al.* 2004) (see section 1.4.6), while $CD4^+$ T cells have been shown to be involved in CD (Allez *et al.* 2007, see sections 1.2.1.3 and 1.4.6). Indeed, a recent study shows that NKG2D expression in $CD4^+$ T cells is a feature of antigen-experienced T_H1/T_H17 cells and that these can contribute to malignancies, such as arthritis and EAE (Babic *et al.* 2020), suggesting that both $CD8^+$ as well as $CD4^+$ T cells are involved in the pathogenesis of EAE. Further, the authors identify IL-12, T-bet and STAT4 as crucial mediators of inducing NKG2D

expression and show that both T-bet and STAT4 bind in close proximity to the *Klrk1* gene, suggesting direct regulation of gene expression. They show that strength of the TCR signal influences NKG2D expression and that NKG2D$^+$ T_H17 cells express higher frequencies of IFN-γ and GM-CSF, but not IL-17, indicating that NKG2D regulates type 1 responses specifically.
NKG2DL has been shown to be upregulated in sera and aortic plaques of patients with type 2 diabetes mellitus as well as aortas and livers in a mouse model of atherosclerosis, suggesting that NKG2D is involved in disease-promoting inflammation. Indeed, lack of NKG2D in *Klrk1*$^{-/-}$ mice resulted in abrogated disease severity, reduced production of IFN-γ by NK and NKT cells and IL-6 by monocytes. Further, cell numbers of NK cells, NKT cells and monocytes were significantly reduced in the absence of NKG2D, suggesting that expression of NKG2DL and engagement of NKG2D not only leads to cell activation, but also immune cell recruitment to the inflamed tissue in a direct or indirect manner (Xia *et al.* 2011). Interestingly, NKG2D-expressing NK cells have not been implicated in the setting of autoimmunity, except in the aforementioned atherosclerosis study and a mouse model of allergic pulmonary inflammation, in which GzB-producing NK cells contribute to pathogenesis (Farhadi *et al.* 2014).
To result in NKG2D-induced pathology, two things are required: NKG2DL, absent on healthy tissue except the intestinal epithelium, must be expressed and NKG2D-expressing cells must be recruited if not already present in the tissue. The studies discussed here underline that different cell types might be involved in different diseases, with exact mechanisms not yet fully understood.

1.4.5 NKG2D plays a dual role in tumorigenesis

A recent study by our group demonstrated that NKG2D can have a pro-tumorigenic role in a setting of chronic inflammation. In a model of HCC, a typical inflammation-driven cancer, mice lacking NKG2D survived longer and showed increased survival, associated with a lower tumor burden (Sheppard *et al.* 2017). In addition to decreased survival of NKG2D-sufficient mice, they displayed a much more severe inflammatory response, accompanied by an enrichment of CD8$^+$ T cells to liver and increased expression of pro-inflammatory cytokines, such as IL-6, TNF-α, IL-1β and IFN-γ, supporting the hypothesis that, in a setting of chronic inflam-

mation, NKG2D fosters rather than inhibits tumorigenesis. A pro-tumor role for NKG2D is in line with a previous study demonstrating the importance of NKG2D-mediated surveillance *in vivo*. In this initial study, Guerra and colleagues noted that in a mouse model of prostate cancer, the transgenic adenocarcinoma of the mouse prostate (TRAMP) model, NKG2D-deficient mice are more susceptible to early aggressive tumors, while late-arising tumors appear to be better controlled, but were unable to identify the cell types involved in the pro- and anti-tumor function (Guerra *et al.* 2008). Similarly, NKG2D-deficient mice were less susceptible to methylcholanthrene (MCA)-induced fibrosarcoma, a mouse model of inflammation-driven cancer (Swann *et al.* 2008). However, this phenotype was only observed when small doses (5 µg) were administered, while high doses (25 µg) resulted in no genotypic differences, suggesting a survival advantage of NKG2D-deficient mice only in slowly arising tumors (Guerra *et al.* 2008). Further, NKG2DL was highly expressed in both mouse models with no indication of downregulation and immunoediting, suggesting continuous activation of NKG2D-expressing effector cells (Table 1.2).

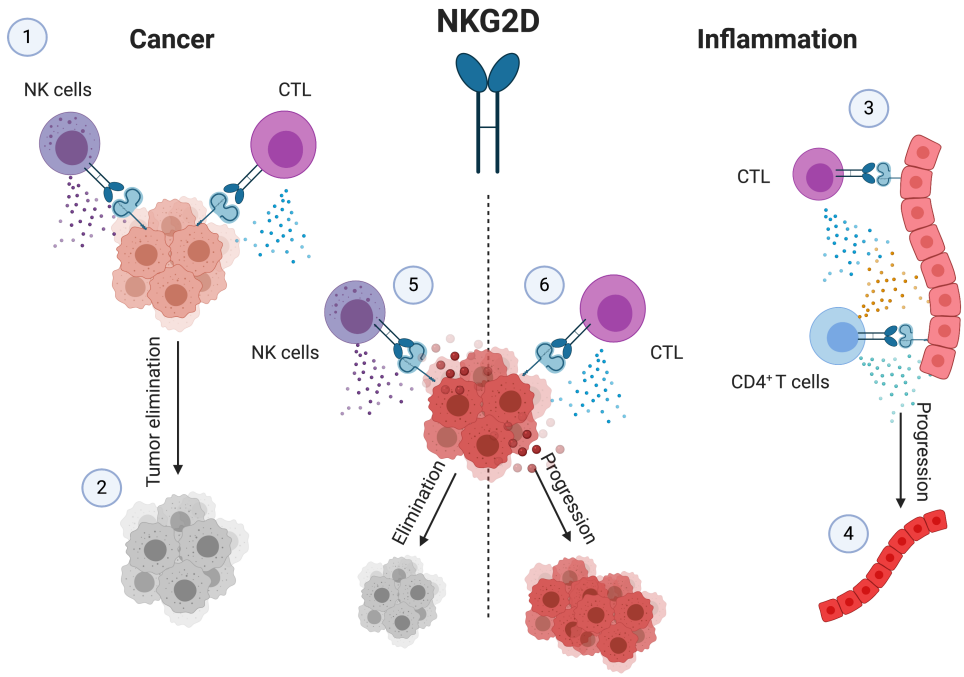

Figure 1.4: Function of NKG2D-expressing cells in cancer and autoinflammatory disorders. NKG2D is important in mediating anti-tumor activity (1+2). NKG2D-expressing NK cells and CTLs (1) mediate elimination of NKG2DL-expressing tumor cells (2) through the secretion of cytotoxic molecules, such as Granzyme B, perforin and cytokines, including IFN-γ. Aberrant NKG2DL expression is associated with autoimmunity and chronic inflammation (3+4). NKG2D-expressing CTLs and $CD4^+$ T cells (3) have been implicated in mediating inflammation through the secretion of pro-inflammatory cytokines, such as IL-17, IFN-γ and GM-CSF, leading to disease progression (4). NKG2D-expressing NK cells (5) can lead to the elimination of nascent tumor cells, whereas sustained expression of NKG2DL in inflammation-driven cancer is thought to constantly engage NKG2D-expressing CTLs, resulting in the sustained secretion of pro-inflammatory cytokines and disease progression (6). CTL = cytotoxic T cell. Image was created using BioRender.

Together, this demonstrates that the role of NKG2D in tumorigenesis is highly context-dependent and that NKG2D promotes slowly arising, inflammation-driven tumors. It further outlines the need to understand tissue environments in which NKG2D expression ultimately favors tumor growth.

Table 1.2: Table summarizing function NKG2D in human diseases and mouse models.

Disease/ Model	Organism	NKG2DL	Cell types	Cytokines	Function	Reference
Transplanted tumors	Mouse	Expressed	$CD8^+$ / $CD4^+$ T cells NK cells	FasL, IFN-γand cytotoxic molecules	Protective	Diefenbach *et al.* 2000 Diefenbach *et al.* 2001 Gilfillan *et al.* 2002 Groh *et al.* 2006
B cell lymphoma (Eμ-Myc model)	Mouse	Upregulated (RAE-1 and MULT1)	Unclear	Unclear	Protective	Guerra *et al.* 2008
Prostate cancer (TRAMP model)	Mouse	Upregulated (RAE-1 and MULT1)	Unclear	Unclear	Protective (early stages)	Guerra *et al.* 2008
Fibrosarcoma (MCA model)	Mouse	Unclear	Unclear	Unclear	Promoting (slowly arising tumors)	Guerra *et al.* 2008
Diabetes (NOD model)	Mouse	Upregulated (RAE-1)	$CD8^+$ T cells	Unclear	Promoting	Ogasawara *et al.* 2004
Diabetes	Human	Upregulated (MICA)	Unclear	Unclear	Promoting	Xia *et al.* 2011
Celiac Disease	Human	Upregulated (MIC/A)	$CD8^+$ / $CD4^+$ T cells	Cytotoxic molecules	Promoting	Meresse *et al.* 2004 Abadie *et al.* 2020
Crohn's Disease	Human	Upregulated (MICA)	$CD4^+$ T cells	IFN-γ, Granzyme B and IL-17	Promoting	Allez *et al.* 2007 Pariente *et al.* 2011
Multiple Sclerosis (EAE model)	Mouse	Upregulated (MULT1)	$CD8^+$ / $CD4^+$ T cells	IFN-γ and IL-17	Promoting	Legroux *et al.* 2019 Babic *et al.* 2020 Guerra *et al.* 2013
Artherosclerosis	Mouse	Upregulated (RAE-1 and H60)	NK and NKT cells	IFN-γ	Promoting	Xia *et al.* 2011
Allergic pulmonary inflammation	Mouse	Upregulated (RAE-1 and MULT1)	NK cells	Granzyme B	Promoting	Farhadi *et al.* 2014
Hepatocellular carcinoma (DEN model)	Mouse	Upregulated (RAE-1)	$CD8^+$ T cells	IFN-γ	Promoting	Sheppard *et al.* 2017

1.4.6 NKG2D/NKG2DL is implicated in intestinal health and disease

NKG2DL are typically absent from healthy tissue, except for MICA, which has been detected on healthy intestinal epithelium (Groh *et al.* 1996). A regulatory role for the NKG2D/NKG2DL axis in the context of intestinal homeostasis has been confirmed by studies showing that upregulation of NKG2DL is associated with NKG2D-mediated intestinal pathology.

One of the first studies ascribing a pathological to NKG2D in intestinal disease dates back to 2004, where Meresse and colleagues demonstrated that NKG2D is involved in CeD pathology. They showed an increased frequency of NKG2D$^+$ IELs as well as increased expression of the NKG2DL MICA/B on intestinal tissue, suggesting direct killing of ligand-expressing epithelial cells (Meresse *et al.* 2004). The authors hypothesized that sustained exposure to IL-15 reprograms CD8$^+$ T cells into Lymphokine-activated killer cell (LAK) cells with cytotoxic activity, leading to epithelial cell death and subsequent inflammation. Recently, the same group described a mouse model of CeD to further study the mechanisms involved in pathology. They showed that NKG2D$^+$CD8$^+$ T cells are increased in mice receiving a gluten-containing diet and that the frequency of NKG2D$^+$CD8$^+$ T cells is strongly correlated with disease severity, measured as crypt length (Abadie *et al.* 2020). Interestingly, both the increase in NKG2D-expressing IELs, as well as the upregulation of the NKG2DL RAE-1 on epithelial cells appeared to be CD4-dependent, as depletion of CD4$^+$ T cells reversed this phenotype. This study confirms that the mechanisms involved in NKG2D-mediated disease are likely more complicated than previously thought and that more research is needed to understand the crosstalk between CD4$^+$ T_H cells and NKG2D-expressing IELs.

Similar to CeD, NKG2D appears to be involved in the inflammatory processes in CD patients. As described in section 1.2.1.3, Allez *et al.* proposed several mechanisms in which NKG2D$^+$ T cells can contribute to pathology, including the disease-promoting secretion of IFN-γ, GzB, IL-17 and IL-22 (Allez *et al.* 2007, Pariente *et al.* 2011). However, as opposed to CeD, where CD8$^+$ IELs appear to be the main drivers of disease, CD4$^+$ are the subtype of T cells proposed to drive CD. Indeed, blocking of NKG2D in a mouse model of colitis prevents IFN-γ secretion

by $CD4^+$ T cells and ameliorates pathology (Ito *et al.* 2007). These studies have fuelled research into targeting NKG2D therapeutically and have led to the development of anti-NKG2D monoclonal antibodies, which are currently being tested in the clinic (Allez *et al.* 2016).

Mechanisms leading to the upregulation of NKG2DL in the setting of human and mouse gut inflammation are not fully understood, but a number of stress-related pathways can lead to the upregulation of NKG2DL on intestinal epithelial cells, including endoplasmic reticulum (ER) stress (Hosomi *et al.* 2017) and heat shock (Groh *et al.* 1998). Additionally, the microbiota has been implicated in regulating NKG2DL expression (Hansen *et al.* 2013), making a microbiota-related mechanism possible. Additionally, it has been shown that binding of *E. coli* leads to the upregulation of MICA on epithelial cells and triggers IFN-γrelease by NK cells (Tieng *et al.* 2002). Indeed, NKG2D has been shown to contribute to the clearance of bacteria in the context of pulmonary (Borchers *et al.* 2006) and intestinal (Li *et al.* 2011) infection. However, many of these studies rely on *in vitro* systems and whether or not these processes are involved *in vivo* remains to be determined.

Less data is available on the role of NKG2D in CRC. Phenotypic analysis of tumor-infiltrating T cells revealed an increased frequency of NKG2D-expressing $CD4^+$, but not $CD8^+$ T cells. In fact, frequencies of NKG2D-expressing $CD8^+$ T cells are reduced compared to healthy control tissue, which the authors attributed to cell activation (Chirica *et al.* 2015). Indeed, they showed that activation through CD3 and NKG2D *in vitro* leads to cell degranulation and downregulation of NKG2D. However, what functional consequences this has *in vivo*, what stimuli induce the increased frequency of NKG2D-expressing $CD4^+$ T cells and whether or not patient survival is influenced by the activation of NKG2D-expressing cells remains to be determined.

Several other studies have tried to investigate the function of NKG2D in CRC, but have relied on serum samples or transcriptional analysis only, offering limited insight on the function of NKG2D-expressing cells within the tissue. Two independent studies showed reduced frequencies of NKG2D-expressing NK cells in peripheral blood of CRC patients (Shen *et al.* 2011, Gharagozloo *et al.* 2015). The later study further compared NKG2D expression between metastatic and non-metastatic disease and showed that disease severity is associated with a further decrease of NKG2D expression. Contrary to this, a more recent study demonstrated increased levels of

NKG2D in CRC. However, rather than measuring protein levels on immune cells infiltrating the tumor, the authors performed transcriptional analysis on peripheral blood (Meckawy *et al.* 2019). Further, performing analysis on bulk peripheral blood mononuclear cell (PBMC)s possibly dilutes out cell-specific changes.

An extensive study measuring expression of six different NKG2DL in tissue from CRC patients revealed improved survival of patients expressing high levels of MIC and RAET1G (ULBP5) on tumors sections (McGilvray *et al.* 2009). All ligands were expressed at high levels and, with the exception of ULBP2, were decreased in advanced disease stages. Interestingly, ULBP2 was the only ligand with a hazard ratio above 1, highlighting a distinct role for ULBP2.

In a separate study, levels of soluble NKG2DL in the sera of CRC patients was measured and shown to be increased from a baseline of 0.8 ng/ml in healthy individuals to 5.5 ng/ml in CRC patients, suggesting that ligand is indeed shed from the surface of colorectal tumors (Salih *et al.* 2002). These studies reveal that the NKG2D/NKG2DL system indeed plays a role in CRC, but demonstrate that evidence is limited and that mechanisms involving NKG2D-mediated immune responses *in vivo* are not fully understood.

Nonetheless, NKG2D has been the subject of therapeutic approaches. As discussed in section 1.4.3, NKG2D is a receptor of interest in the development of CAR T cells. Indeed, several studies have investigated the possibility of using NKG2D CAR T cells against CRC. Testing of NKG2D CAR T cells *in vitro* showed antitumor activity against NKG2DL-expressing cells and rejection of a xenograft model of a human CRC cell line (Deng *et al.* 2019). A second study showed similar results using a slightly different construct (Li *et al.* 2020). While these studies demonstrate that NKG2D CAR T cells are indeed capable of killing NKG2DL-expressing tumor cells, the complex cellular environment is not modeled in the immunodeficient mice used in these studies. Further, cell lines which express high levels of NKG2DL were used, not necessarily reflecting the expression pattern of NKG2DL in patients. Yet, these studies provide evidence not only for the ability to kill tumor cells, but more importantly the potential to infiltrate solid tumors.

In addition to the clinical trials on Celyad's CYAD-01 (see section 1.4.3), studies on human patients were performed at a hospital in China. Rather than using T cells, NKG2D CAR NK

cells were developed and three CRC patients with malignant ascites or liver metastasis were treated (Xiao *et al.* 2019). All three patients showed tumor regression to some extent, but eventually died of the disease. Nonetheless, these results are promising in that they show a direct effect on metastatic colon cancer.

These studies demonstrate a highly complex and context-dependent role for NKG2D. Due to its ability to recognize aberrant cells and induce a strong immune response, it has a crucial role in tumor recognition and elimination. Simultaneously, these features can, when not controlled appropriately, lead to detrimental responses in the context of autoimmunity, chronic inflammation and inflammation-driven cancer.

1.5 Gaps in current knowledge

A dual role for NKG2D has been established and the role of the NKG2D/ NKG2DL axis has been studied in a number of disorders and maladies. Yet, many questions remain:

1. *What is the role of the NKG2D/ NKG2DL axis in the intestine of healthy individuals?*
   Studies showed constitutive expression of NKG2DL on healthy intestinal epithelium as well as presence of NKG2D-expressing immune cells in the lamina propria. What exactly is the role of these cells? Why does the presence of NKG2D and NKG2DL-expressing cells in the intestine not induce an inflammatory response under steady-state conditions? What induces NKG2DL expression in the intestine?

2. *Are mice an appropriate model organism to study the function of NKG2D in the intestine?*
   A few studies have demonstrated a pro-inflammatory role for NKG2D in the mouse intestine, yet the expression pattern of NKG2D and its ligand and the question of whether NKG2DL is constitutively expressed has not been studied in detail. This is of importance in determining whether studies performed in mice are translatable to human disease, in particular due to the differences in NKG2D signalling between humans and mice.

3. *Which cell types are involved in the disease-promoting function of NKG2D?*
   Evidence suggests that while NK cells and $CD8^+$ T cells are involved in NKG2D-mediated elimination of tumor cells, $CD4^+$ and/or $CD8^+$ T cells are the main drivers of autoinflammation. Yet, several of the studies mentioned here are merely observational. Further, due to the recent discovery of ILCs and evidence for their ability to express NKG2D, it is not unlikely that they are involved in inflammatory responses, but have not yet been identified as disease drivers.

4. *What leads to aberrant NKG2DL expression in the context of autoimmunity?*
   Several autoimmune disorders have been shown to be associated with NKG2DL expression. It is not well understood what mechanisms are involved in the upregulation of NKG2DL in the context of autoimmunity. Does inflammation lead to the upregulation

of NKG2DL or does the upregulation of NKG2DL due to unknown mechanisms lead to inflammation?

5. *What tissue environments favor a pro-tumorigenic role for NKG2D?*

   A dual role for NKG2D in the context of cancer immunity has been unraveled by our lab. However, the question of which immune environments favor the pro-tumorigenic role of NKG2D remains to be determined. It is unclear whether NKG2D exerts anti-tumor functions at early disease stages and what stimuli are required to favor the pro-tumorigenic function.

1.6 Aims and objectives of this thesis

The focus of this PhD was to investigate NKG2D in intestinal disease. For this, several mouse models of intestinal tumorigenesis and inflammation were used. The main aims and objectives include:

1. To characterize the expression pattern of NKG2D and NKG2DL in the mouse intestine. (Chapter 1)

2. To immunophenotype the intestinal immune system of NKG2D-deficient mice. (Chapter 1)

3. To investigate the mechanisms involved in NKG2D-mediated intestinal tumorigenesis. (Chapter 2)

4. To investigate the function of NKG2D in a sterile model of colitis. (Chapter 3)

5. To establish and characterize the role of NKG2D in an infection-induced model of colitis. (Chapter 3)

Methods

2.1 Code availability

Software written and/or adapted from open source software is available on: https://github.com/sophiecurio/phd.

2.2 Mouse models

2.2.1 Mice

Mice were bred and maintained in the animal facility at Imperial College London in a specific pathogen-free environment. Work was carried out in compliance with the British Home Office Animals Scientific Procedures Act 1986 (PPL 70/8606).

2.2.2 *Apc*$^{min/+}$ model

NKG2D-sufficient (*Klrk1*$^{+/+}$) and -deficient (*Klrk1*$^{-/-}$) mice (Guerra *et al.* 2008) were intercrossed with *Apc*$^{min/+}$ mice (purchased from Jackson) to generate *Klrk1*$^{+/+}$ *Apc*$^{min/+}$, *Klrk1*$^{-/-}$ *Apc*$^{min/+}$, *Klrk1*$^{+/+}$ *Apc*$^{+/+}$ and *Klrk1*$^{-/-}$ *Apc*$^{+/+}$ mice. The health status of *Apc*$^{min/+}$ mice was checked and evaluated frequently. Disease severity was assessed using a scoring scheme that included parameters such as appearance, natural behavior, provoked behavior, body condition and tumor score. Mice were humanely culled once they reached endpoint.

2.2.3 DSS model of colitis

Mice were treated with 2% DSS (MP Biomedicals, colitis grade) (w/v) in drinking water for 7 days. On day 7, water was changed to regular drinking water. Weight loss was monitored closely, and mice were sacrificed on day 10 for the short-term experiments. To induce chronic inflammation, DSS was administered for 7 days, followed by 7 days of drinking water. This was repeated three times and mice were sacrificed on day 38.

2.2.4 *Citrobacter rodentium* model of colitis

C. rodentium (Strain ICC169, provided by Gad Frankel) was grown overnight from a frozen microbank bead in 15 ml of LB containing nalidixic axis. The culture was centrifuged and resuspended in 1.5 ml sterile phosphate buffered saline (PBS) to achieve a 10x concentrated suspension (approximately $1x10^9$ colony-forming units (CFU)). Mice were inoculated with 200 µl by oral gavage. The number of inoculated bacteria was determined by plating on LB agar containing nalidixic acid and counting CFUs. Mice were weighed, and stool was collected regularly. The number of viable bacteria per gram of stool was determined by plating on LB agar and culturing aerobically at 37°C overnight. On the specified day, mice were sacrificed and the number of viable bacteria in stool, colonic tissue and, if applicable, cecum, liver and spleen, was determined by plating on LB agar. The remaining colonic tissue was used for lamina propria cell isolation and flow cytometric analyses.

Experiments involving a bioluminescent strain of *C. rodentium* (ICC180) were performed by Eve Hopkins and Izabela Glegola-Madejska. Mice were infected following the same procedure as with strain ICC169. Prior to imaging, mice were shaved to expose the abdominal skin and anesthetized using 3% (v/v) isoflurane. Images were acquired using the IVIS SpectrumCT (PerkinElmer) and the Living Image software. Anesthetized mice were removed from the imaging chamber, returned to their cages and monitored frequently for adverse events.

2.2.5 Antibody treatment

To block NKG2D *in vivo*, 200 µg of HMG2D or hamster IgG (BioXCell) was administered intraperitoneal (i.p.) -2, +1, +3 and +5 days post inoculation with *C. rodentium*.

2.2.6 Genotyping

2.2.6.1 DNA extraction

Ear notches were taken from mice aged 10 days or older for identification and genotyping. Tissue was stored at 4°C until extraction. 100 µl lysis buffer (see 2.1) and 2 µl Proteinase K (stock: 25 mg/ml, Sigma-Aldrich) was added to each tube containing the ear notch sample and incubated at 55°C for 2 hours. After incubation, 30 µl of 5M sodium chloride (NaCl) was added to each tube and vortexed for 30 seconds. Samples were centrifuged at 4°C at 14000 x g for 5 minutes before 80 µl of the supernatant was transferred to a fresh tube. 100 µl of cold 100% ethanol was added and liquids were mixed by inverting the tubes. After a 20 minutes incubation at -20°C, tubes were centrifuged (4°C, 14000 x g, 5 minutes), supernatant discarded and 100 µl of 70% ethanol was added. After another centrifugation (4°C, 14000 x g, 5 minutes), supernatant was discarded and tubes left to dry for 10 minutes to allow the ethanol to evaporate. 50 µl of Tris-EDTA (TE) buffer was added and tubes were incubated at 55°C for 20 minutes to allow re-suspension of DNA. 100 µl of water was added to dilute the DNA. Samples were stored at -20°C.

Table 2.1: Lysis buffer

Reagents	**Volume (ml)**
Water	332
Tris, pH = 8.5 (stock: 1M)	40
EDTA, pH = 8 (stock: 0.5M)	4
NaCl, pH = 8 (stock: 5M)	16
SDS (10%)	8

2.2.6.2 PCR

Polymerase chain reaction (PCR) reactions were prepared using GoTaq Hot Start Polymerase (stock 5 U/µl, Promega), deoxynucleoside triphosphates (dNTP)s (stock 10 mM, Promega), 5X Green GoTaq Reaction Buffer (Promega) and primers (see 2.2, stock 10 µM, Invitrogen) according to Table 2.3. PCR programs were run according to Tables 2.4 and 2.5.

Table 2.2: Primers for genotypic PCRs

Target	Name	Sequence 5' to 3'
Klrk1	L1	CAAGTAGTGTGCATTTCATTCAG
	P3	ATTGCTCCCTGTCTCATTGTCTT
	WT3	CAGAGCAAGCTTCCTGTTTGTCTCA
Apc	WT	TTCCACTTTGGCATAAGGC
	Common	GCCATCCCTTCACGTTAG
	KO	TTCTGAGAAAGACAGAAGTTA

Table 2.3: PCR reaction setup

Reagent	Volume (µl)
GoTaq Hot Start Polymerase	0.1
dNTPs	0.4
5X Green GoTaq Reaction Buffer	4
Primer	0.2 (each)
Water	10.3

Table 2.4: PCR program for *Klrk1*

Time	Temperature (°C)	
4 minutes	94	
50 s	94	x 40
80 s	56	
90 s	72	
7 minutes	72	

Table 2.5: PCR program for *Apc*

Time	Temperature (°C)	
4 minutes	94	
50 s	94	x 36
80 s	47	
90 s	72	
7 minutes	72	

2.2.6.3 Agarose gel

A 100 ml 2% (w/v) agarose gel containing 5 µl of SYBR Safe DNA Gel Stain (ThermoFisher) was prepared prior to the gel electrophoresis and left to dry for at least 30 minutes. Before loading the gel, it was transferred to the electrophoresis station. 15 µl of PCR product was transferred to each well and electrophoresis was performed at 70 V for 40 minutes. The gel was transferred to the EC3 Imaging System (UVP), where an image using the SYBR Green filter was acquired.

2.3 Cell isolation

2.3.1 Isolation of tumor cells

Small intestine and colon were removed from the mouse abdomen. The cecum was removed, and the small intestine was separated into duodenum, jejunum and ileum. Remaining fat as well as the gut content was removed from the intestine. The intestine was flushed with PBS and cut open avoiding cutting through tumors. Mucus was removed by carefully scraping it off using blunt tweezers, and tumors were counted before they were removed from the intestinal tissue and minced using a scalpel. Tissue was transferred to a 1.5 ml tube and 1 ml of RPMI containing 5% fetal calf serum (FCS), 25 mM 4-(2-hydroxyethyl)-1-piperazineethanesulfonic acid (HEPES), 150 U/ml collagenase IV (Sigma Aldrich) and 50 U/ml DNase (Roche) was added. Tubes were shaken in a horizontal position on an incubator shaker (37°C, 200 revolutions per minute (rpm), 30 minutes). Tissue and liquid was transferred to a 50 ml tube through a 100 µm cell strainer. To further dissociate the tissue, it was pushed through the filter using the plunger of a 2 ml syringe. To inhibit enzyme activity, 1 ml of PBS containing 10% FCS and 5 mM EDTA was added to the 1.5 ml tube and transferred to the 50 ml tube. Cells were centrifuged for 10 minutes at 500 x g and resuspended in medium.

2.3.2 Isolation of intraepithelial and lamina propria lymphocytes

Intestines were removed and washed as previously described (see section 2.3.1). The tissue was cut into small pieces and transferred to a 15 ml tube containing 10 ml of solution #1 (see Table 2.6). Tubes were vortexed for 30 s and solution #1 was replaced. Tubes were shaken in a horizontal position on an incubator shaker (37°C, 200 rpm, 20 minutes), which resulted in the removal of the mucus layer. Using a 100 µm cell strainer, the tissue was transferred to a new 15 ml tube containing 10 ml of solution #2. It was again shaken in a horizontal position (37°C, 200 rpm, 15 minutes), before it was filtered through a 100 µm strainer. The liquid, containing IEL, was taken up and stored at 4°C, and the tissue transferred back to the 15 ml tube and 10 ml of fresh solution was added. This step was repeated two or three times for large and small intestine, respectively, and resulted in the removal of all epithelial cells. The tissue was transferred to a 6 well plate and minced into small pieces using a pair of scissors. 7 ml of solution #3 containing 100 U/ml collagenase VIII (Sigma Aldrich) and 50 U/ml DNase (Roche) was added to each well. Tissue was incubated on an orbital shaker at 100 rpm for 45 minutes at 37°C. To dissociate the cells further, the tissue was mixed every 15 minutes using tweezers. The digested tissue was taken up into 10 ml stripettes and filtered through 100 µm cell filters into 50 ml tubes. This resulted in a single cell suspension, which was centrifuged for 10 minutes at 500 x g and resuspended in medium.

2.3.3 Isolation of cells from mesenteric lymph nodes and Peyer's patches

MLNs or PPs were minced through a 100 µm cell strainer into the well of a 6 well plate containing 7 ml medium. The suspension was taken up and transferred into a Falcon tube. The well was washed with an additional 7 ml medium and cells were stored on ice until further processing.

Table 2.6: Solutions for intestinal digestions

Solution	Content
#1	1 mM DTT (Sigma Aldrich) 2% FCS 100 U/ml Pencillin (Sigma Aldrich) 100 µg/ml Streptomycin (Sigma Aldrich) HBSS (Lonza)
#2	1 mM EDTA 2% FCS 100 U/ml Pencillin 100 µg/ml Streptomycin HBSS
#3	5% FCS RPMI

2.4 Flow cytometry

2.4.1 Antibody staining

Prior to antibody staining, cells were stimulated with Phorbol 12-myristate 13-acetate (PMA) (final concentration 600 ng/ml), ionomycin (final concentration 100 ng/ml) and Brefeldin A (final concentration, 10 µg/ml) for 4 hours at 37°C to enhance cytokine production (if applicable). Unspecific binding by the Fc receptor was prevented by incubation of anti-mouse CD16/CD32 (BD) for 20 minutes. Dead cells were stained using the LIVE/DEAD Fixable Aqua Dead Cell Stain kit (Thermofisher, dilution 1:400) or Zombie UV Fixable Viability Kit (BioLegend, dilution 1:400), before extracellular antibodies were added and incubated for 30 minutes. Before staining of intracellular cytokines and transcription factors (if applicable), cells were permeabilized, using the Transcription Factor Fixation/Permeabilization kit according to manufacturer's recommendations (eBioscience). Intracellular antibodies were added and incubated for 30 minutes, before cells were washed and transferred to 1.2 ml cluster tubes (Sigma-Aldrich) through a filter mesh.

2.4.2 Sample acquisition

Samples were acquired on a BD LSRFortessa using FACSDiva or a Cytek Aurora using SpectroFlo. Prior to sample acquisition, single-stained compensation beads as well as unstained controls were run and auto-compensation (LSRFortessa) or unmixing (Aurora) was performed. If required, fluorescence minus one (FMO) controls were included in the experiment.

2.4.3 Antibodies

Table 2.7: Antibodies used in this study

Antigen	Clone	Fluorophore	Company	Stock (mg/ml)	Dilution
B220	PE-Cy7	RA3-6B2	BioLegend	0.2	1:200
B220	BV785	RA3-6B2	BioLegend	0.2	1:200
CD107a	PerCp-eFluor 710	1D4B	eBioscience	0.2	1:50
CD11b	PE-CF594	M1/70	BD	0.2	1:100
CD11b	PerCp-Cy5.5	M1/70	eBioscience	0.2	1:150
CD11c	PE	N418	eBioscience	0.2	1:200
CD11c	BV605	N418	BioLegend	0.2	1:200
CD127	BV711	SB/199	BD	0.2	1:100
CD127	FITC	A7R33	Thermofisher	0.5	1:100
CD19	PE-CF594	ID3	BD	0.2	1:200
CD19	BV650	6D5	BioLegend	0.5	1:400
CD200R	VioBright515	REA850	Miltenyi	0.15	1:100
CD206	AF647	C068C2	BioLegend	0.5	1:100
CD206	PerCp-Cy5.5	C068C2	BioLegend	0.2	1:100
CD27	PE	LG.3A11	BioLegend	0.2	1:100
CD3	V450	17A2	BD	0.2	1:100
CD3	PE-CF594	145-2C11	BD	0.2	1:100
CD3	BUV737	145-2C11	BD	0.2	1:200
CD4	APC-eFluor780	RM4-5	eBioscience	0.2	1:200
CD4	BV711	RM4-5	BioLegend	0.2	1:400
CD4	BUV496	GK1.5	BD	0.2	1:200
CD45	FITC	30-F11	BioLegend	0.5	1:400
CD45	AF700	30-F11	BioLegend	0.5	1:1000
CD8α	PerCp-Cy5.5	53-6.7	BioLegend	0.2	1:400
CD8α	BV785	53-6.7	BioLegend	0.2	1:400

CD8α	BUV395	53-6.7	BD	0.2	1:400
DNAM1	PE	10E5	BioLegend	0.2	1:100
F4/80	PE	BM8	eBioscience	0.2	1:50
F4/80	PE-Cy7	BM8	BioLegend	0.2	1:100
F4/80	BV785	BM8	BioLegend	0.2	1:100
F4/80	BV421	BM8	BioLegend	0.2	1:100
Foxp3	APC	FJK-16	eBioscience	0.2	1:50
γδTCR	PerCP-eFluor 710	GL3	eBioscience	0.2	1:100
γδTCR	APC	GL3	eBioscience	0.2	1:100
γδTCR	BV421	GL3	BD	0.2	1:200
γδTCR	PE-Cy5	GL3	eBioscience	0.2	1:400
γδTCR	biotin	GL3	BioLegend	0.5	1:00
Gr-1	APC-Cy7	RB6-8C5	BioLegend	0.2	1:100
Granzyme B	e450	NGZB	eBioscience	0.2	1:50
Granzyme B	AF647	GB-11	BD	0.2	1:50
IFN-γ	PE	XMG1.2	eBioscience	0.5	1:100
IFN-γ	BV421	XMG1.2	eBioscience	0.5	1:50
IFN-γ	e450	XMG1.2	eBioscience	0.2	1:50
IL-17	PE-Cy7	TC11-18H10.1	BioLegend	0.2	1:50
IL-22	PE	1H8PWSR	eBioscience	0.2	1:50
IL-6	APC	MP5-20F3	BioLegend	0.2	1:100
Ki67	eFluor450	SolA15	eBioscience	0.2	1:100
Lineage	AF700			BioLegend	1:100
Ly6C	biotin	HK1.4	BioLegend	0.5	1:100
Ly6C	BV605	HK1.4	BioLegend	0.5	1:2000
Ly6G	APC-Cy7	1A8	BioLegend	0.2	1:100
Ly6G	BUV661	1A8	BD	0.2	1:400
MHC-II	APC-e780	M5/114.15.2	eBioscience	0.2	1:400
NK1.1	PE-Cy7	PK136	BioLegend	0.2	1:200

NK1.1	AF488	PK136	BioLegend	0.5	1:200
NK1.1	BUV395	PK136	BD	0.2	1:100
NK1.1	BV650	PK136	BioLegend	0.2	1:200
NKG2D	APC	CX5	eBioscience	0.2	1:100
NKG2D	biotin	A10	eBioscience	0.5	1:100
NKG2D	PE	CX5	eBioscience	0.2	1:100
NKp46	FITC	29A1.4	eBioscience	0.5	1:100
PD-1	BV650	J43	BD	0.2	1:100
PD-1	PerCP-eFluor 710	J43	eBioscience	0.2	1:200
RAE1	APC	REA723	Miltenyi	0.15	1:100
RAE1	APC	AF1136	R&D	0.2	1:100
RORγt	PE	AFKJS-9	eBioscience	0.2	1:50
RORγt	PE eFluor610	B2D	eBioscience	0.2	1:100
T-bet	BV711	4B10	BioLegend	0.2	1:50
TNF-α	PE	MP6-XT22	eBioscience	0.2	1:50
TNF-α	PerCP-eFluor 710	MP6-XT22	eBioscience	0.2	1:50
TNF-α	APC-Cy7	MP6-XT22	BioLegend	0.2	1:50

2.4.4 Analysis

Flow cytometry analysis was performed using FlowJo Version 9 or 10 (BD). Following auto-compensation on the flow cytometer, compensation parameters were manually checked in FlowJo. Gating was performed visually or on FMO controls. T-distributed stochastic neighbor embedding (tSNE) plots were created using FlowJo. Downstream analysis, including statistical analysis and data visualization was performed using Python scripts (Folder ‘Flow cytometry’).

2.5 Immunohistochemical analysis

2.5.1 Sample preparation

Swiss rolls of intestines were prepared according to published protocols (Bialkowska *et al.* 2016). Tissue was fixed in 10% formalin overnight and then transferred to 70% (v/v) ethanol where it was kept until paraffin embedding (performed by the Research Histology Facility at the Department of Medicine, Imperial College London). Paraffin blocks were cut into 4 µm sections using a microtome (Leica), placed in a 40°C water bath and affixed onto Superfrost Plus Microscope Slides (Thermo Scientific). Prior to staining, slides were deparaffinized and rehydrated.

2.5.2 Immunohistochemical staining

After heat-induced epitope retrieval (HIER), several blocking steps were performed to prevent nonspecific binding. Primary antibody (Anti-murine Rae1 Pan specific antibody, R&D Systems) or appropriate isotype control (Polyclonal goat isotype IgG, NEB) was added at a final concentration of 10 µg/ml and incubated overnight. After several washing steps, the secondary antibody (10 µg/ml of Rabbit anti-goat, Vectorlabs) was added and incubated for 30 minutes. The antigen was revealed using ABC (Vectorlabs) and DAB reagents (Abcam). Slides were counterstained by immersion in Harris Haematoxylin and dehydrated, before coverslips were mounted using HistoMount mounting media (ThermoFisher).

2.5.3 Hematoxylin and eosin stains

After deparaffination and dehydration, slides were immersed in Harris Haematoxylin (Sigma-Aldrich) for 4 minutes. Differentiation was achieved by briefly immersing the slides in 1% acid alcohol. Slides were then places in 1% Eosin (Sigma-Aldrich) for one minute. The sections were dehydrated using an increasing series of ethanol solution, before a final wash in xylene (x3) and mounting on coverslips.

2.5.4 Image acquisition and analysis

Slides were scanned using a Slide Scanner Axio Scan.Z1 (Zeiss). For image analysis of IHC-stained slides, tumors and surrounding tissue were identified and marked using Fiji. Percentage of positivity was determined using a Fiji macro (Folder 'IHC') by comparing stained samples to isotype controls. Analysis of H&E stained slides was based on previously published guidelines (Erben *et al.* 2014) and streamlined by B.Sc. student Alexander Steemers. A scoring system was established to evaluate the severity of inflammation in the tissue (Table 2.8). Crypt length was determined by measuring an average of 20 crypts per sample using Fiji (Figure 2.1a). Goblet cells were counted in four areas of each sample (Figure 2.1b).

Table 2.8: Histomorphological scoring system of H&E stained intestinal tissue sections

Category	Definition	Score
Cell infiltration	Muscularis mucosa	1
	Muscularis mucosa and submucosa	2
Crypt elongation	Minimal (<25%)	1
	Mild (25-35%)	2
	Moderate (36-50%)	3
	Marked (>50%)	4
Goblet cell loss	Minimal (<25%)	1
	Mild (25-35%)	2
	Moderate (36-50%)	3
	Marked (>50%)	4

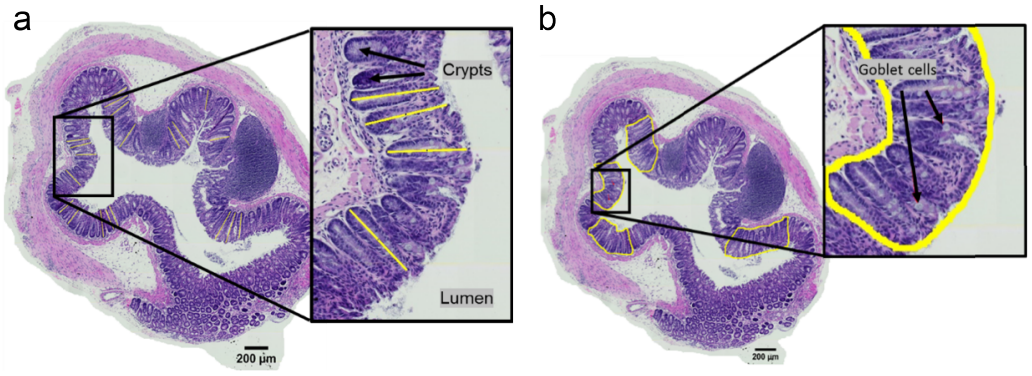

Figure 2.1: Exemplary histomorphological analysis of H&E stained intestinal tissue sections (a) Representative example of crypt length measurement in the colon of mice infected with *C. rodentium*. (b) Representative example of Goblet cell quantification in the colon of mice infected with *C. rodentium*. Image acquired using Slide Scanner Axio Scan.Z1 (Zeiss) at 10x magnification. Scale bar = 200 µm. Image created by Alexander Steemers.

2.6 Gene expression analysis

2.6.1 RNA extraction and cDNA preparation

Tumor and surrounding intestinal tissue was collected from freshly harvested tissue and stored in RNAlater (Invitrogen) until extraction. RNA was extracted from tissue using the RNeasy Plus Mini Kit (Qiagen). Reverse transcription was performed using the High Capacity cDNA Reverse Transcription Kit (Thermo Fisher) with an input of 1750 ng RNA.

2.6.2 Preamplification

cDNA was preamplified using the TaqMan PreAmp Master Mix (Thermo Fisher) and a total of 48 selected TaqMan probes (Thermo Fisher, Table 2.12). Preamplification was performed according to manufacturer's recommendations with a pre-dilution of cDNA of 1:5, 14 cycles and half the recommended volume.

2.6.3 qPCR using TaqMan or SYBR Green

2.6.3.1 TaqMan

The reaction was prepared at half the recommended volume, resulting in a total volume of 10 µl per reaction (Table 2.9). Samples were run in MicroAmp Fast 96-Well Reaction Plates (Applied Biosystems) on the Applied Biosystems 7500 Fast Real-Time PCR System using the 'Fast' run when using the TaqMan Fast Advanced Master Mix and 'Standard' when using the TaqMan Gene Expression Master Mix.

Table 2.9: TaqMan reaction setup

	Volume (µl)
TaqMan Master Mix	5
TaqMan Probe (stock 5µM)	0.5
Water	2
cDNA	2.5

2.6.3.2 SYBR Green

The reaction was prepared according to Table 2.10. Samples were run in MicroAmp Fast 96-Well Reaction Plates (Applied Biosystems) on the Applied Biosystems 7500 Fast Real-Time PCR System following the program outlined in Table 2.11.

Table 2.10: SYBR Green reaction setup

	Volume (µl)
SYBR Green Master Mix	5
Forward primer (stock: 10 µM)	0.9
Reverse primers (stock: 10 µM)	0.9
Water	0.7
cDNA	2.5

Table 2.11: Thermal cycling for SYBR Green reaction

Time (s)	**Temperature°C**	
20	95	
3	95	x 40
30	60	

2.6.4 Fluidigm biomark

Gene expression analysis was performed using the 48.48 integrated fluidic circuit (IFC) Biomark system (Fluidigm). All steps were performed following manufacturer's recommendations.

2.6.5 Analysis

Due to the unavailability of appropriate analysis software for macOS, a Python-based analysis pipeline was developed (Folder 'Biomark'). The 'amplification_plots_all.py' script was used to visualize amplification curves. The 'ct.csv' file was opened, a column named 'Manual Call' added and each failed amplification plot manually assessed. Amplification curves that only reached the threshold after more than 35 cycles were labelled 'Fail' and remaining ones 'Pass'. This was merged with sample information using the 'merge_ct+sample+assign groups.py' script. Data was plotted using the 'plots_biomark.py' and, after calculating the arithmetic means using 'means_biomark.py', the 'heatmap_biomark.py' scripts.

Table 2.12: TaqMan probes used for pre-amplification

Gene name	TaqMan probe
Il22rb	Mm01192969_m1
Csf2	Mm01290062_m1
Il23r	Mm00519943_m1
Mif	Mm01611157_gH
Il21	Mm00517640_m1
Il1r2	Mm00439629_m1
Il33	Mm00505403_m1
Il17f	Mm00521423_m1
Cxcr3	Mm99999054_s1
Ccl17	Mm01244826_g1
Foxp3	Mm00475162_m1
Rorc	Mm01261022_m1
Tbx21	Mm00450960_m1
Stat1	Mm01257286_m1
Stat6	Mm01160477_m1
Gapdh	Mm99999915_g1
Tnfsf14	Mm00444567_m1
Nfkb1	Mm00481872_s1
Il1r2	Mm00439629_m1
Hprt	Mm00446968_m1
Il17a	Mm00439618_m1
Ifng	Mm01168134_m1
Il10	Mm00439614_m1
Il6	Mm00446190_m1
Il12a	Mm00434165_m1
Il15	Mm00434210_m1
Il18	Mm00434226_m1
Il23a	Mm01160011_g1
Tnfa	Mm00443258_m1
Il22	Mm00444241_m1
Il18	Mm00434226_m1
Tnfsf10	Mm01283606_m1
Tgfb	Mm01178820_m1
Cxcl10	Mm00445235_m1
Ccl22	Mm00436439_m1
Cxcl9	Mm00434946_m1
Stat3	Mm01219775_m1
Pdcd1	Mm01285676_m1
Ptgs2	Mm00478374_m1
Nos2	Mm00440502_m1
Prf1	Mm00812512_m1
Btla	Mm00616981_m1
Lag3	Mm00493071_m1
Ctla4	Mm00486849_m1
Mmp9	Mm00442991_m1
Gzmb	Mm00442837_m1
Klrk1	Mm00473603_m1

2.6.6 TCGA

TCGA data was visualized and downloaded using https://xenabrowser.net/. Data was further analyzed using Python scripts (Folder 'TCGA'). Correlations were determined using 'correlations.py', gene expression was plotted by disease stage using 'stage.py' and by pathological features, such as mutation and microsatellite status using 'pathol_features.py'.

2.6.7 RNA sequencing analysis

Data from a human RNAseq study was provided by the University of Otago, Christchurch as a csv file containing gene expression data as transcript per million (TPM) for each gene and each individual patient sample. Data was further analyzed using Python scripts (Folder 'RNAseq'). Correlations were performed using 'correlations.py'. Individual plots comparing gene expression of a specific gene across different CMS were created using 'plot_RNAseq1.py'.

2.7 Protein quantification

2.7.1 ELISA

IL-22 enzyme-linked immunosorbent assay (ELISA)s were performed using the ELISA MAX Deluxe Set Mouse IL-22 kit (BioLegend), following manufacturer's recommendations. Absorbance was measured using a SPECTROStar Nano absorbance reader (BMG LABTECH).

2.8 Microbiota analysis

2.8.1 Sample collection and DNA isolation

Fecal samples were collected at 3, 10 and 18 weeks of age and stored at -80°C until extraction. Tumor samples were collected at 18 weeks and stored in RNAlater at -80°C until extraction. For DNA extraction, samples were thawed and processed using the FastDNA SPIN Kit for Soil (MP Biomedicals), following the manufacturer's recommendations. Concentration and purity

were determined using a NanoDrop spectrophotometer (Thermo Fisher Scientific). Samples with a low 260/230 ratio (< 1.8) were purified further. For this, 30 µl of NaCl was added, samples were vortexed and centrifuged at 4°C, 14000 x g for 5 minutes. Supernatant was transferred to a new tube and 100 µl of 96% ethanol was added. Samples were vortexed and kept at -20°C for 20 minutes. Samples were centrifuged as before, 100 µl of 70% ethanol was added and supernatant discarded after a third centrifugation step. The tubes were left to dry upside down at room temperature for approximately 10 minutes. To elute the DNA, 50 - 100 µl of TE buffer was added and heated up to 50°C for 20 minutes. Samples were stored in -80°C until further use.

2.8.2 16S rRNA gene sequencing

16S rRNA gene sequencing was performed by LC Sciences. After quality control, the 16S ribosomal RNA (rRNA) gene V4 variable region was amplified using the 515F: 5'-GTGYCAGCMGCCGCGGTAA 3' and 806R: 5'-GGACTACHVGGGTWTCTAAT-3' primers. The Illumina Sequencing Library was prepared using adapters and barcodes for sample identification. Before sequencing, the PCR AxyPrep Mag PCR Normalizer kit (Axygen) was used for DNA quantitation and concentration normalization. Samples were sequenced using the Illumina MiSeq following the manufacturer's guidelines.

2.8.3 Analysis

Paired-end sequences were demultiplexed and primers were removed using Quantitative Insights Into Microbial Ecology (QIIME) 2 (Bolyen *et al.* 2019). Using DADA2 (Callahan *et al.* 2016), Illumina-sequenced amplicon errors were corrected, forward reads were truncated at position 220 base pair (bp) and reverse reads at 200 bp and 10 bp were trimmed left and right. Taxonomy was assigned using SILVA132. Sequence variants were analyzed using the R package phyloseq (McMurdie *et al.* 2013). Differences between groups were visualized using Weighted UniFrac Principal Component Analysis (PCoA) and statistical differences were determined using PERMANOVA. Pie charts were created using KronaTools (Ondov *et al.* 2011). R scripts used in the study are available in the Folder 'Microbiota'. Data was merged with macroscopic data and

flow cytometry data and correlations were determined using the 'correlations.py' script (Folder 'Microbiota').

2.9 Statistical analysis

Statistical analysis was performed using Python and Pandas. Shapiro-Wilk tests were performed to test for normality and significance was determined using Mann-Whitey U or unpaired t tests unless stated otherwise. If applicable, Bonferri correction was used to control for multiple testing. Significant differences were indicated as follows: * $p \leq 0.05$, ** $p \leq 0.01$, *** $p \leq 0.001$, **** $p \leq 0.0001$.

Results

3.1 Chapter 1 - The role of NKG2D in the healthy mouse intestine

3.1.1 Introduction

A key study from 1996 demonstrated constitutive expression of NKG2DL on healthy human intestinal epithelium (Groh *et al.* 1996) - a remarkable finding suggesting a particular role for NKG2D in the intestine. Subsequently, NKG2D has been implicated in a number of intestinal disorders, including IBD, CeD and CRC, yet its function under homeostatic conditions has not been studied in detail. Indeed, the only evidence for the presence of NKG2D-expressing cells in the healthy intestine comes from studies comparing healthy or non-inflamed tissue to patients samples and provide limited information on their functionality.

Quantification of NKG2D expression on healthy intestinal immune cells showed low frequencies of NKG2D-expressing $CD4^+$ in the LP of healthy adults and children, ranging from less than 1% to 10% in most samples, but occasionally exceeding 20% (Allez *et al.* 2007, Chirica *et al.* 2015, Scaleia *et al.* 2012). Frequencies of NKG2D-expressing $CD8^+$ T cells were shown to be significantly higher with 40-90% $NKG2D^+$ $CD8^+$ T cells in children (Scaleia *et al.* 2012) and 50-100% in healthy adults (Chirica *et al.* 2015). This is not surprising due to the fact that, as opposed to mice where only activated $CD8^+$ T cells express NKG2D, human naive T cells are $NKG2D^+$ (Bauer *et al.* 1999). NK cells in the intestine are not well studied and little evidence is available on the expression of NKG2D on human intestinal NK cells. Wang *et al.*

observed a mere 2% of NKG2D$^+$ NK1.1$^+$ CD3$^-$ NK cells in healthy controls (Wang *et al.* 2017) and a representative flow cytometry histogram by Takayama *et al.* suggests 10-20% positivity (Takayama *et al.* 2010). The most comprehensive data on human tissue came from a study by Vadstrup *et al.*, in which the frequency of NKG2D-expressing cells of inflamed and non-inflamed tissue from CD patients was compared (Vadstrup *et al.* 2017b). They showed that more than 80% of γδT cells and CD8$^+$ T cells and approximately 60% of NK cells express NKG2D in non-inflamed tissue, while the frequency of NKG2D$^+$ CD4$^+$ is below 5%. Between 40 and 60% of unconventional T cells, such as MAIT cells and CD56$^+$ T cells were shown to express NKG2D. While this study provides valuable information due to the direct comparison of several cell types, non-inflamed tissue from IBD patients is not necessarily comparable to tissue from healthy individuals, due to potential changes in immune cell infiltration and microbial composition affecting apparently healthy adjacent tissue.

Despite easier access to mouse intestinal tissue, even less data is available on the expression pattern of the mouse NKG2D. Data is limited to two studies showing low frequencies ($< 5\%$) of NKG2D-expressing CD4$^+$ T cells in the mouse colonic LP, similar to what was observed in humans (Han *et al.* 2020, Ito *et al.* 2007). In regard to CD8$^+$ T cells, one study specifically investigating NKG2D$^+$ CD8$^+$ γδ IELs, showed less than 2% positivity in healthy mice (Li *et al.* 2011) and a second study less than 5% NKG2D$^+$ intraepithelial CD8$^+$ TCRβ$^+$ cells (Abadie *et al.* 2020).

Similarly, NKG2DL expression has mostly been studied in the context of inflammation. Low levels of protein MICA/B, ULBP1 and ULBP2 were detected on colonic tissue of pediatric control samples (Scaleia *et al.* 2012), confirming the presence of NKG2DL on intestinal epithelial cells. Similarly, flow cytometric analysis of RAE-1, MULT1 and H60 revealed low frequencies of NKG2DL-expressing cells on IECs ($< 5\%$) in the healthy mouse large intestine (Li *et al.* 2017). Hansen *et al.*, who investigated the relationship between NKG2DL expression in the small intestine and the microbiota showed baseline expression of NKG2DL at 20% in male and 3% in female C57BL/6NTac mice (Hansen *et al.* 2013). Differences between female and male mice were attributed to differences in housing facilities and differences in microbial composition rather than sex differences. Further confirming a role for the microbial composition in

regulating NKG2DL expression, the authors showed that administering different antibiotics significantly alters NKG2DL expression. The relationship between NKG2DL and the microbiota was further confirmed by showing that GF mice have a significantly increased percentage of NKG2DL-expressing cells. Which ligands exactly are influenced by changes in the microbiota is unclear, as the authors used an NKG2D-Fc chimera to detect all cells expressing proteins that bind to NKG2D. Transcriptional analysis showed that RAE-1 expression is significantly altered upon antibiotics treatment, while changes in MULT-1 and H60 expression are minor. Further studies are needed to understand which ligands are regulated by which bacteria or bacterial metabolites.

The scarcity of data relating to the function of NKG2D under steady-state conditions illustrates a significant gap in current knowledge. Despite being implicated in a number of intestinal disorders, the expression pattern and function of NKG2D in intestinal homeostasis is poorly understood. In this chapter, I thoroughly characterize the expression pattern of NKG2D in the mouse intestine and determine the impact of germline deletion of NKG2D on the intestinal immune system and the microbial composition.

Flow cytometry is a technique often used in immunology research. The idea is to label cellular antigens, such as surface receptors or intracellular proteins, with fluorescent antibodies or dyes. This allows detection of presence or absence, as well as co-expression of the selected markers. The combination of several markers allows identification of different cell types as well as their functional characterization.

A flow cytometer typically consists of a flow cell, allowing cells to pass through a narrow tube one cell at a time, at least one laser, emitting a light beam as the individual cells pass through, and detectors, capturing the light emitted by the individual cells. Most systems are equipped with bandpass filters, which only allow light of certain wavelengths to pass through, installed in front of photomultiplier tube (PMT)s, which absorb the photons emitted by the fluorophore and generate a corresponding electrical signal (Figure 3.1a). Modern devices, such as the BD FACSymphony™ can theoretically detect up to 50 different fluorophores. However, the high number of different fluorophores inevitably results in high spectral overlap, realistically limiting

the number of usable channels with the current availability of commercial fluorophores to 29 (Filipovic *et al.* 2019).

As opposed to this conventional detection using bandpass filters, spectral analyzers capture the full emission spectrum of each fluorophore. Instead of consisting of filters and detectors, spectral analysers contain prisms or gratings, which disperse the emitted light that is then captured by a Multi Channel Detector Array (Figure 3.1b, Nolan *et al.* 2013). The idea behind this is that each fluorophore has a unique emission spectrum and that based on its spectrum, each fluorophore can be identified. This means that rather than compensating 'spill-over' from a fluorophore to a different filter, spectral unmixing needs to be performed. Single-stained controls provide the required information to mathematically assign each fluorophore to a specific spectrum and differentiate the signals from several fluorophores.

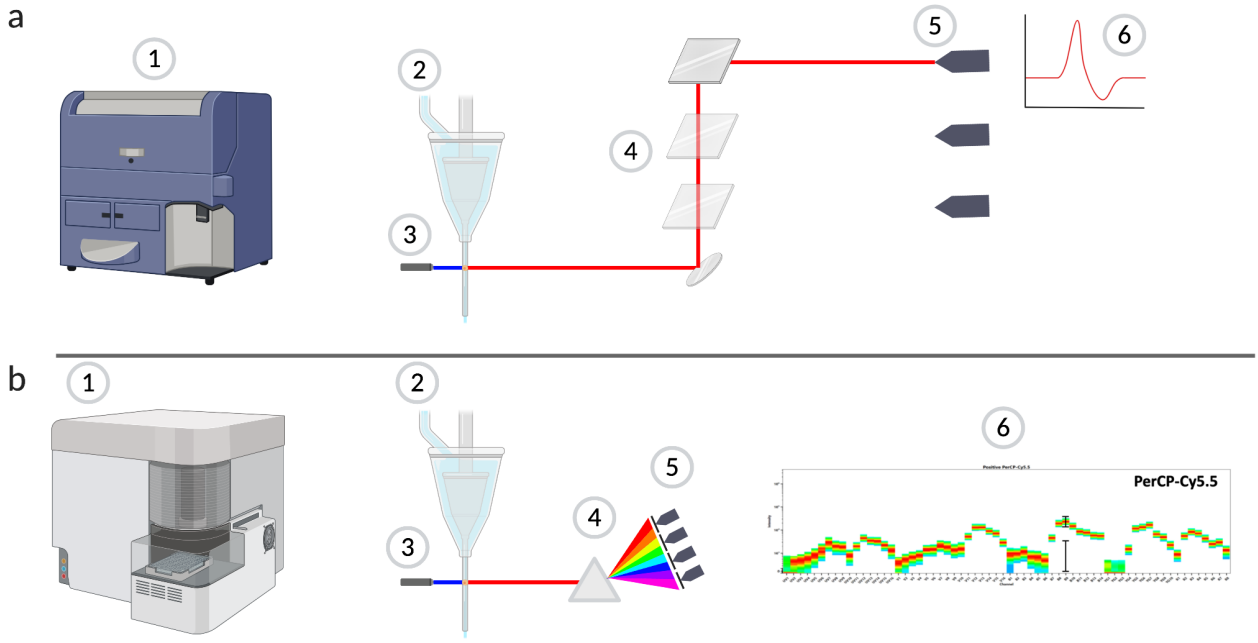

Figure 3.1: Simplified representation of two types of flow cytometers. (a) A filter-based system, such as the BD Fortessa (1), consists of a flow cell (2), at least one laser, which excites each individual cell (3) and several filters (4). Dichroic filters reflect light at a specific wavelength, while photons at different wavelengths can pass through. Reflected light is detected by PMTs (5), which convert photons into an electrical signal (6). (b) In a spectral analyzer, such as the Cytek Aurora, components 1-3 are the same as in a filter-based system. Instead of filters and mirrors, it is equipped with a prism, which disperses the emitted light (4). This light is then captured simultaneously on detector modules (5). This results in an emission spectrum unique to each fluorophore (6). PMT = photomultiplier tube. Image was created using BioRender.

The technique of flow cytometry has led to tremendous advances in immunology research and recent developments in technology now theoretically allow detection of up to 64 different fluorophores. This however comes with a price, and the high number of different fluorophores inevitably results in high spectral overlap. This can be compensated for mathematically, removing spillover from one fluorescent marker to a different channel, however careful panel design and appropriate controls are crucial for successful experiments. Isolation of cells from mucosal tissue often results in the cell suspension containing non-immune cells and high background autofluorescence, making the intestine a particularly difficult tissue to work with.
Here, I demonstrate the successful isolation of LPL and IEL with cell yields high enough to allow me to study rare cells, such as ILCs, as well as the setup of a 18-color panel on the BD Fortessa and 25-color panel on the Cytek Aurora to study intestinal cell function.

Aims:

1. To establish a multi-color panel and gating strategy for flow cytometric analysis of the mouse intestinal immune compartment.

2. To characterize the expression pattern of NKG2D and NKG2D ligands in the healthy intestine.

3. To determine whether NKG2D deficiency impacts the intestinal immune compartment or microbial composition.

4. To establish a 25-color flow cytometry panel for the in-depth characterization of intestinal immune cells using the Cytek Aurora spectral analyzer.

3.1.2 Results

3.1.2.1 Flow cytometric analysis of the intestinal immune compartment using a 18 color panel

Flow cytometry is a method commonly used by immunologists and has greatly advanced our understanding of immune cell composition and function. Increasing numbers of fluorophores of interest complicate designing a suitable antibody panel due to the increasing spectral overlap between fluorophores. In this chapter, I present a flow cytometry panel for the analysis of intestinal immune cells. Several considerations were made when the panel was established to allow easy identification of immune cell subsets and prevent unspecific staining. These included:

1. Reducing spectral overlap of antibodies binding to antigens expressed on the same cell. Example: antibodies binding CD3 (AF647) and CD4 (BUV395), co-expressed on a subset of T cells, were chosen so that spectral overlap was minimized (see Figure 3.2).

2. Combinating bright fluorophores with antigens that are expressed at low levels and vice versa.

3. Configuration of the BD Fortessa used in this study.

4. Limited availability of the needed antibody and fluorophore combinations, in particular of recently developed dyes, such as BUV.

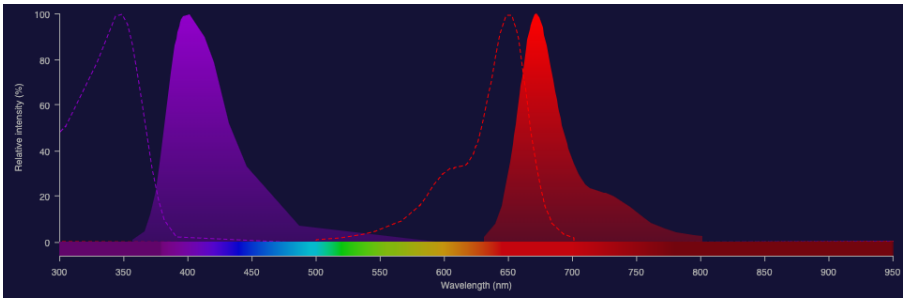

Figure 3.2: Analysis of spectral overlap. Example of two fluorophores used during the panel design. Dotted lines represent excitation and filled lines emission spectra. Purple = BUV395, red = AF647. Figure created using Fluorescence SpectraViewer (ThermoFisher Scientific).

The panel was developed to achieve a broad overview of intestinal cell populations and functionality. As NKG2D was shown to mainly be expressed on NK cells, T cells and ILCs, a particular emphasis was put on these cells. However, myeloid cells are of great importance in the gastrointestinal tract (Joeris *et al.* 2017), which is why markers to identify DCs, neutrophils and monocytes were included. For further functional analysis, antibodies binding to intracellular cytokines were used. Due to a limit of 18 colors on the BDFortessa, these only included IFN-γ and IL-17, two cytokines implicated in NKG2D-mediated inflammation or general intestinal immunity (Table 3.1). Pilot experiments included GzB and IL-22 staining, but low levels of GzB expression on intestinal lymphocytes and lack of evidence of NKG2D-mediated IL-22 regulation ultimately led to omission of these antibodies.

Table 3.1: 18-color flow cytometry panel used to study intestinal immune cell function.

Exitation laser	Emission filter	Fluorophore	Antigen
355	379/28	BUV395	NK1.1
355	450/50	BUV495	CD4
355	730/40	BUV737	Ly6C
405	450/50	BV421	IFNγ
488	525/50	FITC	CD127
561	585/15	PE	NKG2D
405	610/20	BV605	CD11c
561	610/20	PE-CF594	RORγT
640	670/14	AF647	CD3
561	670/30	PE-Cy5	γδTCR
405	660/20	BV650	CD19
640	710/50	AF700	CD45
405	710/50	BV711	T-bet
488	695/40	PerCp Cy5.5	CD8
561	780/60	Pe-Cy7	IL-17
640	780/60	APC-Cy7	Ly6G
405	780/60	BV786	CD11b
405	525/50	Aqua	

The gating strategy to identify immune cell subsets isolated from the colonic LP and the MLN is illustrated in Figure 3.3 and 3.4. In the experimental procedure, I did not include removal of non-lymphocytes and dead cells using Percoll, as suggested by others (Goodyear *et al.* 2014), resulting in low frequencies of live $CD45^+$ cells. The rationale for not using Percoll was that

gradient centrifugation is inevitably associated with a loss of cells and decreased viability. Due to the nature of the project, which included the analysis of ILCs, a very small population of intestinal immune cells, I decided that the benefit of not losing cells outweighed the benefit of having 'clean' cell preparations.

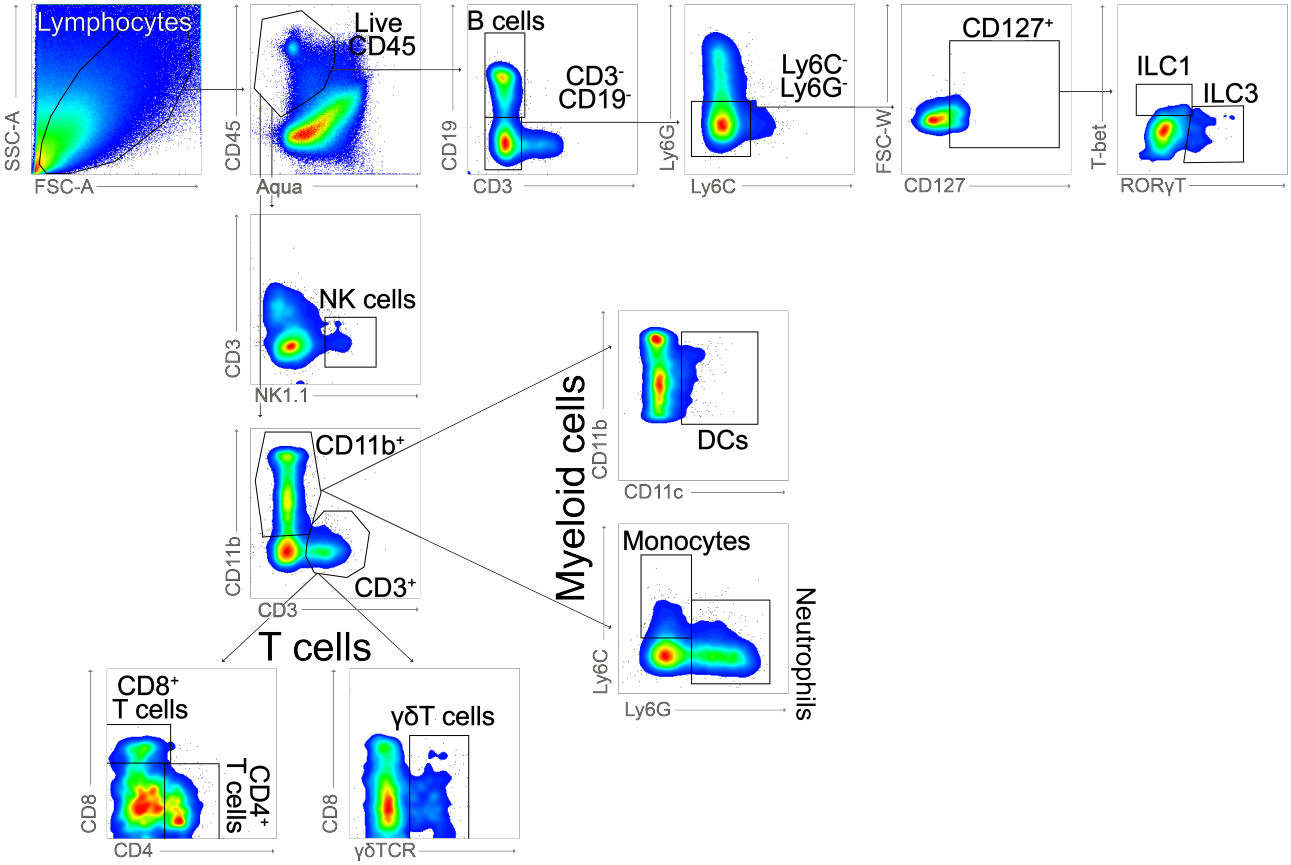

Figure 3.3: Gating strategy and representative flow cytometry plots of cells isolated from the colonic lamina propria. Representative flow cytometry plots of immune cells isolated from the colonic lamina propria of healthy *Klrk1*$^{+/+}$ mice. FMO controls were used to identify ILC1, ILC3, CD127^{+} cells and DCs. FMO = fluorescence minus one.

After exclusion of dead and CD45^{-} cells, further subgating was performed. With the exception of DCs and ILCs, gates were visually identified. For markers identifying DCs (CD11c) and ILCs (CD127, T-bet and RORγT) FMO controls were used. For MLN and other lymphoid tissues, the same panel and gating strategies were used.

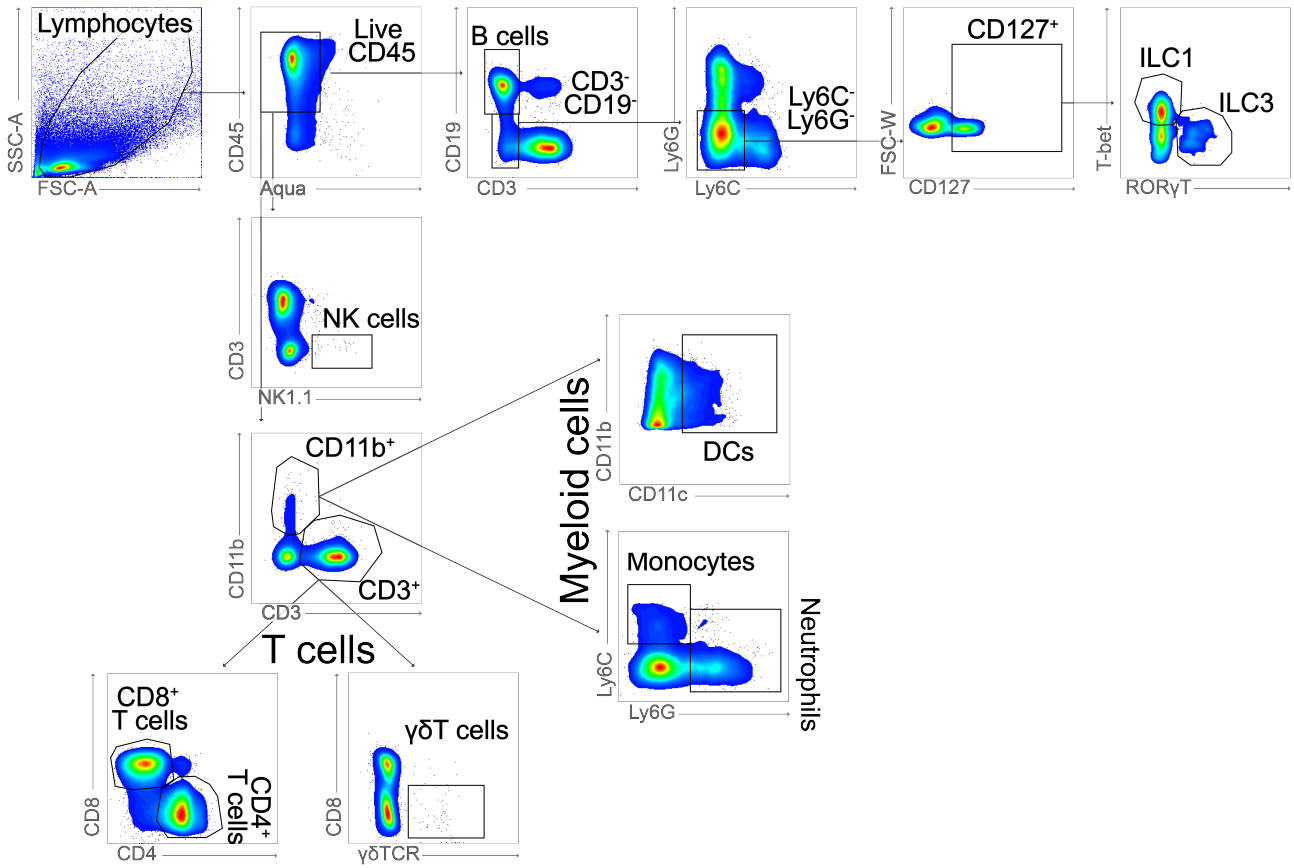

Figure 3.4: Gating strategy and representative flow cytometry plots of cells isolated from the mesenteric lymph nodes. Representative flow cytometry plots of immune cells isolated from the mesenteric lymph nodes of healthy *Klrk1*$^{+/+}$ mice. FMO controls were used to identify ILC1, ILC3, CD127^{+} cells and DCs. FMO = fluorescence minus one.

3.1.2.2 Elevated NKG2D expression in the mouse intestine under steady-state conditions

To better understand the function of NKG2D in intestinal health, I quantified the expression pattern of the mouse NKG2D under homeostatic conditions in the intestine by determining frequencies of NKG2D-expressing cells in the colonic and small intestinal LP, as well as the MLN. Cells isolated from NKG2D-deficient *Klrk1*$^{-/-}$ were used as a negative control and were used to determine the gates identifying NKG2D-expressing cells (Figure 3.5c and d). In addition to detecting NKG2D on NK cells, substantial levels of NKG2D–expressing cells were detected among ILC1, ILC3s and T cells, including CD4^{+}, CD8^{+} and γδT cells. Unsurprisingly, the highest frequency of NKG2D-expressing cells was found within the NK cell subset in MLN (33.2%), SI (31.2%) and in the colon (49.7%). With regard to ILC1, 35.9% of NKG2D^{+} ILC1s

were isolated from the MLN and < 6% of intestinal ILC1s were found to be NKG2D$^+$. The frequency of NKG2D$^+$ ILC3s ranged from 13% (MLN and colon) to 23.4% (SI) (Figure 3.5a and e). Among T cells, frequencies of NKG2D-expressing cells was highest in the γδT cell subset in the MLN (4.6%) and colon (11.2%), compared to the small intestine (SI) (2.1%). In contrast, the proportions of NKG2D-expressing CD4$^+$ and CD8$^+$ T cells were scarce in the MLN (<1%), but significantly elevated in the colon (3.1% and 4.2%) and small intestine (2.0% and 1.49%) (Figure 3.5b and f). With the exception of ILC1 and ILC3s, the frequency of NKG2D-expressing cells was significantly higher in the colonic LP compared to the MLN, suggesting a particular role for NKG2D in the intestine.

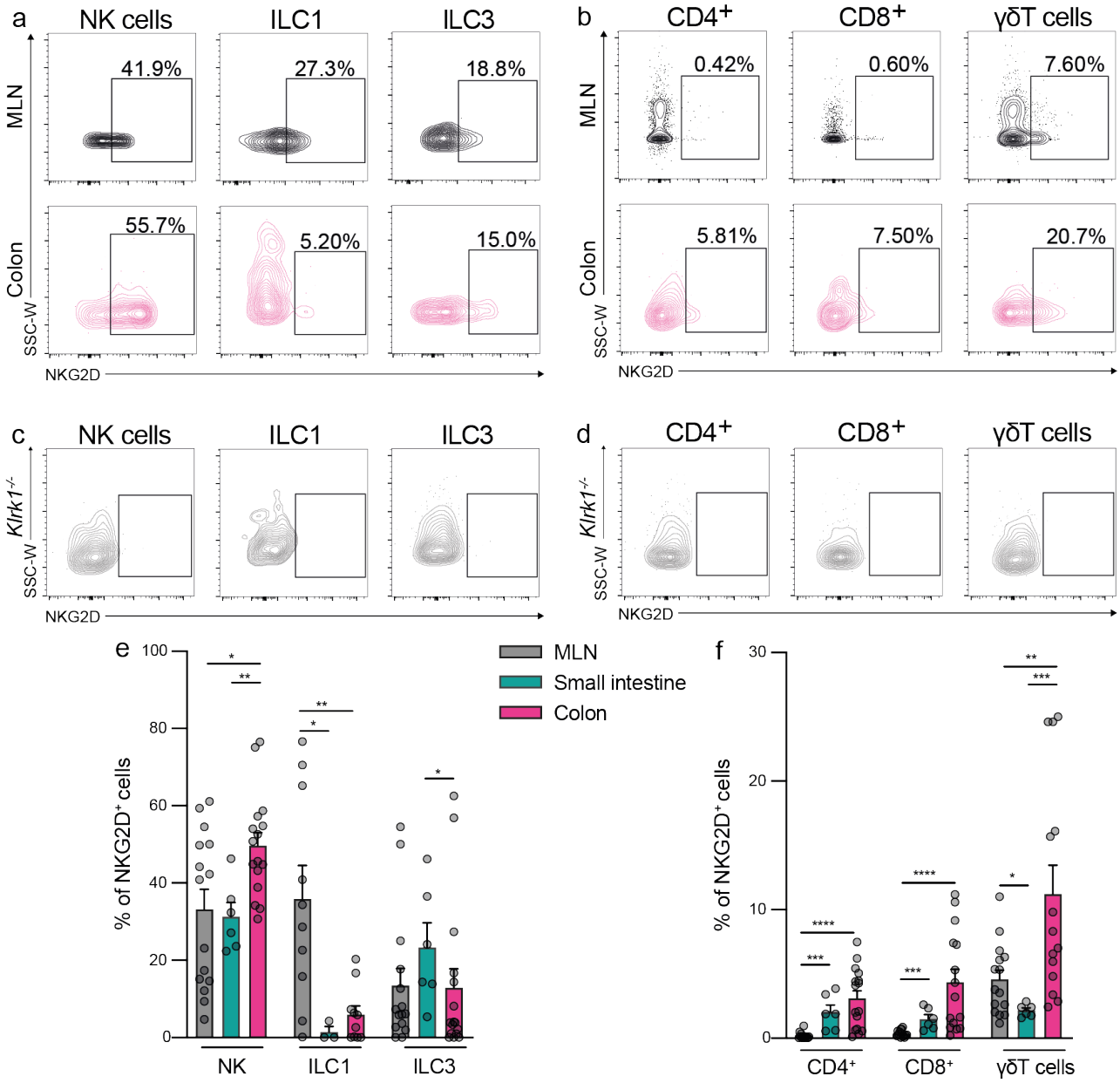

Figure 3.5: NKG2D expression is elevated in the healthy mouse gastrointestinal tract. Representative flow cytometry plots depicting NKG2D expression on innate cells (a) and T cells (b) isolated from the colonic lamina propria of naive *Klrk1*$^{+/+}$ mice. Representative flow cytometry plots depicting NKG2D staining on innate cells (c) and T cells (d) from the colonic lamina propria of naive *Klrk1*$^{-/-}$ mice used as a negative control. Frequencies of NKG2D-expressing cells in the MLN (grey) and on small intestinal (green) and colonic (magenta) LPL among innate cells (e) and T cells (f) of naive *Klrk1*$^{+/+}$ mice. LPL = lamina propria lymphocytes, MLN = mesenteric lymph nodes. n $\geq$ 6. Data in b and d represented as mean $\pm$ SEM of individual mice from at least three independent experiments. * p $\leq$ 0.05, ** p $\leq$ 0.01, *** p $\leq$ 0.001.

I next assessed frequencies of NKG2D-expressing cells within IECs. These IELs can have direct contact with the content of the intestinal lumen and therefore play a significant role in host defence. Frequencies of NKG2D-expressing NK cells and ILC3s were comparable among IELs to LPL, whereas frequencies of NKG2D$^+$ ILC1s were increased from 1.43% LPL in the small intestine to 24.8% among IELs and 5.9% (LPL) to 34.5% (IEL) in the colon (Figure 3.6a). Frequencies of NKG2D-expressing innate cells tended to be higher in the colon compared to the small intestine. Frequencies of NKG2D-expressing CD4$^+$ T cells in the colon were slightly increased among IELs compared to LPLs (Figure 3.6b). I further found that a significantly higher frequency of colonic CD4$^+$ and CD8$^+$ T cells expressed NKG2D compared to the small intestine. With the exception of NKG2D$^+$ ILC1s, which were more abundant among IELs, frequencies of NKG2D$^+$ IELs were comparable to LPLs.

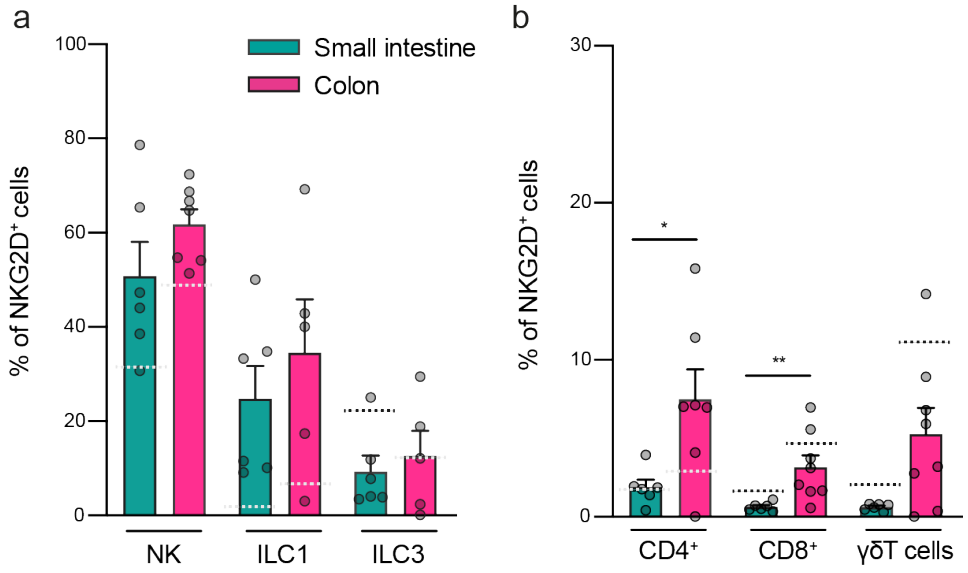

Figure 3.6: Frequencies of NKG2D-expressing IELs are higher in the colon compared to the small intestine of healthy mice. Frequencies of NKG2D-expressing cells in small intestinal (green) and colonic (magenta) IEL among innate cells (a) and T cells (b) isolated from naive *Klrk1*$^{+/+}$ mice. Dotted line (white or black) represents mean frequency of NKG2D-expressing LPL. IEL = intestinal epithelial lymphocytes. n $\geq$ 6. Data is represented as mean $\pm$ SEM of individual mice from at least three independent experiments. * p $\leq$ 0.05, ** p $\leq$ 0.01.

These data indicate:

1. A significant number of NKG2D-expressing cells exist in the healthy intestine.

2. Frequencies of NKG2D-expressing cells are increased in the colon compared to the small intestine.

3. A significantly greater percentage of colonic NK cells and T cells express NKG2D in comparison with MLN.

4. Frequencies of NKG2D-expressing IELs and LPLs are comparable with the exception of ILC1s, which are more frequent within epithelial cells.

3.1.2.3 NKG2D ligand is expressed in the healthy mouse intestine

The study showing constitutive expression on human epithelium (Groh *et al.* 1996) raised the question of whether NKG2DL is present on healthy mouse intestinal epithelium. Indeed, a large RAE-1$^+$ area was detected in both small intestinal (63.0%) and colonic (58.4%) tissue of 10-12 week old wild-type mice (Figure 3.7). Interestingly, RAE-1$^+$ area was decreased in mice older than 20 weeks (33.7% on small intestinal and 37.1% on colonic epithelium, Figure 3.7), suggesting an age-dependent downregulation of NKG2DL expression.

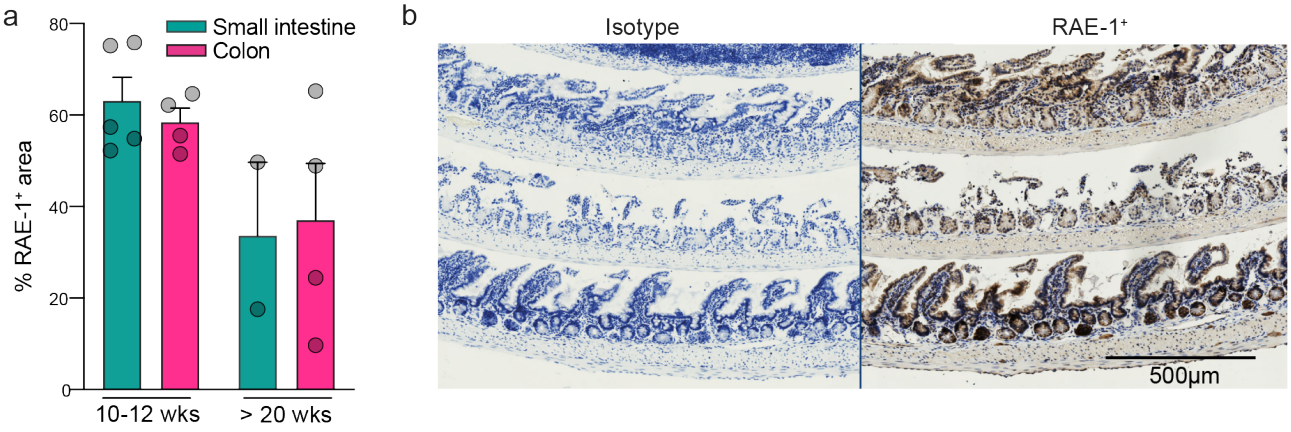

Figure 3.7: The NKG2D ligand RAE-1 is expressed in the healthy mouse gastrointestinal tract. (a) Percentages of RAE-1$^+$ area on small intestinal and colonic tissue of naive *Klrk1*$^{+/+}$ mice aged 10-12 weeks (left) and > 20 weeks (right). (b) Representative RAE-1 staining on intestinal tissue. n $\geq$ 4, except small intestine > 20 weeks, where n = 2. Data represented as mean $\pm$ SEM. IHC staining was performed by M.Sc. student Elena Rondeau.

Low sample numbers, high variations and staining for only one of the several mouse ligands make it difficult to infer on NKG2DL regulation. Nonetheless, we can conclude that RAE-1 is indeed expressed at significant levels on healthy mouse epithelium, underlining similarities with the human NKG2D/NKG2DL system.

3.1.2.4 Frequencies of ILC3s are increased in the NKG2D-deficient intestinal tract

I next asked whether germline deletion of NKG2D would impact the intestinal immune cell compartment. For this, I compared frequencies of the major immune subsets in the LP and MLN of naive *Klrk1*$^{+/+}$ and *Klrk1*$^{-/-}$ mice. Due to the main site of inflammation studied in Chapter 3 being the colon, I focused on characterizing the immune cells in the colonic lamina propria.

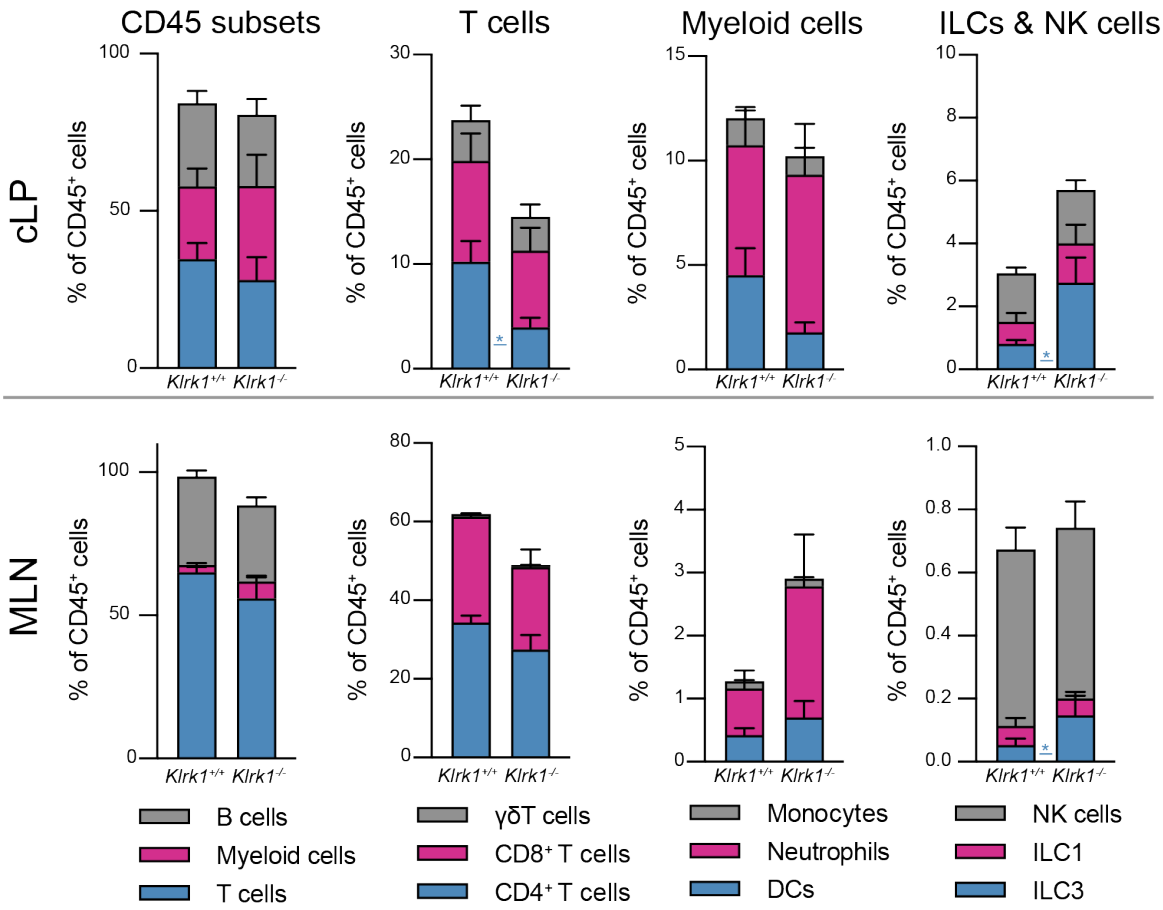

Figure 3.8: NKG2D deficiency is associated with minor changes in the intestinal immune compartment. Stacked bar plots of immune cell subsets in the cLP (top) and MLN (bottom) of naive *Klrk1*$^{+/+}$ and *Klrk1*$^{-/-}$ mice. n $\geq$ 9. cLP = colonic lamina propria. MLN = mesenteric lymph nodes. Data is represented as mean $\pm$ SEM of individual mice from at least six independent experiments. * p $\leq$ 0.05.

No major differences were observed in the frequencies of T cells, B cells or myeloid cells (Figure 3.8), but detected a significant increase of ILC3s in both MLN as well as in the colonic LP in NKG2D-deficient mice. In the intestine, but not MLN, this increase of ILC3s was associated with a decrease of $CD4^+$ T cells (Figure 3.8, 3.9c and data not shown). In *Klrk1*$^{-/-}$ mice, the frequency of ILC3s varied between 0.17% and 6.69% of all $CD45^+$ cells, while the variation in *Klrk1*$^{+/+}$ mice was lower, with frequencies of ILC3s falling between 0.11% and 1.84% (Figure 3.9a and b).

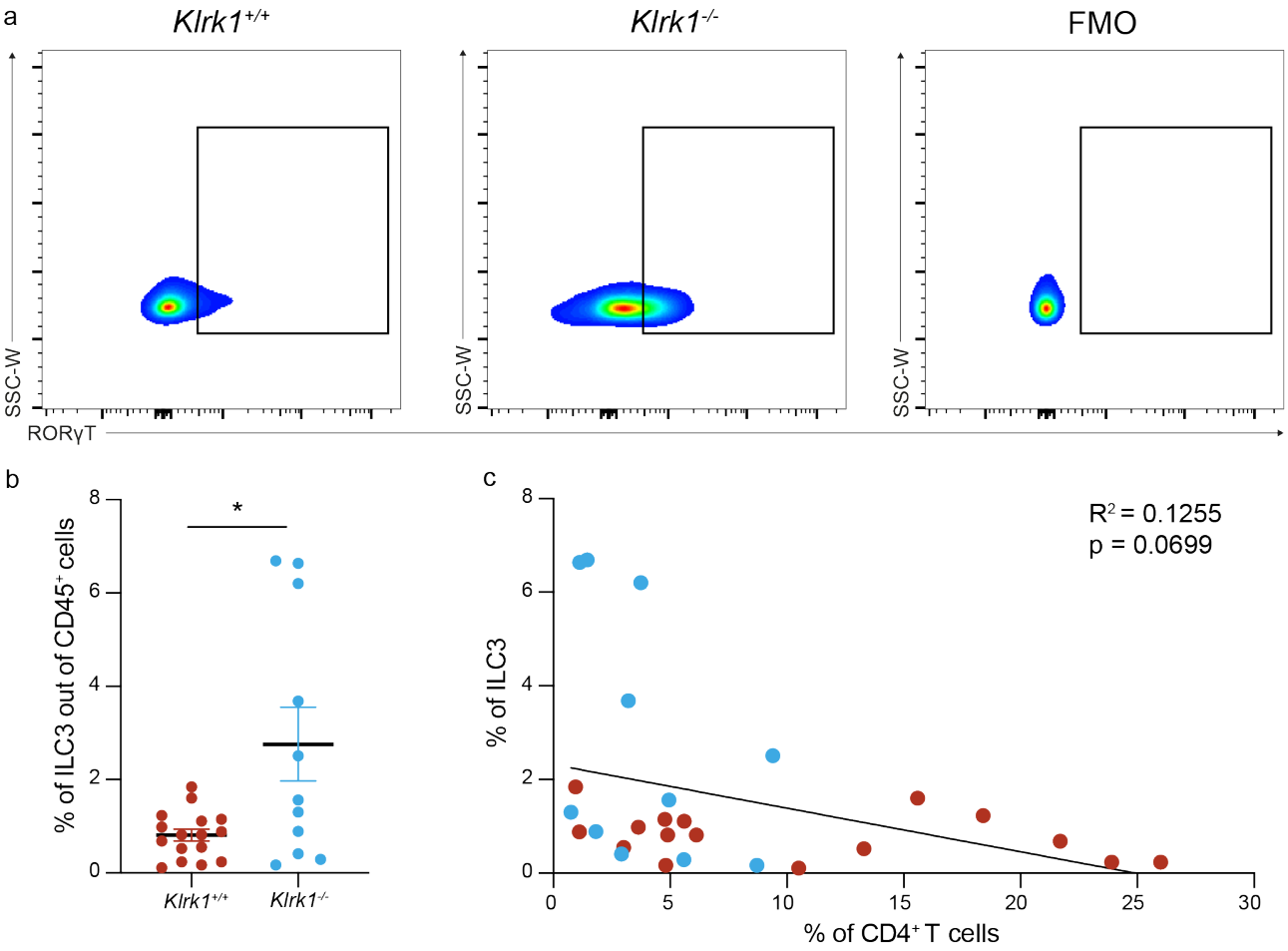

Figure 3.9: Frequencies of ILC3s are increased in the colonic lamina propria of NKG2D-deficient mice. (a) Representative flow cytometry plots depicting RORγT staining to identify ILC3s, comparing naive *Klrk1*$^{+/+}$ and *Klrk1*$^{-/-}$ mice. (b) Scatterplot of frequencies of ILC3s in the cLP of naive *Klrk1*$^{+/+}$ and *Klrk1*$^{-/-}$ mice. (c) Linear regression of frequencies of ILC3s and $CD4^+$ T cells in the cLP of naive *Klrk1*$^{+/+}$ (red) and *Klrk1*$^{-/-}$ (blue) mice. $n \geq 11$. FMO = fluorescence minus one, cLP = colonic lamina propria. Data is represented as mean ± SEM of individual mice from at least four independent experiments. * $p \leq 0.05$.

The top five data points within the *Klrk1*$^{-/-}$ group originated from four independent experiments, suggesting that the difference was not due to one experiment with particular high frequencies of ILC3s. Linear regression analysis to establish whether an increase of ILC3s was correlated with a decrease of CD4^{+} T cells (Figure 3.9b) revealed a subtle, but not statistically significant inverse correlation of ILC3s and CD4^{+} T cells in the colonic LP (Figure 3.9c). Together with the fact that the increase of ILC3s was observed in two organs - the colonic LP and MLN - this supports the hypothesis that NKG2D-deficiency is associated with an increase in ILC3 frequency. One major drawback is the fact that in this study, only frequencies and not absolute numbers were measured. To confirm these findings, cell quantification should be performed by multi-color immunofluorescence (IF).

3.1.2.5 Lack of NKG2D is associated with minor changes in immune cell functionality and cytokine production

Having established that NKG2D-deficiency was associated with minor changes in immune cell composition, I next investigated whether lack of NKG2D was associated with differences in cell functionality. I compared frequencies of IFN-γ and IL-17-expressing ILCs in the colonic LP of *Klrk1*$^{+/+}$ and *Klrk1*$^{-/-}$ mice. Baseline IFN-γ production ranged from 17.2 (NK cells) to 35.9% (ILC3s) in *Klrk1*$^{+/+}$ mice (Figure 3.10a and b). Interestingly, the frequency of IFN-γ-producing ILC1s was significantly increased in *Klrk1*$^{-/-}$ mice (52.4%) compared to *Klrk1*$^{+/+}$ littermates (27.2%). A slight, but not statistically significant difference was observed in the frequency of IFN-γ-producing NK cells, with 17.2% in wild-type and 29.5% in NKG2D-deficient NK cells (Figure 3.10b). Baseline IL-17 production was lower and ranged from 9.0% (NK cells) to 30.2% (ILC1s) (Figure 3.10c and d). No genotypic differences in IL-17 production were observed under steady-state conditions (Figure 3.10d).

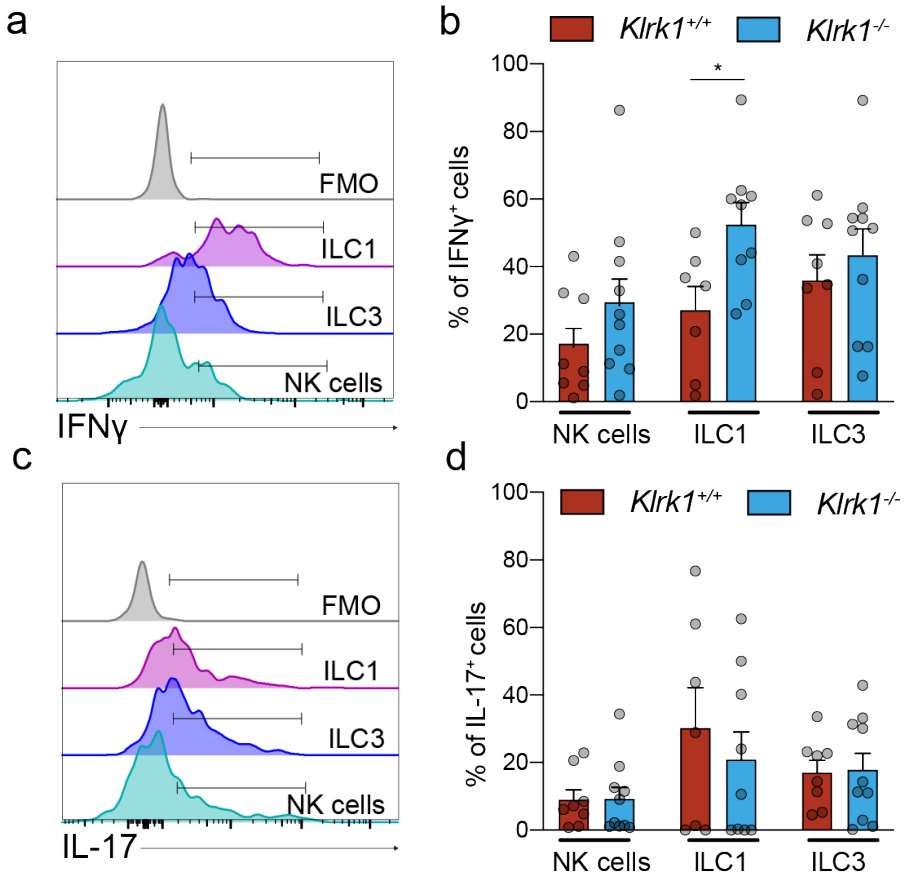

Figure 3.10: IFN-γ production is slightly increased in NKG2D-deficient colonic innate immune cells. (a) Representative flow cytometry histograms of IFN-γ staining on innate cells stimulated with PMA and ionomycin, isolated from the cLP of naive *Klrk1*$^{+/+}$ mice. (b) Quantification of IFN-γ-producing cells stimulated with PMA and ionomycin, in the cLP of naive *Klrk1*$^{+/+}$ and *Klrk1*$^{-/-}$ mice. n ≥ 8. (c) Representative flow cytometry histograms of IL-17 staining on innate cells stimulated with PMA and ionomycin, isolated from the cLP of naive *Klrk1*$^{+/+}$ mice. (d) Quantification of IL-17-producing cells stimulated with PMA and ionomycin, in the cLP of naive *Klrk1*$^{+/+}$ and *Klrk1*$^{-/-}$ mice. n ≥ 9. FMO = fluorescence minus one. Data is represented as mean ± SEM of individual mice from at least four independent experiments. * p ≤ 0.05.

In addition to studying functional characteristics of NKG2D-deficient immune cells, I sought to determine whether there was a functional difference between NKG2D-positive and NKG2D-negative cells within the same (*Klrk1*$^{+/+}$) mouse. For this, I gated on the different cell types as previously described and then determined the frequencies of IFN-γ- and IL-17-producing cells within the NKG2D^{+} and NKG2D^{-} compartments. A higher median fluorescence intensity (MFI) of IFN-γ in the NKG2D^{-} subset of colonic NK cells, and to some extent ILC1s (Figure 3.11a and b), but not MLN was observed. Out of 8 LP samples, the MFI of IFN-γ NK cells was higher in the NKG2D^{-} subset in 6, while it was slightly reduced in 2. Within the ILC1

subset, the MFI of IFN-γ was greatly increased in the NKG2D$^-$ subset in 2 out of 5 samples, with no differences between NKG2D$^+$ and NKG2D$^-$ subsets in the remaining 3 (Figure 3.11c). Only IFN-γ production differed between NKG2D$^+$ and NKG2D$^-$ subsets, while no changes in IL-17 production were observed (data not shown).

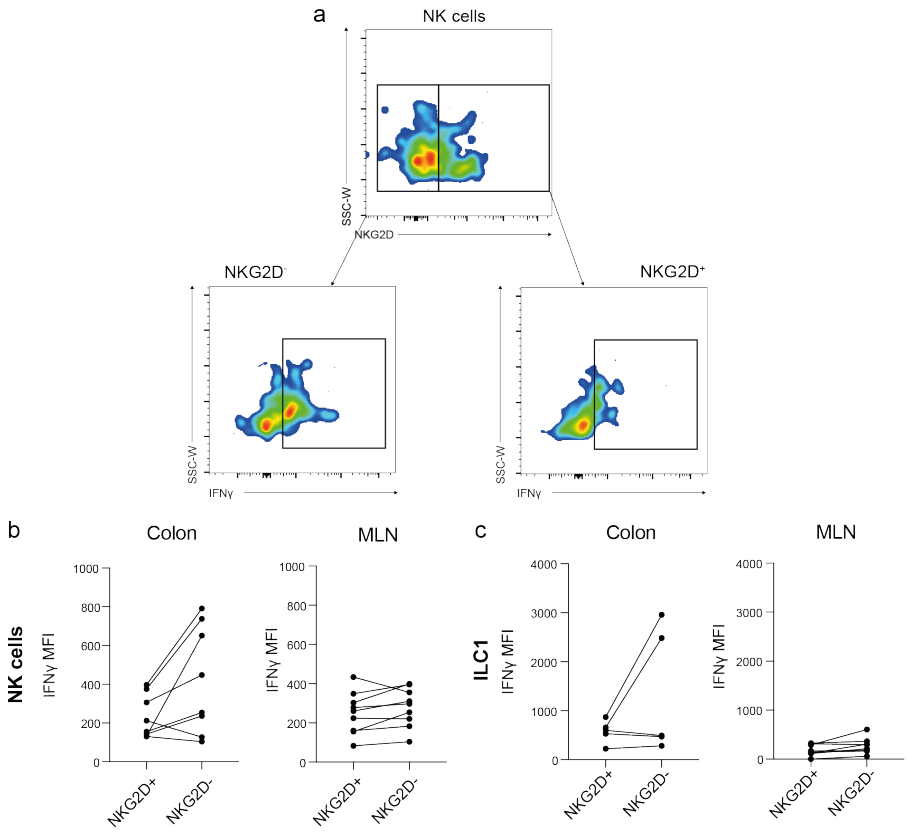

Figure 3.11: NKG2D$^-$ cells display a slightly increased production of IFN-γ in the colon of naive mice. (a) Representative flow cytometry plots of IFN-γ-producing NKG2D$^+$ and NKG2D$^-$ NK cells stimulated with PMA and ionomycin, isolated from the cLP of naive *Klrk1*$^{+/+}$ mice. n ≥ 8. (b) Quantification of IFN-γ-producing cells stimulated with PMA and ionomycin, within NKG2D$^+$ and NKG2D$^-$ NK cells in the cLP (left) and MLN (right) of naive *Klrk1*$^{+/+}$ mice. (c) Quantification of IFN-γ-producing cells stimulated with PMA and ionomycin, within NKG2D$^+$ and NKG2D$^-$ ILC1s in the cLP (left) and MLN (right) of naive *Klrk1*$^{+/+}$ mice. n ≥ 5. cLP = colonic lamina propria, MLN = mesenteric lymph nodes, MFI = median fluorescence intensity. Data represented as individual mice per line.

Together, we conclude that NKG2D-deficient innate immune cells, both cell with a germ-line deletion of *Klrk1* as well as NKG2D$^-$ cells in *Klrk1*$^{+/+}$ mice produce higher levels of IFN-γ compared to their NKG2D$^+$ counterparts. However, further research is needed to determine the validity of these results. The low sample number, high variation and the *ex vivo* stimulation make it difficult to draw conclusions on the physiological function of these cells.

Having established that NKG2D-deficiency influences IFN-γ production by innate cells in the colon, I next assessed functional differences within the T cell compartments. Babic *et al.* showed in a recent study that the frequencies of both IFN-γ as well as GM-CSF-producing NKG2D$^+$ CD4$^+$ T cells were higher compared to NKG2D$^-$ CD4$^+$ T cells in the small intestine (Babic *et al.* 2020).

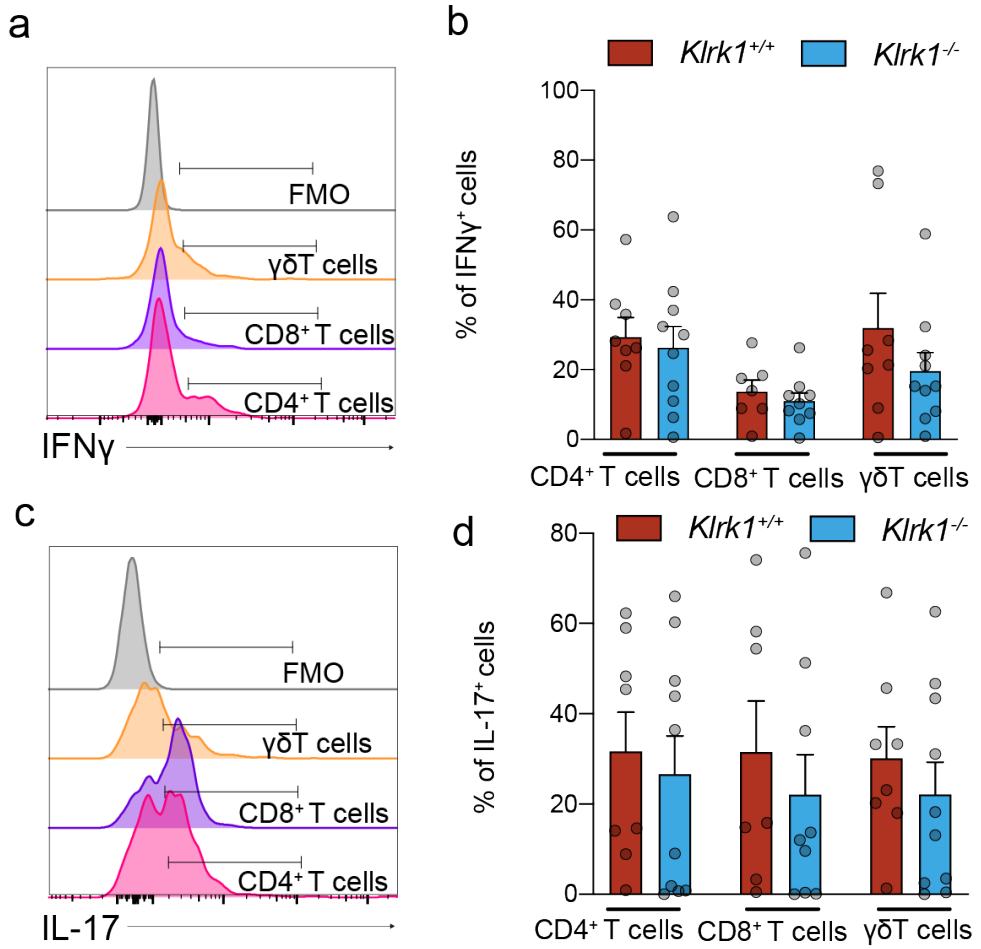

Figure 3.12: NKG2D deficiency leads to no changes in cytokine production in colonic T cells. (a) Representative flow cytometry histograms of IFN-γ staining on T cells stimulated with PMA and ionomycin, isolated from the cLP of naive *Klrk1*$^{-/-}$ mice. (b) Quantification of IFN-γ-producing T cells stimulated with PMA and ionomycin, isolated from the cLP of naive *Klrk1*$^{+/+}$ and *Klrk1*$^{-/-}$ mice. n $\geq$ 8. (c) Representative flow cytometry histograms of IL-17 staining on T cells stimulated with PMA and ionomycin, isolated from the cLP of naive *Klrk1*$^{+/+}$ mice. (d) Quantification of IL-17-producing T cells stimulated with PMA and ionomycin, isolated from the cLP of naive *Klrk1*$^{+/+}$ and *Klrk1*$^{-/-}$ mice. n $\geq$ 9. FMO = fluorescence minus one. Data represented as mean ± SEM of individual mice from at least four independent experiments. * p $\leq$ 0.05.

Comparing MFI of NKG2D$^+$ versus NKG2D$^-$ CD4$^+$ T cells in the colonic LP revealed that while NKG2D-deficiency did not alter the frequency of IFN-γ- (Figure 3.12a and b) or IL-17-producing cells (Figure 3.12c and d), there was a noticeable difference in cytokine production when comparing NKG2D$^+$ to NKG2D$^-$ cells from the same mouse. Similar to what Babic *et al.* reported, I found that NKG2D$^+$ T cells expressed significantly more IFN-γ, measured as MFI, compared to NKG2D$^-$ cells (Figure 3.13a and b). This increased expression of IFN-γ was particularly striking in CD8$^+$ T cells, but a similar trend was observed in CD4$^+$ T cells (data not shown). Similar to observations made by Babic and colleagues who showed no differences in IL-17 production when comparing small intestinal NKG2D$^+$ to NKG2D$^-$ cells, no differences in IL-17-production in the colonic LP were observed (Figure 3.13c). However, MFI of IL-17 was significantly increased in NKG2D$^+$ CD4$^+$ T cells compared to NKG2D$^-$ cells in the MLN. The data shows that there are some differences in immune cell composition in *Klrk1*$^{-/-}$ mice compared to their wild-type littermates. Due to the limited cell yield and the restriction to 18 colors in the flow cytometry experiments, functional data was limited to IFN-γ and IL-17.

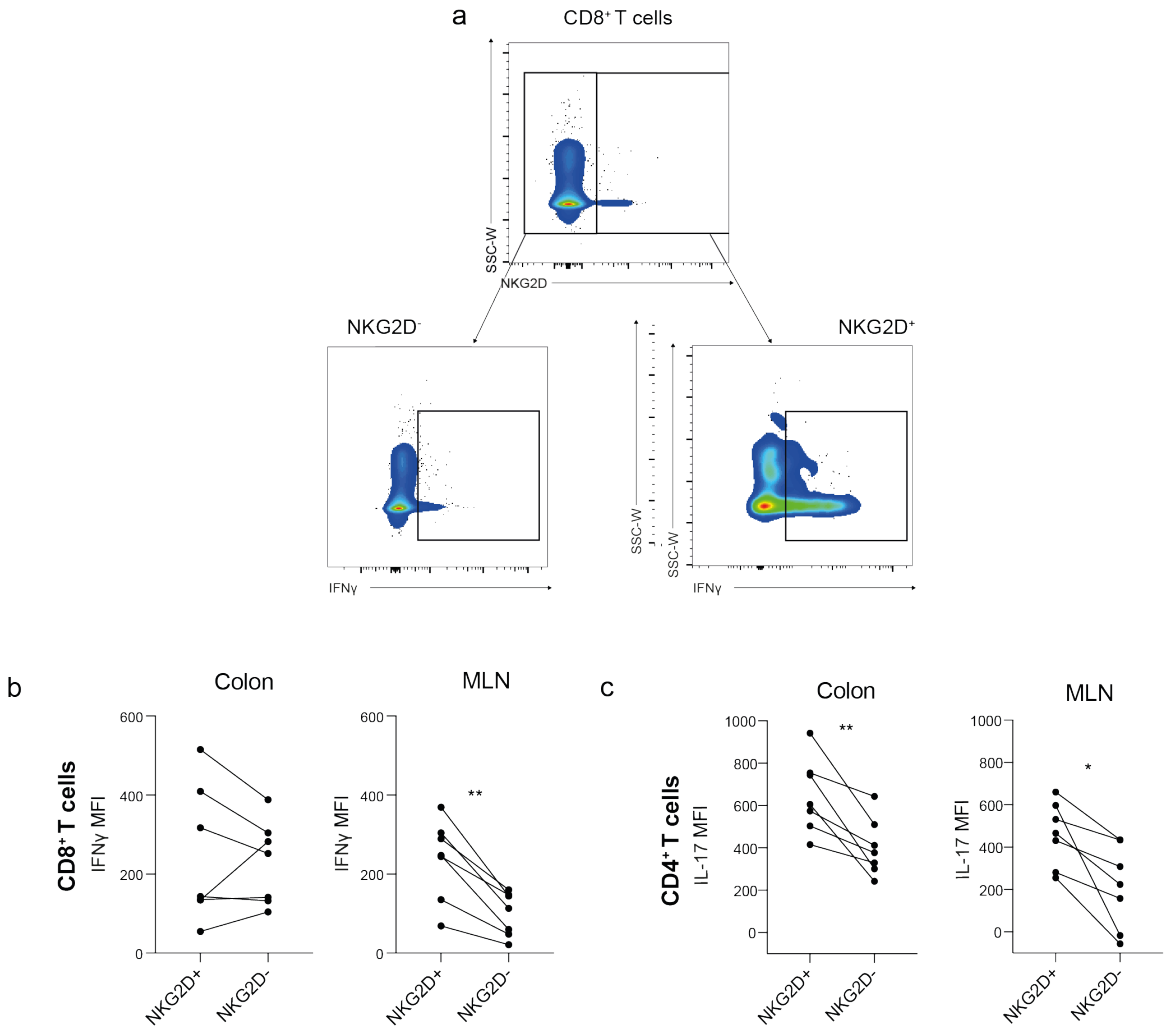

Figure 3.13: NKG2D directly influences IFN-γ and IL-17 production in *Klrk1*$^{+/+}$ mice. (a) Representative flow cytometry plots of IFN-γ-producing NKG2D^{+} and NKG2D^{-} CD8^{+} T cells stimulated with PMA and ionomycin, isolated from the MLN of naive *Klrk1*$^{+/+}$ mice. n $\geq$ 8. (b) Quantification of IFN-γ-producing T cells stimulted with PMA and ionomycin, within NKG2D^{+} and NKG2D^{-} CD8^{+} T cells in the cLP (left) and MLN (right) of naive *Klrk1*$^{+/+}$ mice. (c) Quantification of IFN-γ-producing cells stimulated with PMA and ionomycin, within NKG2D^{+} and NKG2D^{-} CD4^{+} in the cLP (left) and MLN (right) of naive *Klrk1*$^{+/+}$ mice. n $\geq$ 5. cLP = colonic lamina propria, MLN = mesenteric lymph nodes, MFI = median fluorescence intensity. Each line in b and c represents an individual mouse. Significance was determined using paired t-test. * $p \leq 0.05$, ** $p \leq 0.01$.

To achieve a broad overview of any potential major defects in immune cell functionality, I performed a gene expression screen of 30 genes of interest on small intestinal tissue from naive *Klrk1*$^{+/+}$ and *Klrk1*$^{-/-}$ mice. I compared gene expression profile of *Klrk1*$^{+/+}$ and *Klrk1*$^{-/-}$ mice by calculating a fold change ratio (fold change of *Klrk1*$^{+/+}$ over fold change of *Klrk1*$^{-/-}$) (Figure 3.14a). Transcript for Granzyme B (5.7x higher) and CXCL9 (3.3x higher) were expressed at significantly higher levels in tissue from *Klrk*$^{+/+}$ compared to *Klrk1*$^{-/-}$ mice. Interestingly, RORγT was expressed 2x higher in *Klrk1*$^{-/-}$ mice, which supports the observation that NKG2D-deficient mice display an increased frequency of RORγT^{+} ILC3s in the intestine.

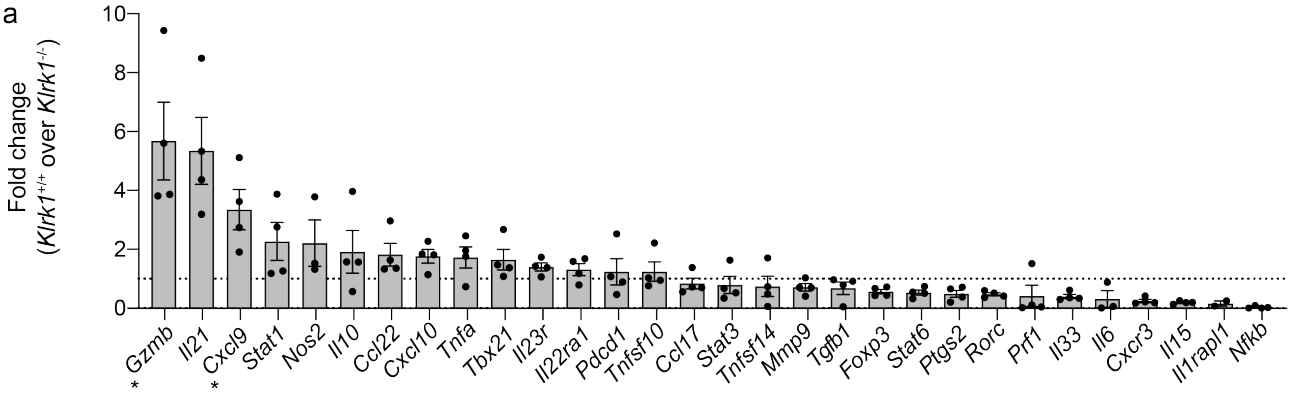

Figure 3.14: Gene expression profile of naive *Klrk1*$^{+/+}$ and *Klrk1*$^{-/-}$ mice. (a) Fold change calculated as fold change (over HPRT) of *Klrk1*$^{+/+}$ over fold change (over HPRT) of *Klrk1*$^{-/-}$ mice, ordered from highest to lowest. Dots represent individual samples. Data represented as mean from n $\geq$ 3. * p $\leq$ 0.05.

3.1.2.6 NKG2D deficiency does not impact NKG2DL expression

I next examined whether NKG2D deficiency influences the expression of NKG2DL in the mouse intestine. For this, I compared the percentage of RAE-1^{+} area from wild-type mice to mice lacking NKG2D. Interestingly, no differences were observed and the average frequency of RAE-1^{+} area was 34.5% in the small intestine and 33.9% in the colon, comparable to what was observed in *Klrk1*$^{+/+}$ mice (Figure 3.7). I therefore conclude that ligand expression is independent of NKG2D and that, under steady-state conditions, NKG2DL-expressing epithelial cells are not targeted and eliminated by NKG2D-expressing immune cells.

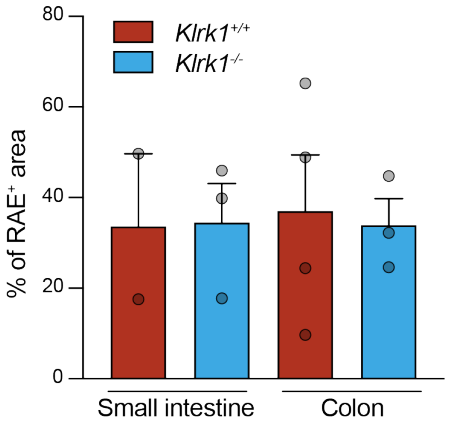

Figure 3.15: Expression of the NKG2D ligand RAE-1 is unaltered *Klrk1*$^{+/+}$ compared to *Klrk1*$^{-/-}$ mice. Immunohistochemical quantification of RAE-1^{+} area in naive *Klrk1*$^{+/+}$ compared to *Klrk1*$^{-/-}$ mice in the small intestine (left) and colon (right) of mice aged 20 weeks and above. n $\geq$ 3, except small intestine *Klrk1*$^{+/+}$, where n = 2. Data represented as mean $\pm$ SEM.

3.1.2.7 NKG2D deficiency does not influence the composition of the fecal microbiota

It is well established that the immune system and the microbiota are tightly connected and evidence suggests a particular role for the NKG2D/NKG2DL axis in microbiota crosstalk (Hansen *et al.* 2013). No differences in NKG2DL expression were observed in the absence of NKG2D and the microbiota of naive *Klrk1*$^{+/+}$ and *Klrk1*$^{-/-}$ mice were therefore expected to be alike. However, various other mechanisms can lead to changes in the microbial composition and I wanted to exclude the possibility of changes in the microbiota due to minor differences in immune composition. I performed 16S rRNA gene sequencing on fecal samples collected from naive *Klrk1*$^{+/+}$ and *Klrk1*$^{-/-}$ mice at 3, 10 and 18 weeks of age. PCoA revealed no genotypic differences (Figure 3.16a) and Alpha diversity was similar between *Klrk1*$^{+/+}$ and *Klrk1*$^{-/-}$ mice (Figure 3.16b). Similar to humans, the most prevalent phyla in the fecal microbiota of were *Bacteroides* and *Firmicutes*. Further, *Actinobacteria*, *Patescibacteria* and *Proteobacteria* were detected, but at much lower frequencies (Figure 3.16c). Analysis at the rank of Family revealed that *Lachnospiraceae* and *Lactobacillaceae* were the most abundant families among *Firmicutes*, while further analysis of *Bacteroidetes* revealed a high frequency of *Muribaculaceae* (Figure 3.16d). I conclude that the microbiota of naive *Klrk1*$^{+/+}$ and *Klrk1*$^{-/-}$ mice is indeed compara-

ble and that lack of NKG2D does not lead to major changes in the fecal microbiota. This study does not exclude the possibility of differential expression of microbial metabolites or changes in the microbiota not detected by the low sample size.

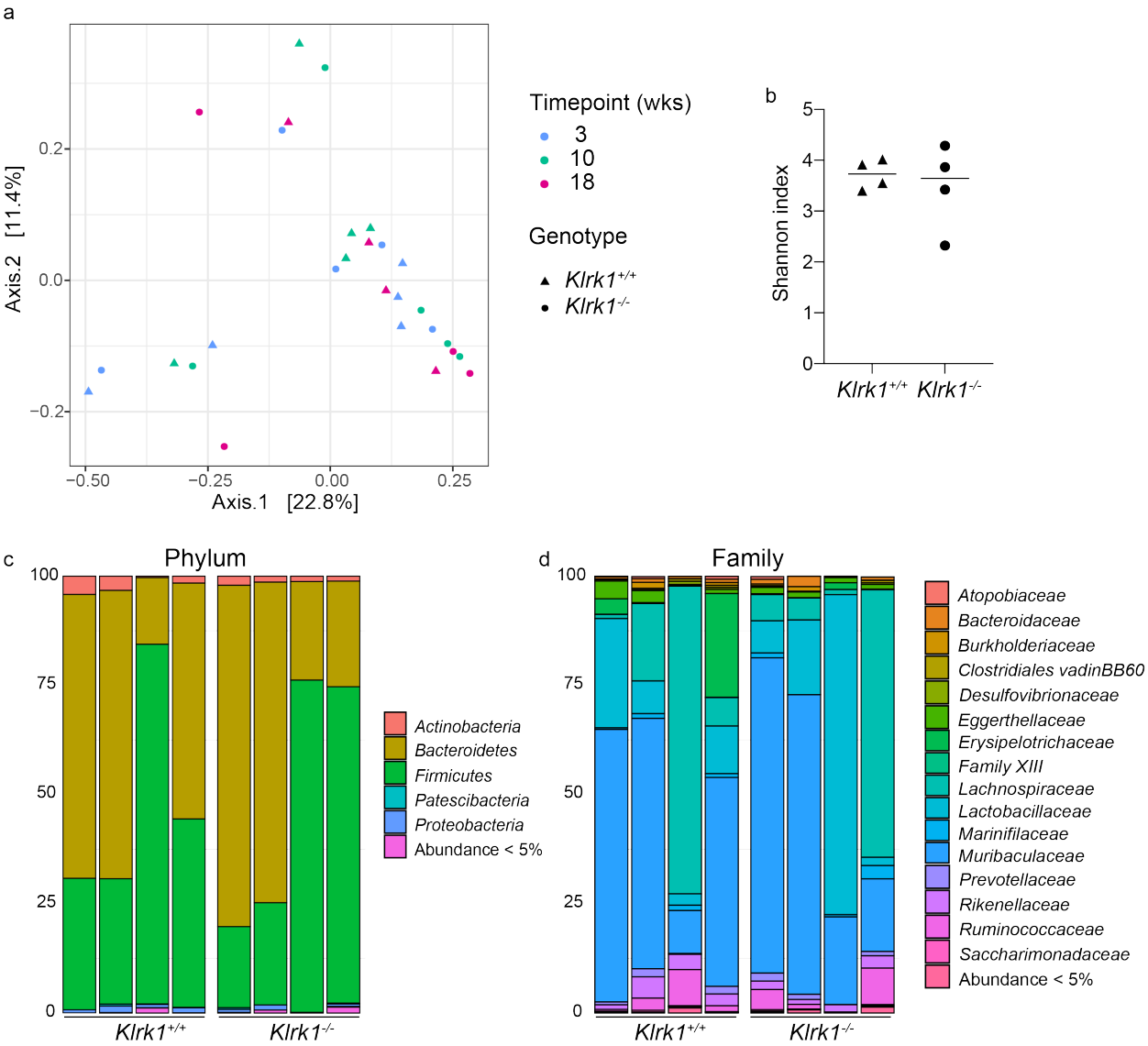

Figure 3.16: Composition of the fecal microbiota of naive *Klrk1*$^{+/+}$ and *Klrk1*$^{-/-}$ mice is alike. (a) Weighted UniFrac PCoA of the fecal microbiota of naive *Klrk1*$^{+/+}$ and *Klrk1*$^{-/-}$ mice at 3, 10 and 18 weeks of age. (b) Alpha diversity, measured as Shannon index, of *Klrk1*$^{+/+}$ and *Klrk1*$^{-/-}$ mice at 18 weeks. (c) Relative abundance of fecal bacteria at the rank of phylum. (d) Relative abundance of fecal bacteria at the rank of family. wks = weeks, PCoA = Principal component analysis.

3.1.2.8 Setting up a 25-color panel to unravel intestinal immune cell function

Our flow cytometric analysis in this and the following chapters was limited to 18 colors due to the setup of the flow cytometer available at the time of experiments. I aimed to increase the previous flow cytometry panel from 18 to 25 colors to allow characterization of further immune cell subsets found in the intestine using a spectral analyzer. For this, I carefully designed a panel with minimal overlap of antibodies binding to proteins co-expressed on the same cell (Table 3.2). I was able to include further markers, including the cytokines Granzyme B and TNF-α , Foxp3 (to identify T_{reg} cells), F4/80 (to identify macrophages) CD206 (to distinguish pro- and anti-inflammatory 'M2' macrophages) and CD107a (a degranulation marker). Instead of CD19, B cells were identified using B220, a protein constitutively expressed by B cells. The panel was designed to be used to characterize not only healthy intestinal tissue, but also TILs.

Table 3.2: Panel for flow cytometric analysis using the Cytek Aurora.

	Fluorophore	Antigen
UV2	BUV395	CD8
UV6	Zombie UV	Viability
UV7	BUV495	CD4
UV11	BUV661	Ly6G
UV14	BUV737	CD3
V1	BV421	F4/80
V3	eFluor450	IFNγ
V7	VioGreen	CD11b
V10	BV605	Ly6C
V11	BV650	NK1.1
V13	BV711	T-bet
V15	BV786	B220
B1	Vio515	CD200R
B2	FITC	CD127
B8	PerCp	CD107a
B9	PerCpCy5.5	CD206
B10	PerCp-eFluor710	PD-1
YG1	PE	NKG2D
YG3	PE-eFluor610	RORgt
YG5	PE-Cy5	γδTCR
YG9	PE-Cy7	IL-17
R1	APC	Foxp3
R2	AF647	Granzyme B
R4	AF700	CD45
R7	APC-Cy7	TNFα

The panel was carefully tested and optimized, which included ensuring minimal unspecific staining and spectral overlap by running FMO samples for all colors. As previously mentioned, one of the main difficulties with working with intestinal tissue is the fact that cell preparations often include dead cells, epithelial cells and mucus resulting in a strong autofluorescent signal. One way to avoid this is to perform Percoll gradient centrifugation, which inevitably results in cell loss. Cytek systems are able to extract autofluorescence from samples by detecting the full spectrum of unstained samples. I tested this by comparing flow cytometry plots of cells where autofluorescent cells were removed versus traditional gating without the removal of autofluorescent cells (Figure 3.17) and concluded that removing autofluorescent cells significantly improves the staining and identification of immune cell populations.

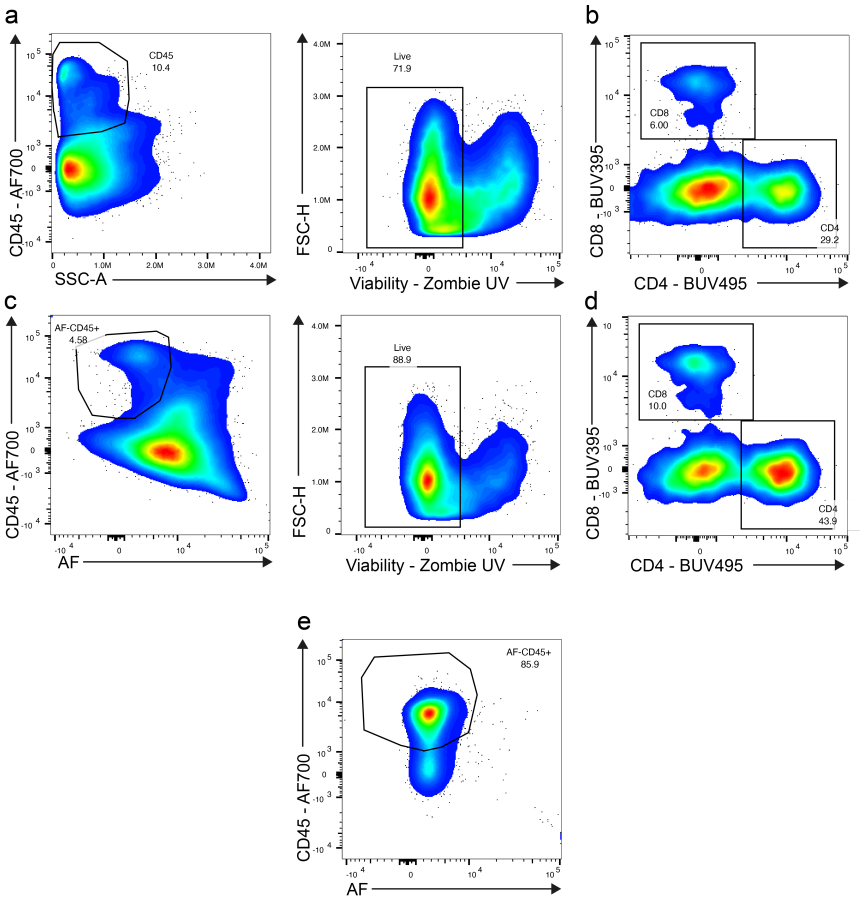

Figure 3.17: Removing autofluorescent cells significantly reduces noise. (a) Exemplary flow cytometry plots of lymphocytes isolated from the cLP of naive *Klrk1*$^{+/+}$ mice. (b) Flow cytometry plot of T cells (gated on CD3^{+} cells). (c) Exemplary flow cytometry plots of lymphocytes including the removal of autofluorescent cells. (d) Flow cytometry plot of T cells (gated on CD3^{+} cells) after the removal of autofluorescent cells. (e) Flow cytometry plot depicting autofluorescent signal on lymphocytes isolated from the MLN, used as a negative control. cLP = colonic lamina propria, MLN = mesentery lymph nodes, AF = autofluorescence.

Previously, live immune cells were identified by selecting lymphocytes singlets using the forward scatter (FSC) and sideward scatter (SSC) and gating on $CD45^+$ and Viability Dye^- cells (Figure 3.17a). The additional autofluorescence channel allowed gating on $CD45^+$ and $autofluorescent^-$ cells before exclusion of dead cells (Figure 3.17c). Directly comparing flow cytometry plots of $CD4^+$ and $CD8^+$ staining on $CD3^+$ T cells revealed that removal of autofluorescent cells significantly improved the quality of the staining. Unspecific noise was removed (seen on the x-axis in Figure 3.17b) and populations were cleaner. Further, frequencies increased from 29.2% to 43.9% $CD4^+$ T cells and 6.0% to 10.0% $CD8^+$ T cells when autofluorescent cells were removed, suggesting that autofluorescent cells skew cell populations by increasing the frequency of unstained cells (Figure 3.17b and d). MLN were used as a negative control as lymph nodes are typically clean and do not contain autofluorescent cells (Figure 3.17e).

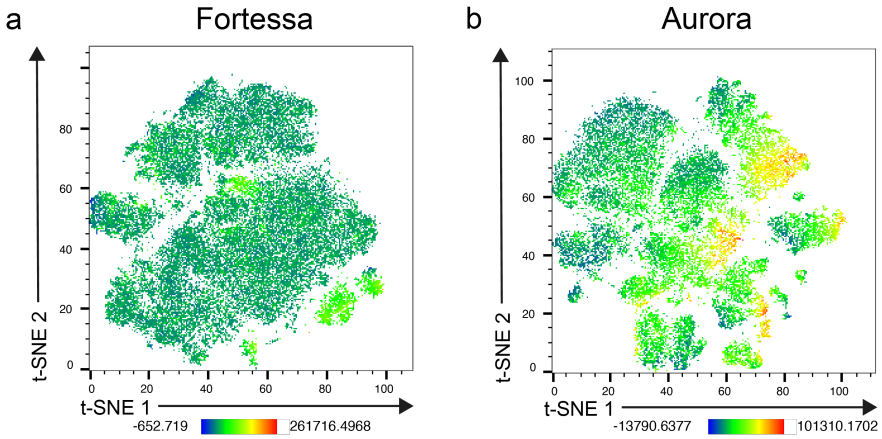

Figure 3.18: tSNE plots of colonic immune cells acquired on different flow cytometers. (a) tSNE plot of cells isolated from the cLP of naive *Klrk1*$^{+/+}$ mice acquired on the BD Fortessa. (b) tSNE plot of cells isolated from the cLP of naive *Klrk1*$^{+/+}$ mice acquired on the Cytek Aurora. Colors indicate median fluorescence intensity of CD3.

Previously, performing complex analysis such as meaningful dimensionality reduction was difficult due to the high level of unspecific staining and background noise. Clustering algorithms, such as tSNE, failed to provide distinct clusters. I directly compared tSNE plots from colonic tissue acquired on the Fortessa to samples acquired on the Aurora. Not only were clusters much more distinct, populations were easier to identify due to higher MFI (Figure 3.18). Together, this confirms that flow cytometric analysis using the Cytek Aurora system provides cleaner cell populations that allow complex downstream analysis.

3.1.3 Discussion

Understanding expression pattern and function of NKG2D and its ligands is of significant importance in understanding mechanisms leading to NKG2D-mediated disease. Here, I provide a in-depth characterization of the NKG2D/NKG2D ligand axis in the healthy mouse intestine and determine the impact of NKG2D deficiency on the intestinal immune composition. Using multi-color flow cytometry, I provide a comprehensive picture of the immune cell composition in the intestine and MLN. I quantified NKG2D expression on intestinal immune cells and found that NKG2D is expressed on a number of intestinal immune cells, including NK cells, ILC1s, ILC3s, $CD4^+$ and $CD8^+$ T cells as well as γδT cells. NKG2D expression is significantly higher on NK cells and T cells isolated from the colonic LP compared to cells isolated from MLN, underlining a particular role for NKG2D-expressing cells in mucosal tissue. I show that germline deletion of NKG2D is not associated with any gross anomalies, but results in minor changes in the immune environment. Specifically, I observed an increased frequency of ILC3s and a decrease of $CD4^+$ T cells in *Klrk1*$^{-/-}$ mice compared to wild-type controls, as well as higher frequencies of IFNγ-producing ILC1s. Gene expression of *Gzmb* and *Cxcl9* was significantly decreased in the absence of NKG2D. No changes in microbial composition or expression of NKG2DL were observed.

3.1.3.1 Intestine-specific changes in ILC3s and $CD4^+$ T cells in NKG2D-deficient mice

Klrk1$^{-/-}$ mice have been studied extensively and some evidence for developmental defects in the absence of NKG2D exists. Differences in frequencies of splenic NK cells (Zafirova *et al.* 2009) as well as reduced expression of the inhibitory NK cell receptors Ly49G2 and Ly49F (Sheppard *et al.* 2013) have been reported. Further, *Klrk1*$^{-/-}$ mice show a minor defect in the development of peritoneal B1a cells (Lenartić *et al.* 2017) compared to *Klrk1*$^{+/+}$ controls. However, to this date, the impact of NKG2D deficiency on the development of the intestinal immune system has not been studied. This study provides evidence for a role of NKG2D in

the development of intestinal immune cells and shows that *Klrk1*$^{-/-}$ mice display decreased frequencies of ILC3s in the colonic LP and MLN and increased frequencies of CD4^{+} T cells in the colon. Despite all mice being bred on the same genetic background and being housed in comparable conditions, variations in the composition of the intestinal immune compartment from mouse to mouse are significant. This variability raises the question of whether changes in cell frequencies are just a consequence of the inherent variations or whether NKG2D deficiency results in true developmental defects. While the frequency of ILC3s in mice lacking NKG2D was comparable to those of *Klrk1*$^{+/+}$ mice in six out of a total of eleven *Klrk1*$^{-/-}$ mice, five *Klrk1*$^{-/-}$ mice displayed a frequency of ILC3s of 2% or higher. The fact that these datapoints derived from four independent experiments in which *Klrk1*$^{-/-}$ mice were directly compared to *Klrk1*$^{+/+}$ littermates, supports the notion that NKG2D-deficiency is indeed associated with an increased frequency of ILC3s. Further adding to the evidence that NKG2D-deficiency impacts frequencies of ILC3s comes from the observation that percentages were increased in both the colonic LP, as well as MLN. Contrary to this, percentages of CD4^{+} T cells were reduced only in the colonic LP and not MLN of *Klrk1*$^{-/-}$ mice. Babic *et al.* suggested that NKG2D impacts CD4^{+} T cell development and showed that CD4^{+} T cells isolated from *Klrk1*$^{-/-}$ mice have impaired T_H1 and T_H17 responses (Babic *et al.* 2020). Their study reports no differences in the frequencies of CD4^{+} T cells contrary to what was observed in this study. Nonetheless, both studies support the hypothesis that NKG2D directly impacts CD4^{+} T cell functionality. CD4^{+} T cells in the intestine are tissue-resident and often antigen-experienced (Wijk *et al.* 2010), making a defect specifically in the mucosal T cell compartment plausible. Nonetheless, further evidence is needed to support our observations. Increasing the sample size as well as using supplementary methods, such as immunofluorescent staining of ILC3s and CD4^{+} T cells in intestinal tissue will provide valuable insight and confirm whether these findings are physiologically relevant.

Other genotypic differences included the significant decrease in gene transcript of GzB and CXCL9 in *Klrk1*$^{-/-}$ mice compared to wild-type controls. Gene expression is not necessarily correlated with protein expression and secretion of the cytokine or chemokine of interest, but can still provide valuable information on functional differences. CXCR3, the receptor for CXCL9,

is expressed on the majority of $CD4^+$ T cells in humans (Papadakis *et al.* 2004) and on 10% in mice (Kristensen *et al.* 2006, Cohen *et al.* 2013). The decreased frequency of $CD4^+$ T cells in the LP of NKG2D-deficient mice could therefore be related to a decrease in chemotactic signals. However, further functional analysis of NKG2D-deficient $CD4^+$ T cells is required.

3.1.3.2 NKG2D/NKG2DL may act as a regulatory barrier to prevent overreaction of intestinal immune cells

To appreciate the function of the NKG2D/NKG2DL axis in the intestine, it is important to understand the physiological function of constitutive NKG2DL expression on healthy intestinal epithelium. One possible explanation is that constitutive low level engagement of NKG2D elevates the activation threshold of immune cells residing in the healthy intestine, preventing overreaction to harmless antigens. This is not a new concept and has been shown to be relevant in the anti-tumor function of NKG2D. Chronic exposure of NKG2D-expressing NK cells to NKG2DL-expressing tumor cells has been shown to abrogate NK cell function, specifically its cytolytic function *in vitro* (Coudert *et al.* 2005) and *in vivo* (Oppenheim *et al.* 2005). Interestingly, the first study, which investigated several aspects of NK cell function, noted that NK cells exposed to NKG2DL for prolonged periods of time produce higher levels of IFN-γ in comparison to the control condition. A follow-up study further showed that not only signaling through NKG2D and its adapter molecules DAP12 and DAP10 was altered, but that DAP10/12-independent pathways, such as ADCC and missing-self recognition was inhibited as well (Coudert *et al.* 2008). Both studies were performed *in vitro* and focused on NK cell functionality only, therefore providing limited evidence of these mechanisms being of relevance *in vivo*. The study by Oppenheim *et al.*, which utilizes a mouse line overexpressing RAE-1 in all tissues noted no significant differences in T cell functionality, but did not exclude the possibility of an undetected effect on these cells. Notably, sustained engagement was associated with a downregulation of NKG2D from the cell surface, which is contrary to the heightened expression of NKG2D in intestinal NK cells and T cells observed in our study. Yet, the fact that sustained engagement of NKG2D reduced the capability of NK cells to mediate ADCC might be of importance in mucosal tissue to prevent an immune response against IgA-coated

commensal bacteria. Interestingly, I observed an increased frequency of IFN-γ^+ ILC1s in the absence of NKG2D, which is contrary to the observation that sustained engagement of NKG2D results in heightened expression of IFN-γ. Directly comparing NKG2D$^+$ to NKG2D$^-$ cells from the same mouse showed that, in the case of NK cells, the MFI of IFN-γ was increased among NKG2D$^-$ cells compared to NKG2D$^+$ cells. ILC1s showed no difference in the MFI of IFN-γ , though low numbers of ILC1s make it difficult to assess functionality. Again low sample numbers and large variations mean that the results obtained in this study are not conclusive and further evidence is needed.

3.1.3.3 NKG2D expression has no impact on the composition of the microbiota

I observed no changes in the microbiota when comparing naive *Klrk1*$^{+/+}$ to *Klrk1*$^{-/-}$ mice. This lack of genotypic differences consistent with experiments previously performed in the lab by visiting PhD student Ana Montalban-Arques, who performed a thorough study comparing the microbial composition fecal samples as well as mucosal tissue from the colon, cecum, small intestine and stomach of 11 *Klrk1*$^{+/+}$ and 8 *Klrk1*$^{-/-}$ mice (Arques 2016). For this, she performed sequencing on the V1-2 region of the 16S rRNA gene using the Roche 454 Life Science platform and found that while the difference in relative abundance of some genera was found to be statistically significant, the microbiota was comparable between the two genotypes and differences were attributed to normal variation, differences in mouse age and co-housing of some, but not all mice. On the basis of this, I only included four samples per genotype in our sequencing experiment, as the main focus was on determining changes during disease progression (see Chapter 2). We cannot exclude the possibility of changes in the microbial composition not captured in our experiments or differences in the production of metabolites. Indeed, while metagenomic analysis can provide valuable information on changes in the microbial composition associated with disease, metabolomic analysis helps gain further insight into molecular mechanisms involved in cross-talk between the host and the microbiota (Vernocchi *et al.* 2016).

3.1.3.4 Limitations

Being limited to 18 colors meant that I was unable to define all immune cell subsets. Two cell types that have important functions in the intestine are not included in our analysis are ILC2s and macrophages. I decided to focus on ILC1s and ILC3s due to their ability to express NKG2D and their known involvement in intestinal disease and not include markers defining ILC2s, such as the transcription factor GATA3 or the IL-33 receptor ST2. Macrophages are of great importance in intestinal immunity, but their function is complex and including general markers such as F4/80 or CD64 without the possibility to assess their functionality would not have provided much valuable information. Further defining DCs using CD103, ILC3s using NKp46, T cells using CD44 and CD62L or Foxp3 to identify T_{reg} cells would have been of great value, but was not feasible in these experiments. Similarly, staining for additional cytokines, such as IL-22 and GzB would have been of interest. Nonetheless, we provide an overview of the immune cells present in the intestine and MLN and assess their capability to produce IFN-γand IL-17.

One major drawback of this study is the lack of cell quantification. The flow cytometric analysis performed in this study provides percentages only, meaning that all comparisons between genotypes and organs are based on ratios rather than absolute cell numbers. From our study, I cannot conclude whether the increased frequency of ILC3s in the colonic LP of *Klrk1*$^{-/-}$ mice compared to wild-type littermates is due to an increase of absolute cell numbers or merely a consequence of a shift in ratios (for example a decrease of another cell population, such as that of $CD4^+$ T cells) and/or changes in cell influx and efflux. A commonly used way to obtain absolute cell numbers from flow cytometric analysis is to add a known number of 'counting beads' to each sample. The absolute cell number can then be calculated as follows:

$$\frac{\#\text{ of counting beads added to each samples}}{\text{volume of sample}} \times \frac{\#\text{ of cells (of interest) acquired}}{\#\text{ of counting beads acquired}}$$

To be able to compare cell numbers between samples, the amount of cells lost during the isolation and staining procedure must be consistent and to be able to conclude on the absolute number of cells in any given tissue, few cells should be lost. Due to the difficulty of isolating

cells from intestinal tissue, the protocol used in this study involves several steps in which loss of cells is inevitable and depending on the amount of residual mucus, size of the tissue and grade of inflammation, this loss of cells is not consistent among samples. Further, counting beads are not recommended for use with samples that were fixed and permeabilized, again due to loss of cells. I therefore decided against using counting beads, as I believe this would have resulted in inaccurate and unreliable results. An alternative way to compare cell numbers is by immunofluorescent or immunohistochemical staining of the cell type of interest on tissue sections. Staining of tissue sections allows cell type quantification, but also provides valuable evidence of the exact location of each cell type. While I do separate IEL and LPL, I do not know which cells have direct interactions and where exactly in the tissue they are located.

We observed similar frequencies of ILC1s and ILC3s in the colon and MLN of wild-type mice, which is contrary to other studies that have demonstrated a larger proportion of ILC3s compared to ILC1s in the LP. Two studies providing a protocol and gating strategy for the characterization of ILCs in the small intestine both showed that ILC3s make up between 50-75% of all ILCs, while ILC1s are much scarcer and only represent 2-15% (Dutton *et al.* 2018, James *et al.* 2020). They further showed that the distribution of ILCs in the MLN was similar with ILC3s being more abundant than ILC1s. ILCs are less well studied in the colon and little data is available on the frequencies of the different cell subsets. Gating on live $CD45^+$ $CD3^-$ $CD19^-$ cells, Robinette *et al.* showed that ILC1s (defined as $ROR\gamma T^-$ $NKp46^+$ Eomesodermin $(EOMES)^-$) are indeed enriched in the colon compared to the small intestine (Robinette *et al.* 2017), but different gating strategies makes it difficult to directly compare these three studies. Nonetheless, these studies, in particular the last study, which compared small intestinal and colonic cells directly, illustrates organ-specific differences. We cannot exclude the possibility of other factors contributing to the low frequencies of ILC3s observed in our mice. Antibiotic treatment has been shown to reduce the frequency of $ROR\gamma T^+$ ILCs (Vonarbourg *et al.* 2010), suggesting that their presence is dependent on the microbiota. Housing mice in an extremely clean environment, as it is the case in our mouse colony, may explain discrepancies between our observations and other studies. Further, technical limitations could result in an underestimation of ILC3s. To identify ILC3s, we used the anti-$ROR\gamma T$ antibody attached to a PE-CF594

fluorophore, a tandem dye consisting of PE and CF594. PE is one of the biggest fluorophores typically used in flow cytometric analysis and might not reach the RORγT epitope in the nucleus efficiently due to the nuclear pore size.

Low sample numbers make it difficult to draw conclusions on changes in NKG2DL expression. The initial experiments were performed by MRes student Elena Rondeau in 2016 and repeating the exact same experimental procedure in recent years resulted in unspecific staining in control samples, which included RAE-1-deficient transplanted tumor tissue as well as intestinal tissue from mice with a germline deletion of RAE-1 (provided by Prof David Raulet, UC Berkeley). Trouble-shooting of the IHC protocol included titration of the primary and secondary antibody, testing different HIER protocols (changing method, time and intensity), replacing reagents and comparing staining of recently cut tissue samples versus samples that were stored for a prolonged period of time, none of which resulted in a clean negative control staining. There are several explanations for this, I. the manufacturer of one of the RAE-1 antibody (R&D Systems) made minor changes to either the antibody or the buffer or II. the experiments in 2016 yielded in unspecific staining, which was not detected at the time. We therefore cannot with certainty exclude the possibility that the staining is unspecific and the data shown here is an overestimation of RAE-1 expression in the mouse intestine. We have no reason to believe that RAE-1 is absent in the intestine, as other studies have detected RAE-1 protein on mouse intestinal tissue (Li *et al.* 2017, Hansen *et al.* 2013). Moreover, we see changes in percentages of RAE-1$^+$ area in an age-dependent manner in both genotypes, further suggesting that we are indeed able to detect differences in protein expression. However, to draw conclusions on the expression level and functional consequences of changes in NKG2DL expression, further experiments need to be performed. Alternative approaches could include quantifying RAE-1 protein expression on epithelial cells by flow cytometry or Western blot.

3.1.3.5 Conclusions

Together, I demonstrate that both NKG2D as well as NKG2DL are expressed at significant levels in the healthy mouse intestine. I show that germline deletion of *Klrk1* has no major impact on immune cell functionality, suggesting that NKG2D is dispensible in maintaining intestinal homeostasis. Genotypic differences observed in this study will need to be investigated further to understand the intricate function of NKG2D-expressing cells at steady-state.

Lastly, I successfully established a 25-color flow cytometry panel that will enable us to perform in-depth analysis of intestinal immune cells in the future. Not only does the Cytek Aurora allow use of more fluorophores, including fluorophores that have a similar excitation/emission spectrum and cannot be distinguished by the BD Fortessa, it also has the great advantage of being able to extract autofluorescence, resulting in clean cell populations that allow complex down-stream analyses.

3.2 Chapter 2 - NKG2D in a mouse model of intestinal cancer

3.2.1 Introduction

NKG2D has been studied extensively in the context of tumor immunity due to its strong anti-tumor properties. NKG2D is a potent immunoreceptor and its ligands are mainly expressed on transformed or stressed cells, thereby acting as danger signals and facilitating NKG2D-mediated elimination of nascent tumor cells. Upon binding to one of its ligands, NKG2D elicits a strong immune response resulting in the secretion of cytokines and cytotoxic molecules and subsequent target cell death. The presence of NKG2DL on tumor tissue makes NKG2D an important receptor in tumor recognition, which has been confirmed *in vitro* and *in vivo* (Diefenbach *et al.* 2000, Diefenbach *et al.* 2001, Guerra *et al.* 2008). Several studies have explored NKG2D as a potential therapeutic target, with clinical trials harnessing the anti-tumor activity of NKG2D-expressing cells currently underway (Baumeister *et al.* 2018, Xiao *et al.* 2019).

Our lab recently identified a dual role for NKG2D in tumorigenesis and showed that in a mouse model of inflammation-driven liver cancer, NKG2D promotes rather than inhibits tumorigenesis (Sheppard *et al.* 2017, Sheppard *et al.* 2018). When treating *Klrk1*$^{+/+}$ and *Klrk1*$^{-/-}$ with Diethylnitrosamine (DEN), a chemical which induces liver damage and ultimately cancer (Lee *et al.* 2004), NKG2D-sufficient mice displayed decreased survival and increased tumor-burden compared to their NKG2D-deficient littermates. This led to the conclusion that NKG2D exacerbates disease in this chronic model of HCC. CD8$^+$ T cells were preferentially enriched in the inflamed liver of *Klrk1*$^{+/+}$ mice, which was associated with an accumulation of pro-inflammatory cytokines, including IFN-γ, TNF-α and IL-6 in both the tumor as well as the surrounding tissue. Further, PD-1 was upregulated on TILs, suggesting chronic engagement and/or T cell exhaustion contributing to disease severity. These data lead to the hypothesis that chronic engagement of NKG2D by its ligands expressed on tumor cells leads to a pro-inflammatory microenvironment and subsequent tissue damage favoring tumorigenesis.

This hypothesis is supported by previous observations in the MCA-induced fibrosarcoma model.

When mice were treated with a high dose, NKG2D deficiency had no impact on survival, however, when a small dose was administered, resulting in slowly arising tumors, NKG2D-deficient mice displayed a survival benefit, supporting a pro-tumor role for NKG2D in certain environments (Guerra *et al.* 2008). Specifically, in settings of chronic inflammation and slowly arising tumors, as is the case in the MCA and DEN model, NKG2D appears to favor tumorigenesis. Indeed, a pro-inflammatory role for NKG2D in chronic inflammation has previously been demonstrated in a number of studies. Dysregulated ligand expression and NKG2D-mediated disease has been observed in atherosclerosis (Xia *et al.* 2011), diabetes (Ogasawara *et al.* 2004), asthma (Farhadi *et al.* 2014) and experimental autoimmune encephalitis (Guerra *et al.* 2013). These studies reveal a disease-promoting role for NKG2D-expressing cells and underline the importance in understanding what mechanisms lead to NKG2D/NKG2DL-mediated disease.

The intestine is of particular interest in studying NKG2D in the setting of inflammation-driven tumorigenesis, as chronic intestinal inflammation, such as IBD, is a known risk factor for the development of CRC. Understanding molecular mechanisms contributing to disease is of great importance as CRC accounts for 600,000 deaths worldwide each year, thereby making it the fourth most common type of cancer (Bray *et al.* 2018). Despite major efforts in improving therapies to treat CRC, the 5-year relative survival rate is only 64% (Bray *et al.* 2018). ICI therapy, which has significantly improved patient outcome in a variety of cancers, only shows limited anti-tumor activity in CRC patients. Only a subgroup of patients, specifically those with dMMR and MSI-H, which make up only 10-20% of all patients (Koopman *et al.* 2009), have shown to benefit from PD-1 blockade immunotherapy (Le *et al.* 2015).

To address the question of whether NKG2D contributes to tissue damage and tumorigenesis in settings of chronic intestinal inflammation and to better understand mechanisms involved in the tumor immune response, we used the $Apc^{min/+}$ mouse model of familial adenomatous polyposis. The $Apc^{min/+}$ mouse harbors a point mutation in the *Apc* gene, resulting in the development of multiple intestinal neoplasia and colon carcinoma. Tumor development in this model is comparable to human familial adenomatous polyposis and due to its chronicity and inflammatory properties, it constitutes a good model to study chronic inflammatory disease leading to tumorigenesis (Moser *et al.* 1995). Indeed, lack of the adapter protein MyD88, a

crucial signaling molecule associated in immune cells and involved in intestinal tissue repair significantly abrogates disease severity in $Apc^{min/+}$ mice (Rakoff-Nahoum *et al.* 2007), suggesting that this model is appropriate in studying the impact of NKG2D in inflammation-driven intestinal cancer.

I studied the expression and function of NKG2D on several immune effector cells localized in the tumor microenvironment during tumor development and demonstrate that NKG2D does indeed promote tumorigenesis and disease severity, underlining the importance of understanding the context-dependent pro- and anti-tumor function of immune cells in the tumor microenvironment. I further analyzed changes in the microbiota associated with disease progression and used RNAseq datasets to study changes in the NKG2D/NKG2DL axis in human intestinal cancer.

This project was initiated by previous lab members Chiara Triulzi and Jenny McGovern, who acquired the majority of data relating to disease endpoint. This included macroscopic data, such as survival, tumor burden (at 10-12 weeks and disease endpoint) and hematocrit (HCT) (at disease endpoint) as well as flow cytometry, with the exception of data relating to PD-1. Further, histological analyses were performed by M.Sc. student Elena Rondeau under the supervision of Jenny McGovern. Previously collected data was critically analyzed, including the reanalysis of all flow cytometry data. The experimental arm of this project focused on the characterization of the immune response and genotypic differences at 18-20 weeks, but additional experiments on tissue collected by previous lab members, such as transcriptional analyses were performed as part of this PhD. Further, as part of an additional scholarship (Stevenson Fund, awarded by Imperial College London), microbiota analysis was performed in collaboration with the University of Otago, Christchurch. A main aim of this PhD was to fill the knowledge gaps and present the results in the format of a scientific paper.

Aims:

1. To collect, interpret and (if required) reanalyze previously acquired data.
2. To characterize the immune response in 18-20 weeks old $Apc^{min/+}$ mice and identify potential genotypic differences between $Klrk1^{+/+}$ and $Klrk1^{-/-}$ mice.
3. To analyze changes in the microbiota relating to disease development in $Apc^{min/+}$ mice and/or NKG2D-deficiency.
4. To compare mouse data to that from human patients.

3.2.2 Results

3.2.2.1 NKG2D promotes tumorigenesis in a mouse model of intestinal tumors

To test the hypothesis that NKG2D exacerbates intestinal inflammation associated with tumorigenesis, we used *Apc*$^{min/+}$ mice intercrossed with *Klrk1*$^{+/-}$ mice to generate NKG2D-sufficient *Apc*$^{min/+}$ *Klrk1*$^{+/+}$ and NKG2D-deficient *Apc*$^{min/+}$ *Klrk1*$^{-/-}$ mice.

In a first step, I examined the level of expression of NKG2D on TILs. To this end, I isolated lymphocytes present in the tumor of *Apc*$^{min/+}$ *Klrk1*$^{+/+}$ mice. NKG2D MFI was increased on CD8$^+$ T cells, γδT cells and NK cells, but not CD4$^+$ TIL compared to IELs from healthy mice. The largest increase in MFI was seen on γδT cells with a 5-fold increase and on NK cells with a 2-fold increase (Figure 3.19a). This was reflected in frequencies with a significant increase of NKG2D$^+$ CD8$^+$ T cells (0.63% among IEL and 4% among TIL) and γδT cells (0.62% to 5.2%) (Figure 3.19b).

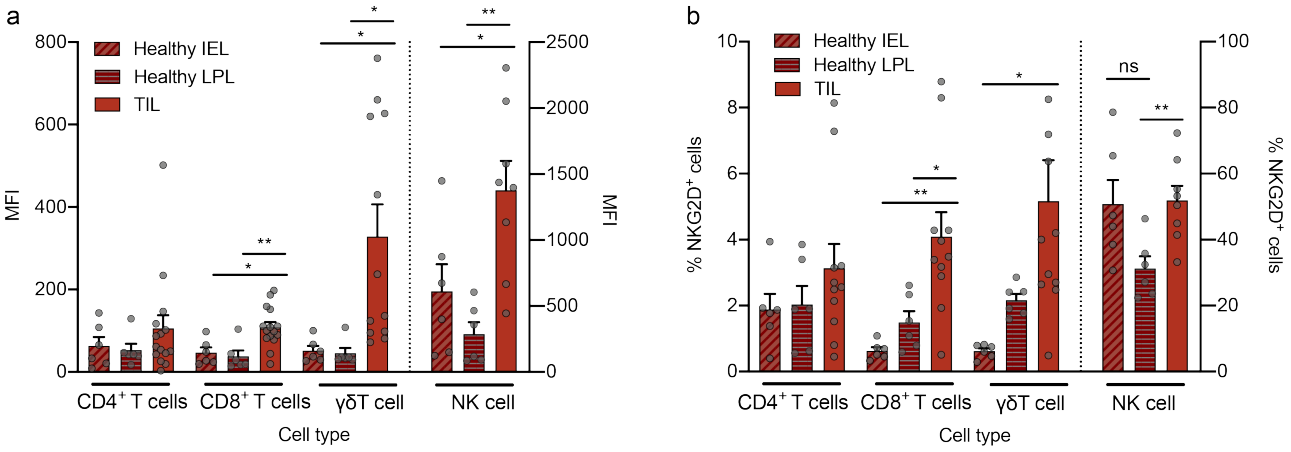

Figure 3.19: Elevated NKG2D expression on TILs in *Apc*$^{min/+}$ mice. (a) Frequencies of NKG2D-expressing cells in healthy IEL and LPL compared to SI TIL in *Apc*$^{min/+}$*Klrk1*$^{+/+}$ mice at 18-20 weeks. n ≥ 6. (b) MFI of NKG2D on in healthy IEL and LPL compared to SI TIL in *Apc*$^{min/+}$*Klrk1*$^{+/+}$ mice at 18-20 weeks. n ≥ 6. TIL = tumor-infiltrating lymphocyte, SI = small intestine, LPL = lamina propria lymphocytes, IEL = intraepithelial lymphocytes, MFI = median fluorescent intensity. Bars represent mean ± SEM of individual mice from at least three independent experiments. n ≥ 6. * p ≤ 0.05, ** p ≤ 0.01.

Having observed this increased expression of NKG2D in the context of tumor growth, we hypothesized that NKG2D plays a pro-inflammatory and pro-tumor role in the *Apc*$^{min/+}$ mice. In line with this hypothesis, survival of *Apc*$^{min/+}$ *Klrk1*$^{+/+}$ mice was significantly decreased

compared to *Apc*$^{min/+}$ *Klrk1*$^{-/-}$ littermates, with a mean survival of 21.8 weeks in *Apc*$^{min/+}$ *Klrk1*$^{+/+}$ mice compared to 26.7 weeks in mice lacking NKG2D (Figure 3.20a), as well as a two-fold increase in colon tumor burden (mean of 1.87 in *Apc*$^{min/+}$ *Klrk1*$^{+/+}$ compared to 0.86 in *Apc*$^{min/+}$ *Klrk1*$^{-/-}$ mice, Figure 3.20b). HCT was measured as an additional read-out of disease severity, as *Apc*$^{min/+}$ mice are known to develop severe anemia as a consequence of intestinal tumor development. Blood collected at disease endpoint show that the anemia was exacerbated in *Apc*$^{min/+}$ *Klrk1*$^{+/+}$ compared to *Apc*$^{min/+}$ *Klrk1*$^{-/-}$ mice (HCT of 13% and 19.9% respectively, compared to 41.6% in control mice) (Figure 3.20c), further supporting the observations that tumor progression is indeed advanced in *Apc*$^{min/+}$ *Klrk1*$^{+/+}$ mice. Anemia is a consequence of the high number of multiple intestinal polyps in the small intestine, which can exceed 100 tumors per mouse and leads to significant blood loss. We assessed the number of small bowel tumors at several time points, with *Apc*$^{min/+}$ *Klrk1*$^{+/+}$ mice showing a 2.8-fold increase at early stages of disease development (10-12 weeks) compared to *Apc*$^{min/+}$ *Klrk1*$^{-/-}$ mice. There were minor differences at 18-20 weeks (mean of 36 in *Apc*$^{min/+}$ *Klrk1*$^{+/+}$ and 25.8 in *Apc*$^{min/+}$ *Klrk1*$^{-/-}$) and at disease endpoint, which varied between 18 and 45 weeks (mean of 60 tumors in *Apc*$^{min/+}$ *Klrk1*$^{+/+}$ versus 54.3 tumors in *Apc*$^{min/+}$ *Klrk1*$^{-/-}$ mice) (Figure 3.20d). We observed an inverse correlation between the number of small bowel polyps at disease endpoint and mouse survival (Figure 3.20e), in both *Apc*$^{min/+}$ *Klrk1*$^{+/+}$ (top, $R^2 = 0.16$, $p = 0.014$) and *Apc*$^{min/+}$ *Klrk1*$^{-/-}$ (bottom, $R^2 = 0.27$, $p = 0.0023$) mice, indicating that the majority of tumors in *Apc*$^{min/+}$ *Klrk1*$^{+/+}$ mice develop before 25 weeks (dotted line), while this appears to be delayed in *Apc*$^{min/+}$ *Klrk1*$^{-/-}$ mice.

Together, the decreased overall survival, increased tumor burden in the colon and exacerbated anemia indicate aggravated disease in *Apc*$^{min/+}$ *Klrk1*$^{+/+}$ compared to *Apc*$^{min/+}$ *Klrk1*$^{-/-}$ mice and supports the hypothesis of a pro-tumor effect of NKG2D in this model.

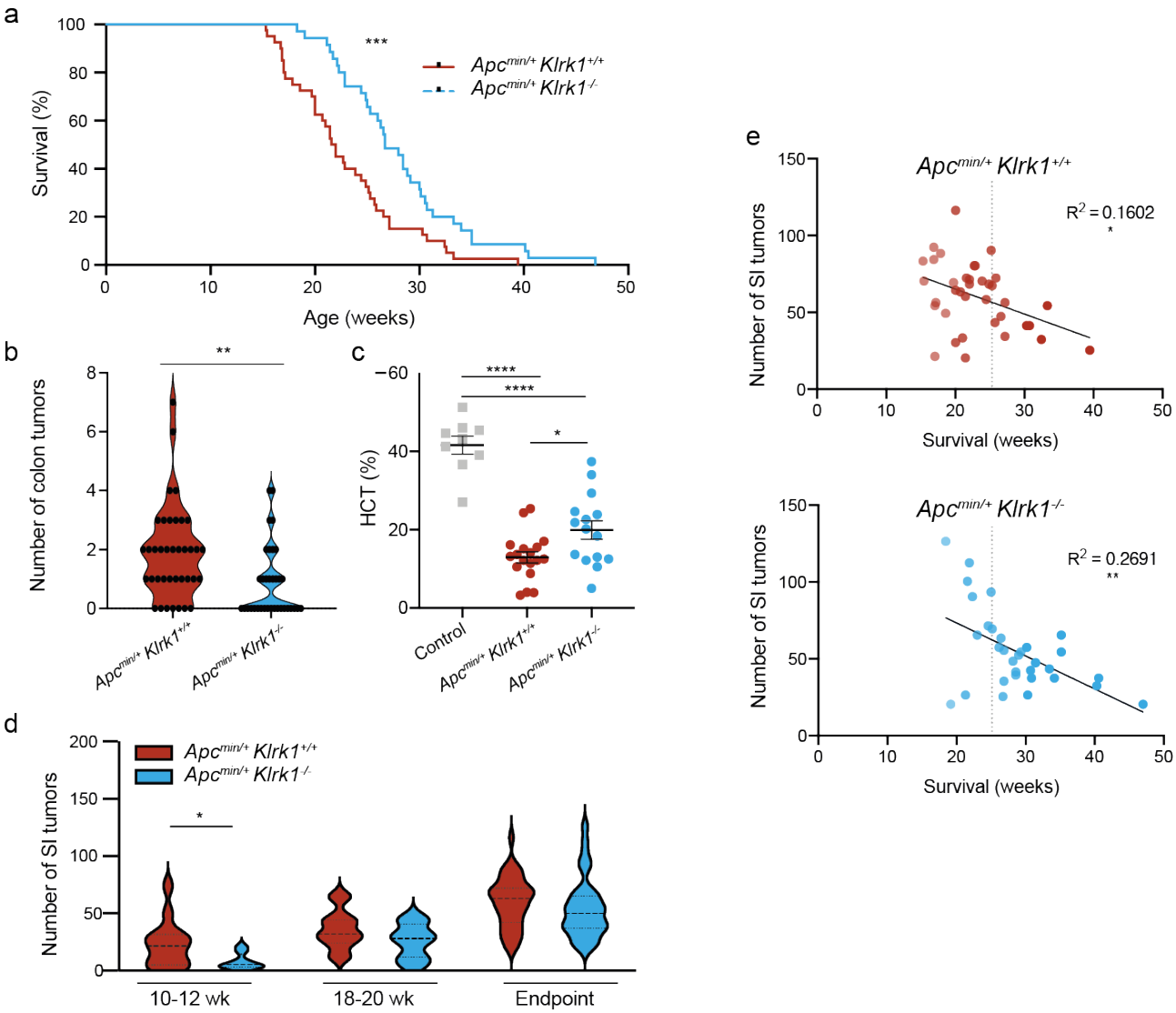

Figure 3.20: NKG2D drives disease in the *Apc$^{min/+}$* model of intestinal cancer. (a) Kaplan-Meier representation of *Apc$^{min/+}$ Klrk1$^{+/+}$* (n = 35) and *Apc$^{min/+}$ Klrk1$^{-/-}$* (n = 40) mice. (b) Number of tumors in the colon at disease endpoint in *Apc$^{min/+}$ Klrk1$^{+/+}$* and *Apc$^{min/+}$ Klrk1$^{-/-}$* mice. n $\geq$ 35. (c) HCT of healthy wild-type control mice and *Apc$^{min/+}$ Klrk1$^{+/+}$* and *Apc$^{min/+}$ Klrk1$^{-/-}$* mice at disease endpoint. n $\geq$ 9. (d) Frequencies of small bowel tumors at 10-12 weeks, 18-20 weeks and disease endpoint of *Apc$^{min/+}$ Klrk1$^{+/+}$* and *Apc$^{min/+}$ Klrk1$^{-/-}$* mice. n $\geq$ 12. (e) Correlation between number of small bowel tumors and survival in *Apc$^{min/+}$ Klrk1$^{+/+}$* (top) and *Apc$^{min/+}$ Klrk1$^{-/-}$* (bottom) mice. wk = week, HCT = haematocrit, IEL = intraepithelial lymphocytes, MFI = median fluorescent intensity. Bars represent mean $\pm$ SEM. n $\geq$ 6. Significance in a was determined using Log-rank (Mantel-Cox) test. * p$\leq$ 0.05, ** p $\leq$ 0.01, *** p $\leq$ 0.001 and **** p $\leq$ 0.0001.

3.2.2.2 NKG2D promotes T cell accumulation and IFN-γ production at advanced stages of the disease

The upregulation of NKG2D on TILs and the decreased survival of *Apc$^{min/+}$ Klrk1$^{+/+}$* compared to *Apc$^{min/+}$ Klrk1$^{-/-}$* mice suggests that the presence of NKG2D triggers an immune response that ultimately favors tumor growth. To assess how and to what extent the presence of NKG2D influences immune cell infiltration into the tumor, we performed flow cytometric analysis to assess frequencies of the tumor-infiltrating immune cell subsets. The analysis was done at 18-20 weeks when tumors are numerous enough to yield sufficient number of lymphocytes for *ex vivo* analysis as well as at disease endpoint. B and T cells made up the largest proportion of TILs at 18-20 weeks with 40-50% and 32-36%, respectively, with few NK cells (1%). Yet, no difference between *Apc$^{min/+}$ Klrk1$^{+/+}$* to *Apc$^{min/+}$ Klrk1$^{-/-}$* mice was seen at that timepoint (Figure 3.21a). Disease endpoint is defined as the humane endpoint, where the disease is so advanced that mice reach a severity limit. Flow cytometric analysis at disease endpoint revealed a decrease in B cells (from 40% at 18-20 weeks to 8% at disease endpoint), an increase in myeloid cells (from 20% at 18-20 weeks to 38.9% (*Apc$^{min/+}$ Klrk1$^{+/+}$*) and 46.2% (*Apc$^{min/+}$ Klrk1$^{-/-}$*) at disease endpoint) and an increase in NK cells (from $< 1\%$ at 18-20 weeks to 2.4% (*Apc$^{min/+}$ Klrk1$^{+/+}$*) and 1.9% (*Apc$^{min/+}$ Klrk1$^{-/-}$*) at disease endpoint). The frequency of T cells was significantly higher in *Apc$^{min/+}$ Klrk1$^{+/+}$* compared to *Apc$^{min/+}$ Klrk1$^{-/-}$* mice, from which we infer that NKG2D promotes T cell infiltration and/or accumulation at late stages of the disease (Figure 3.21b). Further characterization of the T cell subsets showed that the difference in frequency was due to an increased percentage of CD8$^+$ T cells (Figure 3.21c and d) in the tumors of *Apc$^{min/+}$ Klrk1$^{+/+}$* mice compared to *Apc$^{min/+}$ Klrk1$^{-/-}$* littermates.

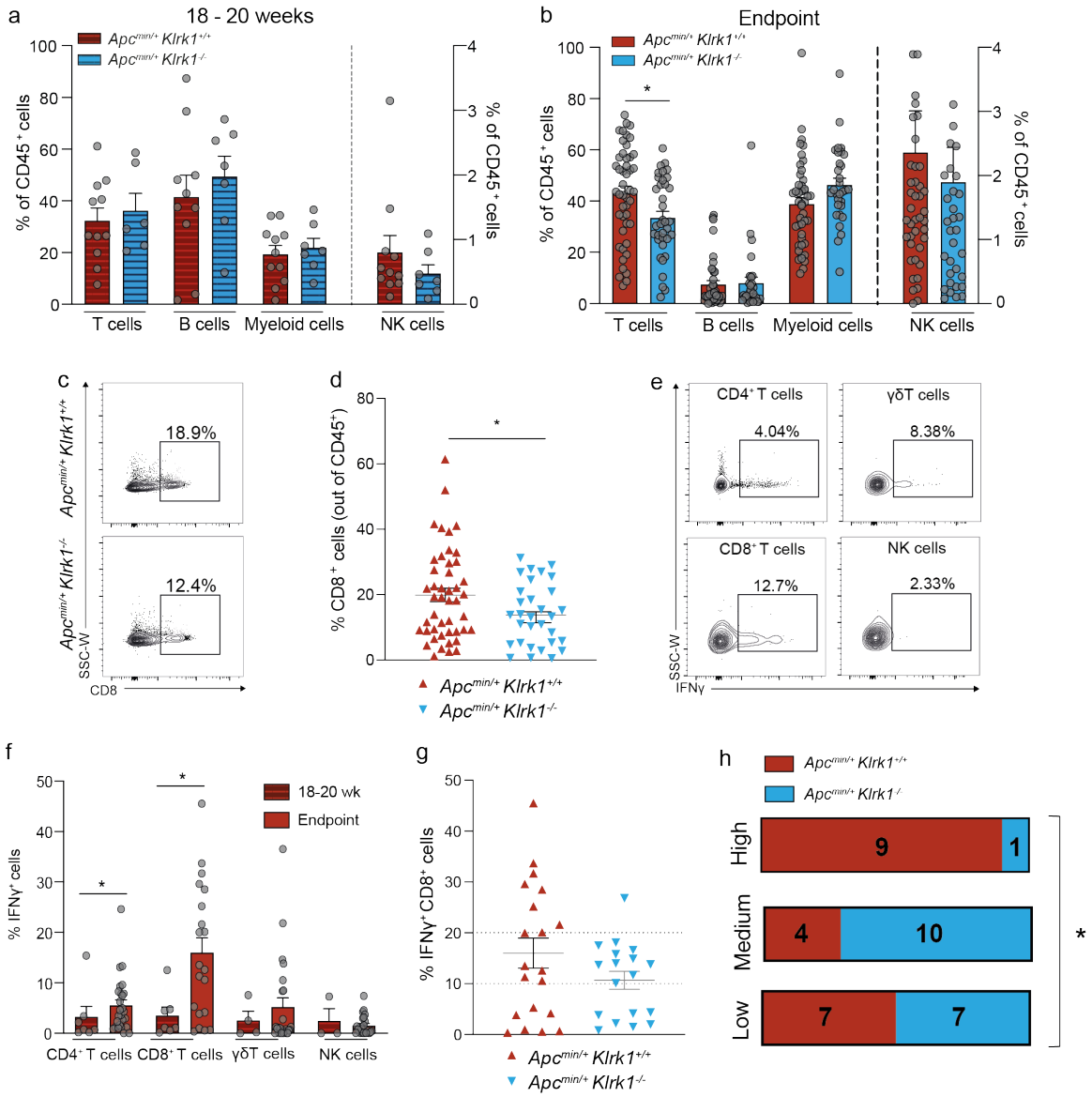

Figure 3.21: IFN-γ-producing CD8$^+$ T cells accumulate in tumors of *Apc$^{min/+}$ Klrk1$^{+/+}$* mice at disease endpoint. (a) Frequencies T cells (CD3$^+$), B cells (CD19$^+$), myeloid cells (CD11b$^+$) and NK cells (NK1.1$^+$CD3$^-$) in the SI TME of *Apc$^{min/+}$ Klrk1$^{+/+}$* compared to *Apc$^{min/+}$ Klrk1$^{-/-}$* mice at 18-20 weeks. n $\geq$ 6. (b) Frequencies T cells, B cells, myeloid cells and NK cells in the SI TME of *Apc$^{min/+}$ Klrk1$^{+/+}$* compared to *Apc$^{min/+}$ Klrk1$^{-/-}$* mice at disease endpoint. n $\geq$ 30. (c) Representative flow cytometry plots of CD8$^+$ T cells in the SI TME, gated on CD3$^+$ lymphocytes. (d) Frequencies of CD8$^+$ T cells (gated on CD3$^+$ lymphocytes) in the SI TME at disease endpoint in *Apc$^{min/+}$ Klrk1$^{+/+}$* compared to *Apc$^{min/+}$ Klrk1$^{-/-}$* mice. (e) Representative flow cytometry plots of IFN-γ-expressing cells (gated on CD8, CD4 or γδTCR following selection of CD3$^+$ lymphocytes) and NK cells (CD3$^-$NK1.1$^+$) following stimulation with PMA and ionomycin, in the SI TME at disease endpoint. (f) Frequencies of IFN-γ-producing cells and NK cells following stimulation with PMA and ionomycin, in the SI TME of *Apc$^{min/+}$ Klrk1$^{+/+}$* mice at 18-20 weeks compared to endpoint. n $\geq$ 5. (g) Frequencies of IFN-γ$^+$ CD8$^+$ T cells (gated on CD3$^+$ lymphocytes) following stimulation with PMA and ionomycin, in *Apc$^{min/+}$ Klrk1$^{+/+}$* compared to *Apc$^{min/+}$ Klrk1$^{-/-}$* mice in the SI TME at disease endpoint. (h) Categories of IFN-γ levels produced by CD8$^+$ T cells (gated on CD3$^+$ lymphocytes) following stimulation with PMA and ionomycin, in *Apc$^{min/+}$ Klrk1$^{+/+}$* compared to *Apc$^{min/+}$ Klrk1$^{-/-}$* mice in the SI TME at disease endpoint. SI = small intestine, TME = tumor microenvironment. Bars represent mean ± SEM of individual mice from at least five independent experiments. * p $\leq$ 0.05. Significance in h determined by Chi-Squared test.

Next, we assessed the functionality of these CD8$^+$ T cell types by means of IFN-γ production - a cytokine which can have both pro- and anti-tumorigenic properties (Wang *et al.* 2015a, Hanada *et al.* 2006). Frequencies of IFN-γ-producing T and NK cells were low at 18-20 weeks, but significantly increased as the disease progressed (Figure 3.21e and f). The most striking increase in the frequency of IFN-γ-producing cells was observed among CD8$^+$ T cells, with 3.5% of cells producing IFN-γ at 18-20 weeks and 16% at disease endpoint (Figure 3.21f).
We categorized the ability of T cells to produce IFN-γ into three categories: 'high' (> 20%), 'medium' (10-20%) and 'low' (< 10%) (Figure 3.21g). When comparing *Apc$^{min/+}$ Klrk1$^{+/+}$* to *Apc$^{min/+}$ Klrk1$^{-/-}$*, we observed a significantly higher fraction of IFN-γ-high producing CD8$^+$ T cells among *Apc$^{min/+}$ Klrk1$^{+/+}$* mice than *Apc$^{min/+}$ Klrk1$^{-/-}$* (Figure 3.21g and h). Mice falling into the 'low' category were evenly distributed among genotypes (7 *Apc$^{min/+}$ Klrk1$^{+/+}$* and 7 *Apc$^{min/+}$ Klrk1$^{-/-}$*), 4 *Apc$^{min/+}$ Klrk1$^{+/+}$* mice were classified as 'medium' and 9 as 'high'. Conversely, 10 *Apc$^{min/+}$ Klrk1$^{-/-}$*, mice had a 'medium' frequency of IFN-γ$^+$ CD8$^+$ T cells and only 1 'high' (Figure 3.21h). We hypothesize that the higher proportion of IFN-γ$^+$ CD8$^+$ T cells in NKG2D-sufficient versus -deficient mice results in an accumulation of IFN-γ in the TME in an NKG2D-dependent manner.

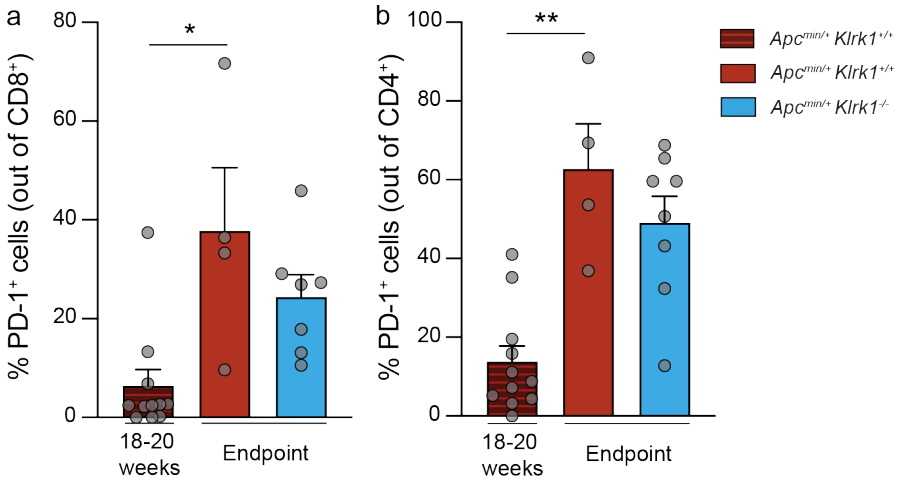

Figure 3.22: High frequencies of CD4$^+$ and CD8$^+$ T cells express PD-1 in the TME. Frequencies of PD-1-expressing CD8$^+$ (a) and CD4$^+$ (b) T cells (gated on CD3$^+$ lymphocytes) in the SI TME of *Apc$^{min/+}$ Klrk1$^{+/+}$* mice at 18-20 weeks (left) (n ≥ 12) and frequencies of PD-1-expressing T cells in the TME of *Apc$^{min/+}$ Klrk1$^{+/+}$* and *Apc$^{min/+}$ Klrk1$^{-/-}$* mice disease endpoint (right) (n ≥ 3). Bars represent mean ± SEM of individual mice from at least three independent experiments. * p ≤ 0.05, ** p ≤ 0.01.

PD-1, a marker associated with T cell activation and exhaustion was expressed by 40% of $CD8^+$ T cells at disease endpoint, but not earlier stages (< 10%) (Figure 3.22 a), suggesting strong activating signals leading to the upregulation of inhibitory receptors as the disease progresses. Similarly, frequencies of PD-1-expressing $CD4^+$ T cells was low at 18-20 weeks (13.8%) and increased to 62.7% in *Apc*$^{min/+}$ *Klrk1*$^{+/+}$ and 49.1% in *Apc*$^{min/+}$ *Klrk1*$^{-/-}$ mice (Figure 3.22b). Together, we demonstrate an increased frequency of IFN-γ-high $CD8^+$ T cells in *Apc*$^{min/+}$ *Klrk1*$^{+/+}$ compared to *Apc*$^{min/+}$ *Klrk1*$^{-/-}$ mice. We hypothesize that the activation of $CD8^+$ T cells through NKG2D leads to increased IFN-γ production through direct or indirect mechanisms.

3.2.2.3 PD-1$^+$ γδT cells preferentially accumulate in NKG2D-sufficient mice

Along $CD8^+$ T cells, γδT cells were significantly increased in *Apc*$^{min/+}$ *Klrk1*$^{+/+}$ compared to *Apc*$^{min/+}$ *Klrk1*$^{-/-}$ mice (Figure 3.23a and b). Recent in-depth analysis of γδT cell subsets revealed that cell expressing Vγ6 are skin tissue-resident cells with the ability to mature into activated, IL-17-producing cells. These cells were shown to express high levels of PD-1, which is in contrast to other γδT cell subsets, among which frequencies of PD-1-expressing cells are typically low (Tan *et al.* 2019). Determining the PD-1 expression pattern in the TME of *Apc*$^{min/+}$ mice revealed low frequencies of PD-1^+ γδT cells at 18-20 weeks (15%), while the vast majority of γδT cells expressed PD-1 at disease endpoint in NKG2D-sufficient *Apc*$^{min/+}$ *Klrk1*$^{+/+}$ mice (Figure 3.23c and d). Strikingly, this increase in PD-1^+ γδT cells was not observed in *Apc*$^{min/+}$ *Klrk1*$^{-/-}$ mice, where only 30% of γδT cells were PD-1^+ at disease endpoint (Figure 3.23d), leading us to hypothesize that the V$\gamma6^+$ subset specifically accumulates in an NKG2D-dependent manner. IL-17, a pro-inflammatory cytokine known to drive intestinal tumorigenesis in the *Apc*$^{min/+}$ mouse model (Chae *et al.* 2010), is produced by certain subsets of γδT cells, including skin-resident V$\gamma6^+$ cells. We therefore determined frequencies of IL-17, specifically IL-17A-producing cells within the tumor and found that similar to IFN-γ, IL-17-producing cells were detected at 18-20 weeks at low frequencies (< 5% among $CD4^+$, $CD8^+$ and γδT cells), but were significantly increased in all subsets at disease endpoint. The main producers of IL-17 were $CD4^+$ T cells with 17% followed by γδT cells with 15% IL-17^+ among

each subset (Figure 3.23e). No differences in frequencies of IL-17-producing cells out of all γδT cells were observed when comparing *Apc*$^{min/+}$ *Klrk1*$^{+/+}$ mice to *Apc*$^{min/+}$ *Klrk1*$^{-/-}$ littermates (Figure 3.23f). Nonetheless, we hypothesized that IL-17 production is influenced by NKG2D expression, based on the observation that NKG2D^{+} γδT cells isolated from the MLN of *Apc*$^{min/+}$ *Klrk1*$^{+/+}$ mice produced significantly higher levels of IL-17 compared to NKG2D^{-} cells from the same mouse (Figure 3.23g). Interestingly, this difference was only evident in *Apc*$^{min/+}$ *Klrk1*$^{+/+}$, but not healthy *Klrk1*$^{+/+}$ mice, suggesting a disease-specific role for NKG2D^{+} IL-17-producing cells.

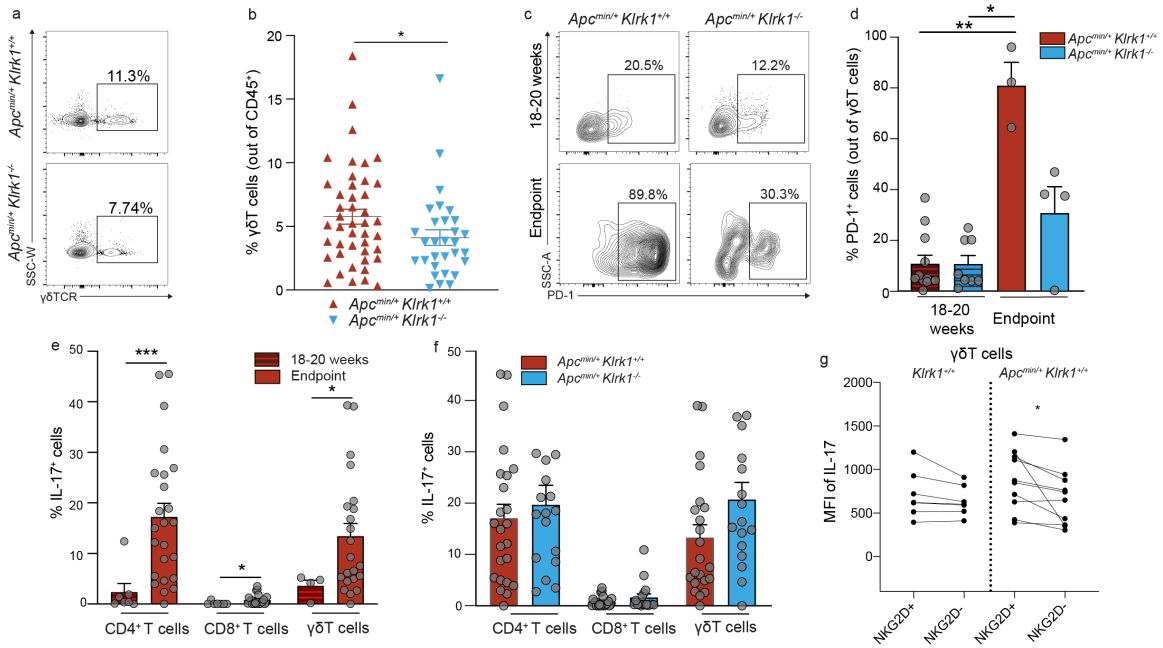

Figure 3.23: PD-1^{+} γδT cells accumulate in the tumor microenvironment in an NKG2D-dependent manner. (a) Representative flow cytometry plots of γδT cells (gated on CD3^{+} lymphocytes). (b) Frequencies of γδT cells at disease endpoint in the SI TME of *Apc*$^{min/+}$ *Klrk1*$^{+/+}$ compared to *Apc*$^{min/+}$ *Klrk1*$^{-/-}$ mice. n ≥ 30. (c) Representative flow cytometry plots depicting PD-1 expression on γδT cells (gated on CD3^{+} lymphocytes). (d) Frequencies of PD-1 expressing γδT cells in the SI TME of *Apc*$^{min/+}$ *Klrk1*$^{+/+}$ and *Apc*$^{min/+}$ *Klrk1*$^{-/-}$ mice at 18-20 weeks compared to endpoint. n ≥ 3. (e) Frequencies of IL-17^{+} T cells stimulated with PMA and ionomycin, in the SI TME of *Apc*$^{min/+}$ *Klrk1*$^{+/+}$ mice at 18-20 weeks compared to disease endpoint. n ≥ 5. (f) Frequencies of IL-17^{+} T cells (gated on CD4^{+}, CD8^{+} or γδTCR^{+}) stimulated with PMA and ionomycing, in the SI TME of *Apc*$^{min/+}$ *Klrk1*$^{+/+}$ compared to *Apc*$^{min/+}$ *Klrk1*$^{-/-}$ mice at disease endpoint. n ≥ 16 (g) Direct comparison of MFI of IL-17 in NKG2D^{+} and NKG2D^{-} γδT cells isolated from the MLN of *Klrk1*$^{+/+}$ and *Apc*$^{min/+}$ *Klrk1*$^{+/+}$ mice. TME = tumor microenvironment, MLN = mesenteric lymph nodes. Bars represent mean ± SEM of individual mice from at least three independent experiments. Lines in g represent individual lines. * p ≤ 0.05, ** p ≤ 0.01, *** p ≤ 0.001. Significance in g was determined using a paired t-test.

In conclusion, we show that PD-1$^+$ γδT cells are enriched in the presence of NKG2D and that NKG2D contributes to their activation and potential accumulation in the TME. A subset of γδT cell produces IL-17 and could contribute to the accumulation of IL-17 in the TME as a consequence of γδT cells enrichment.

3.2.2.4 Gene expression is altered in tumors of *Apc$^{min/+}$* mice

To gain a better understanding of the immune response involved in tumor growth and progression, I performed gene expression analysis on 48 immune-related genes using the Fluidigm Biomark system. For this, we isolated RNA from tumor tissue and healthy surrounding tissue from *Apc$^{min/+}$* mice as well as healthy small intestinal tissue from control mice. Genes upregulated in tumor compared to control tissue included some genes associated with a myeloid response, such as *Il6* (IL-6) and *Il33* (IL-33), demonstrating that myeloid cells contribute to the pro-inflammatory environment within the tumor (Figure 3.24a). *Ptgs2* (COX-2) and *Tnfa* (TNF-α) were increased approximately 2-fold within the tumor compared to healthy control tissue. Interestingly, genes associated with a cytotoxic response, such as *Prf1* (Perforin-1) and *Gzmb* (GzB) were expressed at notably lower levels within the tumor compared to both healthy tissue as well as surrounding tissue of *Apc$^{min/+}$* mice (2- and 6-fold, respectively). Genes associated with cell exhaustion, such as *Pdcd1* (PD-1), *Lag3* (LAG3) and *Btla* (BTLA) were expressed at significant levels in the healthy intestine and the tumor tissue, but decreased in surrounding tissue from *Apc$^{min/+}$* mice. While gene expression analysis only provides limited information on changes associated with cell functionality or infiltration, I made the following observations: I. Genes associated with inflammation, specifically myeloid-cell driven inflammation, were increased in the tumor, II. genes associated with a cytotoxic response typically correlated with a good anti-tumor response were decreased and III. genes encoding cell surface markers associated with cell exhaustion were increased in the tumor compared to surrounding tissue from *Apc$^{min/+}$*, but not healthy mice.

Next, I directly compared the gene expression profile of *Apc$^{min/+}$ Klrk1$^{+/+}$* to *Apc$^{min/+}$ Klrk1$^{-/-}$* mice. Surprisingly, no genes were differentially expressed despite various differences in immune cell composition and functionality. Mild differences were seen in the expression of *Cfs2* (GM-

CSF) and *Il23* (IL-23), which were expressed at lower levels in the tumors of *Apc*$^{min/+}$ *Klrk1*$^{-/-}$ compared to *Apc*$^{min/+}$ *Klrk1*$^{+/+}$ mice (Figure 3.24b). Further, *Tbx21*, encoding for T-bet, a transcription factor associated with a T_H1 and ILC1 response was increased 2-fold in tumors of NKG2D-sufficient mice. While this difference was not statistically significant and is based on only 8 mice per group, it supports the observation that NKG2D-sufficient mice induce a stronger T_H1 response in the TME compared to NKG2D-deficient littermates. Genes encoding IL-17 and IFN-γ were included in the analysis, but fell below the detection threshold.

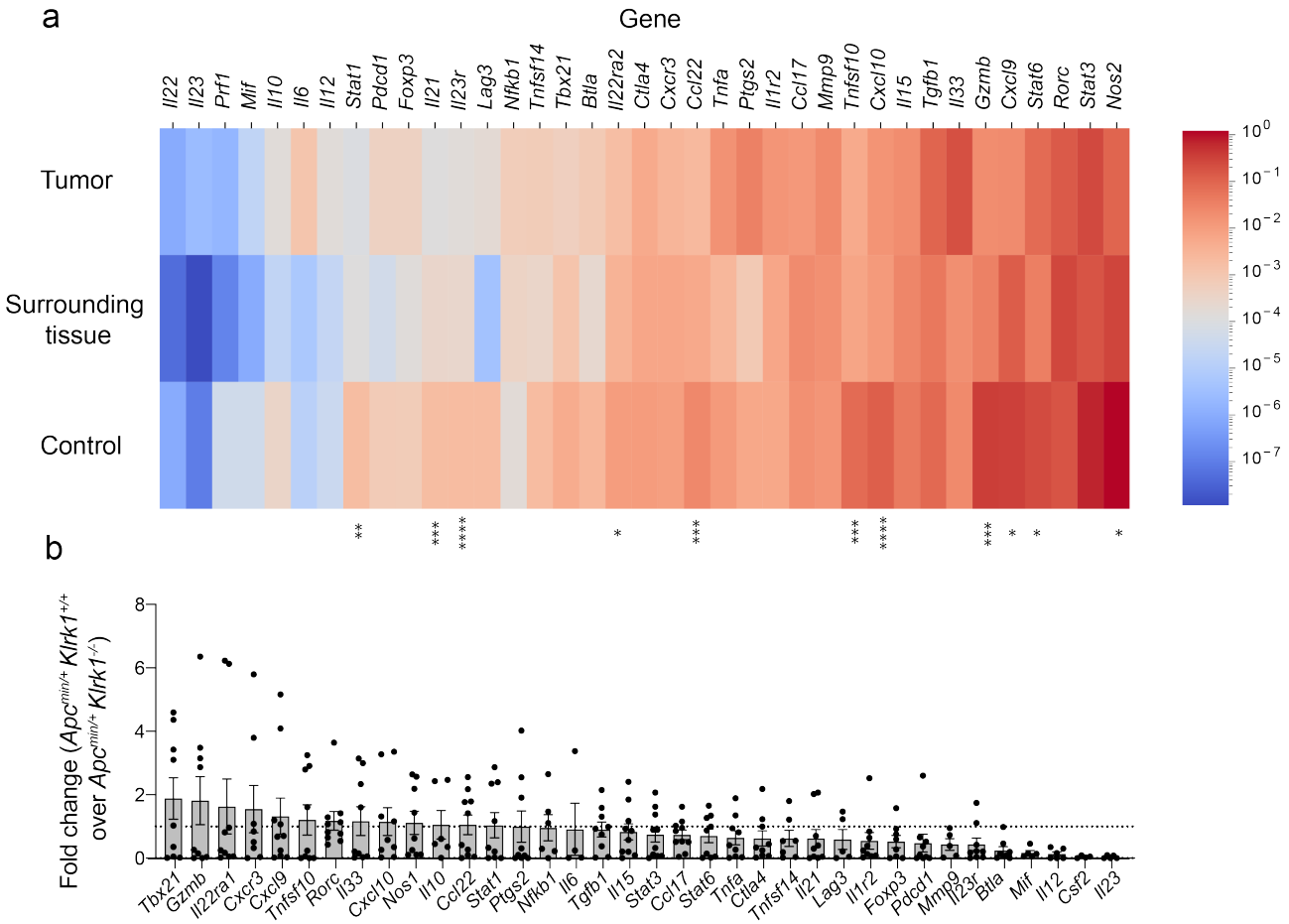

Figure 3.24: Gene expression profile of *Apc*$^{min/+}$ mice. (a) Heatmap of fold change over the housekeeping gene HPRT of an array of immune-associated genes expressed in the tumor (top), surrounding tissue (middle) from *Apc*$^{min/+}$ *Klrk1*$^{+/+}$ and healthy tissue (bottom) from *Apc*$^{+/+}$ mice. Ordered from left to right with increasing expression in the tumor tissue. Tissue was collected at disease endpoint in *Apc*$^{min/+}$ mice and age-matched controls (> 20 weeks). Significance was determined using one-way ANOVA and adjusted for multiple comparisons. (b) Fold change of gene expression in tumors from *Apc*$^{min/+}$ *Klrk1*$^{+/+}$ over *Apc*$^{min/+}$ *Klrk1*$^{-/-}$ mice. Dots represent individual samples. n ≥ 4 per group.

3.2.2.5 NKG2D ligand expression is independent of NKG2D and tumorigenesis

In Chapter 1, we established that RAE-1 is constitutively expressed on healthy mouse epithelium. Human studies have shown that NKG2DL is expressed on various types of cancer, including CRC (Watson *et al.* 2006, McGilvray *et al.* 2009), raising the question of NKG2DL expression in $Apc^{min/+}$ mice. To study changes in NKG2DL expression throughout disease development, we performed immunohistochemical analysis of the mouse NKG2DL RAE-1 in $Apc^{min/+}$ mice at various timepoints and compared this to $Apc^{+/+}$ control mice.

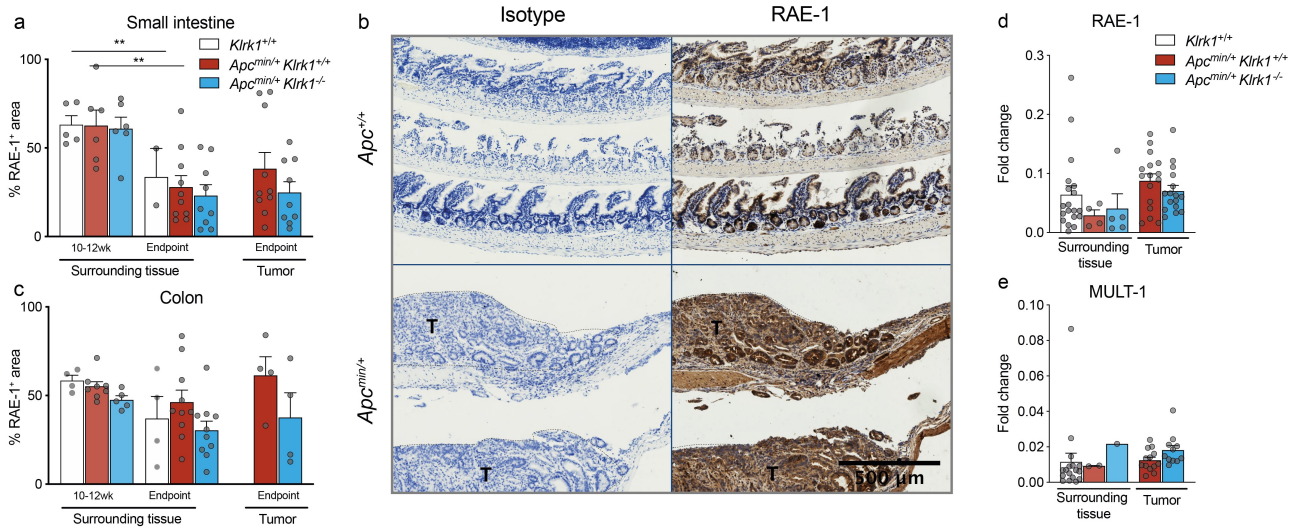

Figure 3.25: NKG2DL expression is independent of NKG2D signaling or tumor development. (a) Immunohistochemical analysis of RAE-1$^+$ area in small intestinal tissue and tumor tissue from $Apc^{min/+}$ $Klrk1^{+/+}$, $Apc^{min/+}$ $Klrk1^{-/-}$ mice as well as non-*Apc* $Klrk1^{+/+}$ littermates. n $\geq$ 6 for $Apc^{min/+}$ mice and n $\geq$ 5 for $Klrk1^{+/+}$ mice. (b) Representative immunohistochemical staining of RAE-1 on intestinal tissue of healthy (top) and $Apc^{min/+}$ mice. n $\geq$ 4. (c) Immunohistochemical analysis of RAE-1$^+$ area in colonic tissue and tumor tissue from $Apc^{min/+}$ $Klrk1^{+/+}$, $Apc^{min/+}$ $Klrk1^{-/-}$ mice as well as non-*Apc* $Klrk1^{+/+}$ littermates. n $\geq$ 4. (d+e) Fold change in RAE-1 (d) and MULT-1 (e) expression in small intestinal tissue and tumor tissue from $Apc^{min/+}$ $Klrk1^{+/+}$, $Apc^{min/+}$ $Klrk1^{-/-}$ mice as well as non-*Apc* $Klrk1^{+/+}$ littermates. n $\geq$ 4 for RAE-1 and n = 1-2 for MULT-1 in surrounding tissue of $Apc^{min/+}$ mice and n $\geq$ 11 for remaining groups. ** p $\leq$ 0.01. IHC staining was performed by M.Sc. student Elena Rondeau.

RAE-1$^+$ area was similar in $Apc^{min/+}$ mice compared to non-*Apc* healthy mice with an average area of 62.6% in the SI of $Apc^{min/+}Klrk1^{+/+}$ mice at 10-12 weeks and a 28% on surrounding tissue at disease endpoint (Figure 3.25a and b). Lack of NKG2D did not impact RAE-1 expression. Frequencies of RAE-1$^+$ area was similar on SI tumor tissue compared to healthy

surrounding tissue at disease endpoint with a mean of 38.2% in *Apc*$^{min/+}$*Klrk1*$^{+/+}$ and 24.9% in *Apc*$^{min/+}$*Klrk1*$^{-/-}$ mice (Figure 3.25a and b). RAE-1 expression in the colon followed a similar trend with a mean of approximately 55% RAE-1^{+} area in young mice independent of the genotype and a mild downregulation to 30-40% in aged control mice or *Apc*$^{min/+}$ mice at disease endpoint (Figure 3.25c). RAE-1 expression on colonic tumors of *Apc*$^{min/+}$*Klrk1*$^{+/+}$ mice was higher (61.3%) in comparison with *Apc*$^{min/+}$*Klrk1*$^{-/-}$ mice (37.6%, Figure 3.25c).

In addition to immunohistochemistry, we performed transcriptional analysis on tissue samples collected from *Apc*$^{min/+}$ mice at disease endpoint. In addition to RAE-1, we analyzed expression levels of an additional NKG2DL, MULT-1. RAE-1 was expressed at higher levels in healthy *Klrk1*$^{+/+}$ mice than MULT-1 with a mean fold change of 0.06 compared to 0.01 (Figure 3.25d and e). Gene expression was not significantly altered in the surrounding tissue or tumor tissue of *Apc*$^{min/+}$ mice compared to healthy controls and was independent of the genotype (Figure 3.25d and e). We observed a slight increase in fold change of RAE-1 in tumor tissue (mean fold change of 0.09) compared to surrounding tissue (0.03) in *Apc*$^{min/+}$ *Klrk1*$^{+/+}$ mice (Figure 3.25d).

This confirms a mild downregulation of RAE-1 with increasing age independent of the genotype in the SI. Expression of RAE-1 on tumor and surrounding tissue in the colon at disease endpoint was mildly increased in *Apc*$^{min/+}$ *Klrk1*$^{+/+}$ mice compared to NKG2D-deficient littermates, suggesting that NKG2D expression influences the regulation of RAE-1 to some extent.

3.2.2.6 Tumorigenesis is associated with subtle changes in the microbiota

NKG2D ligands can be regulated by the microbiota (Hansen *et al.* 2013) and changes in bacterial composition have been shown to play a role in tumorigenesis (Hale *et al.* 2016). I studied changes in the microbiota during disease development by performing 16S rRNA gene sequencing of fecal samples and tumor tissues. At 18 weeks, *Bacteroidetes* and *Firmicutes* were the most abundant phyla in healthy controls and *Apc*$^{min/+}$ mice, together making up $> 90\%$ of the identified bacteria (Figure 3.26a left and middle). *Proteobacteria* were highly represented in tumor, but not fecal samples, ranging from 60% to 90% (Figure 3.26a right). Further in-depth analysis revealed *Stenotrophomonas* as the most abundant genus, making up 50% or more of

tumor-associated bacteira (Figure 3.26b). Principal component analysis of fecal and tumor tissue revealed significant differences between the bacterial composition of fecal samples and tumor tissue (Figure 3.26c).

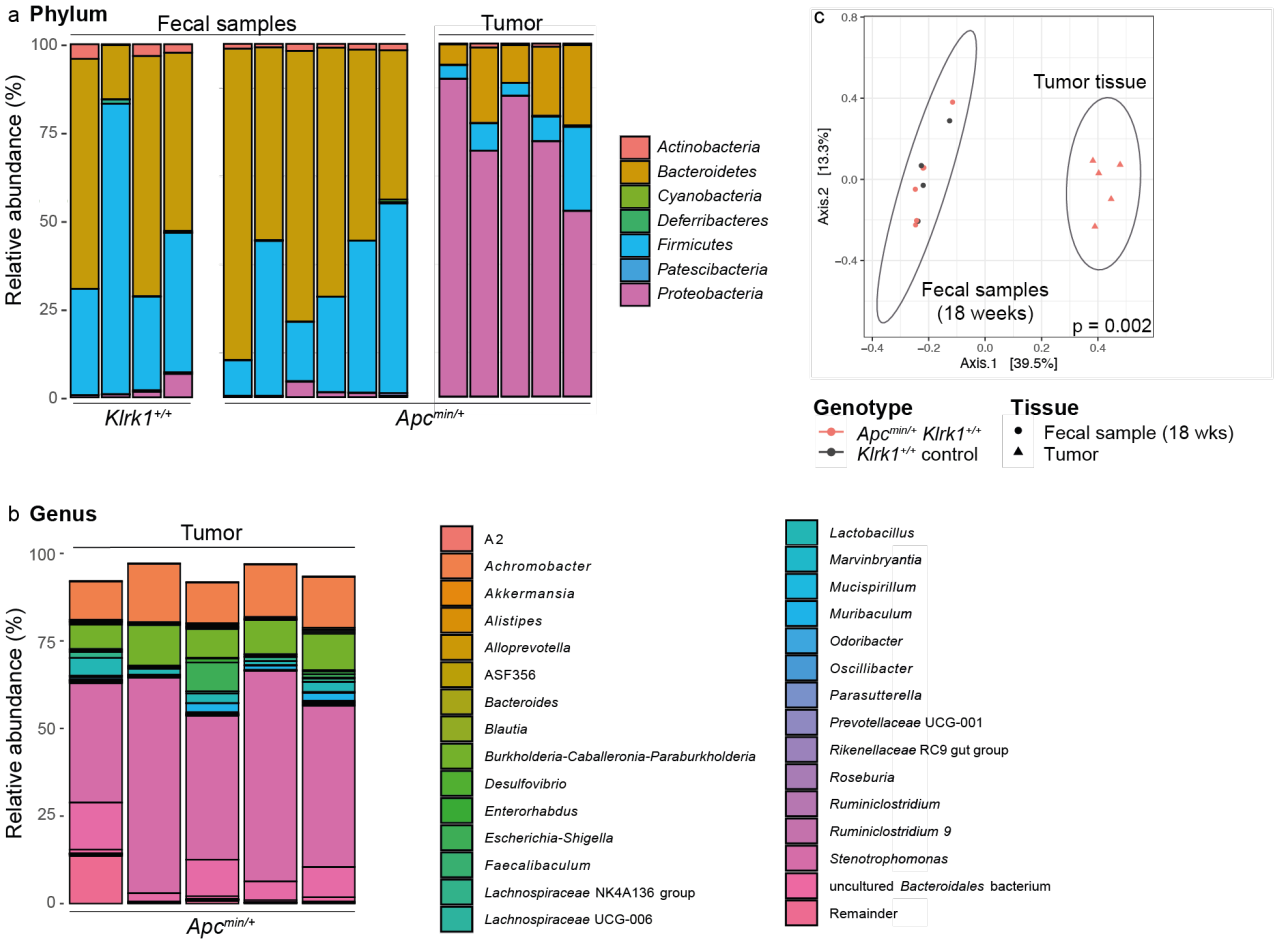

Figure 3.26: Tumorigenesis is associated with changes in the microbiota. (a) Relative abundance of fecal bacteria at the rank of phylum (left), class (middle) and order (right) in naive *Klrk1*$^{+/+}$ and *Apc*$^{min/+}$ *Klrk1*$^{+/+}$ mice. (b) Relative abundance of fecal bacteria at the rank of genus in tumors isolated from *Apc*$^{min/+}$ *Klrk1*$^{+/+}$ mice. (c) Weighted UniFrac PCoA of fecal bacteria and tumor tissue. PCoA = Principal Component Analysis, wks = weeks. n = 4 for control mice, n = 6 for fecal samples and n = 5 for tumor samples. Significance in c compared fecal and tumor samples collected from *Apc*$^{min/+}$ *Klrk1*$^{+/+}$ mice and was determined by PERMANOVA.

Analysis of alterations in the microbiota over time revealed no changes in Shannon diversity in fecal samples of 3, 10 or 18 week old *Apc*$^{min/+}$ *Klrk1*$^{+/+}$ mice compared to 18 week old *Klrk1*$^{+/+}$ controls (Figure 3.27a). The relative abundance of *Firmicutes* decreased over time from a mean of 41.3% in 3-week-old *Apc*$^{min/+}$ *Klrk1*$^{+/+}$ mice to 30.6% at 18 weeks (Figure 3.27b

left), while the relative abundance of *Bacteroidetes* increased from 45.2% at 3 weeks to 54% at 10 weeks and 63.1% at 18 weeks (Figure 3.27b right). Krona plots revealed changes in the composition of *Firmicutes* over time: at 3 weeks, the ratio of *Clostridia* to *Bacilli* was 0.5 (14% and 28%, respectively), while *Clostridia* were more abundant than *Bacilli* at 18 weeks (ratio 0.75, 20% and 15%, Figure 3.27c). From this observation, we conclude that the microbiota of healthy control mice is comparable to young $Apc^{min/+}$ mice and that changes in the bacterial composition occur over time in parallel to disease progression.

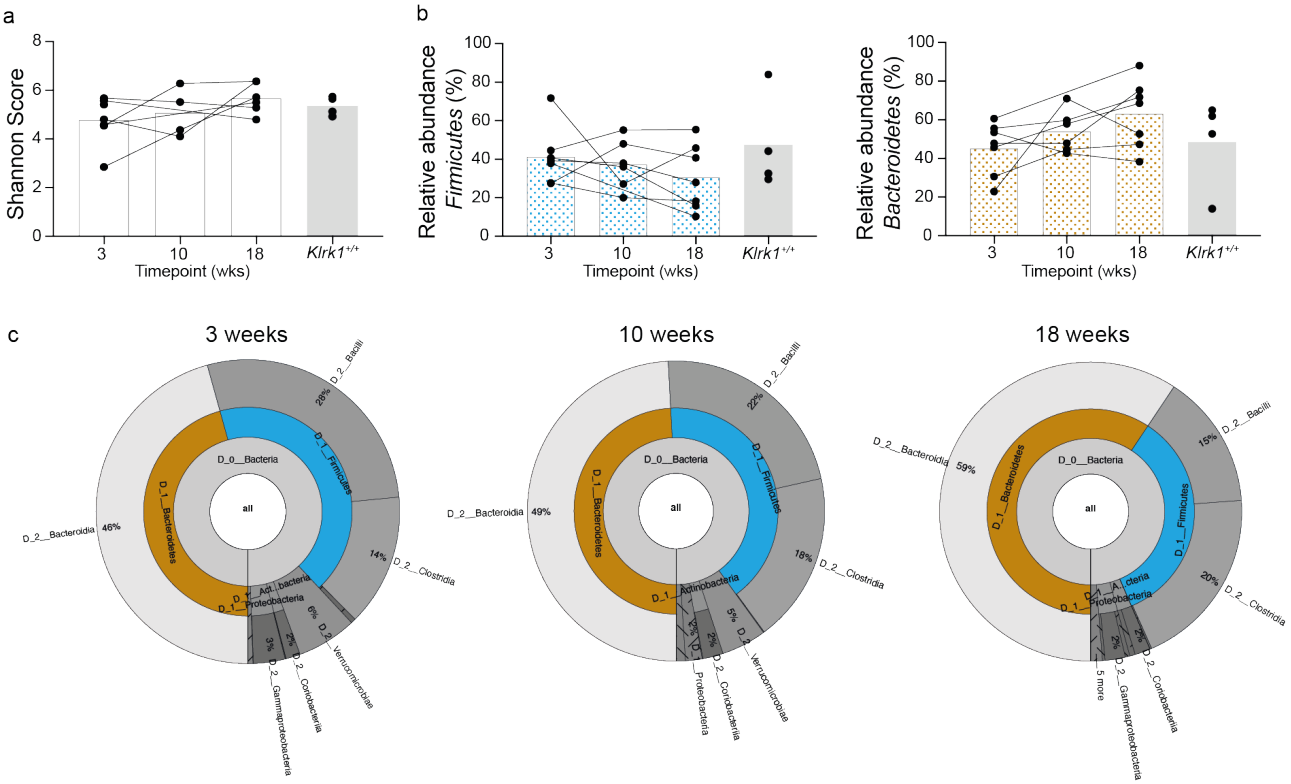

Figure 3.27: Tumorigenesis is associated with changes in the microbiota over time. (a) Shannon diversity index of $Apc^{min/+}$ $Klrk1^{+/+}$ mice over time compared to 18 week old $Klrk1^{+/+}$ mice. (b) Relative abundance of *Firmicutes* (left) and *Bacteroidetes* (right) of $Apc^{min/+}$ $Klrk1^{+/+}$ mice over time compared to 18 week old $Klrk1^{+/+}$ mice. (c) Krona plots showing relative abundance of bacterial taxa in fecal samples of $Apc^{min/+}$ $Klrk1^{+/+}$ mice collected at 3 weeks (left), 10 weeks (middle) and 18 weeks of age (right). wks = weeks. n = 4 for control mice, n = 6 for fecal samples and n = 5 for tumor samples. Bars represent mean and dots represent individual samples.

I next compared the composition of the microbiota in fecal samples and tumor tissue collected from $Apc^{min/+}$ $Klrk1^{+/+}$ and $Apc^{min/+}$ $Klrk1^{-/-}$ mice. PCoA analysis revealed that the composition of the fecal microbiota was similar across all genotypes, which included $Klrk1^{+/+}$ and $Klrk1^{-/-}$ control samples (Figure 3.28a). Similarly, composition of tumor tissue from both

NKG2D-sufficent and -deficient mice clustered together, suggesting no genotypic differences in the composition of tumor-associated bacteria (Figure 3.28a). I studied the relative abundance of the two most common phyla, *Bacteroidetes* and *Firmicutes* in more detail. The relative abundance of *Firmicutes* was reduced from 47.6% in healthy control mice to 30.6% in $Apc^{min/+}$ $Klrk1^{+/+}$ mice (Figure 3.28b), while the abundance of *Bacteroidetes* was slightly increased from 48.4% (control) to 63.1% ($Apc^{min/+}$ $Klrk1^{+/+}$). While these changes were mild and not statistically significant, I made an interesting observation - relative abundances of both *Bacteroidetes* and *Firmicutes* were changed to a lesser extent (38.7% *Firmicutes* and 51.6% *Bacteroidetes*) in fecal samples from NKG2D-deficient mice compared to their $Apc^{min/+}$ $Klrk1^{+/+}$ littermates (Figure 3.28b and c), suggesting that changes associated with tumorigenesis in the $Apc^{min/+}$ mice are less pronounced in mice lacking NKG2D.

I next assessed the bacterial composition of tumor tissue in the presence and absence of NKG2D. Relative abundance of the most common phyla (*Firmicutes*, *Bacteroidetes* and *Proteobacteria*) were unchanged in NKG2D-deficient mice compared to $Apc^{min/+}$ $Klrk1^{+/+}$ littermates (Figure 3.28d). To gain better insight into microbiome differential abundance, I performed DeSeq2 analysis (Anders *et al.* 2010). This revealed one differentially expressed group, namely *Lachnospiraceae* NK4A136 group, which was more abundant in tumors of NKG2D-deficient mice compared to $Apc^{min/+}$ $Klrk1^{+/+}$ littermates (Figure 3.28e and f).

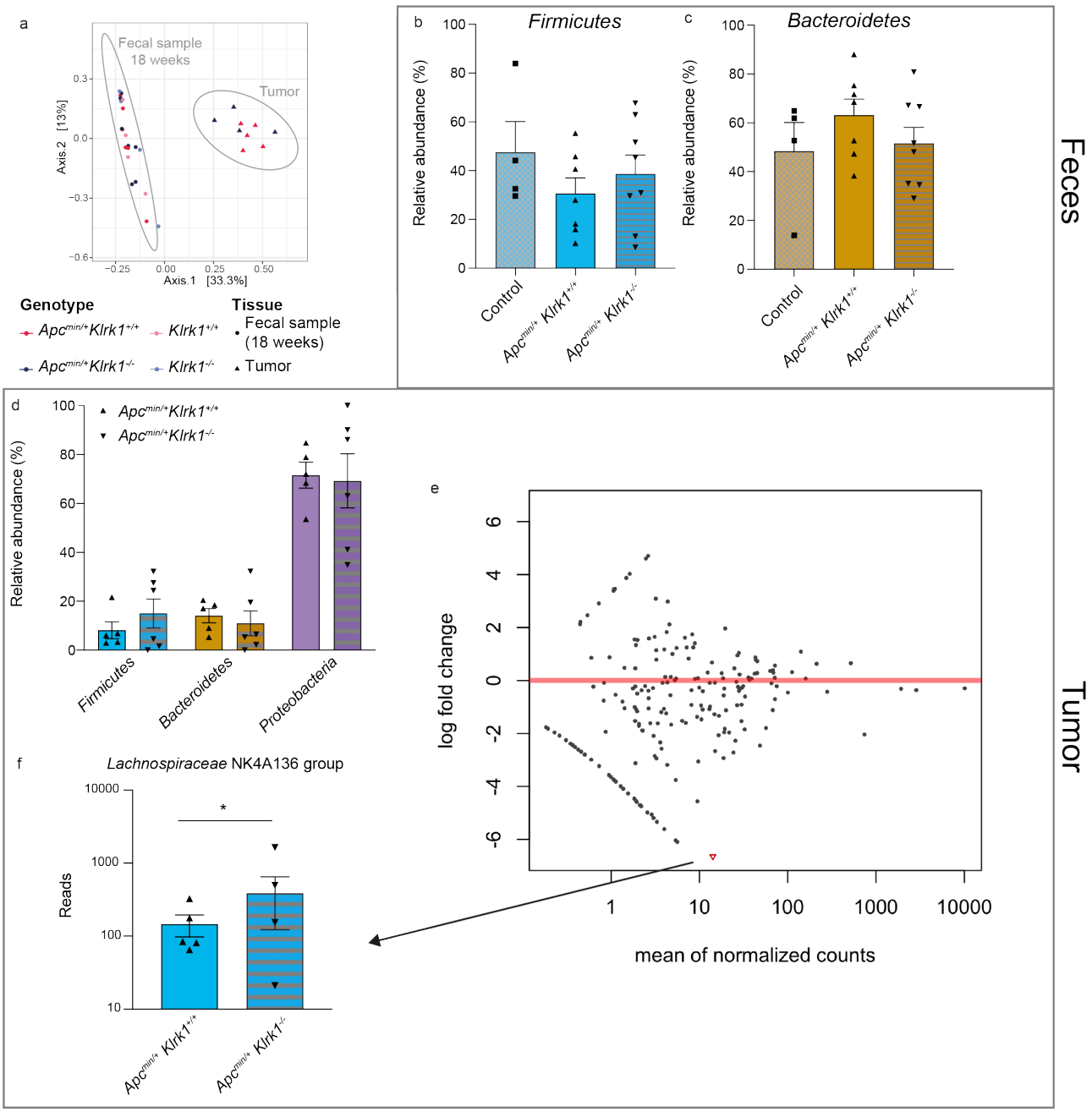

Figure 3.28: NKG2D deficiency is associated with subtle changes in the microbiota in *Apc$^{min/+}$* mice. (a) PCoA of fecal and tumor samples in *Apc$^{min/+}$ Klrk1$^{+/+}$* and *Apc$^{min/+}$ Klrk1$^{-/-}$* mic as well as non-*Apc Klrk1$^{+/+}$* and *Klrk1$^{-/-}$* control mice. (b) Relative abundance of *Firmicutes* in fecal samples from control mice compared to NKG2D-sufficient and -deficient *Apc$^{min/+}$* mice. (c) Relative abundance of *Bacteroidetes* in fecal samples from control mice compared to NKG2D-sufficient and -deficient *Apc$^{min/+}$* mice. (d) Relative abundance of *Firmicutes*, *Bacteroidetes* and *Proteobacteria* in tumor tissue collected from *Apc$^{min/+}$ Klrk1$^{+/+}$* and *Apc$^{min/+}$ Klrk1$^{-/-}$* mice. (e) Volcano plot following DeSeq2 analysis comparing the composition of tumors of *Apc$^{min/+}$ Klrk1$^{+/+}$* and *Apc$^{min/+}$ Klrk1$^{-/-}$* mice. Red indicated statistically significant result. (f) Reads of *Lachnospiraceae* NK4A136 group in tumors of *Apc$^{min/+}$ Klrk1$^{+/+}$* and *Apc$^{min/+}$ Klrk1$^{-/-}$* mice. PCoA = principal component analysis. n $\geq$ 4. * p (adjusted) $\leq$ 0.05.

Next, I examined whether changes in bacterial composition were correlated with disease severity or immune cell infiltration and/or functionality. I performed linear regression analysis on various groups, but decided to focus on identifying correlations between bacterial composition of fecal samples from 18-week old mice at phylum level to macroscopic parameters as well as immune cell frequencies and function. For this, I selected pairs of variables with more than 6 values, on which I performed linear regression analysis (Table 3.3). As expected, *Firmicutes* and *Bacteroidetes* were negatively correlated. Further, *Actinobacteria* was negatively correlated with the frequency of B cells, whereas *Firmicutes* was positively correlated with PMN-MDSCs. None of the changes in the bacterial composition of fecal samples or tumors were striking, yet the fact that bacterial composition of *Apc*$^{min/+}$ *Klrk1*$^{-/-}$ mice was more similar to control mice than that of *Apc*$^{min/+}$ *Klrk1*$^{-/-}$ supports the hypothesis that NKG2D exacerbates disease. The changes are possibly simply a consequence of differences in the severity of intestinal inflammation, but a direct relationship between NKG2D and the microbiota cannot be excluded without further research.

Table 3.3: Correlations of phylum and macroscopic or immune cell function

Variable 1	**Variable 2**	**R^2**	**Adjusted p-value**
Actinobacteria	B cells	-0.92	0.038
Bacteroidetes	*Firmicutes*	-0.83	1.93E-03
Patescibacteria	HCT (10-12wk)	-0.97	1.33E-05
Firmicutes	PMN-MDSC	0.99	8.72E-04

3.2.2.7 Human disease is associated with changes in the NKG2D/NKG2DL system

NKG2D and NKG2DL have been shown to be dysregulated in human CRC cancers (Chirica *et al.* 2015, McGilvray *et al.* 2009), yet the exact role of NKG2D-mediated immunity is not understood. Here, I made use of a large publicly available dataset (TCGA) to study changes in NKG2D and NKG2DL expression in patients diagnosed with COAD, a subtype of CRC.

In a first instance, I determined the expression pattern of NKG2DL in healthy small intestinal tissue compared to tumor tissue from COAD patients. Interestingly, expression of the MIC family was unchanged with both MICA and MICB showing a similar expression pattern in healthy tissue compared to tumor samples (Figure 3.29a and data not shown). In contrast to this, UL16 binding protein (ULBP)s were upregulated in COAD patients (Figure 3.29b and data not shown).

I next asked whether the level of expression was correlated with survival. Kaplan-Meier plots revealed that the level of MICA had no impact on the survival probability in this cohort (Figure 3.29a), while patients with low ULBP2 expression survived significantly longer than patients with high expression (Figure 3.29b). Interestingly, the difference in survival was only obvious in the first 1000 days. Surprisingly and contrary to what we observed in the mouse model of intestinal cancer, expression of *KLRK1*, encoding for human NKG2D, was reduced in tumors compared to healthy small intestinal tissue, potentially suggesting engagement and subsequent downregulation of NKG2D from the cell surface (Figure 3.29c top). Expression level had no impact on patient survival (Figure 3.29c bottom).

MSI-H tumors are often associated with a stronger immune activation than microsatellite stable (MSS) tumors (Kloor *et al.* 2016). Further, mutation on the *KRAS* gene are typically associated with poor response to immunotherapy as well as poor immune cell infiltration (Lal *et al.* 2017). We therefore compared the expression patterns of NKG2D and NKG2DL in patients with MSI and MSS tumors as well as patients with or without *KRAS* mutations. Interestingly, neither the microsatellite, nor the *KRAS* mutation status influenced expression of NKG2D or NKG2DL (3.29d and e).

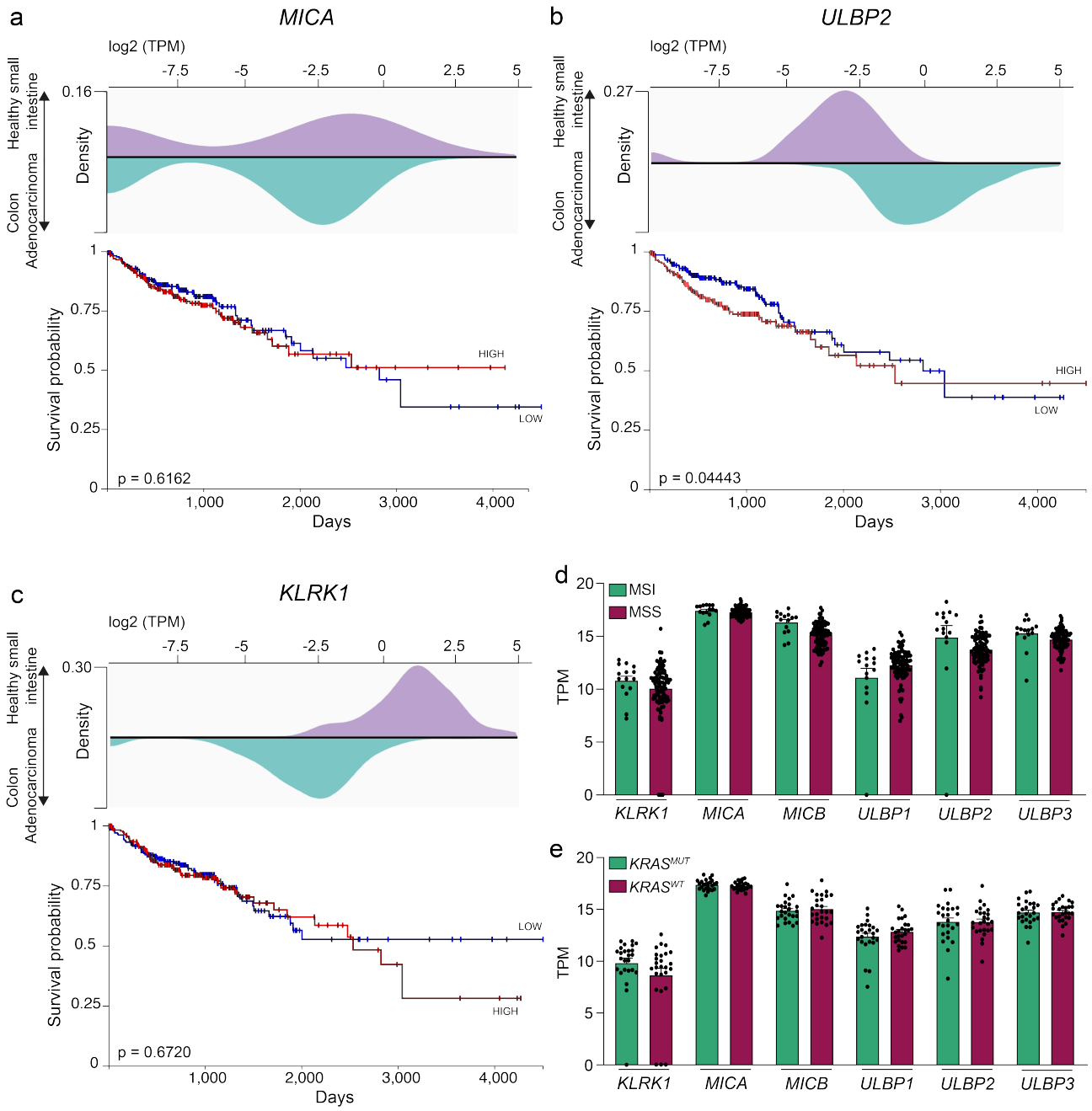

Figure 3.29: NKG2D/NKG2DL are differentially expressed in COAD patients. (a) *MICA* expression in the healthy small intestine (purple) compared to tumors from COAD patients (green) (top) and survival of patients with high (red) compared to low (blue) *MICA*. (b) *ULBP2* expression in the healthy small intestine (purple) compared to tumors from COAD patients (green) (top) and survival of patients with high (red) compared to low (blue) *ULBP2*. (c) *KLRK1* expression in the healthy small intestine (purple) compared to tumors from COAD patients (green) (top) and survival of patients with high (red) compared to low (blue) *KLRK1*. (d) Expression pattern of *KLRK1* and several NKG2D ligands in MSI and MSS tumors. (n = 15 for MSI and n = 88 for MSS patients) (e) Expression pattern of *KLRK1* and several NKG2D ligands in patients with or without *KRAS* mutations (n = 25 for $KRAS^{MUT}$ and n = 26 for $KRAS^{WT}$ patients). Data was obtained from TCGA. Plots a-c were created using https://xenabrowser.net/ with samples being divided into two groups on the median. n = 487 for a-c. TCGA = The Cancer Genome Atlas, COAD = Colon adenocarcinoma, MSI = microsatellite-instability, MSS = microsatellite-stable.

In addition to classification by mutations or microsatellite status, tumors can be classified using the CMS system (Guinney *et al.* 2015). Through our collaborator Rachel Purcell (University of Otago, Christchurch), I obtained access to an unpublished dataset of gene expression data from 308 CRC patients. Patients were classified according to CMS, allowing us to determine changes in the NKG2D/NKG2DL system in the different subtypes of CRC.

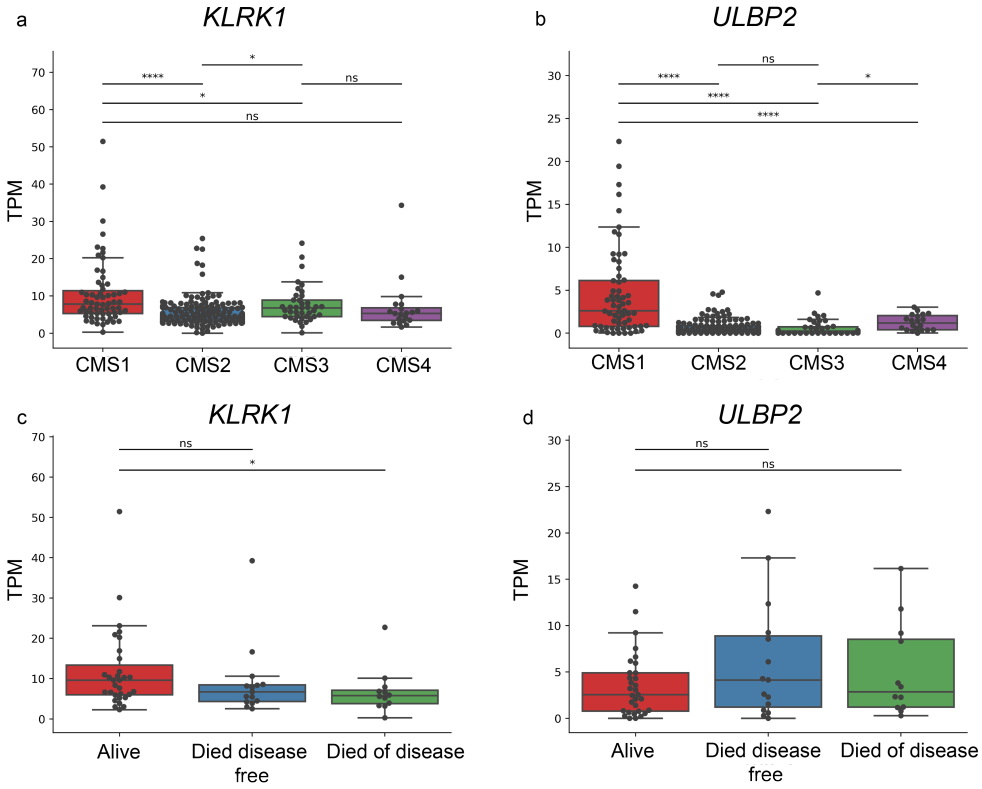

Figure 3.30: NKG2D/NKG2DL are enriched in CMS1 patients. (a) Gene expression of *KLRK1* in CMS1-4. (b) Gene expression of *ULBP2* in CMS1-4. (c) Gene expression of *KLRK1* grouped by disease outcome, CMS1 patients only. (d) Gene expression of *ULBP2* grouped by disease outcome, CMS1 patients only. n (tota) = 308 for a and b, n = 64 for c and d. * $p \leq 0.05$, ** $p \leq 0.01$, *** $p \leq 0.001$, **** $p \leq 0.0001$.

CMS1 is characterized by immune cell infiltration and is a good predictor of response to ICI, posing the question of whether NKG2D-expressing cells are specifically enriched in CMS1 patients. I compared expression levels of NKG2D and NKG2DL across all subtypes and found that *KLRK1* transcript was significantly increased in patients classified as CMS1 compared to CMS2, 3 and 4 (Figure 3.30a). Among NKG2DL, only *ULBP2* transcript was differentially expressed among CRC subtypes, with CMS1 patients displaying significantly higher levels compared to other subtypes (Figure 3.30b and data not shown). I next asked whether expression

levels of *KLRK1* or *ULBP2* were associated with survival. Comparing three categories ('Alive', 'Died disease free' and 'Died of disease') revealed that gene expression of *KLRK1* was higher in CMS1 patients that survived ('Alive') compared to patients that died of disease (Figure 3.30c) No difference was observed in the gene expression of *ULBP2* (Figure 3.30d) or when data from all CMS was analyzed together (data not shown).

I next asked whether NKG2D expression was related to transcript levels of IFN-γ and performed linear regression analysis. I categorized patients into CMS1 and treated all other subtypes as one group. *KLRK1* and *IFNG* were strongly correlated in CMS1 patients, but not other subtypes (Figure 3.31), suggesting that NKG2D and IFN-γ production are interdependent.

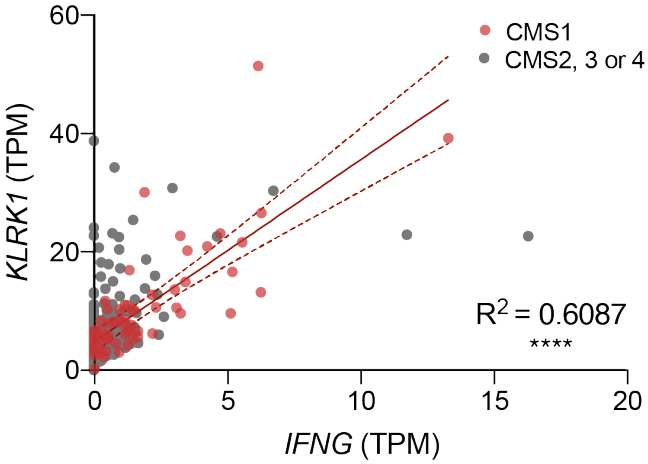

Figure 3.31: Gene expression of *KLRK1* and *IFNG* are positively correlated in CMS1 patients. Correlation of gene expression of *KLRK1* and *IFNG* in CMS1 patients (red) compared to patients classified as CMS2, 3 or 4 (grey). Linear regression curve relates to CMS1 only. TPM = transcript per million. *** $p \leq 0.001$.

3.2.3 Discussion

We have previously shown that NKG2D exacerbates inflammation-driven cancer in a model of liver cancer (Sheppard *et al.* 2017, Sheppard *et al.* 2018), yet mechanisms leading to this pro-tumorigenic role are not fully understood. Identifying settings and tissue environments favoring NKG2D-mediated tumor-promoting inflammation is of great importance in developing new therapies and understanding potentially detrimental side effects of NKG2D-based immunotherapy. In this study, we unravel the function of NKG2D in the setting of inflammation-driven intestinal cancer.

By comparing disease severity and tumor burden of NKG2D-sufficient to NKG2D-deficient $Apc^{min/+}$ mice, a well-established mouse model (Moser *et al.* 1995), that has been shown to be inflammation-driven (Rakoff-Nahoum *et al.* 2007) and has been used in a series of papers studying the immune response in intestinal tumor development (Akeus *et al.* 2014, Bodduluri *et al.* 2018, Zhang *et al.* 2015, Marsh *et al.* 2012), we show that presence of NKG2D is associated with reduced survival, faster tumor progression and increased tumor burden. We further demonstrate that disease progression is associated with subtle changes in the microbiota that are independent of NKG2D. Lastly, we examine expression of NKG2D and NKG2DL in patient samples and show that the NKG2D/NKG2DL is dysregulated in a specific subset of patients.

3.2.3.1 IFN-γ - a driver of disease in intestinal cancer?

We sought to better understand pathways involved in the inflammatory response involved in tumor progression and observed a striking difference in percentages of IFN-γ-producing $CD8^+$ T cells, with an increased frequency of IFN-γ-high $CD8^+$ T cells in tumors of $Apc^{min/+}$ $Klrk1^{+/+}$ compared to $Apc^{min/+}$ $Klrk1^{-/-}$ mice. We confirmed that IFN-γ and NKG2D are strongly correlated in human CRC patients and show that NKG2D was expressed at higher levels among patients classified as CMS1 'immune'. IFN-γ has a dual function in tumor immunity and can be both pro- and anti-tumorigenic. Its anti-tumor functions are well established (Dighe *et al.* 1994) and IFN-γ secretion typically results in effector cell recruitment and activation, tumor cell death and upregulation of MHC-I on tumor cells (Castro *et al.* 2018). A strong IFN-γ response

is therefore often associated with improved survival and a good response to immunotherapy in cancer patients (Weichselbaum *et al.* 2008, Karachaliou *et al.* 2017, Ayers *et al.* 2017). Concurrently, IFN-γ has been shown to facilitate tumorigenesis through a number of mechanisms by rendering tumor cells less susceptible to immunosurveillance through tumor cell dormancy (Müller-Hermelink *et al.* 2008), immunoediting (Takeda *et al.* 2017) and upregulation of inhibitory molecules, such as PD-L1 (Abiko *et al.* 2015). Further, IFN-γ expression can remodel the TME to a tumor-promoting immune environment through the recruitment of MDSC (Hix *et al.* 2013). In the context of CRC, RNAseq analysis revealed a strong positive correlation of IFN-γ expression and several inhibitory receptors, such as PD-1, PD-L1, CTLA-4 and LAG3 (Xu *et al.* 2020). Using the $Apc^{min/+}$ model, we show that PD-1 is indeed upregulated on all T cell subsets at disease endpoint compared to earlier disease stages, suggesting that they have been activated and are potentially exhausted. A study examining subsets of exhausted T cells in the TME of transplanted tumors using RNAseq confirms that 'terminally exhausted' PD-1^{+} T cells are indeed capable of producing IFN-γ and display inferior anti-tumor activity in comparison to PD-1^{low} 'progenitor exhausted' T cells (Miller *et al.* 2019). I analyzed this publicly available dataset further and found that NKG2D gene expression was significantly elevated on 'terminally exhausted' T cells compared to the 'progenitor exhausted' T cells, supporting the presence of tumor-promoting NKG2D^{+} PD-1^{+} IFN-γ^{+} T cells in the TME (data not shown). While it is likely that IFN-γ exerts protective effects at early stages of the disease, as suggested by the aggravated disease in IFN-γ-deficient $Apc^{min/+}$ mice (Wang *et al.* 2015a), we hypothesize that sustained expression and accumulation of IFN-γ-producing T cells contribute to disease progression, either directly as a source of cytokines and/or indirectly due to their impaired anti-tumor killing activity.

The hypothesis that anti-tumor killing activity is indeed impaired was supported by observations we made in a screen quantifying gene expression on tumor tissue from $Apc^{min/+}$ mice, which included 48 genes related to the immune response. We found that genes associated with immune cell exhaustion, such as *Pdcd1* (PD-1), *Ctla4* (CTLA-4), *Lag3* (Lag3) and *Btla* (BTLA) were expressed at high levels, while genes associated with a cytotoxic response, including *Gzmb* (GzB), *Tnfsf10* (TRAIL) and *Prf1* (Perforin) were expressed at lower levels than

in healthy controls. We conclude that the cytotoxic function of TILs is indeed inhibited and supports the hypothesis that they are, at least to some extent, dysfunctional and exhausted. Together, we hypothesize that $CD8^+$ T cells producing high levels of IFN-γ accumulate in the TME in an NKG2D-dependent manner and that at late stages of the disease, where the cytotoxic response is diminished, sustained secretion of IFN-γ favors tumor growth through the accumulation of pro-inflammatory cytokines, recruitment of tumor-promoting immune cells, such as γδT cells and/or immune cell exhaustion.

3.2.3.2 A novel role for γδT cells in NKG2D-mediated disease

In addition to $CD8^+$ T cells, we observed a striking increase in frequencies of γδT cells in NKG2D-sufficient mice. γδT cells as well as IL-17, a cytokine typically produced by $CD4^+$ and γδT cells, have have previously been shown to drive disease in the $Apc^{min/+}$ model (Marsh *et al.* 2012, Chae *et al.* 2010). Interestingly, we found that in addition to an accumulation of γδT cells and thus an accumulation of IL-17 in the TME of NKG2D-sufficient mice, the phenotype of these cells was altered with a majority of γδT cells at disease endpoint expressing PD-1 in $Klrk1^{+/+}$, but not $Klrk1^{-/-}$ mice. PD-1 expression on γδT cells has been ascribed to $V\gamma6^+$ T cells (Tan *et al.* 2019), which promote tumor growth in a model of lung cancer (Jin *et al.* 2019), supporting the hypothesis that these cells are indeed tumor-promoting.

While we lack evidence for a IL-17-specific role in driving disease, personal communication with Seth Coffelt (Beatson Institute, University of Glasgow) revealed similarities in the phenotype and function of tumor-promoting NKG2D-expressing γδT cells across various tissues. By analyzing the lung of pre-metastatic breast cancer, Seth Coffelt and his group found that blocking NKG2D significantly decreased IL-17 production by γδT cells as well as $CD4^+$ T cells. In addition to studying the lung, they employed a model of intestinal cancer similar to the one used in this study and intercrossed these mice lacking *Apc* specifically on epithelial cells ($Villin\text{-}Cre^{ERT2};Apc^{F/+}$) with $Tcrd^{-/-}$ mice lacking all γδT cells, to study the function of these cells specifically. Mice lacking γδT cells survived significantly longer compared to $Tcrd^{+/+}$ littermates, supporting a tumor-promoting role of γδT cells. These findings are combined in the manuscript attached (see Appendix).

3.2.3.3 The function and contribution to disease of CD4$^+$ T cells remains unclear

A study characterizing TILs from CRC patients demonstrates a role for perforin-expressing NKG2D$^+$ CD4$^+$ T cells in the TME, suggesting that they exhibit cytotoxic function, similar to what was observed in Crohn's Disease patients (Chirica *et al.* 2015, Allez *et al.* 2007). Although we see no significant upregulation of NKG2D on CD4$^+$ T cells in the TME or increased infiltration to the TME in the presence of NKG2D (data not shown), we cannot exclude the possibility that they contribute to the cytotoxic and/or IL-17 response in *Apc$^{min/+}$* mice. The decreased frequency of CD4$^+$ T cells observed in naive NKG2D-deficient mice compared to *Klrk1$^{+/+}$* littermates poses the question of whether this subtle difference at steady state impacts disease development in the *Apc$^{min/+}$* model of intestinal cancer.

3.2.3.4 Small intestinal and colonic tumor microenvironments differ and are differentially affected by absence of NKG2D

Apc$^{min/+}$ mice develop numerous tumors in the small intestine and few large tumors in the colon, contrary to human CRC and FAP, where the main site of tumor growth is the colon. We found that NKG2D deficiency led to a strong reduction of colon tumors at disease endpoint, while differences in small tumor burden manifested at early stages, suggesting a delay in small intestinal tumor burden and a decrease of colon tumors in the absence of NKG2D. Throughout the study, we performed flow cytometric analyses on both small intestinal as well as colon tumors, but only observed subtle differences in immune cell infiltration and function in NKG2D-deficient colon tumors compared to tumors from NKG2D-sufficient *Apc$^{min/+}$* mice. Similar to small intestinal tumors, lack of NKG2D was associated with a subtle decrease in frequencies of total CD8$^+$ T cells, as well as IFN-γ-producing CD8$^+$ T cells, but not γδT cells or IL-17 production in the colon (data not shown). The TME is comparable between *Apc$^{min/+}$ Klrk1$^{+/+}$* and *Apc$^{min/+}$ Klrk1$^{-/-}$* mice at disease endpoint and 18-20 weeks and that the difference in colon tumor burden might be a consequence of NKG2D-dependent tumor initiation events at very early stages. We thoroughly investigated differences between immune cell function in small intestinal tumors compared to tumors found in the colon and found that

colon tumors are characterized by a high proportion of myeloid cells and a low frequency of T cells (ratio of 3:1 in colonic and 1:1 in small intestinal tumors, data not shown). Within the T cell subset, $CD4^+$ T cells were more abundant in the colon (1.2x increase compared to small intestinal tumors), while $CD8^+$ T cells dominated in small intestinal tumors (3x increase compared to the colonic tumors). Cytokine production by $CD8^+$ T cells (IFN-γ) and γδT cells (IL-17), but not $CD4^+$ T cells (IL-17 or IFN-γ) was higher in colonic tumors, but independent of NKG2D expression. Colon tumors establish early on in the disease and we hypothesize that this is affected by NKG2D expression, however, mechanisms involved in tumor initiation and how NKG2D is involved are yet to be determined.

3.2.3.5 NKG2D ligands are expressed throughout the disease

The NKG2D ligand RAE-1 is expressed at high levels in the healthy mouse epithelium, in line with what was previously reported on healthy human intestinal epithelium (Groh *et al.* 1996). Similarly, tumor-bearing mice expressed RAE-1 on tumor-surrounding epithelial cells as well as tumors themselves in the small intestine. Surprisingly, RAE-1 expression was independent of NKG2D expression, suggesting no NKG2D-mediated elimination during tumor progression and no immunoediting.

RAE-1 expression in the colon followed a similar trend, but interestingly, the RAE-1^+ area was slightly increased in $Apc^{min/+}$ $Klrk1^{+/+}$ mice compared to NKG2D-deficient $Apc^{min/+}$ mice. The difference was moderate and not statistically significant and further experiments need to be performed to draw conclusions on functional consequences. The higher expression of RAE-1 in $Apc^{min/+}$ $Klrk1^{+/+}$ mice could however point to differences in the extent of inflammation, which is associated with an increase in NKG2DL expression in the human colon (Allez *et al.* 2007).

We cannot exclude the possibility of ligand shedding in this model, which has been shown to promote disease in other settings, including human patients (Paschen *et al.* 2009, Easom *et al.* 2020). Further, our analysis was limited to the quantification of RAE-1 expression and other ligands might be involved in tumor progression. Specifically MULT-1 is of interest

as it has been shown to be upregulated on intestinal epithelial cells following ER stress and DNA damage (Hosomi *et al.* 2017). Nevertheless, the sustained expression of RAE-1 suggests persistent engagement of NKG2D-expressing cells in the TME, potentially promoting cytokine secretion and ultimately cell exhaustion.

3.2.3.6 Altered bacterial composition in $Apc^{min/+}$ mice

The relationship between changes in the microbiota and disease progression has been of great interest in understanding disease pathology, in particular in diseases of the gastrointestinal tract. However, microbial changes associated with disease are often difficult to attribute to pathology, due to the complexity of the microbiota. Often, large cohorts are needed and microbial sequencing, such as 16S rRNA gene sequencing only provides limited information on functional changes. Nonetheless, I was able to confirm that tumorigenesis in $Apc^{min/+}$ mice is associated with changes in the microbiota. Previous studies using $Apc^{min/+}$ mice have focused on colon tumor-infiltrating bacteria (Tomkovich *et al.* 2017), introduced a defined microbiota to study the impact of specific bacteria (Kostic *et al.* 2013, Chung *et al.* 2018) or studied changes in the microbiota following treatment (Huang *et al.* 2017, Sui *et al.* 2020, Kaur *et al.* 2018). A study by Son *et al.* specifically studied changes in the microbiota preceding tumor formation and demonstrated that mice aged 6 weeks exhibited an increase in *Bacteroidetes* compared to non-*Apc* mice (Son *et al.* 2015). This increase in *Bacteroidetes* in young $Apc^{min/+}$ mice supports the observation made in this study that tumorigenesis is associated with gradual changes in the microbiota, specifically an increasing *Bacteroidetes* to *Firmicutes* ratio. In this study, I characterized the composition of SI tumor-infiltrating bacteria and revealed that *Proteobacteria* are the most represented phyla. *Proteobacteria* have not been identified to be particularly abundant in tumor tissue from CRC (Guo *et al.* 2019), but is among the most abundant phyla in both PDA (Pushalkar *et al.* 2018) as well as breast cancer (Urbaniak *et al.* 2014). In the study by Pushalkar *et al.*, who describe high abundance of *Proteobacteria* in PDA, the authors speculate that TLR activation might induce tolerogenic, tumor-promoting macrophages within the TME, but provide no mechanistic proof (Pushalkar *et al.* 2018). Support for this hypothesis comes from the observation that mice lacking TLR5 develop spontaneous colitis associated with an

increase in *Proteobacteria* (Carvalho *et al.* 2012), suggesting inflammatory environments allow expansion of *Proteobacteria*. Future research is needed to determine whether this expansion is specific to our colony or observed in $Apc^{min/+}$ mice across different facilities. Whether *Proteobacteria* plays a significant role in disease progression or is merely a consequence of changes in the TME is of interest for future studies.

Along with characterizing the bacterial composition, I attempted to determine functional consequences by correlating phylum abundance with immune parameters. *Bacteroidetes* was correlated with an increase in NKG2D-expressing NK cells, while *Firmicutes* was correlated with an increase in PMN-MDSCs. The relevance of this is unclear and requires further research. While these changes could be a consequence of the changed inflammatory milieu with *Firmicutes* associated with milder disease, we cannot exclude the possibility that certain bacterial species are directly involved in the recruitment/activation of certain immune cells.

In addition to analyzing fecal and tumor samples on phylum level, I performed in-depth analysis using a variety of bioinformatics tools. DeSeq2 is a valuable tool that allows identification of differentially abundant bacteria and comparing various groups revealed numerous statistically significant results. The biological relevance of these changes is questionable, in particular when the statistical significance is a consequence of single outliers. Further adding to the difficulty of analyzing this dataset and revealing significant and biological relevant changes is the small sample size, in particular of tumor samples. Initially, 8 tumor samples per group were included in the analysis, but not all samples passed quality control due to the low DNA concentration. An additional drawback of this study is that analysis was limited to 16S rRNA gene sequencing, which only provides information on bacterial composition, but not functional differences, such as production of metabolites. Determining the metabolomic profile would greatly add to this dataset, but was outside of the scope of this PhD. Nonetheless, this dataset provides valuable insight into the bacterial composition of $Apc^{min/+}$ mice, something that has not been studied in detail before.

3.2.3.7 The NKG2D/NKG2DL axis is altered in human disease

To better understand the role of the NKG2D/NKG2DL axis in human disease, I made use of publicly available datasets as well as sequencing data provided to us. Crude analysis of TCGA data revealed that MIC ligands were unchanged in patients with COAD, while genes encoding ULBP ligands were upregulated. Only *ULBP2* was a predictor of disease with patients expressing high levels displaying significantly reduced survival. High expression being correlated with poor survival is in contrast to the idea that NKG2DL expression leads to better recognition and killing of tumor cells, but in line with our hypothesis that sustained ligand expression contributes to the chronic inflammatory response driving tumor growth. Previous studies have investigated whether high or low expression is associated with survival probability and while McGilvray *et al.* observed no significant difference, the mean survival of patients with high *ULBP2* expression was 60 months and 67 months in patients with low expression (McGilvray *et al.* 2009). In the second dataset analyzed in this study, *ULBP2* expression was not changed when comparing patients to patients that died of the disease, contrary to the predictive power of *ULBP2* expression in the TCGA cohort. Cohort sizes of all three groups were comparable (> 300), but variations in sample collection, sequencing or patient cohorts could explain the differences. Further, even in the TCGA dataset, differences in survival probability were subtle, raising the question of the clinical relevance.

We were particularly interested in studying transcriptional data from samples that were associated with a strong immune response. Immune cells typically infiltrate MSI-H tumors better than MSS tumors. Using the CMS classification, most MSI-H tumors are categorized as CMS1 based on their transcriptional profile. Interestingly, microsatellite status was not a predictor of NKG2D or NKG2DL expression, whereas tumor samples from CMS1 patients expressed significantly higher levels of both *KLRK1* as well as *ULBP2*. Again, differences in cohorts and differences in classification may explain the discrepancies and using the CMS classification on the TCGA dataset would help better understand regulation of NKG2D and its ligands in immune-enriched tumors. ULBP2 is increased specifically in CMS1 patients and high levels are generally associated with decreased survival, suggesting that sustained ligand expression in immune-rich tumors exacerbates disease, possibly through similar mechanisms as in the

Apc$^{min/+}$ mouse model. It needs to be determined whether the difference in survival probability is specific to CMS1 patients and whether this impacts response to ICI. Publicly available datasets, such as the TCGA contain a tremendous amount of information and potential to understand human disease. However, further in-depth analysis of either of the datasets was outside the scope of this thesis.

3.2.3.8 Conclusion

Together, we unravel a novel role of NKG2D in intestinal immunity and tumorigenesis and confirm a dual function of NKG2D in cancer. We suggest that NKG2D could be an important marker when considering cancer immunotherapy and highlight the need to better understand the function of NKG2D$^+$ cells in the TME at various stages of the disease. We further underline the need to understand tissue-specific immune responses and urge careful considerations of potential tumor-promoting side effects of NKG2D-based immunotherapy. This study confirms that NKG2D plays a role in inflammation-driven cancer and suggest that T cells, in particular CD8$^+$ and γδT cells contribute to disease severity in *Apc*$^{min/+}$ *Klrk1*$^{+/+}$ mice. We observed an increased frequency of both T cell subsets in the TME of NKG2D-sufficient mice compared to *Apc*$^{min/+}$ *Klrk1*$^{-/-}$ mice, an increased fraction of CD8$^+$ T cells producing high levels of IFN-γ and a higher frequency of PD-1$^+$ γδT cells at disease endpoint. We propose two non-exclusive mechanisms in which NKG2D can contribute to enhanced disease progression: I. Accumulation and activation of CD8$^+$ T cells secreting IFN-γ and γδT cells secreting IL-17 leads to a pro-inflammatory milieu, which promotes disease though tissue damage and pro-tumorigenic inflammation or II. sustained activation through NKG2D leading to immune cell exhaustion and dysfunction.

Our findings are important in the light of recent clinical studies using NKG2D-based approaches for immunotherapy (Lonez *et al.* 2018, Murad *et al.* 2018, Lu *et al.* 2015, Andrade *et al.* 2020). While NKG2D has the potential to recognize tumor cells and initiate an anti-tumor response, we provide further evidence for a pro-tumorigenic role, specifically in slowly arising, inflammation-driven cancers. We underline the need to better understand the function of tumor-infiltrating NKG2D$^+$ cells and raise the question of whether reactivation of NKG2D-

expressing cells through immune checkpoint blockade therapy will unleash a pro-inflammatory and tumor-promoting immune response or whether it would reactivate NKG2D$^+$ T cells to specifically kill NKG2D ligand-expressing target cells. Current studies on anti-NKG2D antibodies used to treat CD patients as well as ongoing trials on NKG2D CAR T cells in CRC patients (Celyad, clinical trial NCT03310008) will provide crucial information on the function of NKG2D in advanced disease.

3.3 Chapter 3 - NKG2D in mouse colitis

3.3.1 Introduction

The first evidence that NKG2D is implicated in IBD pathology came from Allez *et al.*, who showed that NKG2DL as well as NKG2D are upregulated in CD patients (Allez *et al.* 2007). This discovery fuelled further research into understanding the function of NKG2D in intestinal disorders and how it can be targeted therapeutically, yet, exactly mechanisms remain unclear. In the initial report, Allez *et al.* described an increased frequency of NKG2D$^+$ CD4$^+$ T cells in the LP of CD patients. Functionally, these cells exhibit a T_H1 signature with high production of TNF-α, IFN-γ and IL-2, but were also shown to produce perforin, indicating that they can be cytotoxic. A follow-up study showed that in addition to T_H1 cytokines, these NKG2D$^+$ CD4$^+$ T cells are the main source of T_H17 cytokines, including IL-17 and IL-22 (Pariente *et al.* 2011). While the authors of the first study hypothesize direct killing of NKG2DL-expressing epithelial cells through NKG2D-expressing CD4$^+$ T cells, the second study showed that mechanisms are likely more complex and that engagement of NKG2D can lead to an inflammatory response and exacerbated disease through a number of pathways. Further adding to the complexity is a study by Vadstrup *et al.* who suggested that CD8$^+$ T cells are involved in CD pathology. They proposed NKG2D-dependent chemotaxis of CD8$^+$ T cells to the inflamed tissue and showed that NKG2D is downregulated on a variety of T cell subsets in inflamed compared to unaffected tissue (Vadstrup *et al.* 2017b). Showing an inverse correlation between the frequency of NKG2D$^+$ γδT cells, and C-reactive protein (CRP), a marker of disease severity, the authors suggested that engagement of NKG2D leads to a disease-promoting inflammatory response and downregulation of NKG2D from the cell surface. Conversely, frequencies of NKG2D$^+$ CD56$^+$ T cells are positively correlated with CRP, suggesting that these unconventional T cells have distinct functions. The authors did not address the functionality of these cells, but showed that high expression of NKG2DL is associated with the release of several cytokines, including IL-1β, TNF-α and IL-10. The correlations presented in the study by Vadstrup *et al.* are weak and NKG2D-dependent migration of CD8$^+$ T cells was only shown *in vitro*. Further, their sample

numbers were low (n = 6 compared to n = 16 in the Allez *et al.* 2007 study n = 49 in the Pariente *et al.* 2011 study), making it difficult to draw conclusions and suggesting causative relationships. Nonetheless, a function for $CD8^+$ T cells cannot be ruled out.

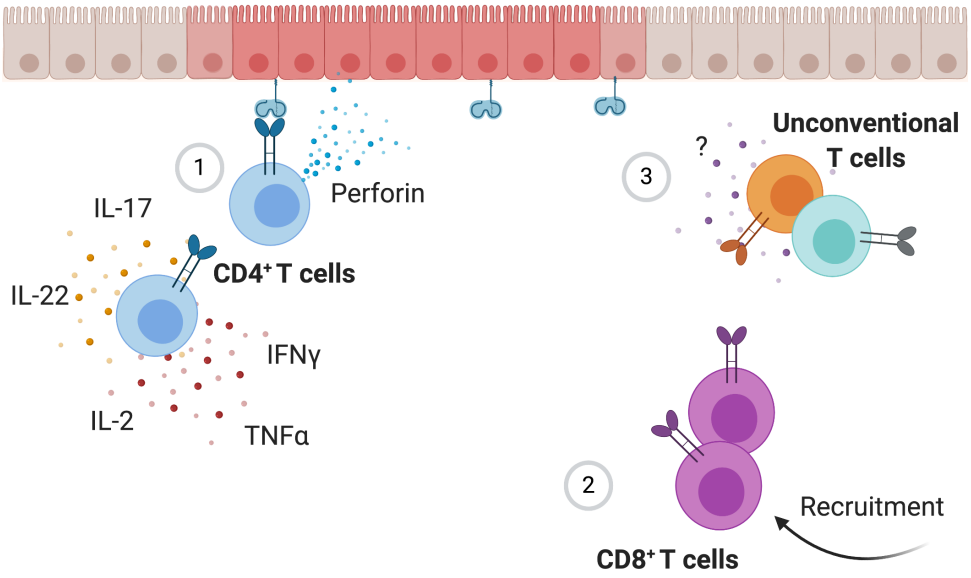

Figure 3.32: Function of NKG2D-expressing cells in Crohn's Disease patients. Simplified representation of different NKG2D-expressing T cells in the inflamed lamina propria of Crohn's Disease patients. $CD4^+$ T cells (1) have been shown to secrete T_H1 and T_H17 cytokines, but can also have cytotoxic properties. $CD8^+$ T cells are preferentially recruited to the inflamed intestine, possibly in an NKG2D-dependent manner, but their role in the tissue is unclear. Unconventional T cells (3), including γδT cells and $CD56^+$ T cells are thought to downregulate NKG2D within the inflamed tissue. The frequency of γδT cells is inversely correlated with disease severity, while there is a positive correlation between $CD56^+$ T cells and CRP. Mechanisms involving unconventional T cells are not understood. (1) is based on Allez *et al.* 2007 and (2+3) on Vadstrup *et al.* 2017b. Image was created using BioRender.

.

Despite a lack of understanding of exact mechanisms involved in NKG2D-mediated disease, these studies were key in the development of an anti-NKG2D antibody to treat CD patients (Allez *et al.* 2016). This antibody developed by Janssen Research & Development, LLC is an antagonizing human IgG4 antibody that blocks interactions between NKG2D and its ligands, but does not deplete or activate NKG2D-expressing cells. A Phase I trial raised no safety concerns, and a safety and efficacy trial, which included 78 patients with moderate-to-severe CD was performed. In this trial, patients received a subcutaneous injection of either the antibody or a placebo and disease activity was assessed after 4 and 12 weeks. While the disease activity

index was not significantly reduced in the treated group compared to the group receiving a placebo, further analysis revealed that patients with particularly severe disease (n = 23, defined as patients with calprotectin levels > 250 µg/g) significantly benefited from the treatment. They further showed that the frequencies of NKG2D-expressing NK and $CD8^+$ T cells was significantly reduced in the first weeks after treatment and returned to baseline level around week 12. In a study where the authors cultured biopsies from CD patients *in vitro* with either an isotype control or an anti-NKG2D blocking antibody, blocking NKG2D reduced secretion of a number of cytokines, including IL-1β GM-CSF, IFN-γ and TNF-α, further supporting the anti-inflammatory effect of the anti-NKG2D antibody (Vadstrup *et al.* 2017a). Interestingly, IL-10 was reduced along the pro-inflammatory cytokines upon blocking of NKG2D, suggesting that the regulation of NKG2D-dependent cytokine production is complex and cannot be reduced to certain pro-inflammatory mediators. While the clinical trial testing the anti-NKG2D antibody showed promising results, more research is needed to understand mechanisms involved in NKG2D-mediated disease. Further, biomarkers to identify patients who are most likely to benefit from the therapy, such as high expression of MICA and/or NKG2D, should be developed.

To better understand the function of NKG2D in IBD, studies using mouse models of colitis have been conducted. One study using the DSS model of intestinal inflammation showed that NKG2D is upregulated on LPL during acute inflammation and returned to baseline levels in mice in remission (Wang *et al.* 2017). Interestingly, they showed that the frequency of $NKG2D^+$ NK cells is reduced during acute colitis and hypothesize that other cell types were responsible for the observed increased overall frequency. However, they did not investigate which other cell types might be involved or elaborate on the function of NKG2D-expressing cells. A second study using the DSS model showed that $NKG2D^+$ $CD4^+$ T cells are protective, while a subset of unconventional $CD4^+$ T cells coexpressing NKG2D and NK1.1, are disease-promoting (Qian *et al.* 2017). By adoptively transferring either $NK1.1^+$ $NKG2D^+$ $CD4^+$ or $NK1.1^-$ $NKG2D^+$ $CD4^+$ T cells, the authors demonstrated that the NK1.1-expressing subset specifically exacerbate disease, while the $NK1.1^-$ subset alleviate disease severity. Mechanistically, the tissue-protective properties were shown to be mediated by the production of TGF-β, demonstrating that, at

least in mice, different subsets of $CD4^+$ T cells may have opposing functions.

In a different model of mouse colitis, which is induced by transfer of $CD4^+$ T cells to Severe combined immunodeficient mice (SCID) mice, blocking of NKG2D abrogates disease severity (Kjellev *et al.* 2007). A similar observation was made by an independent group, confirming the anti-colitogenic effect of administration of anti-NKG2D antibody (Ito *et al.* 2007). Again, data on functionality was limited, but the authors showed that stimulation of LP $CD4^+$ T cells *ex vivo* induces significantly less IFN-γ in mice treated with anti-NKG2D antibody compared to untreated controls. However, other cytokines were not assessed and may contribute to the NKG2D-mediated inflammation observed in this study. Interestingly, Ito *et al.* observed a much stronger effect with virtually no weight loss in the treated mice, which was contrary to a similar weight loss observed in both groups in the first study. The discrepancies in disease severity could be due to the use of different blocking antibodies (clone CX5 in the first and HMG2D in the second study), different dosage (200 µg twice per week and 250 µg three times per week) or differences in transfer protocol (transfer of all $CD4^+$ $CD25^-$ T cells in the first and transfer of $CD4^+$ $CD45RB^{high}$ T cells in the second study).

Regulation of NKG2DL expression during mouse colitis was addressed by two of the aforementioned studies. Qian *et al.* reported a reduction of RAE-1 protein upon administration of DSS, which was in contrast with the reported upregulation of human NKG2DL in IBD patients. Ito *et al.* measured expression of RAE-1, MULT-1 and H60 on a transcriptional level and showed a similar reduction of RAE-1, no difference in gene expression of MULT-1 and a significant upregulation of H60 in colitogenic mice.

NKG2D has clearly been shown to contribute to intestinal inflammation, both in mice and human patients, and in particular T cells have been implicated in NKG2D-mediated inflammation. Yet, exact mechanisms are not fully understood. Studies in human patients have demonstrated that perforin, IFN-γ, TNF-α, IL-17 and IL-22 may be involved in NKG2D-mediated inflammation, while this has not yet been demonstrated in mice. Nonetheless, the fact that blocking NKG2D abrogates mouse colitis suggests that similar mechanisms are in place and that mice constitute a good model organism to study this in more detail.

In an attempt to better understand the function of NKG2D in intestinal disease, our group

made use of the NKG2D-deficient *Klrk1*$^{-/-}$ mice and induced colitis in both *Klrk1*$^{+/+}$ and *Klrk1*$^{-/-}$ mice using DSS. Based on the evidence showing a disease-promoting role for NKG2D, we hypothesized that in a model of acute inflammation, *Klrk1*$^{-/-}$ mice would be protected from disease. In experiments performed by two postdoctoral researchers in the lab, Jenny McGovern and Chiara Triulzu, an interesting observation was made: NKG2D-deficient mice appeared to be more susceptible to DSS-induced colitis in the acute phase, but showed decreased weight loss compared to wild-type littermates at chronic stages of disease (Figure 3.33).

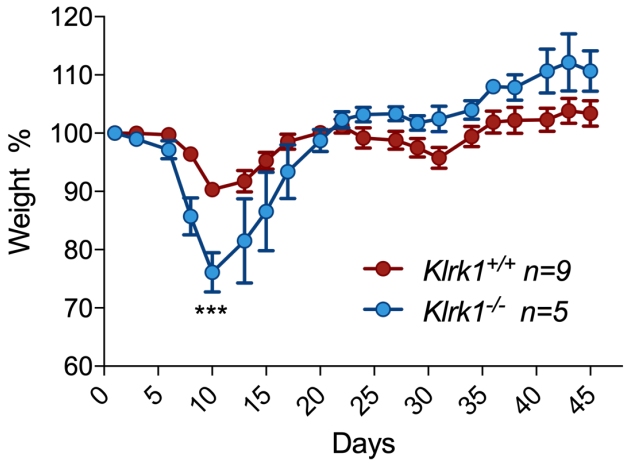

Figure 3.33: Weight loss of *Klrk1*$^{+/+}$ and *Klrk1*$^{-/-}$ mice in a DSS colitis model. *Klrk1*$^{+/+}$ and *Klrk1*$^{-/-}$ mice were treated with 2% DSS 3 x 7 days with 14 days of receiving normal drinking water in between treatments. DSS = dextran sodium sulfate. ***p $\leq$ 0.001.

.

However, this phenotype was not consistent and while a strong genotypic difference was observed in some experiments, other experiments showed no differences. In this chapter, the aim was to dissect the function of NKG2D further by repeating DSS experiments in a tightly controlled manner and complementing findings from sterile colitis to a model of infectious-induced colitis using *C. rodentium*. *C. rodentium* is routinely used to induce mouse colitis, but has not been studied in the context of NKG2D-mediated immunity. Studying the course of disease in *C. rodentium*-mediated colitis in NKG2D-deficient mice will not only add to the understanding of NKG2D in mouse colitis, but also unravel infection-specific components. In the DSS model, the response to non-physiological tissue damage is studied, while the aspect of host defense and elimination of the invading pathogen, something that the NKG2D/NKG2DL axis has been implicated in, will be considered in the *C. rodentium* model.

Aims:

1. To reanalyze previously acquired data on DSS-induced colitis to dissect experimental factors leading to differences in some, but not other experiments.

2. To repeat DSS experiments in a tightly controlled manner and with an improved flow cytometry panel.

3. To set up a model of infection-induced colitis using *C. rodentium*.

4. To determine impact of NKG2D-deficiency on *C. rodentium*-induced colitis.

3.3.2 Results

3.3.2.1 Analysis of previously acquired data revealed no impact on colitis severity in NKG2D-deficient mice

In an attempt to understand what factors led to differences in disease susceptibility and whether lack of NKG2D is indeed associated with heightened susceptibility to DSS-induced colitis, I performed a thorough analysis of previously acquired data. In a first instance, all data was pooled and analyzed as one experiment. A total of 13 experiments were performed by previous lab members, which included 6 short-term (ST) (DSS 1 x 7 days followed by 9 days of normal drinking water) and 7 long-term (LT) experiments (DSS 3 x 7 days with 14 days of normal drinking water in between treatments) (Table 3.4).

Table 3.4: Number of mice and experiments performed by two postdoctoral researchers in the lab between 2012 and 2014.

	Short-term (ST)	**Long-term (LT)**
***Klrk1*$^{+/+}$**	36	22
***Klrk1*$^{-/-}$**	37	23
Rounds	5	7

The data depicted in Figure 3.34 is a pool of all 5 rounds of ST experiments as well as initial weight loss, but not colon length and weight data from the 7 rounds of LT treatment. All mice started losing weight around day 4 with the most severe weight loss on day 8 averaging at 85% of the initial weight. In the recovery phase starting around day 10 mice gained weight, reaching approximately 95% of their initial bodyweight by day 16 (Figure 3.34a). No differences in weight loss were observed between *Klrk1*$^{+/+}$ and *Klrk1*$^{-/-}$ mice, with both groups losing comparable amounts of weight and showing a similar recovery curve.

As an additional read-out of disease, colon length and weight was measured. Inflamed colons are typically significantly shorter and heavier due to the vast infiltration of immune cells. Indeed, colons of DSS-treated mice were significantly shorter (8 cm in DSS-treated mice compared to 10 cm in control mice) and heavier (0.3 g in DSS-treated mice compared to 0.24 g in control mice, Figure 3.34b and c). Similar to the lack of differences in weight loss, no differences were observed between *Klrk1*$^{+/+}$ and *Klrk1*$^{-/-}$ mice.

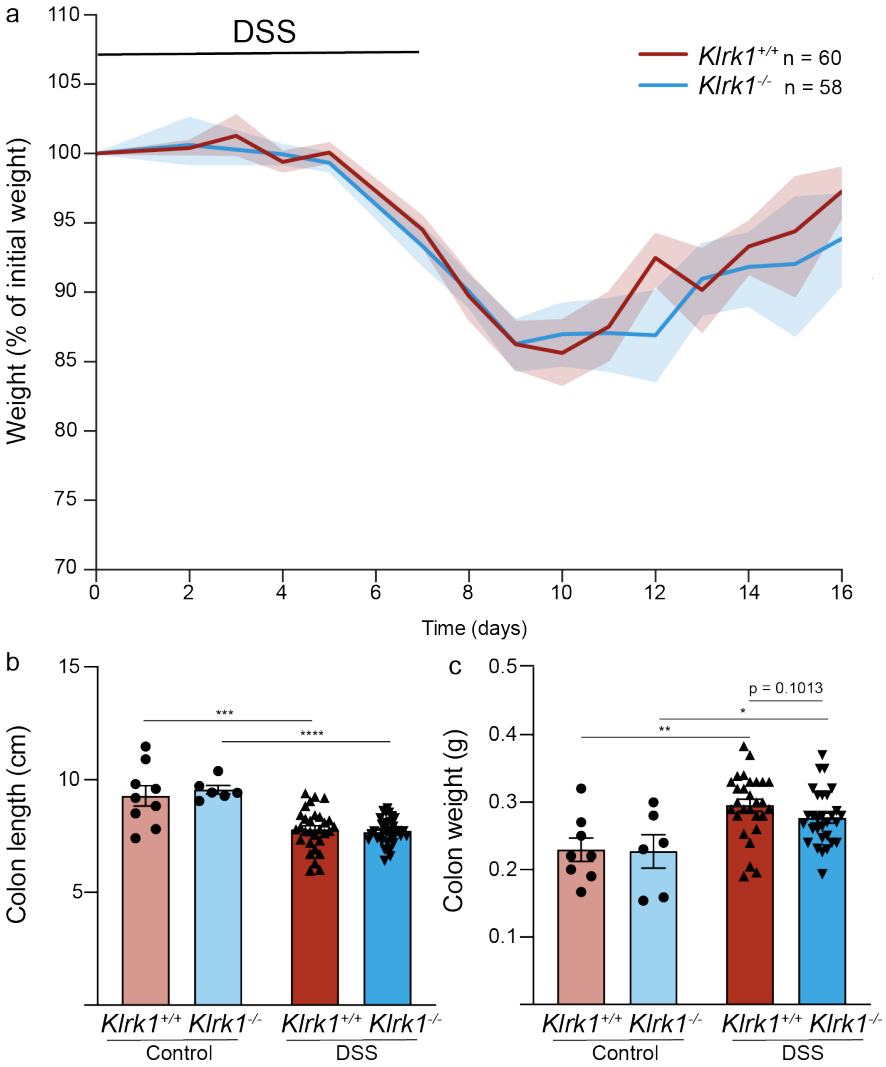

Figure 3.34: NKG2D does not influence disease severity in a short-term model of DSS-induced colitis. (a) Weight loss over time in *Klrk1*$^{+/+}$ compared to *Klrk1*$^{-/-}$ mice treated with 2% DSS for 7 days and normal drinking water for the remaining 9. Data plotted as mean with a 95% CI. (b) Colon length (in cm) and (c) colon mass (in g) of control and DSS-treated mice on day 16. n $\geq$ 6 for control condition and n $\geq$ 25 for DSS-treated mice. DSS = dextran sodium sulfate, CI = confidence interval. Data represented as mean $\pm$ SEM of individual mice from at least five independent experiments. * $p \leq 0.05$, ** $p \leq 0.01$, *** $p \leq 0.001$, **** $p \leq 0.0001$.

.

In a next step, we plotted individual experiments to determine whether there were any batch effects as a result of the composition of experimental groups, changes in the microbiota over the years or differences in the molecular weight of the DSS. Out of the 5 experiments performed, only 3 had sufficient numbers of both *Klrk1*$^{+/+}$ and *Klrk1*$^{-/-}$ mice to directly compare disease susceptibility of the two strains. In the first experiment, *Klrk1*$^{-/-}$ displayed more severe weight

loss with an average of 82% of the initial bodyweight on day 10 compared to *Klrk1*$^{+/+}$ mice (average of 88%) (Figure 3.35a). Contrary to this, in the second experiment, *Klrk1*$^{+/+}$ lost significantly more weight with an average of 83% of initial bodyweight on day 10 compared to 89% in *Klrk1*$^{-/-}$ mice (Figure 3.35b). In the third experiment (Figure 3.35b), no differences were observed and the minimum weight was approximately 88% in both genotypes.

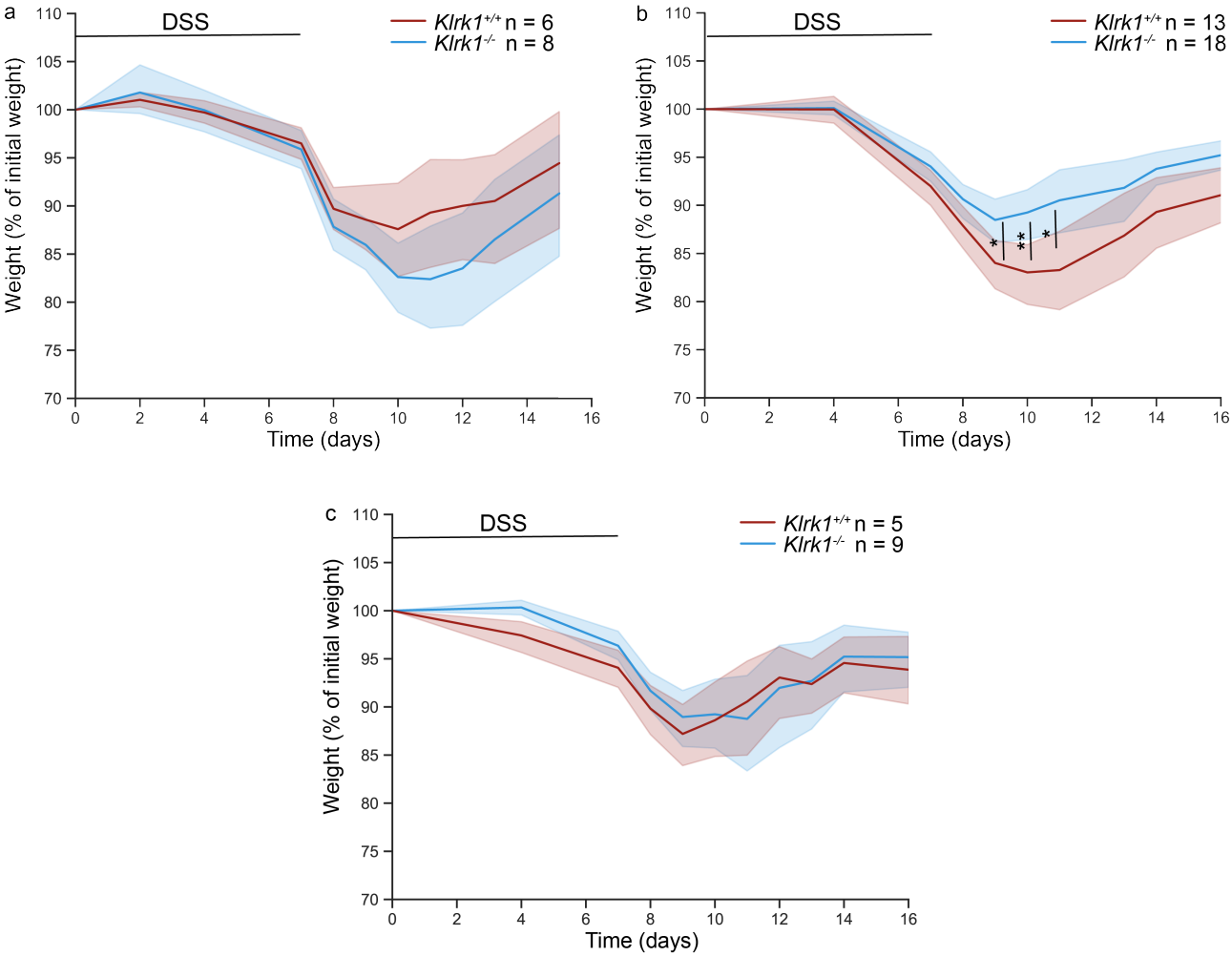

Figure 3.35: Weight loss of *Klrk1*$^{+/+}$ and *Klrk1*$^{-/-}$ mice in three individual short-term DSS colitis experiments reveals inter-experimental variations. Data plotted as mean with a 95% CI. CI = confidence interval. DSS = dextran sodium sulfate. Data represented as mean ± SEM. * $p \leq 0.05$, ** $p \leq 0.01$.

Susceptibility to DSS-induced colitis depends on many factors, including sex (Bábíčková *et al.* 2015) and molecular weight of the DSS (Perše *et al.* 2012). To understand whether any of these factors contributed to the contradicting results observed in Figure 3.35, we performed Analysis of covariance (ANCOVA). The aim of this statistical analysis is to adjust for preexisting differences that are not affected by treatment. Baseline characteristics are depicted in Table

3.5 and in addition to age, sex and bodyweight, each experimental round was included as a covariant. Including experimental rounds as a covariant was thought to adjust for different batches of DSS with different molecular weights that were used. ANCOVA was performed using different disease severity readouts as dependent variables, including percentage of initial bodyweight on day 10, colon length and colon weight and the genotype as the independent variable.

Table 3.5: Baseline characteristics of mice used in previous short-term DSS experiments.

	***Klrk1*$^{+/+}$** (n = 36)	***Klrk1*$^{-/-}$** (n = 37)
Age (weeks)	21.08 (± 4.33)	20.44 (± 4.71)
Sex	27 ♀ 9 ♂	33 ♀ 4 ♂
Bodyweight (g)	25.56 (± 3.59)	25.27 (± 3.73)

None of the dependent variables yielded a p-value below 0.05 (Table 3.6), meaning that the null hypothesis that lack of NKG2D does not influence susceptibility to DSS-induced colitis was accepted.

Table 3.6: Results of ANCOVA analysis.

Dependent variable	% of bodyweight (day 10)	Colon weight	Colon length
p-value	0.212162	0.831000	0.111350

Lastly, we performed similar analysis on the LT DSS dataset. Similar to the ST data, no differences in weight loss or colon length at disease endpoint were observed (Figure 3.36). This was confirmed by ANCOVA and the null hypothesis that lack of NKG2D does not influence disease susceptibility in a LT DSS model of chronic inflammation was accepted (data not shown).

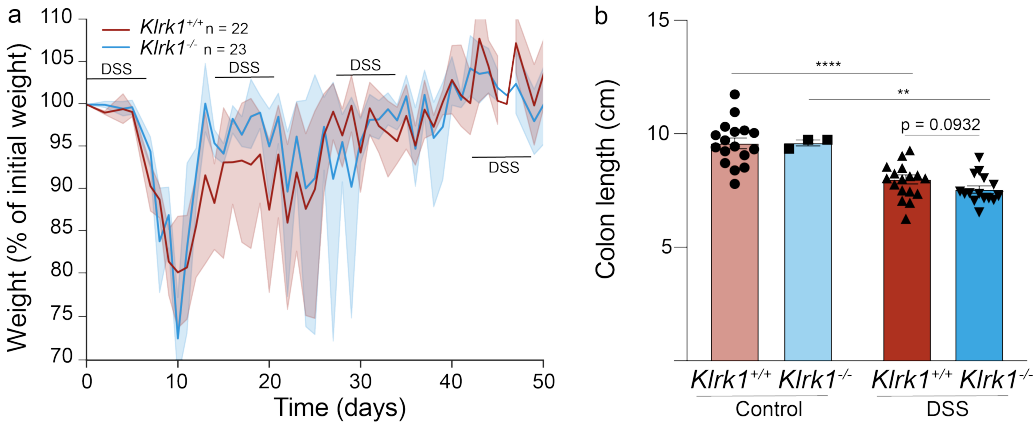

Figure 3.36: NKG2D does not affect disease susceptibility to DSS model of chronic intestinal inflammation. (a) Weight loss over time in *Klrk1*$^{+/+}$ compared to *Klrk1*$^{-/-}$ mice treated with 3 rounds of 2% DSS for 7 days and 14 days normal drinking water. Data plotted as mean with a 95% CI. (b) Colon length (in cm) of control and DSS-treated mice on day 50. n $\geq$ 3 for control condition and n $\geq$ 14 for DSS-treated mice. DSS = dextran sodium sulfate, CI = confidence interval. Data represented as mean $\pm$ SEM of individual mice from at least three independent experiments. **p $\leq$ 0.01, ****p $\leq$ 0.0001

.

Analysis of previously acquired data in the lab revealed that *Klrk1*$^{+/+}$ and *Klrk1*$^{-/-}$ mice are equally susceptible to acute, as well as chronic intestinal inflammation. However, there were several drawbacks to the study. I. mice were not age-, sex- and bodyweight-matched and II. different lots of 'Reagent-grade' DSS with differing sulfur content and molecular weight were used. We therefore performed a small study using only female mice of similar ages and treating them with the same batch of 'Colitis grade' DSS (MP Biomedicals).

3.3.2.2 Optimization of DSS colitis experiments

Before setting up a new round of DSS experiments, I performed two test experiments to I. get familiar with the experimental procedure, II. test the flow cytometry panel and ensure sufficient cell yields to study ILCs, III. determine the right dose and length of the DSS treatment and IV. determine the impact of age and starting weight on disease severity.

In a first instance, I performed two ST experiments in which we determined whether the chosen dose of 2% Colitis-grade DSS reliably induces weight loss within the severity limit (weight loss not below 85% for more than 72 hours and not below 80% at any given point). To reduce variations in mouse weight caused by food or water intake, weight was measured at the same time every day.

Indeed, all mice started losing weight around day 4 with a maximum weight loss on day 8 or

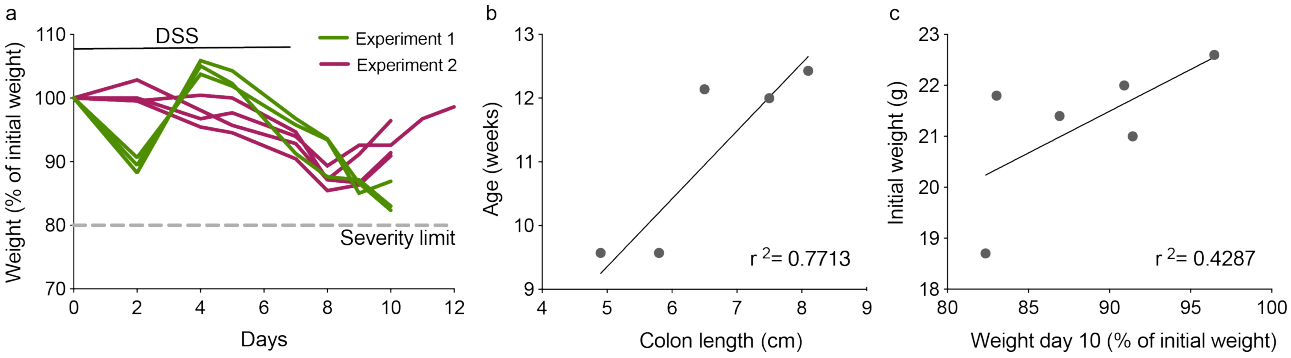

Figure 3.37: Starting weight and age of mice influences disease susceptibility to DSS treatment. (a) Weight loss curve from two independent experiments. n = 3 for Experiment 1 and n = 4 for Experiment 2. Dotted line indicates severity limit. (b) Correlation of age at the beginning of the experiment and colon length as a read-out of disease severity. n = 6 (b) Correlation of weight at the beginning of the experiment and weight at day 10 as a read-out of disease severity. n = 6. Data points represent individual mice. DSS = dextran sodium sulfate.

.

9 (Figure 3.37a). The observed weight loss on day two in the 'Experiment 1' group was most likely caused by external factors, such as a cage change. All mice used in the test experiment were female and between 9.5 and 12.5 weeks of age at the start of the experiment with an initial bodyweight ranging from 18.5 to 22.5 g. To determine how these parameters influence disease susceptibility, age and initial bodyweight was plotted against colon length and weight on day 10. Indeed, age and colon length was strongly correlated (r^2 = 0.7713, p = 0.0213) (Figure 3.37b). I further observed a weak correlation of initial weight and bodyweight on day 10 (r^2 =

0.4287, p = 0.1582) (Figure 3.37c) and concluded that both age and weight at the start of the experiment influence disease severity.

3.3.2.3 NKG2D deficiency does not influence susceptibility to DSS-induced acute or chronic colitis

I set up a small, but extremely tightly controlled study to confirm that NKG2D does not influence disease susceptibility to DSS-induced colitis. Due to the importance of age-matched mice, experimental groups were small. A total of 4 ST experiments with 5 *Klrk1*$^{+/+}$ and 8 *Klrk1*$^{-/-}$ mice and a total of 3 LT experiments with 3 *Klrk1*$^{+/+}$ and 7 *Klrk1*$^{-/-}$ were performed (Table 3.7). One *Klrk1*$^{-/-}$ mouse in the LT group reached the severity limit on day 10 and was therefore retrospectively included in the ST group.

Table 3.7: Baseline characteristics of mice used in DSS experiments.

	Short-term		**Long-term**	
Genotype	*Klrk1*$^{+/+}$ (n=5)	*Klrk1*$^{-/-}$ (n=8)	*Klrk1*$^{+/+}$ (n=3)	*Klrk1*$^{-/-}$ (n=7)
Age (weeks)	7.42 ± 0.80	7.32 ± 0.93	9.05 ± 0.79	8.64 ± 0.81
Weight (g)	19.30 ± 1.57	19.60 ± 1.53	19.69 ± 0.76	19.30 ± 1.15

As a readout of disease severity, weight loss over time as well as colon length at the experimental endpoint (day 10 for ST experiments and day 38 for LT experiments) was measured. As expected, mice reached their minimum weight around day 10, which was set as the endpoint for the ST experiments (Figure 3.38a). In LT experiments, mice started recovering after day 10 and reached their starting weight shortly after (Figure 3.38b). Each round of DSS treatment was associated with a reduction in weight of 5-10% and subsequent recovery. The average colon length of healthy controls was 7.6 cm, which was significantly reduced upon both ST and LT DSS treatment (Figure 3.38c). Average colon length on day 10 was between 5.6 and 6 cm and between 6 and 6.2 cm following repeated cycles of DSS. No differences between *Klrk1*$^{+/+}$ and *Klrk1*$^{-/-}$ mice were observed, indicating that lack of NKG2D does not influence susceptibility to DSS-induced acute or chronic colitis.

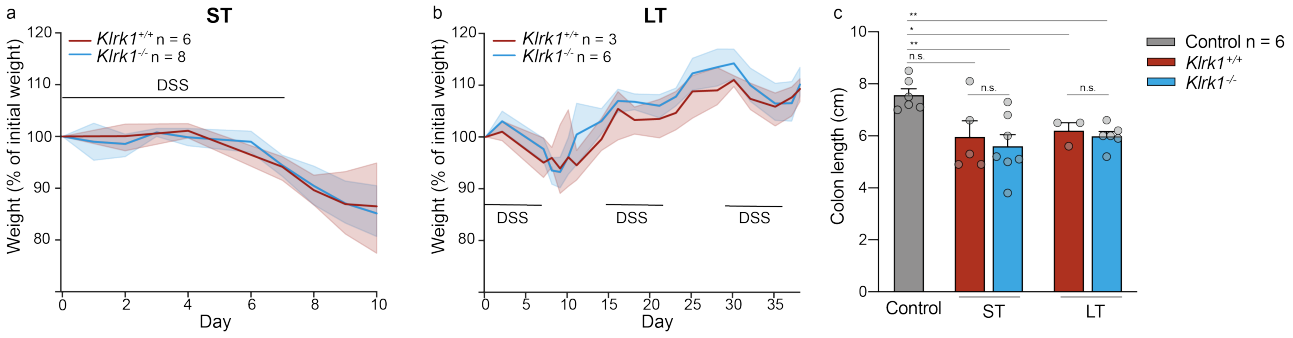

Figure 3.38: Weight loss and colon length following DSS treatment is not influences by NKG2D. (a) Weight loss in *Klrk1*$^{+/+}$ and *Klrk1*$^{-/-}$ mice following ST DSS treatment. (b) Weight loss in *Klrk1*$^{+/+}$ and *Klrk1*$^{-/-}$ mice following LT DSS treatment. (c) Colon length following ST or LT DSS treatment comparing control mice to *Klrk1*$^{+/+}$ and *Klrk1*$^{-/-}$ littermates. n = 6 for control condition and n $\geq$ 3 for DSS-treated mice. Data in a + b plotted as mean with a 95% CI. Data in c represented as mean $\pm$ SEM of individual mice from at least three independent experiments. ST = short-term, LT = long-term, DSS = dextran sodium sulfate, n.s. = not significant, CI = confidence interval. *p $\leq$ 0.05, **p $\leq$ 0.01.

.

3.3.2.4 NKG2D expression remains unchanged upon DSS-induced colitis

To determine whether NKG2D-expressing cells are involved in the immune response following ST or LT DSS treatment, I compared frequencies of NKG2D-expressing immune cells in the inflamed colonic LP to healthy mice. I found that neither ST nor LT treatment induced changes in NKG2D expression with frequencies of NKG2D^{+} T cells, ILC3s and NK cells being similar in the inflamed colon compared to healthy controls (Figure 3.39). ILC1s were nearly absent in chronically inflamed intestines and NKG2D expression was therefore not determined. Frequencies of NKG2D^{+} ILC1s were slightly increased in mice undergoing ST DSS treatment compared to healthy controls, however the difference was small and not statistically significant (Figure 3.39a and b). These data demonstrate that NKG2D expression and frequencies of NKG2D-expressing cells do not change during the course of DSS-induced colitis and could explain the lack of genotypic differences in disease susceptibility.

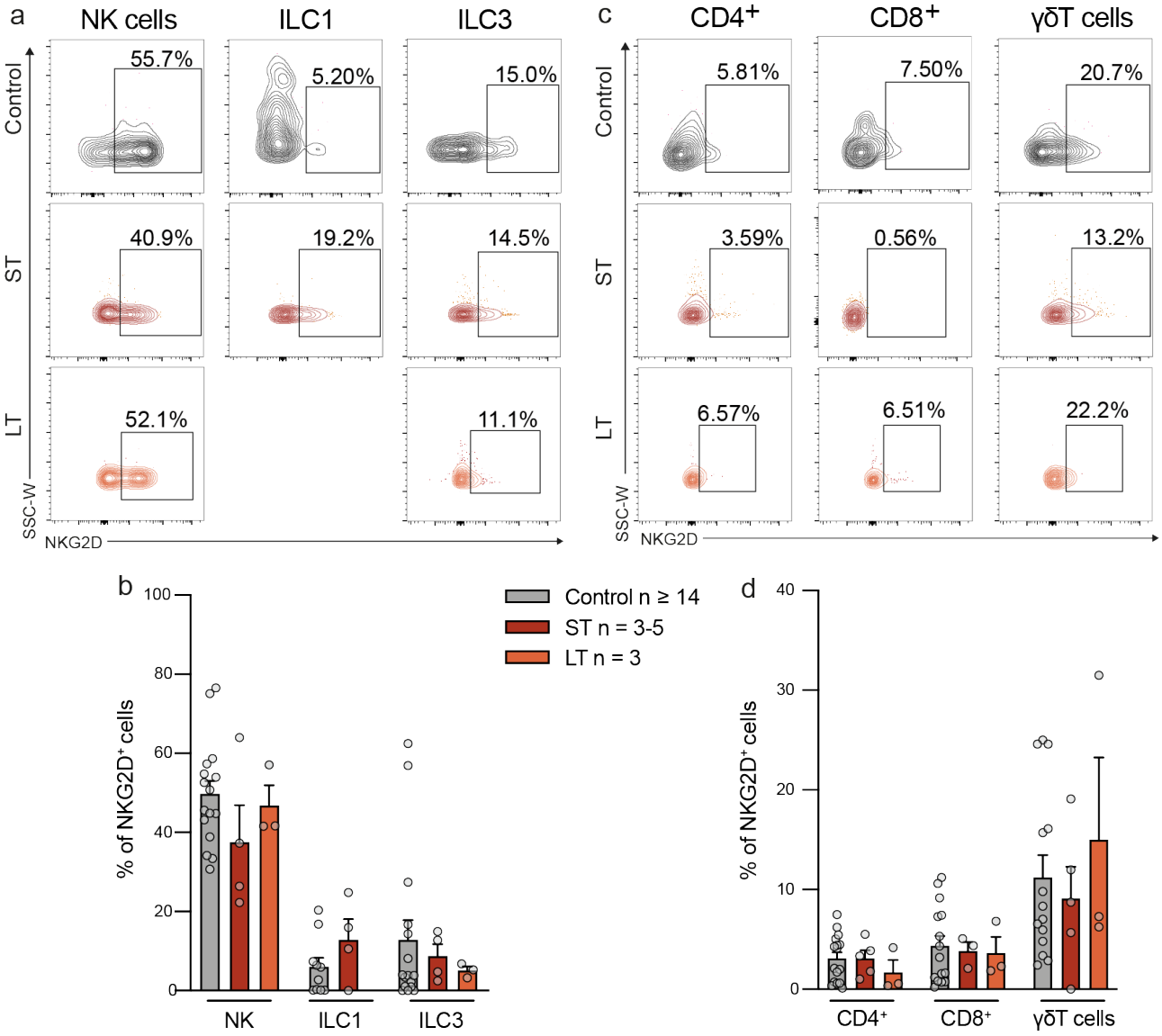

Figure 3.39: NKG2D expression remains unchanged upon treatment with DSS. (a) Representative flow cytometry plots depicting NKG2D expression on innate cells (NK cells gated on $CD3^+$ $NK1.1^-$, ILC1 gated on $CD3^-$ $CD19^-$ $Ly6G^-$ $Ly6C^-$ $CD127^+$ T-bet^+ and ILC3 gated on ILC1 gated on $CD3^-$ $CD19^-$ $Ly6G^-$ $Ly6C^-$ $CD127^+$ $ROR\gamma T^+$) in naive control mice (grey), as well as *Klrk1*$^{+/+}$ mice undergoing ST (red) or LT (orange) DSS treatment. (b) Frequencies of NKG2D-expressing innate cells. (c) Representative flow cytometry plots of NKG2D expression on T cells (gated on $CD4^+$, $CD8^+$ or $\gamma\delta TCR^+$) in naive control mice (grey), as well as *Klrk1*$^{+/+}$ mice undergoing ST (red) or LT (orange) DSS treatment. (d) Frequencies of NKG2D-expressing T cells. Data represented as mean ± SEM of individual mice from at least three independent experiments. ST = short-term, LT = long-term, DSS = dextran sodium sulfate.

3.3.2.5 NKG2D deficiency does not lead to changes in immune cell subsets of the acutely inflamed intestine

Using a similar 18-color flow cytometry panel to the one presented in Chapter 1, I thoroughly characterized changes in the intestinal immune compartment upon ST treatment with DSS. For this, I compared the healthy colonic LP and MLN to inflamed tissue isolated from *Klrk1*$^{+/+}$ and *Klrk1*$^{-/-}$ on day 10 of treatment. Frequencies of T cells, B cells and myeloid cells were comparable in the healthy and inflamed intestine (data not shown), while the composition of the T cell compartment changed upon DSS treatment, with lower frequencies of CD4$^+$ T cells, and a slight increase of CD8$^+$ T cells from an average of 7.8% of all CD45$^+$ cells to 15.0% and 16.0% in *Klrk1*$^{+/+}$ and *Klrk1*$^{-/-}$, respectively (Figure 3.40a left and b). Frequencies of γδT cells remained unchanged, while percentages of ILC1s and ILC3s, which are as low as 0.7% and 0.8% respectively in healthy mice, increased upon treatment with DSS (Figure 3.40a right). ILC1s were increased to 1.5% in *Klrk1*$^{+/+}$ and 3.0% in *Klrk1*$^{-/-}$ DSS-treated mice, while the average frequency of ILC3s was 2.4% in *Klrk1*$^{+/+}$ and 4.0% in *Klrk1*$^{-/-}$ mice. Frequencies of NK cells remained unchanged. Surprisingly, we found that ST treatment resulted in decreased frequencies of IL-17- and IFN-γ-producing T cells, with a significant reduction of IL-17$^+$ CD4$^+$ T cells (29.4% to 5.1%), IL-17$^+$ γδT cells (22.8% to 12.0%) and IFN-γ$^+$ CD8$^+$ T cells (13.8% to 1.2%) in DSS-treated *Klrk1*$^{+/+}$ mice compared to healthy controls (Figure 3.40c left). This reduction was less pronounced in *Klrk1*$^{-/-}$ mice, in which 11.4% of CD4$^+$ T cells and 16.2% of γδT cells were IL-17$^+$ and 7.3% of CD8$^+$ T cells IFN-γ$^+$. Contrary to this reduction of cytokine-producing T cells, we observed an increase in cytokine-producing ILCs and NK cells. Specifically, the average frequency of IFN-γ$^+$ ILC1s was increased from 27.1% to 46.3% in *Klrk1*$^{+/+}$ and 38.5% in *Klrk1*$^{-/-}$ mice (Figure 3.40c right and d). Similar changes were observed in frequencies of IL-17$^+$ ILC3 and IFN-γ$^+$ NK cells.

Together, these data demonstrate that acute DSS-induced colitis is associated with a reduction in CD4$^+$ T cells and an increase in CD8$^+$ T cells as well as increased frequencies of ILC1s and ILC3s. Cytokine-producing T cells were reduced, while frequencies of IL-17- and IFN-γ-producing ILCs and NK cells was slightly increased. In conclusion, we hypothesize that inflammation at early stages is driven by an innate rather than an adaptive immune response.

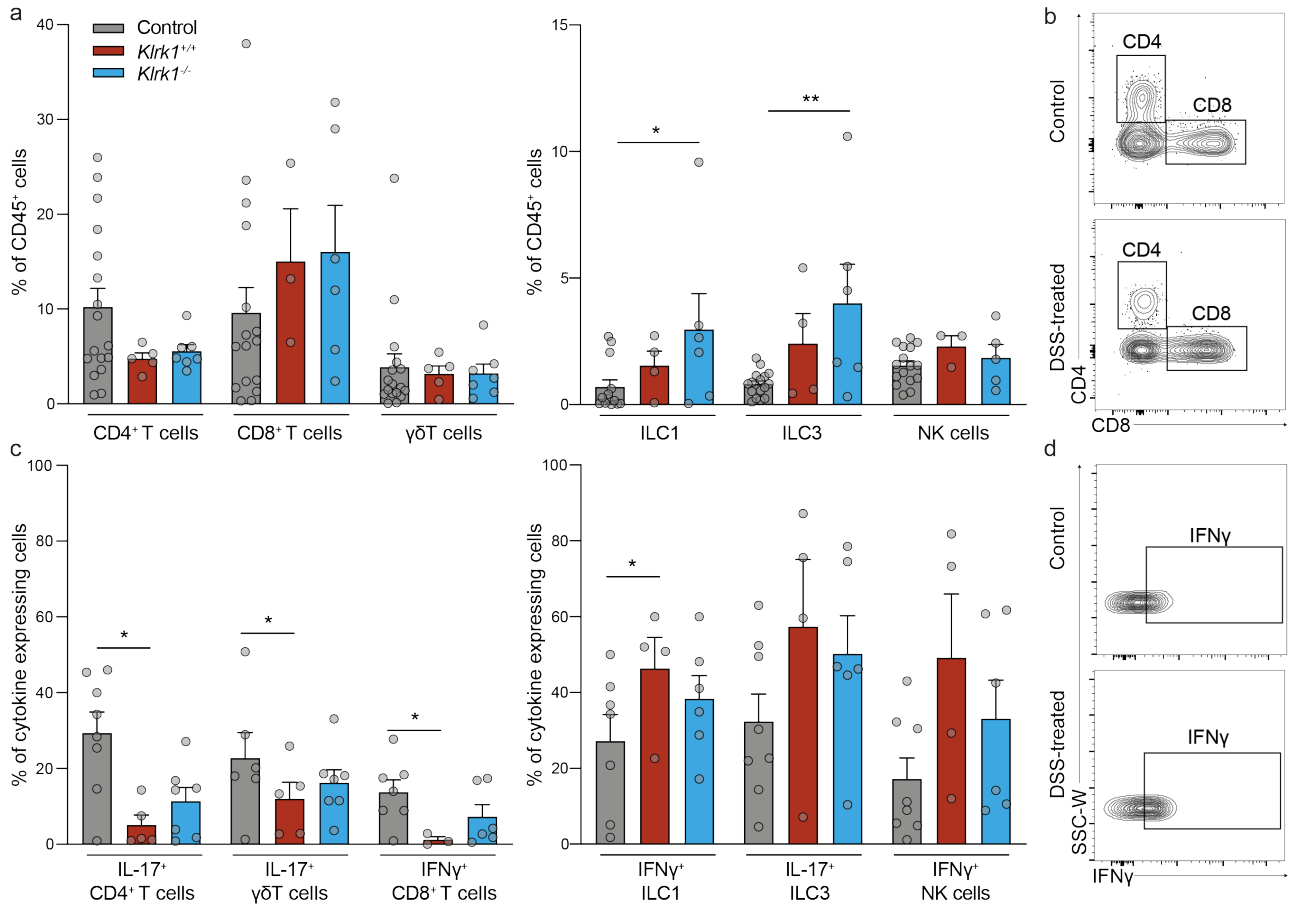

Figure 3.40: Short-term DSS treatment is associated with changes in the T cell compartment and cytokine production by innate cells. (a) Frequencies of T cells (left) (gated on $CD4^+$, $CD8^+$ or $\gamma\delta TCR^+$) and innate cell (right) (NK cells gated on $CD3^+$ $NK1.1^-$, ILC1 gated on $CD3^-$ $CD19^-$ $Ly6G^-$ $Ly6C^-$ $CD127^+$ $T\text{-}bet^+$ and ILC3 gated on ILC1 gated on $CD3^-$ $CD19^-$ $Ly6G^-$ $Ly6C^-$ $CD127^+$ $ROR\gamma T^+$) in the colonic LP of naive control mice (grey), as well as *Klrk1*$^{+/+}$ (red) and *Klrk1*$^{-/-}$ (blue) mice undergoing ST DSS treatment. (b) Representative flow cytometry plots of T cells (gated on live $CD45^+$ $CD3^+$) in control (top) and DSS-treated mice (bottom) (c) Frequencies of cytokine-producing T cells (left) and innate cell (right) stimulated with PMA and ionomycin in the colonic LP of control mice (grey), as well as *Klrk1*$^{+/+}$ (red) and *Klrk1*$^{-/-}$ (blue) mice undergoing ST DSS treatment. (d) Representative flow cytometry plots of IFN-γ^+ ILC1s (gated on live $CD45^+$ $CD3^-$ $CD19^-$ $Ly6G^-$ $Ly6C^-$ $CD127^+$ $T\text{-}bet^+$) in control (top) and DSS-treated mice (bottom). $n \geq 8$ for control mice, $n \geq 3$ for *Klrk1*$^{+/+}$ and $n \geq 5$ for *Klrk1*$^{-/-}$ mice. LP = lamina propria, DSS = dextran sodium sulfate. Data represented as mean ± SEM of individual mice from at least four independent experiments. * $p \leq 0.05$, ** $p \leq 0.01$.

3.3.2.6 Transcriptional changes in response to DSS-induced acute colitis depend on disease severity, but not NKG2D expression

To further characterize the immune response following ST DSS treatment, we performed transcriptional analysis of a number of genes associated with inflammation. For this, we isolated RNA from colons of healthy or DSS-treated mice and performed quantitative PCR (qPCR) analysis using TaqMan probes. Genes associated with a T_H1 (*Ifng* encoding IFN-γ) and T_H17 (*Il17* encoding IL-17 and *Il22* encoding and IL-22) were expressed at low levels (IFN-γ and IL-17) or were undetermined (IL-22) in control mice, but increased in both *Klrk1*$^{+/+}$ and *Klrk1*$^{-/-}$ DSS-treated mice (Figure 3.41). *Il10*, encoding IL-10, an anti-inflammatory cytokine was expressed at low levels in control mice and increased 60-fold in *Klrk1*$^{+/+}$ mice and 5-fold in *Klrk1*$^{-/-}$ DSS-treated mice, suggesting IL-10 is upregulated in response to DSS-induced damage. *Tgfb1* (TGF-β), a second anti-inflammatory cytokine studied in this experiment was expressed at high levels at baseline and did not change significantly upon DSS treatment. *Nos2* (iNOS) (26-fold increase) and *Il6* (IL-6) (200-fold increased), typically secreted by myeloid cells were significantly increased in both genotypes, while gene expression of *Tnfa* encoding TNF-α was unaffected. *Muc1* (Mucin-1 precursor (MUC1)) is often associated with colitis-associated CRC (Beatty *et al.* 2007), but its expression remained unchanged upon DSS treatment. Interestingly, NKG2D expression was undetected in control mice, but detected in DSS-treated *Klrk1*$^{+/+}$ mice. Albeit low expression levels, the increased expression of NKG2D upon DSS treatment is contrary to what was observed at protein level, where no difference in frequencies of NKG2D-expressing cells was observed when comparing control mice to DSS-treated *Klrk1*$^{+/+}$ mice. Of the genes quantified in this experiment, no significant differences between genotypes were observed apart from the expression level of NKG2D. This is in line with the lack of changes immune cell composition and functionality in *Klrk1*$^{+/+}$ compared to *Klrk1*$^{-/-}$ mice.

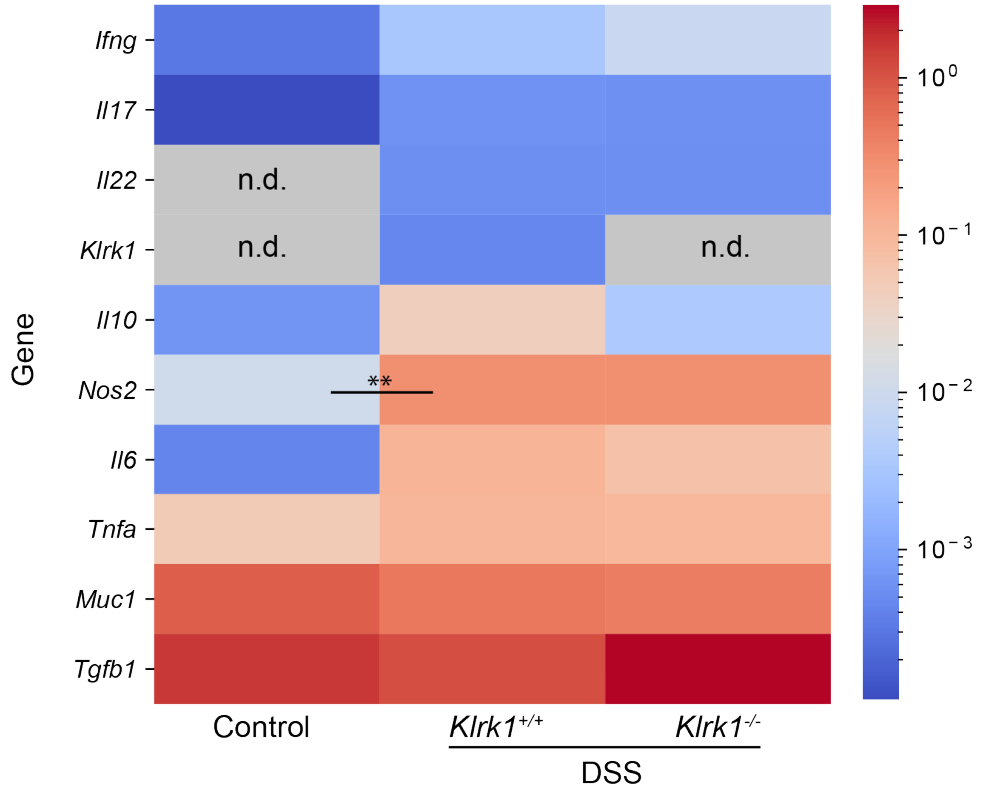

Figure 3.41: Transcriptional changes in mice upon short-term DSS treatment are independent of NKG2D expression. Heatmap depicting fold change of each gene over the housekeeping gene HPRT in the colon of naive control or DSS-treated *Klrk1*$^{+/+}$ and *Klrk1*$^{-/-}$ mice. n = 4 per group, except *Klrk1*$^{-/-}$ where n = 5. n.d. = not detected, ST = short-term, DSS = dextran sodium sulfate. Data depicted as average. **p $\leq$ 0.01. Reverse transcription and qPCR were performed by undergraduate student Harry Baird.

Throughout the analysis of macroscopic parameters, flow cytometric data and gene expression data, we noticed high variability among mice of the same genotype, despite being genetically identical and in many cases littermates. Despite it being a small study with a small sample size, we sought to exploit this variability to better understand mechanisms involved in DSS-mediated colitis. For this we categorized mice into three groups: 'mild', 'intermediate' and 'severe' disease. Disease severity was defined as the minimum weight relative to the starting weight with 'severe' being $<$ 80% of the initial weight, 'intermediate' between 80 and 90% and 'mild' $>$ 90%. Fold changes of *Il17*, *Il22*, *Klrk1* and *Il6* followed disease severity, with the lowest expression in control mice and the highest in mice falling into the 'severe' category (Figure 3.42).

Fold changes of both *Il10* and *Tgfb1* were higher in mice falling into the 'mild' compared to the 'intermediate' category, potentially revealing a relationship between the expression of anti-inflammatory cytokines and disease severity. However, both cytokines were increased in mice with 'severe' disease. This demonstrates that *Klrk1*$^{+/+}$ and *Klrk1*$^{-/-}$ mice have a similar gene expression profile that is dependent on disease severity.

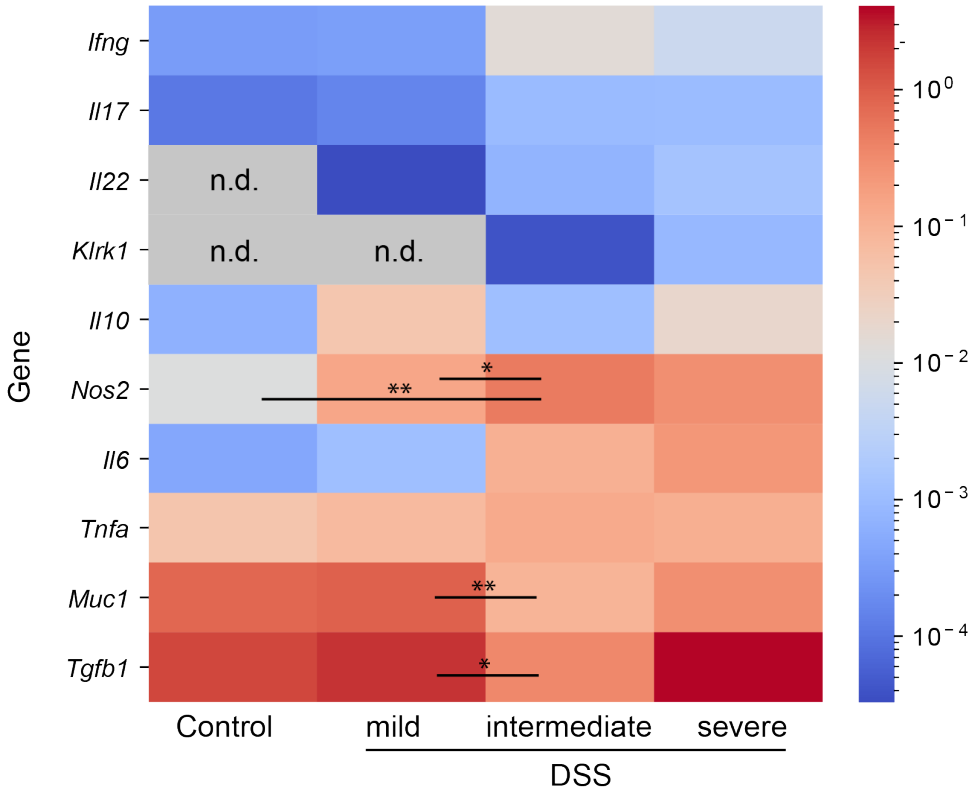

Figure 3.42: Transcriptional changes in mice upon short-term DSS treatment depending on disease severity. Heatmap depicting fold change of naive control or DSS-treated *Klrk1*$^{+/+}$ and *Klrk1*$^{-/-}$ mice ordered by disease severity. n = 4 for control group, n = 2 for 'severe', n = 3 for 'intermediate' and n = 4 for 'mild'. n.d. = not detected, ST = short-term, DSS = dextran sodium sulfate. Data depicted as average. *p $\leq$ 0.05, **p $\leq$ 0.01. Reverse transcription and qPCR were performed by undergraduate student Harry Baird.

.

3.3.2.7 NKG2D deficiency leads to no changes in immune cell subsets of the chronically inflamed intestine

Lastly, I investigated the immune cell composition and functionality of the intestine of *Klrk1*$^{+/+}$ and *Klrk1*$^{-/-}$ mice undergoing LT DSS. While acute colitis was associated with an increase in ILCs and CD8$^+$ T cells, LT treatment resulted in a slight increase in CD4$^+$ and CD8$^+$ T cells and a reduction in γδT cells, ILCs and NK cells (Figure 3.43a and b). The decrease in ILC1s and NK cells was striking, with a decrease from 0.7% ILC1s in control mice to 0.02% and 0.03% in *Klrk1*$^{+/+}$ and *Klrk1*$^{-/-}$ mice, respectively. Similarly, NK cells were decreased from 1.54% to 0.67% and 1.0% in *Klrk1*$^{+/+}$ and *Klrk1*$^{-/-}$ mice. Frequencies of cytokine-producing T cells were reduced (Figure 3.43c), including frequencies of IL-17$^+$ CD4$^+$ and γδT cells, as well as IFN-γ$^+$ CD8$^+$ T cells. Interestingly, frequencies of IL-17-producing ILC3s were increased, from 7.6% in control mice to 15.2% in *Klrk1*$^{+/+}$ and 34.1% in *Klrk1*$^{-/-}$ mice. IFN-γ production by NK cells was significantly reduced from an average frequency of 32.4% IFN-γ$^+$ NK cells in control mice to 5.9% and 6.0% in *Klrk1*$^{+/+}$ and *Klrk1*$^{-/-}$ mice, respectively (Figure 3.43c and d). No significant differences were observed when comparing *Klrk1*$^{+/+}$ to *Klrk1*$^{-/-}$ mice, further supporting the observation that lack of NKG2D does not influence disease susceptibility or the immune response following DSS-mediated injury.

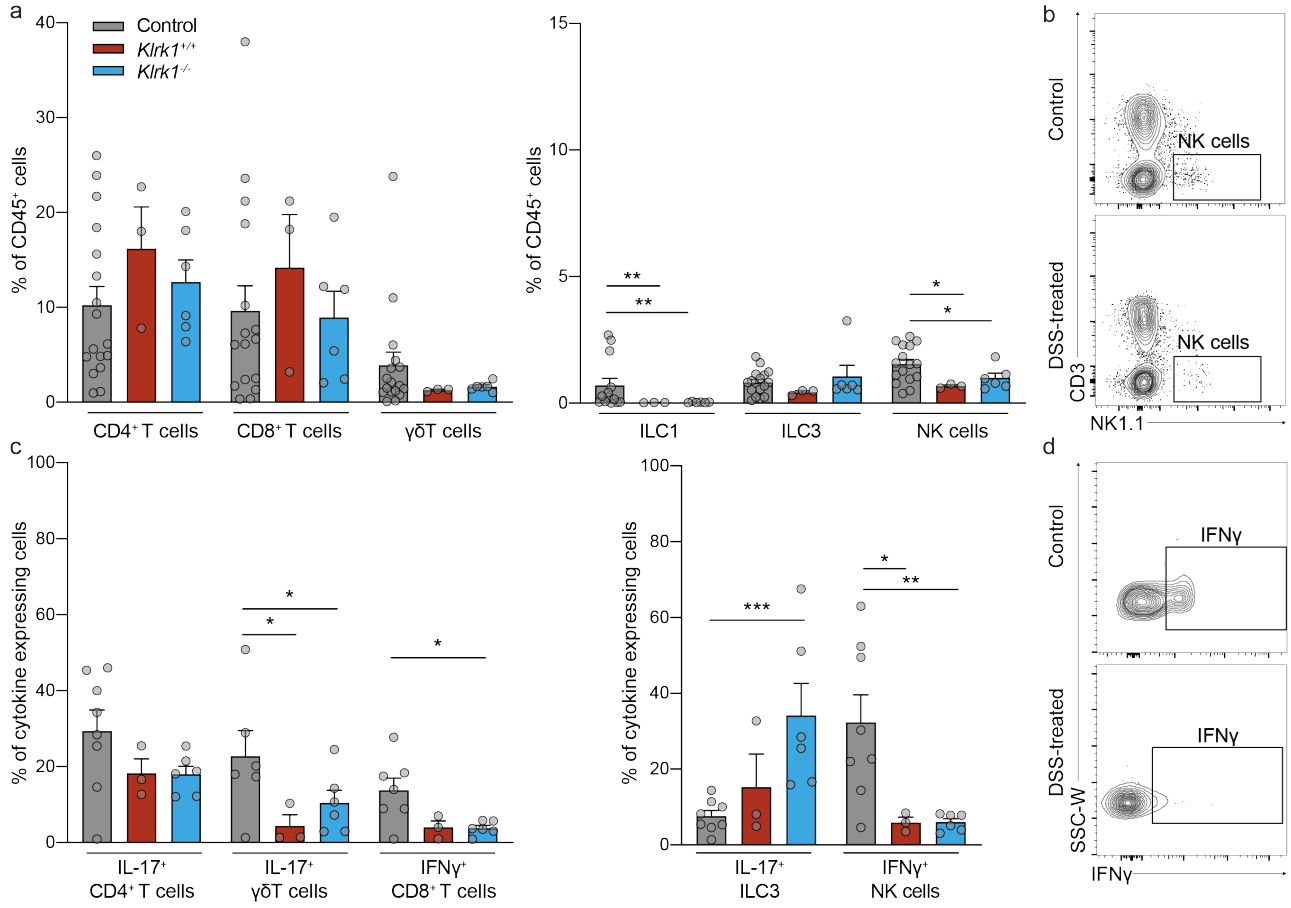

Figure 3.43: Chronic DSS treatment is associated with changes in innate and adaptive intestinal immune cell subsets. (a) (a) Frequencies of T cells (left) (gated on $CD4^+$, $CD8^+$ or $\gamma\delta TCR^+$) and innate cell (right) (NK cells gated on $CD3^+$ $NK1.1^-$, ILC1 gated on $CD3^-$ $CD19^-$ $Ly6G^-$ $Ly6C^-$ $CD127^+$ T-bet^+ and ILC3 gated on ILC1 gated on $CD3^-$ $CD19^-$ $Ly6G^-$ $Ly6C^-$ $CD127^+$ $ROR\gamma T^+$) in the colonic LP of naive control mice (grey), as well as *Klrk1*$^{+/+}$ (red) and *Klrk1*$^{-/-}$ (blue) mice undergoing LT DSS treatment. (b) Representative flow cytometry plots of NK cells (gated on live $CD45^+$) in naive control (top) and DSS-treated mice (bottom) (c) Frequencies of cytokine-producing T cells (left) and innate cell (right) stimulated with PMA and ionomycin, in the colonic LP of naive control mice (grey), as well as *Klrk1*$^{+/+}$ (red) and *Klrk1*$^{-/-}$ (blue) mice undergoing LT DSS treatment. (d) Representative flow cytometry plots of IFN-γ^+ NK cells (gated on live $CD45^+$ $CD3^-$ $NK1.1^+$) stimulated with PMA and ionomycin in naive control (top) and DSS-treated mice (bottom). $n \geq 7$ for naive control mice, $n \geq 3$ for *Klrk1*$^{+/+}$ and $n \geq 5$ for *Klrk1*$^{-/-}$ mice. LP = lamina propria, DSS = dextran sodium sulfate. Data represented as mean ± SEM of individual mice from three independent experiments. *$p \leq 0.05$, **$p \leq 0.01$, ***$p \leq 0.001$.

.

3.3.2.8 Optimization of *Citrobacter rodentium*-induced colitis

Having determined that NKG2D is dispensible for DSS-induced acute and chronic colitis, I sought to employ a model that would better recapitulate human disease. Administration of DSS leads to a very abrupt and acute destruction of the epithelium, whereas *C. rodentium* induces an immune response, which can be compared to the immune response following epithelial disruption and translocation of bacteria in human intestinal inflammation. However, infection with *C. rodentium* does not model human disease perfectly. Being a pathogen, the host immune response is triggered to eliminate *C. rodentium*, whereas human disease is often characterized by an immune response against the harmless commensal microbiota. Further, the infection model used here is acute and sustained inflammation, as it is the case in IBD patients, is not modeled. Nonetheless, infection-induced colitis is of interest in the context of NKG2D-dependent immunity to not only study the susceptibility to infection-induced colitis in NKG2D-deficient mice, but also to determine the efficacy of NKG2D-deficient cells in eliminating mucosal pathogens.

To ensure consistent experimental procedures, a small pilot experiment was set up, in which the experimental procedure, which included preparing agar plates, growing bacteria, determining the correct amount of bacteria for the infection, oral gavage of prepared solution containing a specific amount of bacteria and determining CFU in stool and tissue samples, was practiced. Further, the susceptibility of our mouse colony and specifically that of *Klrk1*$^{-/-}$ mice was tested to rule out serious adverse effects like sudden weight loss. A total of 6 mice were included in the experiment, 2 *Klrk1*$^{-/-}$ mice and 4 *Klrk1*$^{+/-}$ littermates. Of the 6 mice included in the experiment, one mouse unexpectedly lost weight in a short time-frame and was required to be euthanized (Figure 3.44a). The weight of the remaining mice remained stable as expected (Bouladoux *et al.* 2001 and personal communication with Gad Frankel) over the period of the infection. Bacterial burden was measured throughout the experiment by determining the number of CFU in fecal samples every second day. The height of bacterial burden was reached on day 6 post infection (between 1.76 x 10^8 and 2.93 x 10^9 CFU/g, Figure 3.44b). Mucosa-associated bacteria was measured on day 8 by determining the number of CFU per gram of colon tissue, which ranged from 4^7 to 7.07 x 10^8 CFU/g. Both the kinetic of fecal bacterial burden

as well as mucosa-associated bacterial burden was in line with previous experiments performed by Gad Frankel, confirming that the experimental procedure as well as the susceptibility of our mouse colony were adequate. The adverse effects observed in one mouse were attributed to inexperience in the execution of administration of substances by oral gavage rather than strain susceptibility.

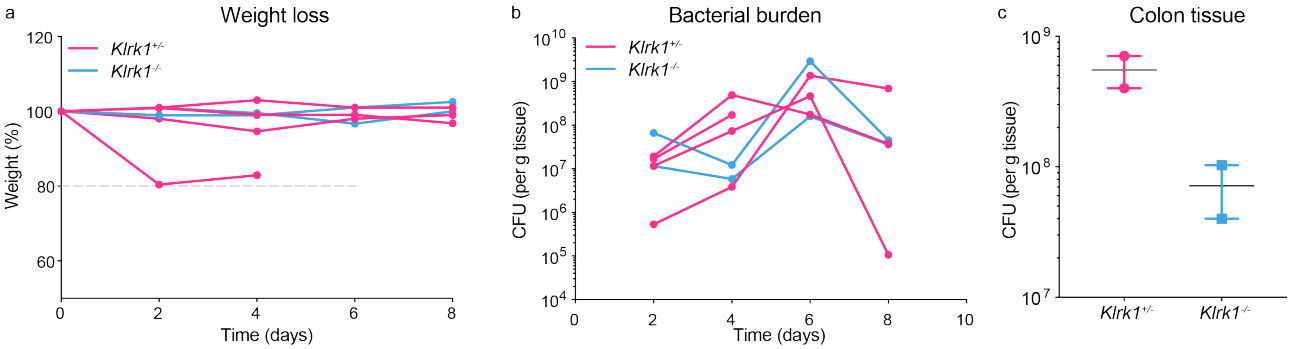

Figure 3.44: Kinetics of weight loss and bacterial burden in *Klrk1*$^{+/-}$ and *Klrk1*$^{-/-}$ mice infected with *C. rodentium*. (a) Weight loss of individual mice over time. (b) Fecal bacterial burden measured as CFU over time. (c) Colonic bacterial burden measured as CFU on day 8 post infection. Dotted grey line in a indicates the severity limit. CFU = colony forming unit. Data in c represented as mean ± SEM.

.

3.3.2.9 The immune response following infection with *Citrobacter rodentium*

Using the DSS mouse model of colitis, we demonstrated that NKG2D expression was unchanged in both the acute and chronic phase of inflammation. We hypothesized that a model in which NKG2D-expressing cells are activated either through the recruitment of NKG2D$^+$ cells or the upregulation of NKG2D and/or its ligands, would better model NKG2D-mediated disease, similar to the pathogenesis in CD patients. *E. coli*, which is closely related to *C. rodentium* has been shown to upregulate MICA on the surface of an epithelial cell line (Tieng *et al.* 2002), suggesting that the *C. rodentium* model of mouse intestinal inflammation is an appropriate model to study NKG2D-mediated responses.

Using an improved flow cytometry panel, which allowed better identification of myeloid cells, we performed a thorough characterization of the immune response within the colonic LP following infection with *C. rodentium* at various time-points, including during the acute phase (2, 4, 7 dpi) and following clearance of the infection on day 25 post infection (p.i.) in NKG2D-

sufficient *Klrk1*$^{+/+}$ mice. Within the T cell compartment, infection was associated with changes in frequencies of different T cell subsets (Figure 3.45a and b), while functionality of T cells (Figure 3.45c) and NKG2D expression (Figure 3.45d) remained comparable to non-infected controls. Acute infection was associated with an increase in CD4$^+$ T cells, which increased from 10.2% in healthy controls to 17.6% on day 2 p.i., while frequencies of CD8$^+$ and γδT cells remained stable (Figure 3.45a and b). CD4$^+$ T cells were slightly decreased on day 4 p.i. (14.4%) compared to the initial increased on day 2 p.i. and returned to baseline levels by day 7 (9.4%). Interestingly, the frequency of CD4$^+$ T cells was increased to 23.4% on day 25, potentially suggesting an accumulation of tissue-resident memory (T_{RM}) following clearance of the infection. Minor changes were detected in T cell functionality, with IL-17$^+$ γδT cells being significantly increased from 13.4% on day 2 p.i. to 39.4% on day 4 (Figure 3.45c). NKG2D expression on CD4$^+$, CD8$^+$ and γδT cells remained stable throughout the infection (Figure 3.45d).

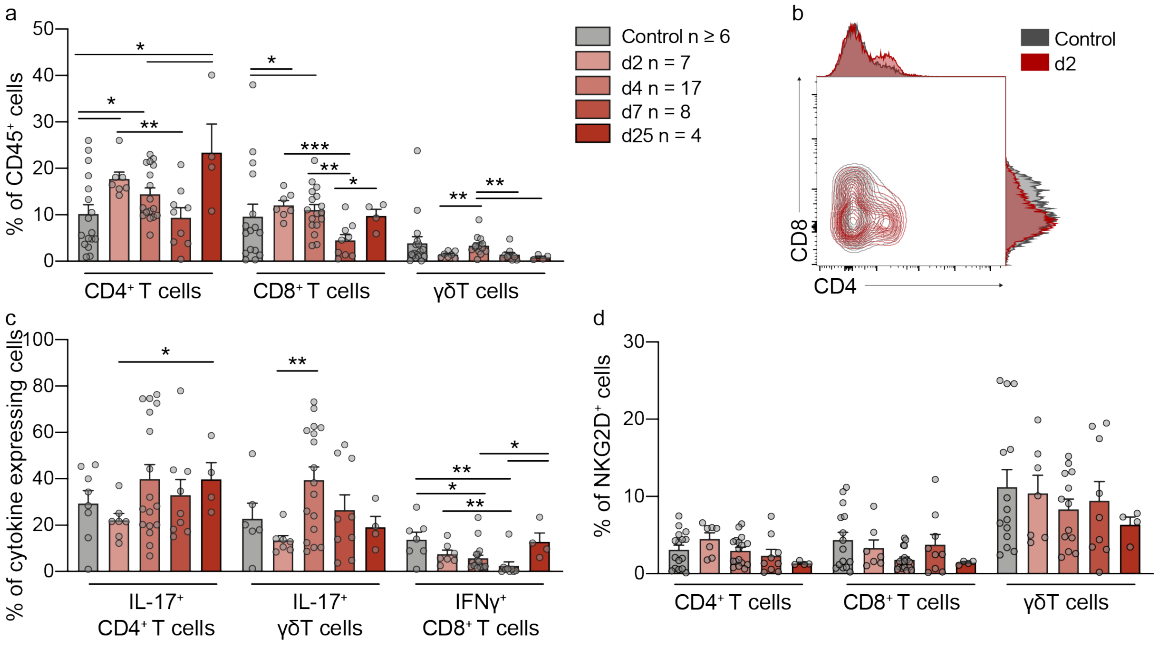

Figure 3.45: Infection with *C. rodentium* is associated with mild changes in the composition and functionality of the T cell compartment, but no changes in NKG2D expression. (a) Frequencies of T cells (gated on $CD4^+$, $CD8^+$ or $\gamma\delta TCR^+$) 2, 4, 7 and 25 dpi compared to naive control mice. (b) Representative flow cytometry plot of $CD8^+$ and $CD4^+$ T cells (gated on live $CD45^+$) in naive control mice (grey) compared to 4 dpi. (c) Cytokine production by T cells 2, 4, 7 and 25 dpi stimulated with PMA and ionomycin compared to naive control mice. (d) Frequencies of $NKG2D^+$ T cells 2, 4, 7 and 25 dpi compared to naive control mice. dpi = days post infection. Data represented as mean ± SEM of individual mice. * $p \leq 0.05$, ** $p \leq 0.01$, *** $p \leq 0.001$.

.

I next asked what role innate cells plays in the immune response to infection. For this, I determined frequencies of ILC1, ILC3 and NK cells, measured their ability to produce cytokines and characterized NKG2D expression throughout the course of infection. As opposed to T cells, frequencies of ILCs changed over the course of infection, with an increase of ILC1s from 0.70% in control mice to 1.53% on day 2 p.i. and an increase of ILC3s from 0.81% to 2.3% (Figure 3.46a and d right). This increase appeared to be temporary, with frequencies returning to baseline on day 4 p.i.. Interestingly on day 7 p.i., frequencies of ILC1s were low (0.23%), while ILC3s were increased (1.83%) compared to control mice and mice on day 4 p.i.. Frequencies of NK cells did not change significantly throughout the disease. There were no significant changes in their ability to produce cytokines during the acute phase of infection (Figure 3.46b). Interestingly, all three cell types studied produced higher than baseline levels of cytokines on day 25 p.i. (increase from 27.2% IFN-γ^+ ILC1s to 48.3%, increase from 32.4% IL-17^+ ILC3s to 68.0% and increase from 17.2% IFN-γ^+ NK cells to 42.2%). Further, production of IFN-γ by NK cells was significantly decreased on day 2, 4 and 7 p.i. compared to control mice. NKG2D expression was altered upon infection with the most striking increase on ILC1s from 5.9% in control mice to 12.7% on day 2 p.i. (Figure 3.46c), which appeared transient and was reduced to 3.1% on day 7 p.i. A similar trend was observed on NK cells, with a less drastic initial increase on day 2 p.i. (Figure 3.46c and d). Expression of NKG2D on ILC3s was not increased following infection, instead, a significant decrease was observed from day 2 to day 7 and day 25 p.i..

While cytokine production was stable throughout acute phases of the infection, an increased frequency of ILC1s and ILC3s suggests that these cells are recruited and/or activated in early stages of infection preceding activation of T cells. Changes in NKG2D expression were subtle but followed a similar pattern in both ILC1s and NK cells with an initial increase and a subsequent decrease of NKG2D$^+$ cells, suggesting that NKG2D is indeed involved in the response to *C. rodentium*.

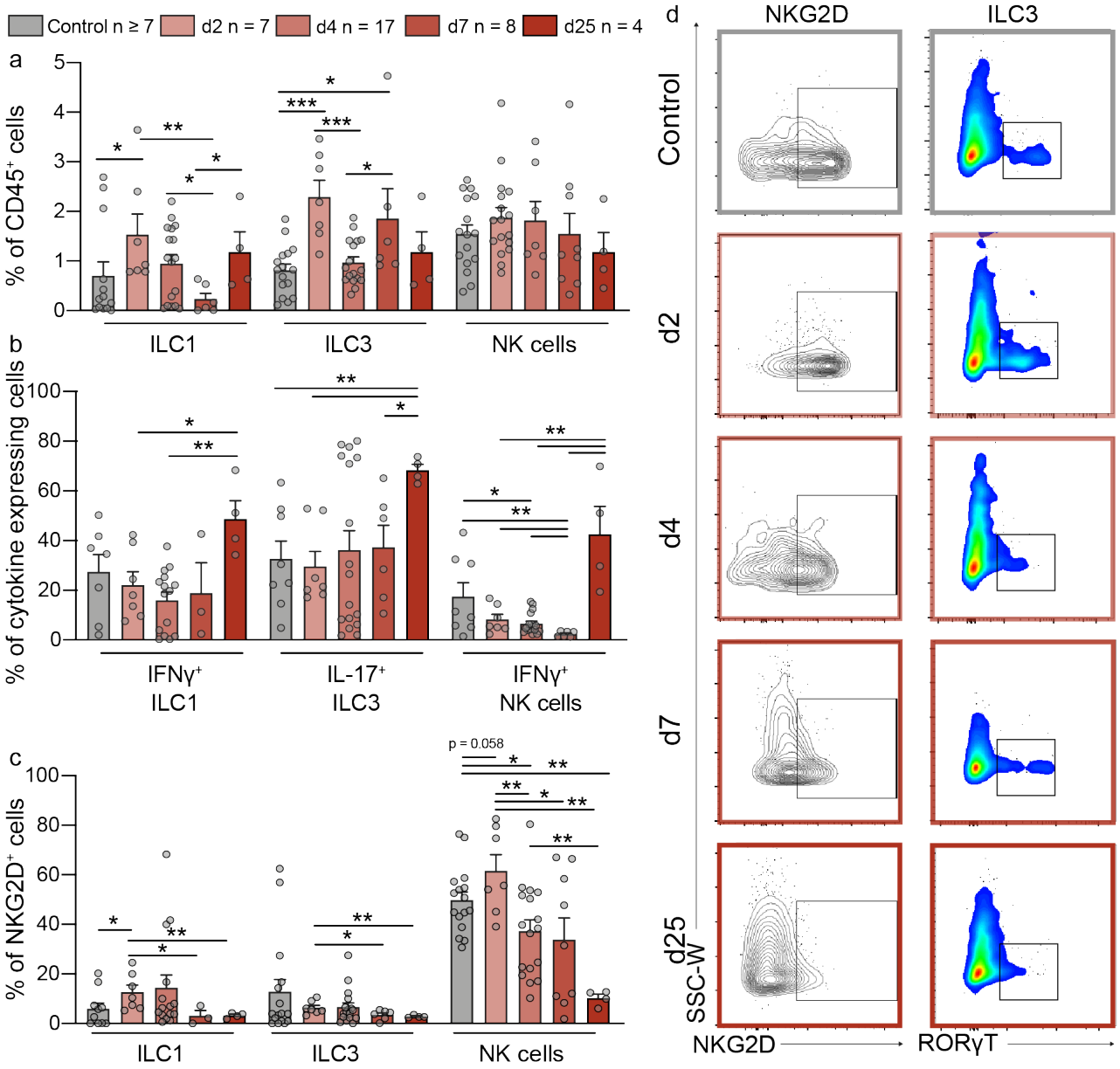

Figure 3.46: Frequencies and cytokine production by innate cells changes throughout infection with *C. rodentium* and is associated with mild changes in NKG2D expression. (a) Frequencies of ILCs (NK cells gated CD3$^-$ NK1.1$^+$, ILC1s gated on CD3$^-$ CD19$^-$ Ly6C$^-$ Ly6G$^-$ CD127$^+$ T-bet$^+$ and ILC3s gated on CD3$^-$ CD19$^-$ Ly6C$^-$ Ly6G$^-$ CD127$^+$ RORγT$^+$) 2, 4, 7 and 25 dpi compared to control mice. (b) Cytokine production by ILCs stimulated with PMA and ionomycin 2, 4, 7 and 25 dpi compared to naive control mice. (c) Frequencies of NKG2D$^+$ ILCs 2, 4, 7 and 25 dpi compared to control mice. (d) Representative flow cytometry plot of NKG2D$^+$ NK cells (left) (gated CD3$^-$ NK1.1$^+$) and ILC3s (gated on CD3$^-$ CD19$^-$ Ly6C$^-$ Ly6G$^-$ CD127$^+$) in control mice and at various stages of the infection. dpi = days post infection. Data represented as mean ± SEM of individual mice. * $p \leq 0.05$, ** $p \leq 0.01$, *** $p \leq 0.001$.

Lastly, we determined frequencies of myeloid cells, including DCs, Ly6C$^+$ monocytes and neutrophils following infection. Interestingly, frequencies of all myeloid cell subsets remained unchanged throughout the infection (3.47). A slight increase in frequencies of Ly6C$^+$ monocytes was observed on day 7 p.i., but only in a subset of mice, suggesting that this was not a *C. rodentium*-specific response.

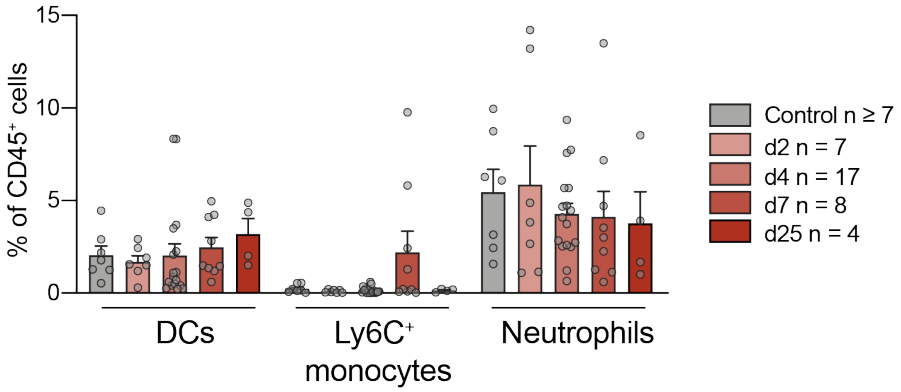

Figure 3.47: Frequencies of myeloid cells remain stable throughout infection with *C. rodentium*. Frequencies of DCs (gated on CD11b$^+$ CD11c$^+$), monocytes (gated on CD11b$^+$ Ly6G$^-$ Ly6C$^+$) and neutrophils (CD11b$^+$ Ly6G$^+$) 2, 4, 7 and 25 dpi compared to control mice. dpi = days post infection. DCs = dendritic cells. Data represented as mean ± SEM.

.

In this study, I provide a thorough characterization of the immune response following infection with *C. rodentium* during acute infection (day 2, 4 and 7 p.i.) as well as post clearance (day 25 p.i.). I show that early stages are associated with an increased frequency of CD4$^+$ T cells, as well as ILC1s and ILC3s. Cytokine productions only changes slightly throughout the infection with a striking increase in cytokine-producing ILCs on day 25 p.i.. NKG2D expression remains stable within the T cell subset, while ILC1s and NK cells display an increased frequency of NKG2D$^+$ cells on day 2 p.i. before a decrease below baseline level on day 7 and 25 p.i.. NKG2D expression on ILC3s decreases over time and shows no transient upregulation, suggesting that specifically NK cells and ILC1s may be involved in the NKG2D-mediated host response following intestinal infection.

3.3.2.10 Fecal bacterial burden is slightly reduced at early stages of infection in the absence of NKG2D but not associated with histological changes

Changes in frequencies of NKG2D-expressing cells indicates that NKG2D is involved in the host response following infection with *C. rodentium*. NKG2D has been shown to be a critical mediator of host defense in a model of respiratory infection (Wesselkamper *et al.* 2008), prompting the hypothesis that NKG2D plays a crucial role in clearing the infection. I further hypothesized that while initially resulting in an improved host response and faster bacterial clearance, activation of NKG2D-expressing cells would equally lead to an exacerbated inflammatory response, resulting in increased injury and aggravated colitis. To test this hypothesis, I assessed disease susceptibility and the inflammatory response following infection in NKG2D-sufficient and -deficient mice. In a first experiment, 5 *Klrk1*$^{+/+}$ and 5 *Klrk1*$^{-/-}$ were infected with *C. rodentium*. As a read-out of disease severity, fecal bacterial burden was measured at several timepoints throughout the infection up to day 7, which was set as the experimental endpoint. Additionally, mucosa-associated bacterial burden was measured on day 7, as well as colon length as an indication of the severity of intestinal inflammation.

In the first experiment, we observed a striking and unexpected difference. Bacterial burden was increased in *Klrk1*$^{+/+}$ mice compared to NKG2D-deficient mice at early stages of infection, with a significant difference on day 4 p.i. (Figure 3.48a and b, 1.37 x 10^9 CFU/g feces in *Klrk1*$^{+/+}$ mice and 5.87^7 in *Klrk1*$^{-/-}$ mice). With the bacterial burden being comparable from day 5 p.i., we hypothesize that differences at earlier timepoints are due to a delayed colonization in NKG2D-deficient mice. Colon length, a read-out of severity of inflammation, was significantly decreased in NKG2D-sufficiente mice on day 7 p.i. (Figure 3.48c and d), with an average length of 7.0 cm in *Klrk1*$^{+/+}$ and 7.8 cm in *Klrk1*$^{-/-}$ mice. Mucosa-associated bacterial burden, measured on day 7 p.i. was comparable in both genotypes (Figure 3.48e).

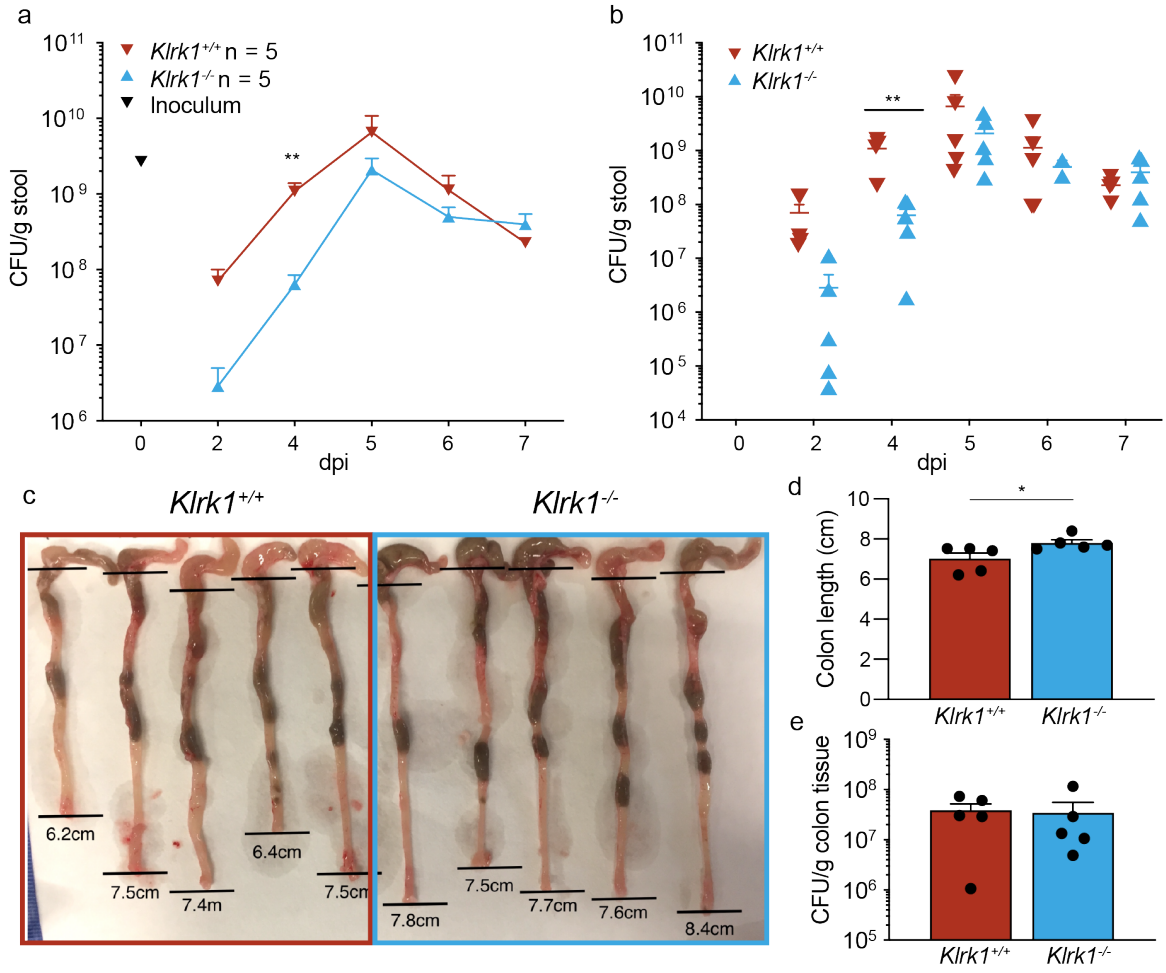

Figure 3.48: Bacterial colonization is delayed in NKG2D-deficient mice and associated with less severe inflammation compared to *Klrk1*$^{+/+}$ littermates. (a) Average bacterial burden measured as CFU per gram of feces collected from *Klrk1*$^{+/+}$ and *Klrk1*$^{-/-}$ mice at various timepoints throughout infection. (b) Bacterial burden measured as CFU per gram of feces collected from *Klrk1*$^{+/+}$ and *Klrk1*$^{-/-}$ mice at various timepoints throughout infection plotted as individual values. (c) Photographs of colons of *Klrk1*$^{+/+}$ and *Klrk1*$^{-/-}$ mice 7 dpi. (d) Quantification of (c). (e) Bacterial burden in colonic mucosa measured as CFU per gram of tissue in *Klrk1*$^{+/+}$ and *Klrk1*$^{-/-}$ mice 7 dpi. CFU = colony forming units, dpi = days post infection. Data in d and e represented as mean ± SEM of individual mice from one experiment. * $p \leq 0.05$, ** $p \leq 0.01$.

One of the limitations of this study was the need to use sex- and age-matched littermates to reduce variations within experimental groups. To further increase the power of the experiments, large experimental groups are needed to reduce variations from one experiment to the other. I therefore considered that using a commercially available NKG2D-specific blocking antibody would circumvent the need to use *Klrk1*$^{-/-}$ mice and would allow us to increase the size of experimental groups. HMG2D (Bio X Cell) is a monoclonal antibody, which has been reported to block NKG2D *in vivo* (Crosby *et al.* 2015) and has been used in the context of studying mouse colitis (Ito *et al.* 2007, Kjellev *et al.* 2007). Before setting up an infection experiment using the HMG2D antibody, I determined its efficiency and ability to block NKG2D in mucosal tissue. I administered 200 µg i.p. on day 0, 2 and 5 and quantified NKG2D expression on day 7 (Figure 3.49a). Indeed, NKG2D expression was not detectable on colonic NK cells on day 7, suggesting that the HMG2D antibody works as expected and blocks NKG2D in mucosal tissue efficiently. I therefore decided to address the question of whether lack of NKG2D affects susceptibility to *C. rodentium*-induced infection using either germline-deficient *Klrk1*$^{-/-}$ (NKG2D-deficient) mice or *Klrk1*$^{+/+}$ mice treated with HMG2D antibody (NKG2D-blocked).

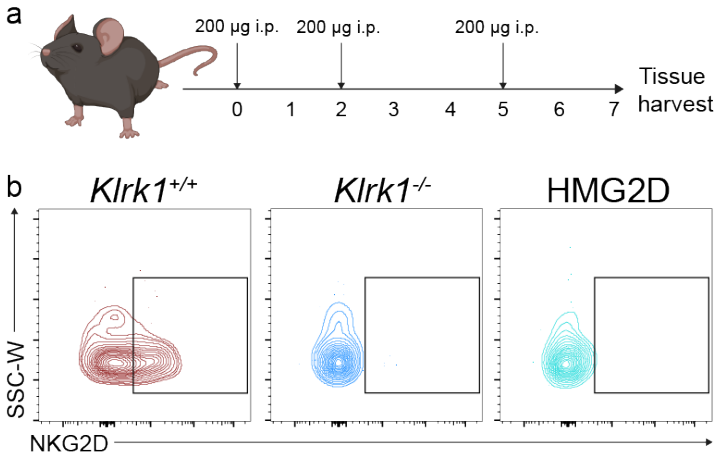

Figure 3.49: Administration of the HMG2D antibody efficiently blocks NKG2D on intestinal NK cells (a) Experimental setup. (b) NKG2D expression on NK cells isolated from the colonic lamina propria on day 7 comparing NKG2D-sufficient *Klrk1*$^{+/+}$ to NKG2D-deficient *Klrk1*$^{-/-}$ mice treated with an isotype control or mice treated with αNKG2D blocking antibody (HMG2D). i.p. = intraperitonal

In a series of experiments with endpoints on day 2, 4 or 7 p.i., I determined the fecal bacterial burden at various timepoints. I observed a striking difference on day 2 p.i., but not at later stages, with a significantly decreased bacterial burden in NKG2D-deficient/-blocked mice (2.5 x 10^6 CFU/g feces) compared to NKG2D-sufficient littermates (4.2 x 10^7 CFU/g feces) (Figure 3.50a). To determine whether the reduced bacterial burden observed in *Klrk1*$^{-/-}$ mice resulted in changes in the severity of inflammation, we measured colon length on day 4 and 7 p.i., but found that there were no differences among groups or compared to uninfected control mice, suggesting only mild inflammation (Figure 3.50b). Being a very crude read-out of disease severity, we complemented measurement of colon length with histological analysis. For this, we followed a published guide for the histomorphological evaluation of intestinal inflammation (Erben *et al.* 2014) and measured crypt length and quantified Goblet cells. Additionally, overall inflammation was evaluated using a scoring system (described in Table 2.8). While infection with *C. rodentium* was associated with mild crypt length elongation (Figure 3.50c and d) and an increased inflammation score (Figure 3.50c and f), no difference between *Klrk1*$^{+/+}$ and *Klrk1*$^{-/-}$ or HMG2D-treated mice was observed. Goblet cells appeared slightly reduced in *Klrk1*$^{+/+}$ mice on day 7 p.i. compared to NKG2D-deficient/-blocked littermates (Figure 3.50e), however the differences were not statistically significant and drawing conclusions is difficult due to low sample numbers and high variations.

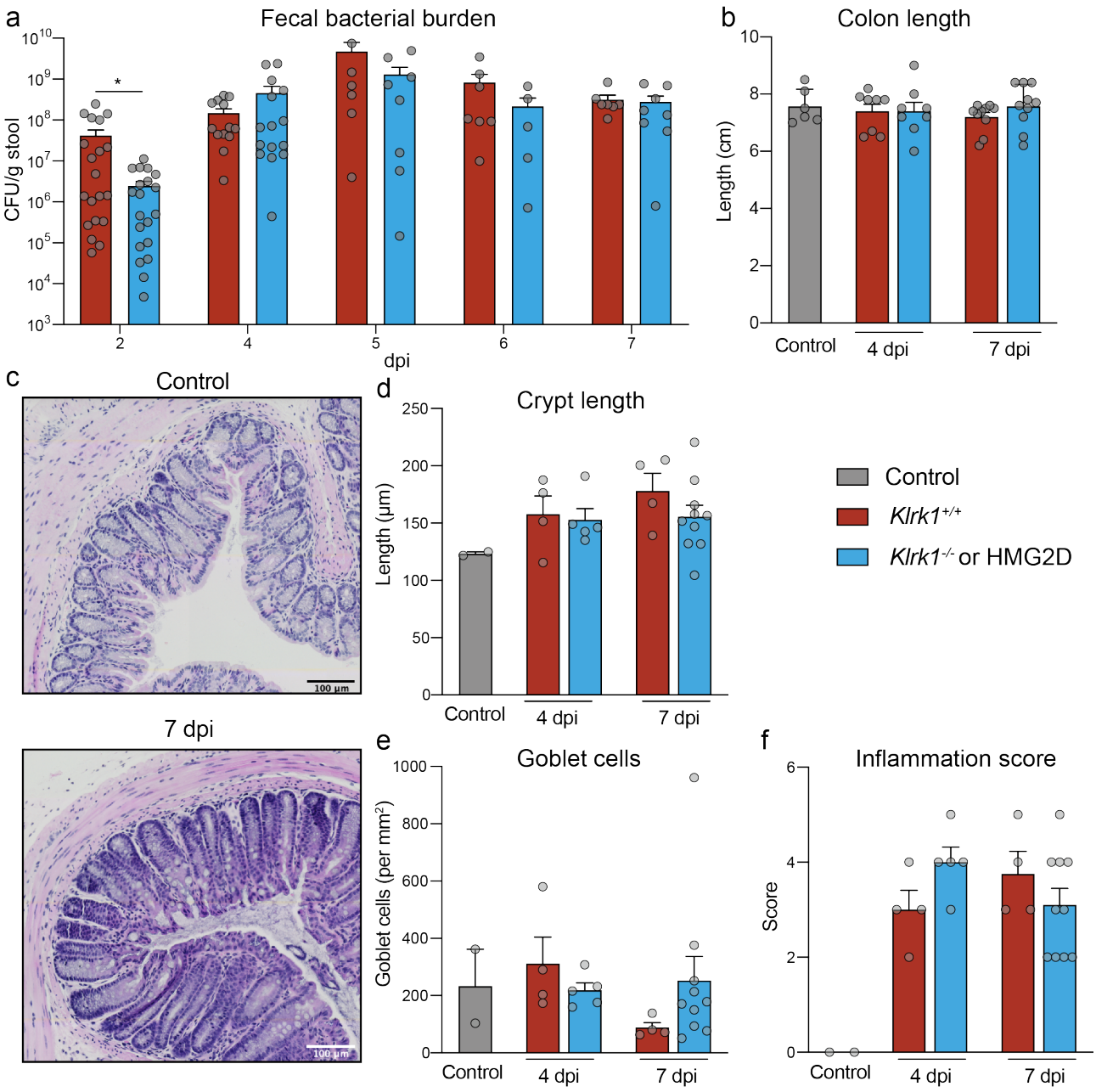

Figure 3.50: Bacterial burden is reduced on day 2 post infection in the absence of NKG2D, but does not result in macroscopic or histological changes associated with intestinal inflammation. (a) Fecal bacterial burden 2, 4, 5, 6 and 7 dpi. n $\geq$ 5. Data collected from a total of 7 individual experiments of varying length. (b) Colon length following infection with *C. rodentium* on day 4 or 7 p.i.. n = 6 for control, n = 8 for day 4, n = 10 for day 7. (c) Representative H&E staining of uninfected (top) colon and colon on day 7 p.i. (bottom). Quantification of crypt length (d), Goblet cell numbers (e) and inflammation score (e) following infection. n = 2 for control, n = 4 for *Klrk1*$^{+/+}$ mice, n = 5 for *Klrk1*$^{-/-}$/HMG2D-treated mice on day 4 and n = 9 for *Klrk1*$^{+/+}$/HMG2D-treated mice on day 7 p.i. CFU = colony forming units, dpi = days post infection, p.i. = post infection. Data in c-f was collected and analyzed by B.Sc. student Alexander Steemers. Data represented as mean $\pm$ SEM of individual mice from at least two independent experiments per timepoint. * p $\leq$ 0.05.

Determining CFU in mucosal colonic tissue and the cecum, where *C. rodentium* attaches before colonizing the colon (Bhinder *et al.* 2013), is a more accurate read-out of bacterial burden compared to fecal samples. Further, *C. rodentium* infection is not restricted to the intestine and bacteria can invade the spleen and liver. To better understand early phases of infection, I quantified bacterial burden in these four organs on day 2 and 4 p.i.. Bacterial burden in colonic mucosal tissue and the liver was similar in *Klrk1*$^{+/+}$ mice compared to NKG2D-deficient/-blocked littermates (Figure 3.51a and c), while a slightly higher burden of spleen-associated bacteria was measured on day 4 p.i. in NKG2D-sufficient compared to NKG2D-deficient/-blocked mice (Figure 3.51c). The most striking difference was observed in the cecum on day 2 p.i., where the CFU per gram of tissue on day 2 p.i. averaged 2.1^6 in *Klrk1*$^{+/+}$ mice and only 19200 in NKG2D-deficient/-blocked mice (Figure 3.51d). This difference supports the previous observation that only very early stages of infection are affected by lack of NKG2D.

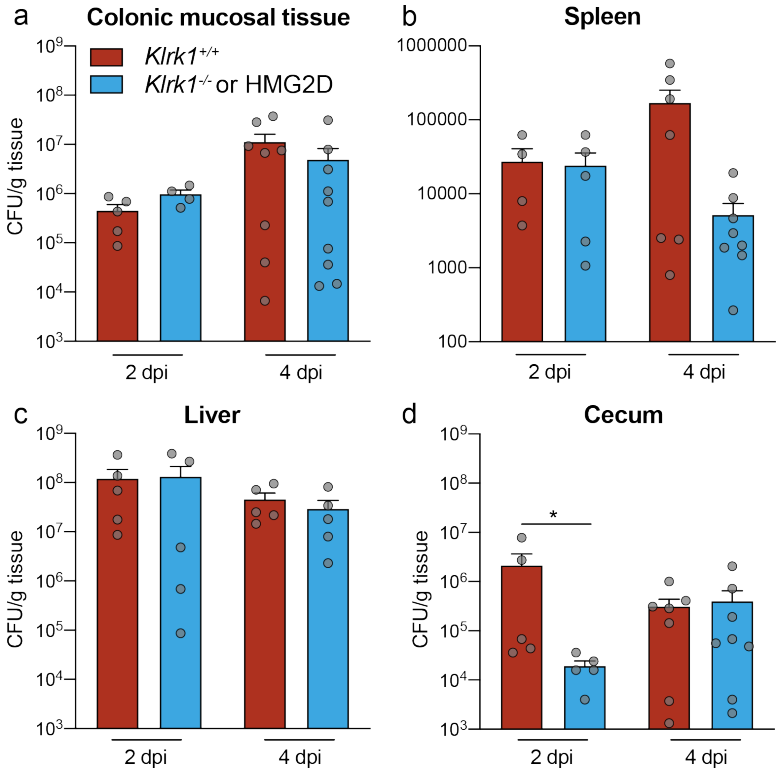

Figure 3.51: Bacterial burden is significantly reduced in the cecum, but not other organs on day 2 post infection in mice lacking NKG2D. Bacterial burden in colonic mucosal tissue (a), spleen (b), liver (c) and cecum (d) 2 and 4 dpi in *Klrk1*$^{+/+}$ mice compared to *Klrk1*$^{+/+}$/HMG2D-treated mice. n $\geq$ 5. CFU = colony forming units, dpi = days post infection. Data represented as mean $\pm$ SEM of individual mice from two individual experiments (a) and one experiment (b-d). * p $\leq$ 0.05.

In a next step, and to better determine kinetics of the infection, we collaborated with Prof. Gad Frankel and his PhD student Eve Hopkins. Using a bioluminescent strain of *C. rodentium*, we were able to observe colonization *in vivo*. We performed two experiments with three and two mice per genotype, respectively. No obvious differences in colonization were detected when comparing bacterial load, measured as radiance at various timepoints (Figure 3.52a and b). In the first experimental group, two *Klrk1*$^{-/-}$ mice had a low bacterial burden on day 3 p.i. compared to *Klrk1*$^{+/+}$ mice, in line with the lower bacterial burden in both fecal samples on day 2 p.i. and the cecum (Figure 3.52a). However, one mouse in the *Klrk1*$^{-/-}$ mice displayed a particularly high bacterial burden, meaning we were unable to confirm the striking genotypic difference seen in previous experiments using this experimental setup.

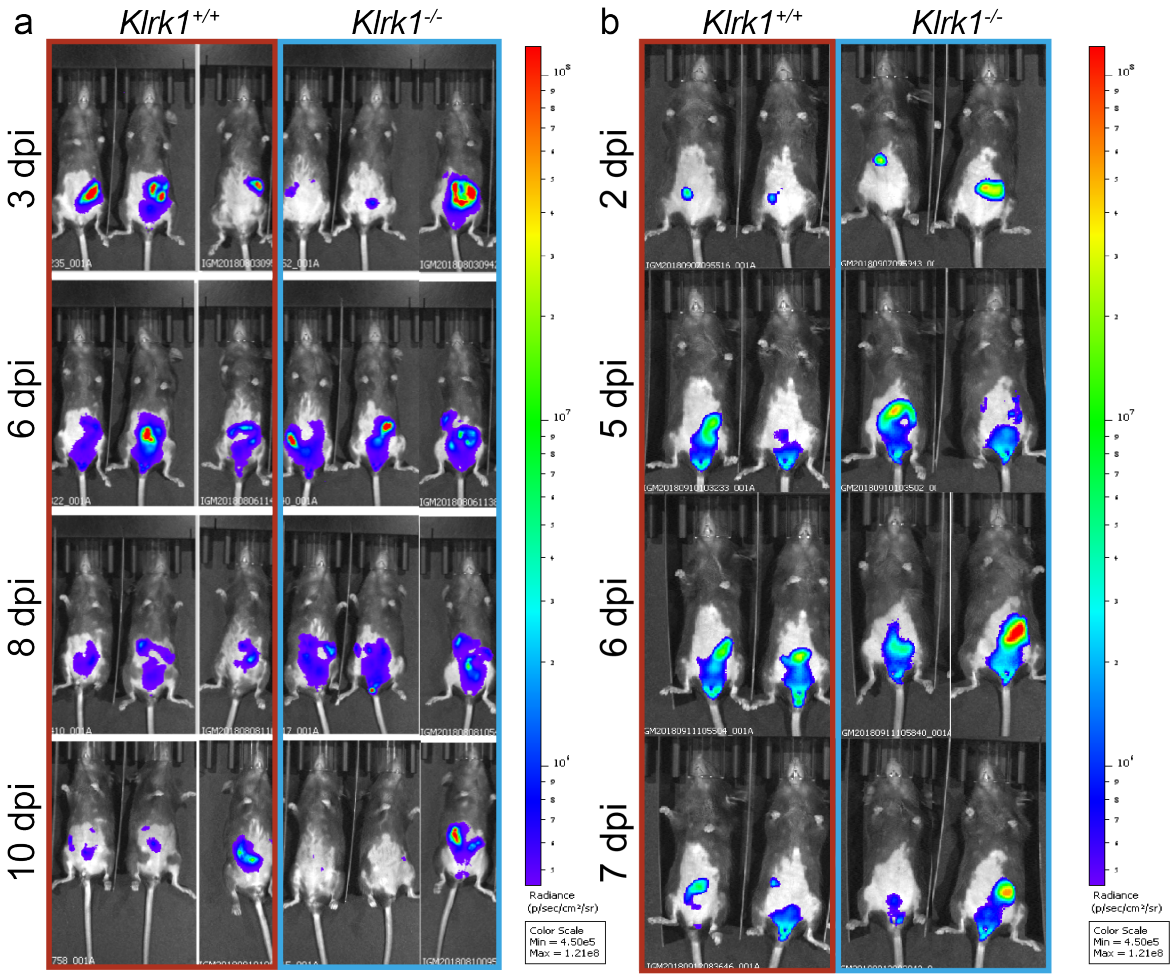

Figure 3.52: *In vivo* visualization of *C. rodentium* reveals no genotypic differences in *Klrk1*$^{+/+}$ and *Klrk1*$^{-/-}$ mice. Bacterial burden in *Klrk1*$^{+/+}$ and *Klrk1*$^{-/-}$ mice measured as photons $s^{-1}cm^{-2}sr^{1}$ in two individual experiments (a and b). The experimental procedure including infection and imaging was performed by Eve Hopkins.

Lastly, we asked whether clearance of bacteria is altered in the absence of NKG2D. For this, we infected four *Klrk1*$^{+/+}$ and four *Klrk1*$^{-/-}$ mice and measured fecal bacterial burden at regular intervals until complete clearance of the infection (Figure 3.53a). We observed no differences between genotypes, suggesting that NKG2D is not involved in later stages of the infection. We further found no differences in colon length on day 25 p.i. (Figure 3.53b), indicating that there are no major differences in the severity of inflammation.

Together this suggests that, while we observed an obvious trend in fecal and cecal bacterial burden on day 2 p.i., lack of NKG2D does not lead to any changes in morphological or macroscopic changes associated with inflammation or deficiencies in clearing the infection.

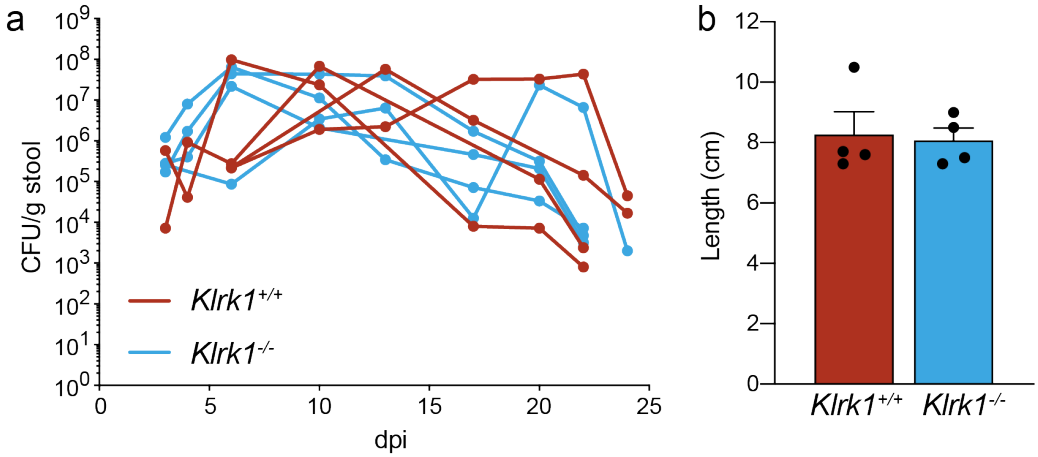

Figure 3.53: Bacterial clearance of *C. rodentium* is independent of NKG2D. (a) Fecal bacterial burden measured at different timepoints until complete clearance of infection following infection with *C. rodentium* in *Klrk1*$^{+/+}$ and *Klrk1*$^{-/-}$ mice. Each line represents one mouse. (b) Colon length 25 dpi. Data in a is represented as individual mice and in b as mean ± SEM of individual mice from one experiment. CFU = colony forming units, dpi = days post infection.

3.3.2.11 Immune function is slightly altered in the absence of NKG2D at early stages of infection

I next asked whether lack of NKG2D leads to differences in immune cell function, which could potentially explain the differences observed in fecal bacterial burden on day 2 p.i.. For this, I isolated LPL and MLN from infected mice at various timepoints and compared the frequencies and functionality of several immune cell subsets in *Klrk1*$^{+/+}$ to mice lacking NKG2D or HMG2D-treated mice.

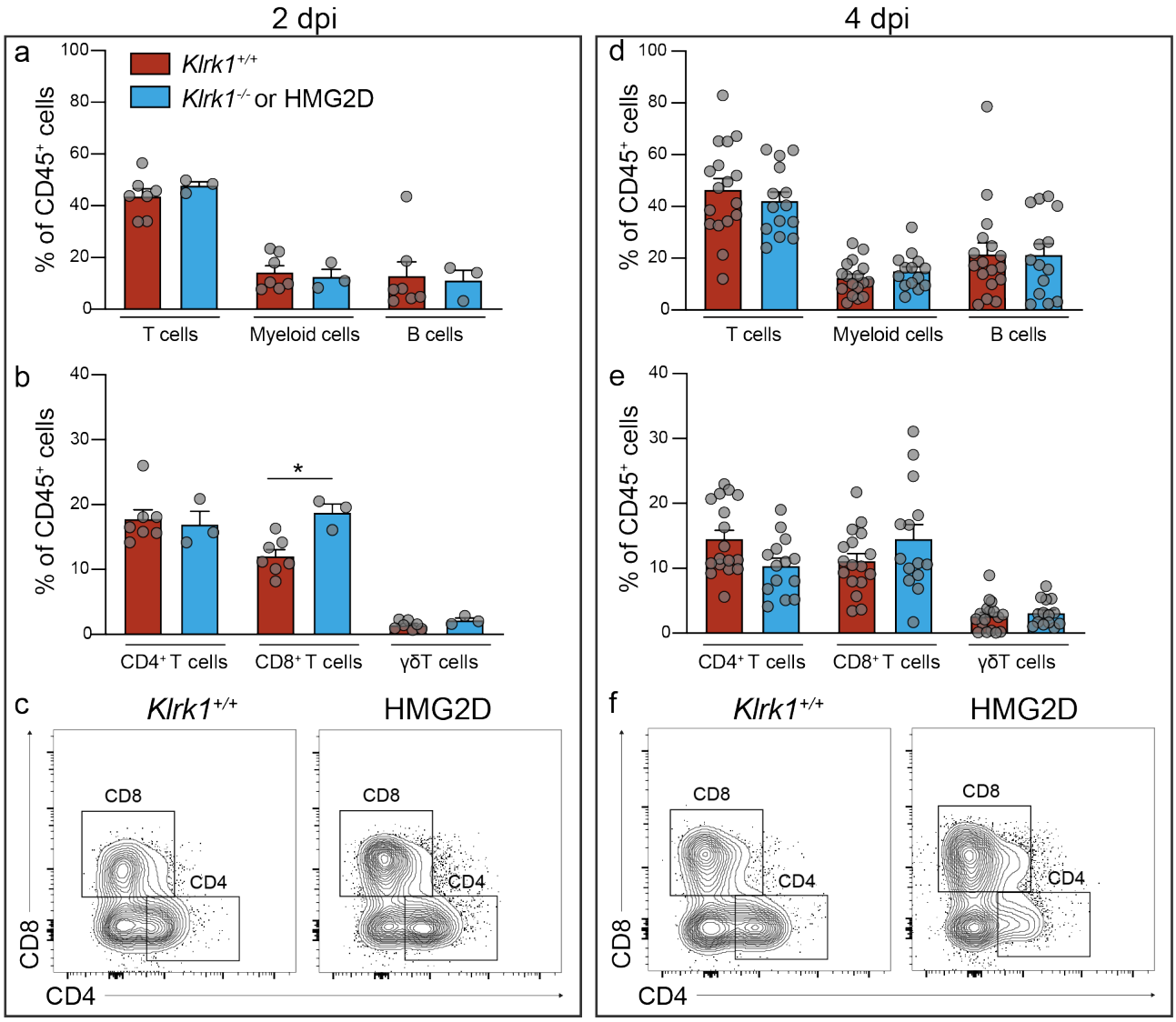

Figure 3.54: Immune cell frequencies on day 2 and 4 post infection are similar in *Klrk1*$^{+/+}$ and NKG2D-deficient/-blocked mice. (a) Frequencies of immune cell subsets (T cells gated on CD3$^+$, myeloid cells gated on CD11b$^+$ and B cells gated on CD19$^+$ lymphocytes) 2 dpi. (b) Frequencies of T cell (gated on CD4$^+$, CD8$^+$ or γδTCR$^+$ after selection of CD3$^+$ lymphocytes) subsets 2 dpi. (c) Representative flow cytometry plots of T cells (gated on CD3$^+$ lymphocytes) 2 dpi. (d) Frequencies of immune cell subsets 4 dpi. (e) Frequencies of T cell subsets 4 dpi. (f) Representative flow cytometry plots of T cells (gated on CD3$^+$ lymphocytes) 4 dpi. n $\geq$ 3 for data 2 dpi and n $\geq$ 14 for data 4 dpi. dpi = days post infection. Data represented as mean ± SEM of individual mice from one (2 dpi *Klrk1*$^{-/-}$/HMG2D), two (2 dpi *Klrk1*$^{+/+}$) or at least three (4 dpi) individual experiments. * p $\leq$ 0.05.

In line with the lack of differences in disease susceptibility, I observed no genotypic differences on day 7 p.i.. Immune cell frequencies as well as cytokine production were comparable in *Klrk1*$^{+/+}$ and *Klrk1*$^{-/-}$ or HMG2D-treated mice (data not shown). Focusing on day 2 and 4 p.i., I observed no major differences in the frequencies of T cells, myeloid cells and B cells (Figure

3.54a and d). Interestingly, CD8$^+$ T cells were significantly increased on day 2 p.i. in NKG2D-deficient/-blocked mice (18.7% of all lymphocytes) compared to NKG2D-sufficient littermates (12.0% of all lymphocytes) (Figure 3.54b and c). Similarly, the average frequency of CD8$^+$ T cells was slightly increased from 11.1% in *Klrk1*$^{+/+}$ mice to 14.5% in NKG2D-deficient/-blocked mice on day 4 p.i., while CD4$^+$ T cells were more frequent in *Klrk1*$^{+/+}$ mice (14.5% compared to 10.4% in NKG2D-deficient/-blocked mice, Figure 3.54e and f). While differences at day 4 p.i. were subtle and sample numbers were low for day 2, this potentially suggests a higher ratio of CD8$^+$ to CD4$^+$ T cells following infection in mice lacking NKG2D. In addition to T cells, I determined frequencies of ILCs (NK cells, ILC1 and ILC3) as well as myeloid cells (DCs, Neutrophils and Ly6C$^+$ monocytes), but observed no NKG2D-dependent differences (data not shown).

I next assessed the functionality of the intestinal T cells by means of cytokine secretion. I observed a striking difference in the frequency of IL-17-producing γδT cells, which was significantly lower in NKG2D-deficient/-blocked mice (4.9%) compared to *Klrk1*$^{+/+}$ mice (13.4%) (Figure 3.55a and b). A similar trend was observed in CD4$^+$ T cells (22.0% in *Klrk1*$^{+/+}$ mice and 13.6% in NKG2D-deficient/-blocked mice), while frequencies of IFN-γ producing CD8$^+$ T cells were independent of NKG2D (Figure 3.55a).

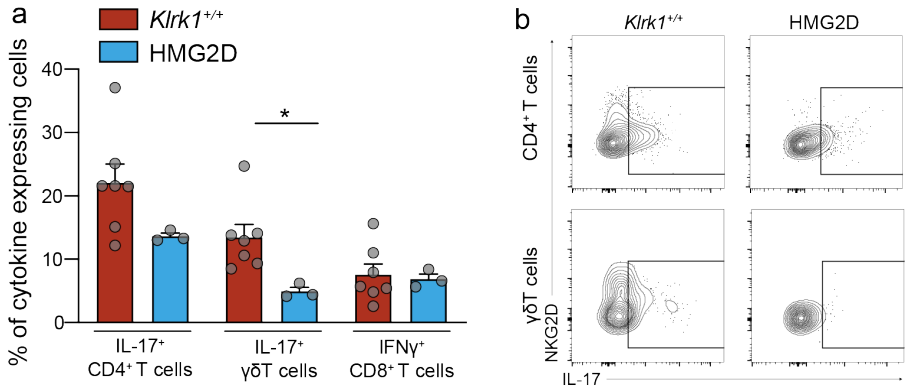

Figure 3.55: Frequencies of IL-17-producing intestinal γδT cells are significantly decreased upon blocking of NKG2D on day 2 post infection. (a) Frequencies of cytokine producing T cells (gated on CD4$^+$, γδTCR$^+$ or CD8$^+$) stimulated with PMA and ionomycin 2 dpi in *Klrk1*$^{+/+}$ mice and mice treated with HMG2D blocking antibody. (b) Representative flow cytometry plots of IL-17 producing CD4$^+$ and γδT cells isolated from *Klrk1*$^{+/+}$ mice and mice treated with HMG2D blocking antibody and stimulated with PMA and ionomycin 2 dpi. n $\geq$ 3. dpi = days post infection. Data represented as mean ± SEM of individual mice from one experiment. * p $\leq$ 0.05.

In all experiments, MLN were analyzed alongside LPL. Typically, no genotypic differences were observed and MLN were used as an internal control for staining and *ex vivo* stimulation. I did however observe striking NKG2D-dependent differences in the frequencies and functionality of ILCs residing in the MLN upon infection with *C. rodentium*. ILC1s, ILC3s and NK cells were reduced in the MLN of NKG2D-deficient/-blocked mice with a significant reduction of ILC3s from 0.05% in *Klrk1*$^{+/+}$ mice to 0.02% in NKG2D-deficient/-blocked mice and a striking reduction of NK cells from 0.60% to 0.19% (Figure 3.56a and b). This change was associated with a change in functionality, specifically of the frequencies of IFN-γ-producing ILC1s and NK cells. I observed a slight reduction in IFN-γ^{+} ILC1s (3.64% in NKG2D-sufficient comapred to 1.22% in NKG2D-deficient/-blocked mice) and a marked reduction in IFN-γ^{+} NK cells (3.38% to 0.16%, Figure 3.56d). This suggests a potential delay in the activation of ILCs residing in the MLN, in particular in the production of IFN-γ.

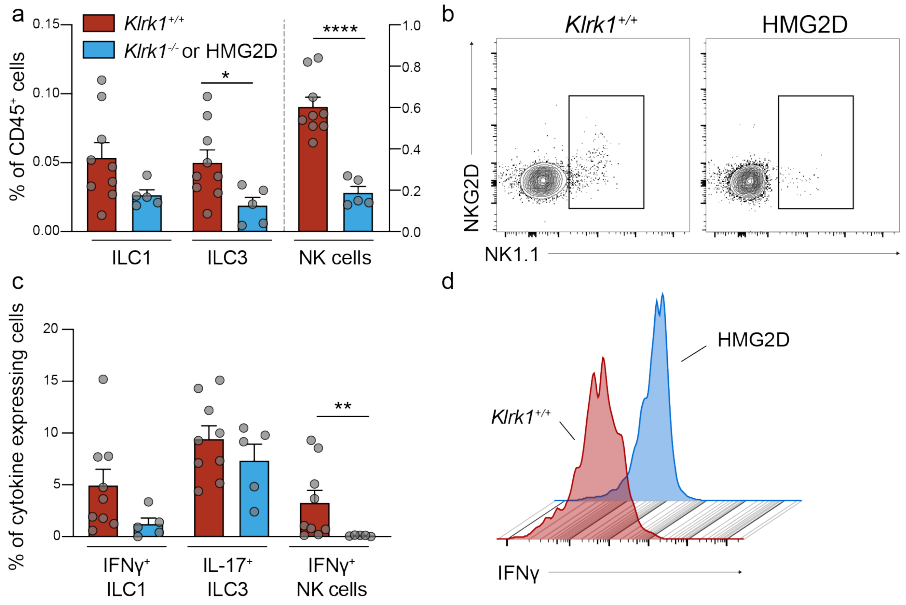

Figure 3.56: Frequencies and cytokine production of innate cell subsets in the MLN are reduced in the absence of NKG2D on day 2 post infection. (a) Frequencies of innate cells (ILC1s gated on CD3^{-} CD19^{-} Ly6C^{-} Ly6G^{-} CD127^{+} T-bet^{+}, ILC3s gated on CD3^{-} CD19^{-} Ly6C^{-} Ly6G^{-} CD127^{+} RORγT^{+} and NK cells gated CD3^{-} NK1.1^{+}) isolated from the MLN 2 dpi. (b) Representative flow cytometry plots of NK cells (gated on CD3^{-}) isolated from the MLN 2 dpi. (c) Frequencies of cytokine-producing innate cell stimulated with PMA and ionomycin, isolated from the MLN 2 dpi. (d) Representative flow cytometry histogram of IFN-γ-producing NK cells (gated on NK1.1^{+} CD3^{-} lymphocytes) stimulated with PMA and ionomycin isolated from the MLN 2 dpi. n ≥ 5. dpi = days post infection, MLN = mesenteric lymph nodes. Data represented as mean ± SEM of individual mice from one experiment. * p ≤ 0.05, ** p ≤ 0.01, **** p ≤ 0.0001.

IL-22 is a cytokine indispensable in the host defense against *C. rodentium* (Zheng *et al.* 2008), but was not included in our flow cytometric analysis. IL-22 induces the expression of antimicrobial proteins in colonic epithelial cells and thereby regulate the early host response to *C. rodentium*. To understand NKG2D-dependent differences in IL-22 production and secretion, I performed an ELISA assay on supernatant from tissue incubated *ex vivo* for 24 hours. I observed an increase of IL-22 on day 4 p.i. (100.6 pg/ml in *Klrk1*$^{+/+}$ mice) compared to day 2 (3.7 pg/ml in *Klrk1*$^{+/+}$ mice), which was reduced to 24.2 pg/ml on day 7. Interestingly on day 25, the average IL-22 concentration was 87.0 pg/ml, but with a standard deviation of 66.1 (Figure 3.57). No statistically significant differences were observed comparing *Klrk1*$^{+/+}$ mice to *Klrk1*$^{-/-}$ mice or mice receiving HMG2D antibody, suggesting that IL-22 expression is not affected by lack of NKG2D. One of the *Klrk1*$^{-/-}$ control mice showed a particular high baseline concentration of IL-22 (231.5 pg/ml), but due to the limited number of mice in the control group, we are unable to draw conclusions on potential differences in NKG2D-dependent IL-22 production in uninfected mice.

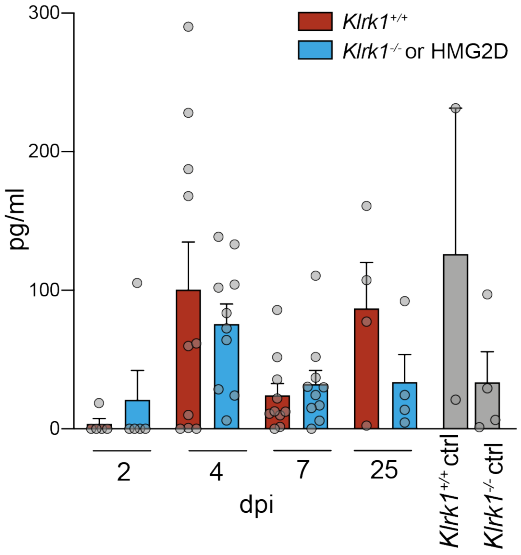

Figure 3.57: IL-22 secretion by *ex vivo* tissue transplants is independent of NKG2D. Protein quantification of supernatant collected from 24 hour *ex vivo* tissue transplants using ELISA. n $\geq$ 4 for infected tissue and n $\geq$ 2 for control tissue. ctrl = control.

3.3.3 Discussion

3.3.3.1 The role of NKG2D in DSS-induced colitis

The DSS mouse model has been used to study the immune response involved in intestinal inflammation for decades (Okayasu *et al.* 1990b) and using mice lacking specific parts of the immune system, mechanisms leading to intestinal inflammation are now well understood. Due to the fact that most studies focus on specific parts of the immune system, few studies provide a broad characterization of the immune response following treatment with DSS. Further complicating this is the fact that immune responses often vary from colony to colony due to differences in the microbiota, genetic background and environmental factors, such as food and housing conditions. Here, I provide a characterization of the immune response following short- and long-term treatment with DSS. The immune response in the ST model is associated with an increase in ILCs, in particular ILC1 and ILC3, as well as an increased production of IFN-γ and IL-17 by innate cells compared to healthy controls (Figure 3.58). A role for ILCs has been demonstrate by other studies, such as a key study by Bernink *et al.* showing an accumulation of ILC1s in the inflamed tissue of both human patients as well as mice (Bernink *et al.* 2013) as well as an increase of IL-17A and IFN-γ mRNA (Yang *et al.* 2017). Nonetheless, the fact that production of IL-17 and IFN-γ by T cells is reduced following treatment with DSS is surprising. Studies demonstrating a clear role for IFN-γ and IL-17 in mediating disease were unable to attribute this to T cells (Ito *et al.* 2006, Ito *et al.* 2008), leaving the possibility that the inflammatory response is mostly independent of the adaptive immune response. Yet, a clear involvement of adaptive immune cells has been demonstrated using Recombination Activating Gene 1 (RAG1)-deficient mice, which display significantly reduced weight loss and milder disease in a ST DSS model (Kim *et al.* 2006). Our study only provides limited insight into the functionality of T cells and many other mechanisms, including direct killing of $CD8^+$ T cells of epithelial cells as well as secretion of other cytokines or cytotoxic molecules, are not considered.

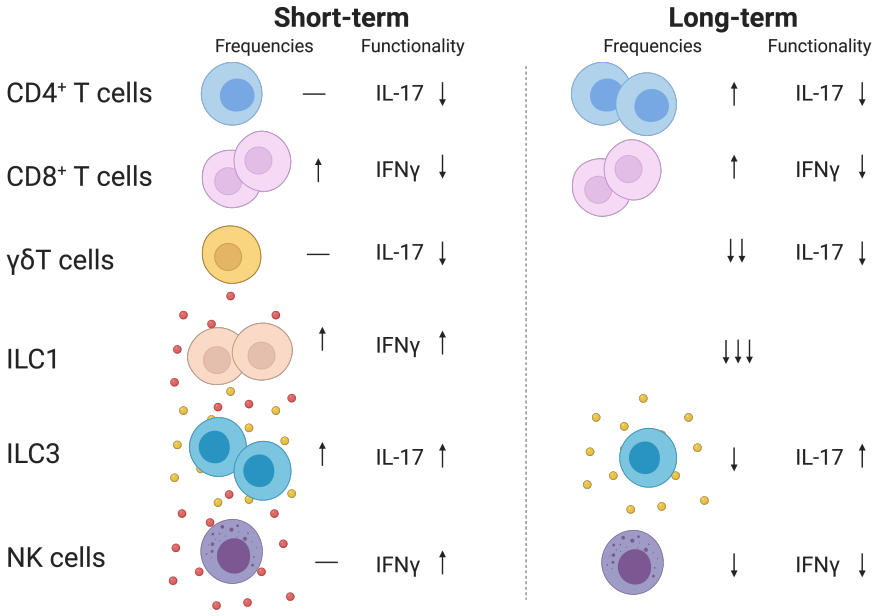

Figure 3.58: Simplified representation of changes in immune cell subsets and functionality upon shot-term and long-term DSS treatment compared to naive control mice. Image was created using BioRender.

Human IBD often develops over a period of years, raising the question of how comparable this acute, seemingly ILC-driven model is with human pathology. Chronic exposure to DSS, as it is the case in our LT model, has not been studied in detail and little is known about the immune response following repeated cycles of DSS treatment. In a slightly different experimental setup with a longer recovery phase following the last round of DSS treatment, blocking of IFN-γ and TNF-α ameliorated disease (Obermeier *et al.* 1999), suggesting that these two cytokines at least partially contribute to the chronic inflammation. Another study using Swiss-Webster mice showed an accumulation of $CD4^+$ T cells in chronically inflamed intestines (Dieleman *et al.* 1998). Both $CD4^+$ and $CD8^+$ T cells, but not γδT cells are increased in the LT model (Figure 3.58). Similar to the acute phase, $CD4^+$ and $CD8^+$ produce little IL-17 and IFN-γ in our study. The low frequency of IL-17 and IFN-γ-producing cells after repeated treatment with DSS indicates that the chronic phase is either characterized by the secretion of other cytokines that were not determined in this study or that the accumulation of T cells results in an overall increase of secreted cytokine, even if frequencies of cytokine-producing T cells are unchanged or even decreased. Frequencies of ILCs are significantly decreased with an almost complete loss of ILC1s, indicating a remodelling of the intestinal immune cell compartment.

Using NKG2D-deficient *Klrk1*$^{-/-}$ mice, we set out to determine the role of NKG2D in DSS-induced colitis. The project had two main experimental aims, I. reanalyze previously acquired data to determine potential covariants leading to differences in disease susceptibility and II. validate these findings in a tightly controlled study. The complexity of factors potentially influencing disease susceptibility made it impossible to directly compare macroscopic parameters of *Klrk1*$^{+/+}$ and *Klrk1*$^{-/-}$ mice and further statistical analysis was needed to determine the impact of covariants in these experiments. ANCOVA revealed that even taking into account sex, age, bodyweight and the experimental round, NKG2D-deficiency did not lead to changes in disease susceptibility. Nonetheless, it must be considered that with increasing numbers of covariants and a relatively low sample size, the statistical power of these experiments is low. I therefore repeated the experiments in a small, but tightly controlled study. I was able to confirm the lack of genotypic differences and further found that NKG2D expression is not altered upon treatment with DSS, possibly indicating that the NKG2D/NKG2DL axis is not involved in mediating inflammation. The lack of phenotypic differences in *Klrk1*$^{-/-}$ mice compared to wild-type controls was surprising considering ER stress, which is a consequence of treatment with DSS (Takagi *et al.* 2018) has been shown to induce upregulation of NKG2DL on epithelial cells (Hosomi *et al.* 2017). Unfortunately, I was unable to determine changes in NKG2DL expression due to the lack of a working IHC staining and without this information, we cannot exclude the possibility of NKG2D-mediated killing of NKG2DL-expressing epithelial cells, similar to what was reported in CD patient. Lack of differences in disease susceptibility as well as unchanged frequencies of NKG2D-expressing cells suggest that if NKG2DL is upregulated upon DSS treatment, the effects of NKG2D-mediated killing of epithelial cells is masked by the overall inflammatory response. DSS-induced colitis differs from human disease in many aspects, one of which is that tissue injury is mediated by a chemical, rather than physiological processes, meaning a much harsher and faster destruction of the epithelium. It is therefore plausible that NKG2D-mediated effects do not become apparent in such an acute and harsh model of tissue injury.

While protein expression of NKG2D on ILCs and T cells remains unchanged upon ST treatment of DSS, we observed differences in the abundance of *Klrk1* transcript. In control mice

and mice with mild disease, *Klrk1* is not detectable, while it is expressed at low levels in intermediate and severe disease. There are two plausible explanations for this, I. DSS-mediated injury induces transcriptional changes, which do not translate to changes in protein levels due to the involvement in other pathways potentially leading to a suppression of protein translation or II. the accumulation of NKG2D-expressing ILCs observed in acute phases of DSS-mediated colitis results in an overall increase of *Klrk1* transcript found in the tissue.
The key data missing from this study is changes in NKG2DL expression, without which it is difficult to draw conclusions on the involvement of the NKG2D/NKG2DL axis. Nonetheless, we can conclude that lack of NKG2D does not influence susceptibility to DSS-mediated colitis, either in a ST, or a LT model. It should however be noted that susceptibility to DSS-induced colitis is highly dependent on the microbiota and that differences within the microbiota might alter the strain's susceptibility, resulting in NKG2D-dependent differences and leading to changes in NKG2D expression during the course of disease, as observed in the study by Wang *et al.* (Wang *et al.* 2017).

3.3.3.2 The role of NKG2D in *Citrobacter rodentium*-induced colitis

The *C. rodentium* model has been used to study host responses following infection with intestinal pathogens, as well as intestinal inflammation to better understand pathogenesis of human IBD. In the context of NKG2D-mediated immunity, two main questions arise: I. is NKG2D involved in pathogen recognition and elimination? And II. does NKG2D mediate the inflammatory response? Evidence exists for the importance of NKG2D in the clearance of respiratory infection, where blocking of NKG2D results in decreased production of T_H1 cytokines and delayed clearance of bacteria (Borchers *et al.* 2006). Bacterial clearance was later shown to be mediated by NK cells through the recognition of NKG2DL (Wesselkamper *et al.* 2008), leading us to hypothesize that similar mechanisms might be involved in clearance of *C. rodentium*. This hypothesis was supported by two papers, one showing upregulation of NKG2DL on epithelial cells infected with *E. coli*, which is closely related to *C. rodentium* (Tieng *et al.* 2002) and a second study demonstrating protective effects of NK cells against intestinal infection (Hall *et al.*

2013b). We therefore hypothesized that lack of NKG2D would lead to delayed recognition of *C. rodentium* and higher bacterial burden at early stages of the disease. Interestingly, we observed the opposite and found that bacterial colonization is delayed in NKG2D-deficient mice. This was only evident on day 2 p.i., raising the question of not only the biological relevance, but also the validity of these results. *C. rodentium* first colonizes the cecum before it progresses to the distal colon 2 to 3 days p.i. (Bhinder *et al.* 2013), resulting in high variations in fecal bacterial burden at early stages of infection (personal communication with Gad Frankel). Analysis of all data collected revealed a statistically significant difference in fecal bacterial burden on day 2 p.i. between *Klrk1*$^{+/+}$ and NKG2D-deficient/-blocked mice, yet, this difference was not always observed in individual experiments. Our revised hypothesis that colonization is indeed delayed in NKG2D-deficient/-blocked mice is supported by the observation that cecal bacterial burden was significantly reduced on day 2, but not 4 p.i. in the absence of NKG2D.

In this study, I provide a thorough characterization of the immune response following infection with *C. rodentium*. Previous studies investigating the immune response have focused on specific timepoints, most often the peak of infection and beyond (Hall *et al.* 2013b, Dann *et al.* 2014, Chen *et al.* 2014). A recently published study provides insight into host responses preceding the peak of infection. Specifically, responses on day 4 p.i. were studied and revealed upregulation of DNA damage repair and replication as well as changes in cell metabolism (Hopkins *et al.* 2019). However, the immune response was not studied in detail. Indeed, even studies addressing the role of ILCs in *C. rodentium*-infection fail to address very early stages and instead focus on changes from day 4 (Lin *et al.* 2019, Guo *et al.* 2015, Giacomin *et al.* 2015).

I show that as early as day 2 p.i. frequencies of CD4$^+$ T cells, ILC1s and ILC3s increase, but that this was not associated with changes in cytokine production. On day 4, where frequencies return to baseline levels, CD4$^+$ and γδT cells start producing IL-17, while functionality of CD8$^+$ and ILCs remain unchanged (Figure 3.59). I observed an unexpected high frequency of IFN-γ-producing ILC1s and IL-17-producing ILC3s on day 25, suggesting remodelling of the immune cell composition and heightened production of cytokines beyond bacterial clearance. No markers to identify T_{RM} cells were included in this study, but the accumulation of CD4$^+$ T cells on day 25 p.i. suggests that they are indeed memory cells. Indeed, IL-17 and IL-22-

producing T_{RM} cells have been found in the mouse intestine up to 3 months after infection (Bishu *et al.* 2019).

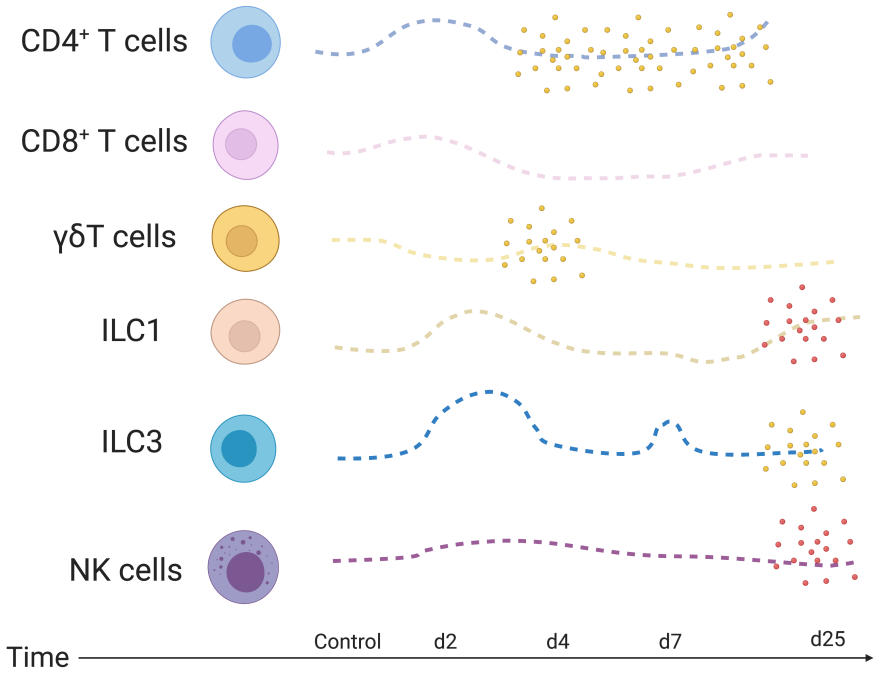

Figure 3.59: Simplified representation of changes in immune cell subsets and functionality upon infection with *C. rodentium*. $CD4^+$ T cells transiently increase on day 2 and 4 p.i. and accumulate at late stages of the infection. IL-17 production is evident from day 4. Cytokine production by $CD8^+$ T cells does not change and frequencies remain similar throughout the infection. γδT cells produce IL-17 at acute phases of the infection (day 4 p.i.). ILC1s transiently increase on day 2 and 4 p.i. and, similar to $CD4^+$ T cells, accumulate in the intestine at late stages of the infection. Frequencies of ILC3s increase on day 2 and day 7, whereas frequencies of IL-17-producing ILC3s remain unchanged during acute phases of the infection and is increased, similar to frequencies of IFN-γ-producing ILC1s, only at late stages (day 25 p.i.). Frequencies of NK cells remain stable and produce similar levels of IFN-γ throughout acute phases of the infection. Similar to other innate cells, frequencies of cytokine-producing NK cells are only increased on day 25 p.i.. Red molecules = IFN-γ, yellow molecules = IL-17. p.i. = post infection. Image was created using BioRender.

Frequencies of NKG2D-expressing T cells remain unchanged throughout infection, similar to what was observed following treatment with DSS. Frequencies of $NKG2D^+$ ILC1s and NK cells increase on day 2 p.i., potentially suggesting an activation of these cells. However, the differences were subtle, making it difficult to draw conclusions on potential functional consequences of this increase (Figure 3.59).

A major drawback of this study is that I only characterized the immune response in the colonic

LP and not the cecum. Considering that *C. rodentium* first colonizes the cecum and that the differences observed in this study preceded colonization of the colon, studying the immune response in the cecum would have been of great value. Indeed, only mild differences were observed in the colonic immune response when comparing *Klrk1*$^{+/+}$ to NKG2D-deficient/-blocked mice. The most striking differences in immune cell composition and functionality in the colonic LP is the increased frequency of CD8$^+$ T cells in NKG2D-deficient/-blocked mice and the decrease of IL-17-producing γδT cells and, to a lesser extent, CD4$^+$ T cells. However, both observations are based on a sample size of 3 and more experiments are required to confirm these findings.

I routinely isolate immune cells from the MLN in all our experimental setups. While I observed no changes in cell frequencies or functionality following treatment with DSS, I observed striking differences of ILCs in the MLN with a reduced frequency and reduced IFN-γ produced by ILC1s and NK cells in NKG2D-deficient/-blocked mice infected with *C. rodentium*. One of the MLN specifically drains the cecum (Bernier-Latmani *et al.* 2017) and differences observed in immune cell composition and function within the MLN might, at least to some extent, reflect the cecal immune response. Further, bacterial translocation to the MLN has been demonstrated (Skinn *et al.* 2006). It is plausible that the reduced frequencies of ILCs and IFN-γ-producing cells in the MLN of NKG2D-deficient/-blocked mice was due to a lack of recognition of the infection and a subsequently delayed host response. However, both NK cells (Hall *et al.* 2013b) as well as IFN-γ (Simmons *et al.* 2002) are crucial in host defense and clearance of *C. rodentium*, and the delay in the innate response contradicts the reduced bacterial burden in NKG2D-deficient/-blocked mice. The host response to *C. rodentium* at early stages is not understood and we hypothesize that the contradicting results can be explained by non-redundant host responses. A heightened responsiveness to infection by mice lacking NKG2D could result in enhanced release of AMPs and better initial bacterial clearance despite the delayed host immune response. However, further research is needed to understand the relationship between NKG2D and early host defense and to improve the general understanding of acute immune responses following infection with *C. rodentium* in various organs.

In summary, I was unable to reveal a mechanism explaining the delayed colonization in NKG2D-deficient/-blocked mice. This leaves two possible explanations for the differences observed, I.

despite a statistical significance, the differences are a result of high variation and are independent of NKG2D and II. other unknown mechanisms are involved. Identifying mechanisms resulting in NKG2D-dependent bacterial clearance are of interest, but the physiological relevance is questionable. The effect observed in this model was subtle and did not affect the outcome of infection. Further, targeting early stages of infection in human patients are difficult to achieve in practice due to the delay in diagnostics.

3.3.3.3 Summary

We initially hypothesized that the two models used in this study - DSS-induced sterile colitis and *C. rodentium*-induced infectious colitis would complement each other and provide us with a clear picture of the role of NKG2D in mouse colitis. However, our studies suggest that neither of the models are appropriate in studying NKG2D-mediated mechanisms observed in CD patients. Nonetheless, the studies provide us with valuable information and raise several questions. We conclude that lack of NKG2D only mildly influence the inflammatory response in either of the models, most likely due to a lack of activation of NKG2D-expressing cells. At this stage, we do not know whether this is due to a lack of upregulation of NKG2DL, which is a critical piece of information missing, or lack of engagement of NKG2D on immune effector cells. We further found that NKG2D is dispensable for clearance of *C. rodentium*, but that initial colonization is delayed in NKG2D-deficient mice. The physiological relevance of differences seen at early stages of infection remain to be determined, but it can be concluded that NKG2D is not a critical mediator in host defense against *C. rodentium*.

3.4 Final discussion and future work

The studies presented in this thesis provide valuable and novel insight into the function of NKG2D in intestinal inflammation and tumorigenesis. The main conclusions are:

1. NKG2D expression in the intestine is elevated compared to other tissues, suggesting that the mucosal environment favors upregulation of NKG2D.

2. Intestinal health under homeostatic conditions is not affected by germline deletion of NKG2D.

3. NKG2D promotes tumorigenesis in a model of intestinal cancer.

4. Exacerbated tumorigenesis in NKG2D-sufficient mice is associated with an increased infiltration of $CD8^+$ T cells producing high levels of IFN-γ as well as a unique subset of PD-1^+ $\gamma\delta$T cells.

5. Composition of the intestinal microbiota and expression of NKG2D ligands in the intestine are independent of NKG2D.

6. NKG2D is dispensable in sterile colitis.

7. Early stages of infection with *C. rodentium* are affected by NKG2D deficiency, but NKG2D does not contribute to the inflammatory response or disease outcome.

NKG2D has been implicated in various intestinal disorders, yet, NKG2D expression has not been studied in detail in the intestine. We provide a thorough characterization of NKG2D-expressing cells in the mouse intestine and show that NKG2D expression is elevated on intestinal immune cells compared to lymphoid organs such as the MLN (Figure 3.60a). We provide evidence for constitutive NKG2DL expression on healthy mouse epithelium, which is in line with observations made on human intestinal tissue (Groh *et al.* 1996). We show that germline deletion of NKG2D does not lead to major changes in the composition of the intestinal immune system, immune cell function, expression pattern of NKG2DL or the intestinal microbiota, suggesting that *Klrk1*$^{-/-}$ mice develop normally and without any immunological defects, making

them a good model organism to study NKG2D in the setting of intestinal dysbiosis and disease. A unique characteristic of the intestine is that NKG2DL are constitutively expressed on healthy tissue. This constititutive expression raises the question why NKG2D-expressing cells are not activated despite the presence of both NKG2D on immune effector cells and NKG2DL on epithelial cells under steady-state conditions. Being constantly exposed to foreign antigens, the intestine is particularly susceptible to misdirected inflammatory responses, which can eventually lead to chronic intestinal inflammation and IBD. Immune cells therefore need to be tightly controlled to prevent overreaction against harmless antigens.

The NKG2D/NKG2DL axis may act in a regulatory manner: constant engagement of NKG2D through its ligand may lower the activation threshold of NKG2D-expressing cells, making them less reactive to harmless foreign antigens or mild and non-pathogenic changes in the intestinal microenvironment. The fact that NKG2D-deficient mice develop normally and display no signs of aberrant inflammation in the healthy intestine however suggests that NKG2D is not crucial to maintaining intestinal health or that other mechanisms are in place to maintain intestinal homeostasis in *Klrk1*$^{-/-}$ mice. It would be of interest to study the impact of NKG2D deficiency further and perform single-cell sequencing analysis to establish transcriptional changes associated with the lack of NKG2D signaling in individual cell types. Transcriptional analysis on a single cell level would further allow validation of the subtle differences observed in this study, such as heightened IFN-γ productions by ILC1s in *Klrk1*$^{-/-}$ mice. RNAseq could be accompanied by *ex vivo* analysis of different immune cell subsets isolated from the intestines of *Klrk1*$^{+/+}$ and *Klrk1*$^{-/-}$ mice to determine their response to certain stimuli. Testing the ability of *Klrk1*$^{-/-}$ to react to certain stimuli in a controlled setting would allow us to determine whether NKG2D-deficient cells are indeed hyperreactive, one hypothesis that arose from observations made in Chapter 3.

Another explanation for the co-existence of NKG2D and NKG2DL is the spatial distribution - despite the presence of NKG2D on IEL, we do not know whether these cells are in direct contact with NKG2DL expressed by epithelial cells. If NKG2DL are expressed on the apical surface, NKG2D may not bind to NKG2DL under homeostatic conditions. Only when the intestinal barrier breaks down, NKG2D-expressing cells bind to NKG2DL and are activated.

Following this hypothesis, the elevated expression of NKG2D on intestinal immune cells would likely be a consequence of a refined danger sensing system which allows an immediate response to disruptions of the epithelial barrier. To address this question, high-resolution microscopy or electron microscopy should be performed to determine the exact location of NKG2DL on epithelial cells. This study is limited to the analysis of one NKG2DL, RAE-1. To better understand the function of different ligands, expression patterns of the other mouse ligands need to be determined.

Our findings on the role of NKG2D in intestinal tumorigenesis are intriguing. While some similarities to the HCC model are evident, such as an increased infiltration of IFN-γ-producing $CD8^+$ T cells in NKG2D-sufficient mice compared to NKG2D-deficient littermates (Sheppard *et al.* 2017), we identified novel mediators specific to the intestinal tumor response. Specifically, we demonstrated a unique role for γδT cells, which accumulate in intestinal tumors in an NKG2D-specific manner (Figure 3.60b). We observed no NKG2D-dependent differences in IL-17 production among these γδT cells, but hypothesize that the increased frequency of γδT cells producing similar levels of IL-17 results in an accumulation of pro-tumorigenic and pro-inflammatory IL-17 in the TME of $Apc^{min/+}$ $Klrk1^{+/+}$ mice. Further, studying the phenotype of these γδT cells revealed that a large percentage expresses PD-1 in the $Apc^{min/+}$ $Klrk1^{+/+}$, but not $Apc^{min/+}$ $Klrk1^{-/-}$ mice. A certain subset of γδT cells, namely Vγ6 cells, has been shown to express PD-1 (Tan *et al.* 2019), suggesting that the accumulation of γδT cells in $Apc^{min/+}$ $Klrk1^{+/+}$ mice is due to an accumulation of this specific subset or $V\gamma6^+$ γδT cells. This hypothesis was further supported by experiments performed by our collaborators from Seth Coffelt's lab (Beatson Institute, University of Glasgow), who demonstrated a relationship between NKG2D signaling and IL-17 in the lung and further showed that NKG2D is expressed largely by $V\gamma6^+$ T cells. Yet, several questions remain and further experiments are needed to confirm a pro-tumorigenic, NKG2D-dependent role of $V\gamma6^+$ T cells. Firstly, we need to determine which subset of γδT cells infiltrate the tumor by comparing expression of different Vγ receptors in TILs of $Apc^{min/+}$ $Klrk1^{+/+}$ and $Apc^{min/+}$ $Klrk1^{-/-}$ mice. We further need to determine whether IL-17 accumulates in the tumors of NKG2D-sufficient mice by quantifying

numbers of IL-17-producing cells or IL-17 protein.

Mechanisms involved in NKG2D-mediated immunity in the context of intestinal tumorigenesis are likely complex and cannot be reduced to one or two celltypes. Nonetheless, cell-type specific deletion of *Klrk1* using $Klrk1^{flox/flox}$ mice on the $Apc^{min/+}$ background intercrossed with $Cd8a^{Cre}$ or $Rorc^{Cre}$ mice could provide valuable information on the role of $CD8^+$ T cell and IL-17-producing cells, respectively. Studying the contribution of $CD4^+$ T cells is of further interest. While we observed no differences in frequencies of tumor-infiltrating $CD4^+$ T cells, tumorigenesis was associated with an upregulation of NKG2D on these cells. Cytokines that have previously been implicated in NKG2D-mediated intestinal inflammation, such as GzB (Allez *et al.* 2007) were not specifically studied in these experiments and we can therefore not exclude the possibility of $NKG2D^+$ $CD4^+$ T cells contributing to inflammation and tumor growth by specifically eliminating NKG2DL-expressing epithelial cells.

Another question that requires further research is the role of NKG2DL in this model of intestinal cancer. We observed no NKG2D-dependent differences in NKG2DL expression on tumors in the SI - we expected tumor cells to escape NKG2D-mediated destruction by downregulating NKG2DL. There are various explanations for this: I. NKG2D-expressing effector cells do not interact with NKG2DL-expressing tumor cells, meaning that these cells are not eliminated in an NKG2D-dependent manner, II. NKG2DL-expressing cells are eliminated, but high cell turnover and chronic inflammation results in consistent upregulation and constant expression of NKG2DL similar to tumors of NKG2D-deficient mice, where NKG2DL-expressing cells are not eliminated and III. NKG2DL interacts with NKG2D on immune effector cells but fails to induce a response leading to target cell death, instead promoting the production of pro-inflammatory cytokines and eventually immune cell exhaustion.

To fully understand the function of the NKG2D/NKG2DL axis, we need to study the expression pattern of other NKG2DL. Further, NKG2DL protein levels should be measured in the serum of mice, as NKG2DL shedding can occur in the context of tumorigenesis (Groh *et al.* 2002). Nonetheless, our data suggests that expression of NKG2DL throughout the disease results in constitutive activation of NKG2D-expressing effector cells leading to an aberrant immune response and/or immune cell exhaustion. This immune cell dysfunction could be the result of

the host response described earlier where NKG2D-expressing cells in the intestine only sense NKG2DL upon epithelial layer disruption, as it is the case in intestinal cancer, due to the location of NKG2DL on the cell surface. While nascent tumor cells are possibly eliminated through NKG2D-mediated immunity, it is plausible that chronic engagement eventually leads to a cell state ultimately favoring tumor growth.

In an attempt to study NKG2D-dependent changes in the microbiota, we found that composition of the microbiota is largely independent of NKG2D. We were able to confirm that tumorigenesis in $Apc^{min/+}$ mice is associated with mild changes in microbial composition. These changes are likely due to differences in the inflammatory milieu, which can alter microbial composition (Belkaid *et al.* 2014). Differences in the severity of inflammation may explain why the composition microbiota of NKG2D-deficient mice, which present with milder inflammation and delayed disease, is more comparable to control mice than that of NKG2D-sufficient littermates.

To ensure that our findings are of clinical relevance and can be translated to human disease, we studied changes in the NKG2D/NKG2DL axis in data obtained from CRC patients, which confirmed that NKG2D and NKG2DL are indeed dysregulated in human disease. While our analysis was limited and only provides a crude overview of the expression pattern in human patients, it is encouraging to see that changes in the NKG2D/NKG2DL axis occur in CRC patients, suggesting that NKG2D is indeed involved in disease progression. Nonetheless, further research is needed to determine how our findings can be translated to human patients. Publicly available datasets provide a valuable platform to study the transcriptional profile of patients and further analyzing these datasets is a valuable tool allowing direct comparison between humans and mice. Ultimately, analysis of transcriptional data will need to be complemented with experiments involving fresh patient samples to study immune cell infiltration of tumors with more accuracy and on protein level.

Further evidence of the function of NKG2D in CRC will come from clinical trials. Celyad is currently testing NKG2D CAR T cells in CRC patients (clinical trial NCT03692429) and have recently announced a collaboration with Merck & co. to test a combination therapy of NKG2D CAR T cells and pembrolizumab, an anti-PD-1 monoclonal antibody (clinical trial KEYNOTE-B79). Interestingly, both trials are conducted primarily on patients with MMR-

proficient tumors, which often present with poor immune cell infiltration. In light of this thesis, targeting a patient group which presents with a poor immune response is a rational approach - we demonstrate that NKG2D contributes to inflammation, but we believe that this only holds true in 'hot', immune cell-rich tumors that provide a pro-inflammatory environment and sustained engagement of NKG2D-expressing effector cells. 'Cold' tumors that lack immune cells or contain dysfunctional and exhausted immune cells, but express NKG2DL could greatly benefit from NKG2D CAR T cell therapy, where transfused cells would directly target and kill the NKG2DL-expressing tumor cells. Complementing this with anti-PD-1 therapy may additionally invigorate exhausted T cells that further contribute to the anti-tumor immune response. Nonetheless, there are risks of side effects that need to be considered and our research builds a foundation that we hope will improve selection of suitable patients for certain therapies and prediction of adverse effects.

Lastly, we studied the role of NKG2D in models of intestinal inflammation not associated with tumorigenesis. We employed two models of mouse colitis hoping the findings from each model would complement each other. Lack of NKG2D had no effect on the disease susceptibility or immune response to DSS-induced colitis (Figure 3.60c). Similarly, infection with *C. rodentium* led to a similar inflammatory response in *Klrk1*$^{+/+}$ mice and mice lacking NKG2D (Figure 3.60d). Surprisingly, we observed a delay in bacterial colonization in *Klrk1*$^{-/-}$ mice, but were unable to determine the mechanisms resulting in this phenotype. Further experiments are needed to study differences at early stages of infection and determine potential mechanisms involved in the host response. Together, we conclude that NKG2D is dispensable for clearance of *C. rodentium* and that further studies addressing early timepoints, such as day 1 and 2 p.i. are needed.

A series of experiments were planned for spring and summer 2020. We planned to further characterize the phenotype and functionality of γδT cells in the TME of *Apc*$^{min/+}$ mice, with particular emphasis on increasing the sample size of data relating to PD-1 expression at disease endpoint. We further planned to stain for different Vγ receptors to prove our hypothesis that

Vγ6$^+$ T cells specifically infiltrate tumors in an NKG2D-dependent manner. Transcriptional analysis measuring changes in gene expression of NKG2DL following treatment with DSS and *C. rodentium* was planned to determine the impact of either treatment on NKG2DL expression. We were unable to perform these experiments due to COVID-19, but hope to address these questions in the future.

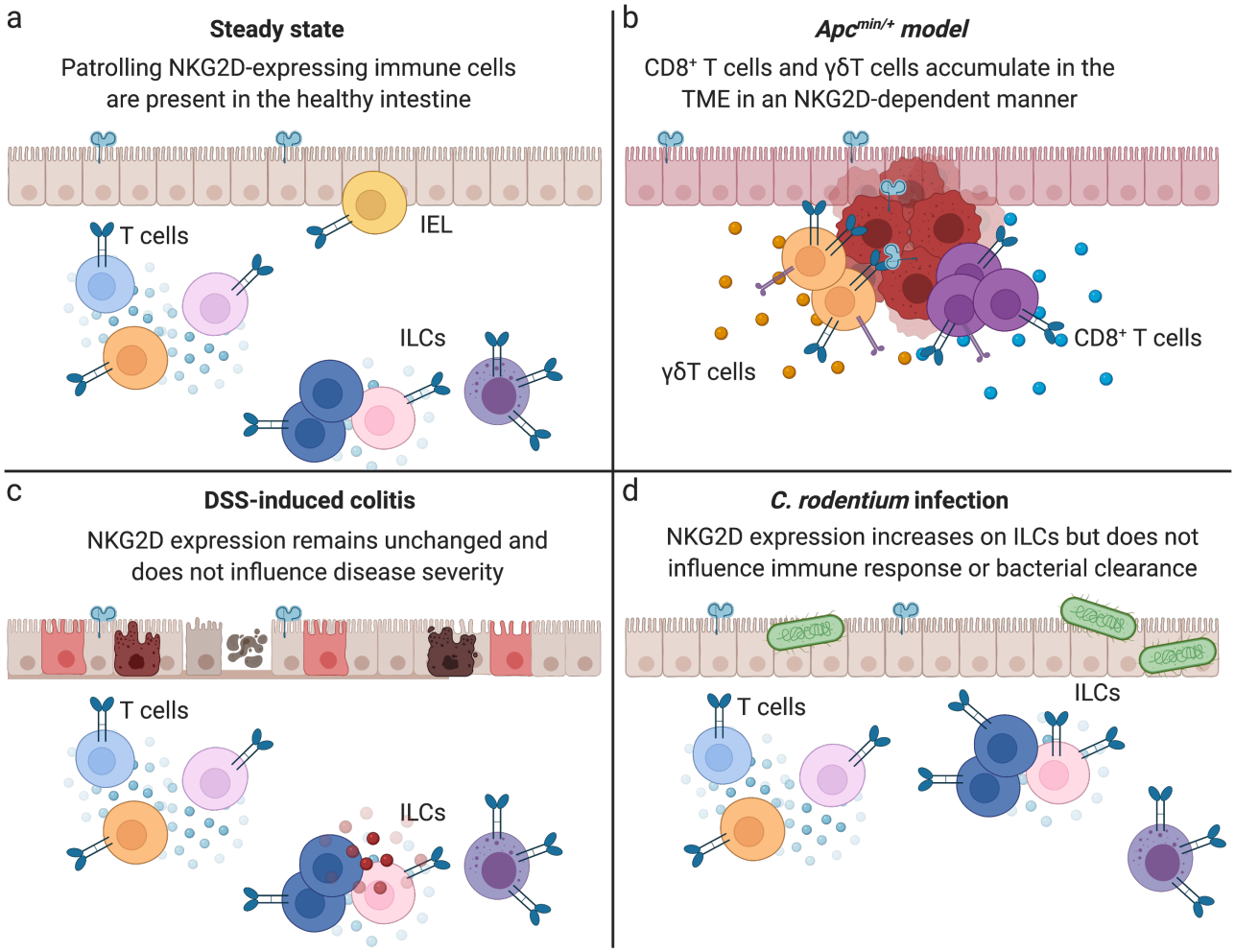

Figure 3.60: Summary of the main findings of this thesis. (a) NKG2D-expressing cells are present in the healthy intestine and include CD4$^+$ and CD8$^+$ T cells, γδT cells, ILC1, ILC3 and NK cells. NKG2DL are expressed on healthy epithelial cells. (b) Intestinal tumorigenesis in the *Apc$^{min/+}$* mouse model is associated with an increase of NKG2D expression on various immune cells, sustained expression of NKG2DL and an NKG2D-dependent accumulation of IFN-γ-producing CD8$^+$ T cells as well as PD-1-expressing γδT cells contributing to the inflammatory milieu. (c) DSS-induced colitis is associated with no changes in NKG2D expression and the immune response following epithelial damage is independent of NKG2D. (d) Infection with *C. rodentium* is associated with mild changes in NKG2D expression on ILCs. NKG2D deficiency does not influence bacterial clearance or affects the immune response following infection. Representation is extremely simplified and does not cover all aspects of NKG2D-mediated immunity. Image was created using BioRender.

3.5 Concluding remarks

Collectively, this work provides further insight into tissue-specific functions of NKG2D in the context of intestinal health and disease. We show that NKG2D promotes inflammation-driven intestinal tumorigenesis and underline the need to understand tissue-specific pathways and mechanisms regulating anti- and pro-tumor function. This is of particular importance in the era of immunotherapy, where immune pathways are specifically targeted to dampen or stimulate the immune response. To improve targeted therapy and avoid detrimental side effects, immune responses in different environments need to be understood. While many questions remain, this thesis improves our understanding of intestinal immunity and reveals a novel role for NKG2D in mediating intestinal homeostasis and pathology.

Acronyms

A. finegoldii *Alistipes finegoldii*

A. muciniphila *Akkermansia muciniphila*

Apc$^{min/+}$ *Adenomatous polyposis coli$^{multiple\ intestinal\ neoplasia/+}$*

Apc *adenomatous polyposis coli*

B. fragilis *Bacteroides fragilis*

E. coli *Escherichia coli*

F. nucleatum *Fusobacterium nucleatum*

H. hepaticus *Helicobacter hepaticus*

P. asaccharolytica *Porphyromonas asaccharolytica*

P. gingivalis *Porphyromonas gingivalis*

P. intermedia *Prevotella intermedia*

P. micra *Parvimonas micra*

S. bovis *Streptococcus bovis*

T. acidaminovorans *Thermanaerovibrio acidaminovorans*

C. rodentium *Citrobacter rodentium*

5-FU Fluorouracil

A/E attaching and effacing

ADCC antibody-dependent cellular cytotoxicity

AhR Aryl hydrocarbon receptor

AML acute myeloid leukemia

AMP anti-microbial peptides

ANCOVA Analysis of covariance

APC antigen presenting cells

bp base pair

CAR chimeric antigen receptor

CD cluster of differentiation

CD Crohn's disease

CeD Celiac Disease

CFU colony-forming units

CMS consensus molecular subtype

COAD colon adenocarcinoma

COX cyclooxygenase

CRC colorectal cancer

CRP C-reactive protein

CSF1R Colony stimulating factor 1 receptor

CTL cytotoxic T lymphocytes

CTLA-4 cytotoxic T-lymphocyte-associated protein 4

DC dendritic cells

DDR DNA damage response

DEN Diethylnitrosamine

dMMR deficient mismatch-repair

DN double-negative

DNA deoxyribonucleic acid

DNAM1 DNAX Accessory Molecule-1

dNTP deoxynucleoside triphosphates

dpi days post infection

DSS dextran sodium sulfate

EAE Experimental Autoimmune Encephalomyelitis

EGFR Epidermal growth factor receptor

EHEC Enterohemorrhagic *Escherichia coli*

ELISA enzyme-linked immunosorbent assay

EOMES Eomesodermin

EPEC Enteropathogenic *Escherichia coli*

ER endoplasmic reticulum

FAP familial adenomatous polyposis

Fap2 Fusobacterial apoptosis protein 2

FasL Fas ligand

FCS fetal calf serum

FMO fluorescence minus one

FMT Fecal microbiota transplant

Foxp3 Forkhead box P3

FSC forward scatter

g grams

GF germ-free

GM-CSF Granulocyte-macrophage colony-stimulating factor

GzB Granzyme B

H60 Histocompatibility 60

HCC hepatocellular carcinoma

HCMV Human Cytomegalovirus

HCT hematocrit

HEPES 4-(2-hydroxyethyl)-1-piperazineethanesulfonic acid

HIER heat-induced epitope retrieval

HLA human leukocyte antigen

i.p. intraperitoneal

IBD inflammatory bowel disease

ICI Immune Checkpoint Inhibitors

IEC Intestinal epithelial cells

IEL intraepithelial cells

IF immunofluorescence

IFC integrated fluidic circuit

IFN interferon

Ig immunoglobulin

IHC immunohistochemistry

IL interleukin

ILC innate lymphoid cells

iNKT Invariant Natural Killer

iNOS inducible nitric oxide synthase

ISC intestinal stem cell

ITAM Immunoreceptor tyrosine-based activation motif

LAG3 Lymphocyte-activation gene 3

LAK Lymphokine-activated killer cell

LP lamina propria

LPL lamina propria lymphocytes

LPS lipopolysaccharide

LSC leukemic stem cells

LT long-term

LTi lymphoid tissue-inducer

mAb monoclonal antibody

MAIT Mucosal associated invariant T cell

MCA methylcholanthrene

mCRC metastatic colorectal cancer

MDS myelodysplastic syndrome

MDSC Myeloid-derived suppressor cell

MFI median fluorescence intensity

MHC Major histocompatibility complex

MIC MHC class I chain-related protein

Min multiple intestinal neoplasia

MLN mesenteric lymph nodes

MM multiple myeloma

MMP Matrix metalloproteinase

MS Multiple Sclerosis

MSI-H microsatellite instability high

MSS microsatellite stable

MUC1 Mucin-1 precursor

MULT1 Murine UL16 binding protein-like transcript

MyD88 Myeloid differentiation primary response 88

NaCl sodium chloride

NCR natural cytotoxicity receptors

NET Neutrophil extracellular traps

NF-$\varkappa$B nuclear factor kappa-light-chain-enhancer of activated B cells

NK natural killer

NKG2A Natural killer group 2A

NKG2D Natural killer group 2D

NKG2DL NKG2D ligands

NKT Natural killer T

NOD2 Nucleotide-binding oligomerization domain-containing protein 2

NOS2 Nitric oxide synthase 2

NSCLC Non-small-cell lung carcinoma

OPN osteopontin

p.i. post infection

PARP1 Poly [ADP-ribose] polymerase 1

PB peripheral blood

PBMC peripheral blood mononuclear cell

PBS phosphate buffered saline

PC plasma cell

PCoA Principal Component Analysis

PCR Polymerase chain reaction

PD-1 Programmed cell death protein 1

PD-L1 Programmed death-ligand 1

PDA pancreatic ductal adenocarcinoma

PI3K Phosphoinositide 3-kinase

PMA Phorbol 12-myristate 13-acetate

PMT photomultiplier tube

PP Peyer's patch

PRR pattern recognition receptors

QIIME Quantitative Insights Into Microbial Ecology

qPCR quantitative PCR

RA retinoic acid

RAE-1 Retinoic acid early inducible 1

RAG1 Recombination Activating Gene 1

RAG2 Recombination Activating Gene 2

RCC Renal cell carcinoma

RegIII Regenerating islet-derived protein 3

RELM Resistin-Like Molecule

RNA ribonucleic acid

RNAseq RNA sequencing

RORγT RAR-related orphan receptor gamma

ROS reactive oxygen species

rpm revolutions per minute

rRNA ribosomal RNA

SCFA Short-chain fatty acid

SCID Severe combined immunodeficient mice

SFB segmented filamentous bacteria

SI small intestine

SOS1 Son of sevenless homolog 1

SSC sideward scatter

ST short-term

STAT Signal transducer and activator of transcription

T-bet T-box transcription factor

T3SS Type III secretion system

$\mathbf{T_{reg}}$ regulatory T cells

$\mathbf{T_{RM}}$ tissue-resident memory

TAM tumor-associated macrophage

TCGA The Cancer Genome Atlas

TCR T cell receptor

TE Tris-EDTA

Tfh T follicular helper

TGF Transforming growth factor

TIL tumor-infiltrating lymphocyte

TLR toll-like receptors

TME tumor microenvironment

TNBS 2,4,6-trinitrobenzene sulfonic acid

TNF tumor necrosis factor

TPM transcript per million

TRAMP transgenic adenocarcinoma of the mouse prostate

TRIF TIR-domain-containing adapter-inducing interferon-β

tSNE T-distributed stochastic neighbor embedding

UC ulcerative colitis

ULBP UL16 binding protein

VEGF Vascular endothelial growth factor

Bibliography

1. Abadie, V. *et al.* IL-15, gluten and HLA-DQ8 drive tissue destruction in coeliac disease. *Nature,* 1–5 (2020).

2. Abed, J. *et al.* Colon Cancer-Associated Fusobacterium nucleatum May Originate From the Oral Cavity and Reach Colon Tumors via the Circulatory System. *Frontiers in Cellular and Infection Microbiology* **10,** 400 (2020).

3. Abegunde, A. T., Muhammad, B. H., Bhatti, O. & Ali, T. Environmental risk factors for inflammatory bowel diseases: Evidence based literature review. *World Journal of Gastroenterology* **22,** 6296–6317 (2016).

4. Abiko, K. *et al.* IFN-γ from lymphocytes induces PD-L1 expression and promotes progression of ovarian cancer. *British Journal of Cancer* **112,** 1501–1509 (2015).

5. Ahern, P. P. *et al.* Interleukin-23 drives intestinal inflammation through direct activity on T cells. *Immunity* **33,** 279–88 (2010).

6. Akeus, P. *et al.* Altered chemokine production and accumulation of regulatory T cells in intestinal adenomas of APC(Min/+) mice. *Cancer Immunology, Immunotherapy : CII* **63,** 807–819 (2014).

7. Akeus, P. *et al.* Regulatory T cells control endothelial chemokine production and migration of T cells into intestinal tumors of APCmin/+ mice. *Cancer Immunology, Immunotherapy : CII* **66,** 683–11 (2018).

8. Allez, M., Skolnick, B. E., Wisniewska-Jarosinska, M., Petryka, R. & Overgaard, R. V. Anti-NKG2D monoclonal antibody (NNC0142-0002) in active Crohn's disease: a randomised controlled trial. *Gut* **66,** 1824–1925 (2016).

9. Allez, M. *et al.* CD4+NKG2D+ T Cells in Crohn's Disease Mediate Inflammatory and Cytotoxic Responses Through MICA Interactions. *Gastroenterology* **132,** 2346–2358 (2007).

10. Amicarella, F. *et al.* Dual role of tumour-infiltrating T helper 17 cells in human colorectal cancer. *Gut* **66,** 692–704 (2015).

11. Anders, S. & Huber, W. Differential expression analysis for sequence count data. *Genome Biology* **11,** R106 (2010).

12. Andrade, L. F. d. *et al.* Antibody-mediated inhibition of MICA and MICB shedding promotes NK cell-driven tumor immunity. *Cancer Immunity,* 1–7 (2018).

13. Andrade, L. F. d. *et al.* Inhibition of MICA and MICB Shedding Elicits NK cell-mediated Immunity against Tumors Resistant to Cytotoxic T cells. *Cancer Immunology Research,* canimm.0483.2019 (2020).

14. Ardi, V. C., Kupriyanova, T. A., Deryugina, E. I. & Quigley, J. P. Human neutrophils uniquely release TIMP-free MMP-9 to provide a potent catalytic stimulator of angiogenesis. *Proceedings of the National Academy of Sciences* **104,** 20262–20267 (2007).

15. Arques, A. M. *The NKG2D system as modulator of host-microbial interactions in the gut* PhD thesis (2016).

16. Atreya, R. *et al.* Antibodies against tumor necrosis factor (TNF) induce T-cell apoptosis in patients with inflammatory bowel diseases via TNF receptor 2 and intestinal $CD14^+$ macrophages. *Gastroenterology* **141,** 2026–2038 (2011).

17. Ayers, M. *et al.* IFN-γ-related mRNA profile predicts clinical response to PD-1 blockade. *The Journal of Clinical Investigation* **127,** 2930–2940 (2017).

18. Babic, M. *et al.* NK cell receptor NKG2D enforces proinflammatory features and pathogenicity of Th1 and Th17 cells. *The Journal of Experimental Medicine* **217** (2020).

19. Bábíčková, J. *et al.* Sex Differences in Experimentally Induced Colitis in Mice: a Role for Estrogens. *Inflammation* **38,** 1996–2006 (2015).

20. Bai, X., Yi, M., Jiao, Y., Chu, Q. & Wu, K. Blocking TGF-β Signaling To Enhance The Efficacy Of Immune Checkpoint Inhibitor. *OncoTargets and Therapy* **Volume 12,** 9527–9538 (2019).

21. Bain, C. C. & Mowat, A. M. The monocyte-macrophage axis in the intestine. *Cellular Immunology* **291,** 41–48 (2014).

22. Bandeira, A. *et al.* Localization of gamma/delta T cells to the intestinal epithelium is independent of normal microbial colonization. *The Journal of Experimental Medicine* **172,** 239–244 (1990).

23. Bando, J. K. *et al.* ILC2s are the predominant source of intestinal ILC-derived IL-10. *The Journal of Experimental Medicine* **217** (2020).

24. Basher, F., Jeng, E. K., Wong, H. & Wu, J. Cooperative therapeutic anti-tumor effect of IL-15 agonist ALT-803 and co-targeting soluble NKG2D ligand sMIC. *Oncotarget* **7,** 814–30 (2016).

25. Basher, F. *et al.* Antibody targeting tumor-derived soluble NKG2D ligand sMIC reprograms NK cell homeostatic survival and function and enhances melanoma response to PDL1 blockade therapy. *Journal of Hematology & Oncology* **13,** 74 (2020).

26. Bates, G. J. *et al.* Quantification of Regulatory T Cells Enables the Identification of High-Risk Breast Cancer Patients and Those at Risk of Late Relapse. *Journal of Clinical Oncology* **24,** 5373–5380 (2006).

27. Bauché, D. *et al.* IL-23 and IL-2 activation of STAT5 is required for optimal IL-22 production in ILC3s during colitis. *Science Immunology* **5,** eaav1080 (2020).

28. Bauer, S. *et al.* Activation of NK cells and T cells by NKG2D, a receptor for stress-inducible MICA. *Science* **285,** 727–729 (1999).

29. Baumeister, S. H. *et al.* Phase 1 Trial of Autologous CAR T Cells Targeting NKG2D Ligands in Patients with AML/MDS and Multiple Myeloma. *Cancer Immunology Research,* 0307 2018 (2018).

30. Baumgart, D. C. & Sandborn, W. J. Crohn's disease. *Lancet (London, England)* **380,** 1590–1605 (2012).

31. Beatty, P. L., Plevy, S. E., Sepulveda, A. R. & Finn, O. J. Cutting Edge: Transgenic Expression of Human MUC1 in IL-10-/- Mice Accelerates Inflammatory Bowel Disease and Progression to Colon Cancer. *The Journal of Immunology* **179,** 735–739 (2007).

32. Belkaid, Y. & Hand, T. W. Role of the Microbiota in Immunity and Inflammation. *Cell* **157,** 121–141 (2014).

33. Bernardo, D. *et al.* Human intestinal pro-inflammatory CD11chighCCR2+CX3CR1+ macrophages, but not their tolerogenic CD11c-CCR2-CX3CR1- counterparts, are expanded in inflammatory bowel disease. *Mucosal Immunology* **11,** 3 (2018).

34. Bernier-Latmani, J. & Petrova, T. V. Intestinal lymphatic vasculature: structure, mechanisms and functions. *Nature Reviews Gastroenterology & Hepatology* **14,** 510–526 (2017).

35. Bernink, J. H. *et al.* Human type 1 innate lymphoid cells accumulate in inflamed mucosal tissues. *Nature Immunology* **14,** 221–229 (2013).

36. Bhagat, G. *et al.* Small intestinal CD8+TCRγδ+NKG2A+ intraepithelial lymphocytes have attributes of regulatory cells in patients with celiac disease. *Journal of Clinical Investigation* **118,** 281–293 (2008).

37. Bhinder, G. *et al.* The Citrobacter rodentium mouse model: studying pathogen and host contributions to infectious colitis. *Journal of Visualized Experiments : JoVE,* e50222 (2013).

38. Bialkowska, A. B., Ghaleb, A. M., Nandan, M. O. & Yang, V. W. Improved Swiss-rolling Technique for Intestinal Tissue Preparation for Immunohistochemical and Immunofluorescent Analyses. *Journal of Visualized Experiments,* e54161–e54161 (2016).

39. Bishu, S. *et al.* Citrobacter rodentium induces tissue-resident memory CD4+ T-cells. *Infection and Immunity,* 87(7):e00295–19 (2019).

40. Bodduluri, S. R. *et al.* Mast cell dependent CD8+ T cell recruitment mediates immune surveillance of intestinal tumors in ApcMin/+ mice. *Cancer Immunology Research* **6,** canimm.0424.2017–347 (2018).

41. Boleij, A., Gelder, M. M. H. J. v., Swinkels, D. W. & Tjalsma, H. Clinical Importance of Streptococcus gallolyticus infection among colorectal cancer patients: systematic review and meta-analysis. *Clinical Infectious Diseases* **53,** 870–8 (2011).

42. Bolyen, E. *et al.* Reproducible, interactive, scalable and extensible microbiome data science using QIIME 2. *Nature Biotechnology* **37,** 852–857 (2019).

43. Borchers, M. T. *et al.* The NKG2D-activating receptor mediates pulmonary clearance of Pseudomonas aeruginosa. *Infection and Immunity* **74,** 2578–2586 (2006).

44. Bouladoux, N., Harrison, O. J. & Belkaid, Y. *The Mouse Model of Infection with Citrobacter rodentium* (John Wiley & Sons, Inc., 2001).

45. Bradford, E. M. *et al.* Epithelial TNF Receptor Signaling Promotes Mucosal Repair in Inflammatory Bowel Disease. *The Journal of Immunology* **199,** 1886–1897 (2017).

46. Bray, F. *et al.* Global Cancer Statistics 2018: GLOBOCAN Estimates of Incidence and Mortality Worldwide for 36 Cancers in 185 Countries. *CA: A Cancer Journal for Clinicians* **68,** 394–424 (2018).

47. Brennan, K. *et al.* Human Natural Killer cell expression of ULBP2 is associated with a mature functional phenotype. *Human Immunology* **77,** 876–885 (2016).

48. Brenner, H., Kloor, M. & Pox, C. P. Colorectal cancer. *Lancet (London, England)* **383,** 1490–1502 (2014).

49. Brown, J. M. & Hazen, S. L. Microbial modulation of cardiovascular disease. *Nature Reviews Microbiology* **16,** 171–181 (2018).

50. Bruno, A. *et al.* Angiogenin and the MMP9-TIMP2 axis are up-regulated in proangiogenic, decidual NK-like cells from patients with colorectal cancer. *The FASEB Journal* **32,** fj201701103R–5377 (2018).

51. Bry, L. & Brenner, M. B. Critical role of T cell-dependent serum antibody, but not the gut-associated lymphoid tissue, for surviving acute mucosal infection with Citrobacter rodentium, an attaching and effacing pathogen. *The Journal of Immunology* **172,** 433–441 (2004).

52. Buonocore, S. *et al.* Innate lymphoid cells drive interleukin-23-dependent innate intestinal pathology. *Nature* **464,** 1371–1375 (2010).

53. Callahan, B. J. *et al.* DADA2: High-resolution sample inference from Illumina amplicon data. *Nature Methods* **13,** 581–583 (2016).

54. Carter, M. J., Lobo, A. J., Travis, S. P. L. & Gastroenterology IBD Section, B. S. o. Guidelines for the management of inflammatory bowel disease in adults. *Gut* **53,** v1 (2004).

55. Carvalho, F. A. *et al.* Transient Inability to Manage Proteobacteria Promotes Chronic Gut Inflammation in TLR5-Deficient Mice. *Cell Host & Microbe* **12,** 139–152 (2012).

56. Castriconi, R. *et al.* Transforming growth factor 1 inhibits expression of NKp30 and NKG2D receptors: Consequences for the NK-mediated killing of dendritic cells. *Proceedings of the National Academy of Sciences* **100,** 4120–4125 (2003).

57. Castro, F., Cardoso, A. P., Gonçalves, R. M., Serre, K. & Oliveira, M. J. Interferon-Gamma at the Crossroads of Tumor Immune Surveillance or Evasion. *Frontiers in Immunology* **9,** 847 (2018).

58. Castro-Dopico, T. *et al.* GM-CSF Calibrates Macrophage Defense and Wound Healing Programs during Intestinal Infection and Inflammation. *Cell Reports* **32,** 107857 (2020).

59. Cella, M. *et al.* A human natural killer cell subset provides an innate source of IL-22 for mucosal immunity. *Nature* **457,** 722–725 (2009).

60. Chae, W.-J. *et al.* Ablation of IL-17A abrogates progression of spontaneous intestinal tumorigenesis. *Proceedings of the National Academy of Sciences of the United States of America* **107,** 5540–5544 (2010).

61. Chalabi, M. *et al.* Neoadjuvant immunotherapy leads to pathological responses in MMR-proficient and MMR-deficient early-stage colon cancers. *Nature Medicine* **26,** 566–576 (2020).

62. Chen, G. *et al.* Polarizing the T helper 17 response in Citrobacter rodentium infection via expression of resistin-like molecule α. *Gut Microbes* **5,** 363–368 (2014).

63. Chen, J., Xu, H. & Zhu, X.-X. Abnormal expression levels of sMICA and NKG2D are correlated with poor prognosis in pancreatic cancer. *Therapeutics and Clinical Risk Management* **12,** 11–8 (2015).

64. Chen, M. L. & Sundrud, M. S. Cytokine Networks and T-Cell Subsets in Inflammatory Bowel Diseases. *Inflammatory Bowel Diseases* **22,** 1157–1167 (2016).

65. Cheroutre, H., Lambolez, F. & Mucida, D. The light and dark sides of intestinal intraepithelial lymphocytes. *Nature Reviews Immunology* **11,** 445–56 (2011).

66. Chirica, M. *et al.* Phenotypic analysis of T cells infiltrating colon cancers: Correlations with oncogenetic status. *Oncoimmunology* **4,** e1016698 (2015).

67. Chulada, P. C. *et al.* Genetic disruption of Ptgs-1, as well as Ptgs-2, reduces intestinal tumorigenesis in Min mice. *Cancer Research* **60,** 4705–4708 (2000).

68. Chung, L. *et al.* Bacteroides fragilis Toxin Coordinates a Pro- carcinogenic Inflammatory Cascade via Targeting of Colonic Epithelial Cells. *Cell Host and Microbe* **23,** 1–18 (2018).

69. Clemente, J. C., Ursell, L. K., Parfrey, L. W. & Knight, R. The impact of the gut microbiota on human health: an integrative view. *Cell* **148,** 1258–70 (2012).

70. Coca, S. *et al.* The prognostic significance of intratumoral natural killer cells in patients with colorectal carcinoma. *Cancer* **79,** 2320–2328 (1997).

71. Cohen, S. B. *et al.* CXCR3-dependent $CD4^+$ T cells are required to activate inflammatory monocytes for defense against intestinal infection. *PLoS Pathogens* **9,** e1003706 (2013).

72. Collins, J. W. *et al.* Citrobacter rodentium: infection, inflammation and the microbiota. *Nature Reviews Microbiology* **12,** 612–623 (2014).

73. Colombel, J.-F. *et al.* Adalimumab for Maintenance of Clinical Response and Remission in Patients With Crohn's Disease: The CHARM Trial. *Gastroenterology* **132,** 52–65 (2007).

74. Coudert, J. D., Scarpellino, L., Gros, F., Vivier, E. & Held, W. Sustained NKG2D engagement induces cross-tolerance of multiple distinct NK cell activation pathways. *Blood* **111,** 3571–8 (2008).

75. Coudert, J. D. *et al.* Altered NKG2D function in NK cells induced by chronic exposure to NKG2D ligand–expressing tumor cells. *Blood* **106,** 1711–1717 (2005).

76. Coutzac, C. *et al.* Systemic short chain fatty acids limit antitumor effect of CTLA-4 blockade in hosts with cancer. *Nature Communications* **11,** 2168 (2020).

77. Crosby, E. J., Clark, M., Novais, F. O., Wherry, E. J. & Scott, P. Lymphocytic Choriomeningitis Virus Expands a Population of NKG2D+CD8+ T Cells That Exacerbates Disease in Mice Coinfected with Leishmania major. *The Journal of Immunology* **195,** 3301–3310 (2015).

78. Dai, Z. *et al.* Multi-cohort analysis of colorectal cancer metagenome identified altered bacteria across populations and universal bacterial markers. *Microbiome* **6,** 70 (2018).

79. Dann, S. M. *et al.* Attenuation of intestinal inflammation in interleukin-10-deficient mice infected with Citrobacter rodentium. *Infection and Immunity* **82,** 1949–1958 (2014).

80. Dekker, E., Tanis, P. J., Vleugels, J. L. A., Kasi, P. M. & Wallace, M. B. Colorectal cancer. *Lancet (London, England)* **394,** 1467–1480 (2019).

81. Deng, X. *et al.* Antitumor activity of NKG2D CAR-T cells against human colorectal cancer cells in vitro and in vivo. *American Journal of Cancer Research* **9,** 945–958 (2019).

82. Denning, T. L. *et al.* Mouse TCRαβ + CD8αα Intraepithelial Lymphocytes Express Genes That Down-Regulate Their Antigen Reactivity and Suppress Immune Responses. *The Journal of Immunology* **178,** 4230–4239 (2007).

83. Diefenbach, A., Jamieson, A. M., Liu, S. D., Shastri, N. & Raulet, D. H. Ligands for the murine NKG2D receptor: expression by tumor cells and activation of NK cells and macrophages. *Nature Immunology* **1,** 119–126 (2000).

84. Diefenbach, A., Jensen, E. R., Jamieson, A. M. & Raulet, D. H. Rae1 and H60 ligands of the NKG2D receptor stimulate tumour immunity. *Nature* **413,** 165–171 (2001).

85. Dieleman *et al.* Chronic experimental colitis induced by dextran sulphate sodium (DSS) is characterized by Th1 and Th2 cytokines. *Clinical & Experimental Immunology* **114,** 385–391 (1998).

86. Dighe, A. S., Richards, E., Old, L. J. & Schreiber, R. D. Enhanced in vivo growth and resistance to rejection of tumor cells expressing dominant negative IFN gamma receptors. *Immunity* **1,** 447–56 (1994).

87. Dosset, M. *et al.* PD-1/PD-L1 pathway: an adaptive immune resistance mechanism to immunogenic chemotherapy in colorectal cancer. *OncoImmunology* **7,** e1433981 (2018).

88. Dullemen, H. M. v. *et al.* Treatment of Crohn's disease with anti-tumor necrosis factor chimeric monoclonal antibody (cA2). *Gastroenterology* **109,** 129–135 (1995).

89. Dunn, C. *et al.* Human Cytomegalovirus Glycoprotein UL16 Causes Intracellular Sequestration of NKG2D Ligands, Protecting Against Natural Killer Cell Cytotoxicity. *The Journal of Experimental Medicine* **197,** 1427–1439 (2003).

90. Dunne, M. R. *et al.* Enrichment of Inflammatory IL-17 and TNF-α Secreting CD4(+) T Cells within Colorectal Tumors despite the Presence of Elevated CD39(+) T Regulatory Cells and Increased Expression of the Immune Checkpoint Molecule, PD-1. *Frontiers in Oncology* **6,** 50 (2016).

91. Dutton, E. E. *et al.* Characterisation of innate lymphoid cell populations at different sites in mice with defective T cell immunity. *Wellcome Open Research* **2,** 117 (2018).

92. Easom, N. J. W. *et al.* ULBP1 Is Elevated in Human Hepatocellular Carcinoma and Predicts Outcome. *Frontiers in Oncology* **10,** 971 (2020).

93. Edin, S. *et al.* The distribution of macrophages with a M1 or M2 phenotype in relation to prognosis and the molecular characteristics of colorectal cancer. *PLoS ONE* **7,** e47045 (2012).

94. Eichele, D. D. & Kharbanda, K. K. Dextran sodium sulfate colitis murine model: An indispensable tool for advancing our understanding of inflammatory bowel diseases pathogenesis. *World Journal of Gastroenterology* **23,** 6016–6029 (2017).

95. Eisele, G. *et al.* TGF- and metalloproteinases differentially suppress NKG2D ligand surface expression on malignant glioma cells. *Brain* **129,** 2416–2425 (2006).

96. Erben, U. *et al.* A guide to histomorphological evaluation of intestinal inflammation in mouse models. *International Journal of Clinical and Experimental Pathology* **7,** 4557–4576 (2014).

97. Erdman, S. E. CD4+CD25+ Regulatory Lymphocytes Induce Regression of Intestinal Tumors in ApcMin/+ Mice. *Cancer Research* **65,** 3998–4004 (2005).

98. Esplugues, E. *et al.* Control of TH17 cells occurs in the small intestine. *Nature* **475,** 514–518 (2011).

99. Fagarasan, S., Kinoshita, K., Muramatsu, M., Ikuta, K. & Honjo, T. In situ class switching and differentiation to IgA-producing cells in the gut lamina propria. *Nature* **413,** 639–643 (2001).

100. Fagarasan, S. *et al.* Critical Roles of Activation-Induced Cytidine Deaminase in the Homeostasis of Gut Flora. *Science* **298,** 1424–1427 (2002).

101. Fais, S. *et al.* Interferon expression in Crohn's disease patients: increased interferon-gamma and -alpha mRNA in the intestinal lamina propria mononuclear cells. *Journal of Interferon Research* **14,** 235–238 (1994).

102. Falcone, A. *et al.* Phase III Trial of Infusional Fluorouracil, Leucovorin, Oxaliplatin, and Irinotecan (FOLFOXIRI) Compared With Infusional Fluorouracil, Leucovorin, and Irinotecan (FOLFIRI) As First-Line Treatment for Metastatic Colorectal Cancer: The Gruppo Oncologico Nord Ovest. *Journal of Clinical Oncology* **25,** 1670–1676 (2007).

103. Farhadi, N. *et al.* Natural killer cell NKG2D and granzyme B are critical for allergic pulmonary inflammation☆ *Journal of Allergy and Clinical Immunology* **133,** 827–835.e3 (2014).

104. Fearon, E. R. & Vogelstein, B. A genetic model for colorectal tumorigenesis. *Cell* **61,** 759–767 (1990).

105. Feng, P.-H. *et al.* NKG2D-Fc fusion protein promotes antitumor immunity through the depletion of immunosuppressive cells. *Cancer Immunology, Immunotherapy : CII,* 1–9 (2020).

106. Filipovic, I. *et al.* 29-Color Flow Cytometry: Unraveling Human Liver NK Cell Repertoire Diversity. *Frontiers in Immunology* **10,** 2692 (2019).

107. Fodde, R., Smits, R. & Clevers, H. APC, signal transduction and genetic instability in colorectal cancer. *Nature Reviews Cancer* **1,** 55–67 (2001).

108. Forbes, S. J., Eschmann, M. & Mantis, N. J. Inhibition of Salmonella enterica serovar typhimurium motility and entry into epithelial cells by a protective antilipopolysaccharide monoclonal immunoglobulin A antibody. *Infection and Immunity* **76,** 4137–44 (2008).

109. Forkel, M. & Mjösberg, J. Dysregulation of Group 3 Innate Lymphoid Cells in the Pathogenesis of Inflammatory Bowel Disease. *Current Allergy and Asthma Reports* **16,** 73 (2016).

110. Forssell, J. *et al.* High Macrophage Infiltration along the Tumor Front Correlates with Improved Survival in Colon Cancer. *Clinical Cancer Research* **13,** 1472–1479 (Mar. 2007).

111. Fort, M. M., Leach, M. W. & Rennick, D. M. A role for NK cells as regulators of CD4+ T cells in a transfer model of colitis. *The Journal of Immunology* **161,** 3256 3261 (1998).

112. Fox, J. G., Ge, Z., Whary, M. T., Erdman, S. E. & Horwitz, B. H. Helicobacter hepaticus infection in mice: models for understanding lower bowel inflammation and cancer. *Mucosal Immunology* **4,** 22–30 (2011).

113. Friese, M. A. *et al.* RNA Interference Targeting Transforming Growth Factor-β Enhances NKG2D-Mediated Antiglioma Immune Response, Inhibits Glioma Cell Migration and Invasiveness, and Abrogates TumorigenicityIn vivo. *Cancer Research* **64,** 7596–7603 (2004).

114. Fuchs, A. *et al.* Intraepithelial type 1 innate lymphoid cells are a unique subset of IL-12- and IL-15-responsive IFN-γ-producing cells. *Immunity* **38,** 769–781 (2013).

115. Fuss, I. J. *et al.* Nonclassical CD1d-restricted NK T cells that produce IL-13 characterize an atypical Th2 response in ulcerative colitis. *Journal of Clinical Investigation* **113,** 1490–1497 (2004).

116. Galdiero, M. R. *et al.* Occurrence and significance of tumor-associated neutrophils in patients with colorectal cancer. *International Journal of Cancer* **139,** 446–56 (2016).

117. Galon, J. *et al.* Type, density, and location of immune cells within human colorectal tumors predict clinical outcome. *Science* **313,** 1960–1964 (2006).

118. Gálvez, J. Role of Th17 Cells in the Pathogenesis of Human IBD. *ISRN inflammation* **2014,** 928461–14 (2014).

119. Gao, Y. *et al.* Tumor immunoevasion by the conversion of effector NK cells into type 1 innate lymphoid cells. *Nature Immunology* **18,** 1004–1015 (2017).

120. Garrett, W. S. *et al.* Communicable ulcerative colitis induced by T-bet deficiency in the innate immune system. *Cell* **131,** 33–45 (2007).

121. Geremia, A. *et al.* IL-23–responsive innate lymphoid cells are increased in inflammatory bowel disease. *The Journal of Experimental Medicine* **208,** 1127–1133 (2011).

122. Gershkovitz, M. *et al.* TRPM2 Mediates Neutrophil Killing of Disseminated Tumor Cells. *Cancer Research* **78,** 2680–2690 (2018).

123. Ghadially, H. *et al.* MHC class I chain-related protein A and B (MICA and MICB) are predominantly expressed intracellularly in tumour and normal tissue. *British Journal of Cancer* **3,** 95–1217 (2017).

124. Gharagozloo, M. *et al.* The decrease in NKG2D+ Natural Killer cells in peripheral blood of patients with metastatic colorectal cancer. *Bratislava Medical Journal* **116,** 296–301 (2015).

125. Giacomin, P. R. *et al.* Epithelial-intrinsic IKKα expression regulates group 3 innate lymphoid cell responses and antibacterial immunityEpithelial regulation of ILC3 responses. *The Journal of Experimental Medicine* **212,** 1513–1528 (2015).

126. Gibson, D. L. *et al.* MyD88 signalling plays a critical role in host defence by controlling pathogen burden and promoting epithelial cell homeostasis during Citrobacter rodentium-induced colitis. *Cellular Microbiology* **10,** 618–631 (2008).

127. Gilfillan, S., Ho, E. L., Cella, M., Yokoyama, W. M. & Colonna, M. NKG2D recruits two distinct adapters to trigger NK cell activation and costimulation. *Nature Immunology* **3,** 1150–1155 (2002).

128. Ginsburg, C. H., Dambrauskas, J. T., Ault, K. A. & Falchuk, Z. M. Impaired Natural Killer Cell Activity in Patients With Inflammatory Bowel Disease: Evidence for a Qualitative Defect. *Gastroenterology,* 1–6 (1983).

129. Glocker, E.-O. *et al.* Inflammatory bowel disease and mutations affecting the interleukin-10 receptor. *The New England Journal of Medicine* **361,** 2033–2045 (2009).

130. Goodyear, A. W., Kumar, A., Dow, S. & Ryan, E. P. Optimization of murine small intestine leukocyte isolation for global immune phenotype analysis. *Journal of Immunological Methods* **405,** 97–108 (2014).

131. Gopalakrishnan, V. *et al.* Gut microbiome modulates response to anti-PD-1 immunotherapy in melanoma patients. *Science* **15,** eaan4236 (2017).

132. Griffen, A. L. *et al.* Distinct and complex bacterial profiles in human periodontitis and health revealed by 16S pyrosequencing. *The ISME journal* **6,** 1176–85 (2011).

133. Griseri, T. *et al.* Granulocyte Macrophage Colony-Stimulating Factor-Activated Eosinophils Promote Interleukin-23 Driven Chronic Colitis. *Immunity* **43,** 187–199 (2015).

134. Groh, V. *et al.* Cell stress-regulated human major histocompatibility complex class I gene expressed in gastrointestinal epithelium. *Proceedings of the National Academy of Sciences* **93,** 12445–12450 (1996).

135. Groh, V., Smythe, K., Dai, Z. & Spies, T. Fas-ligand-mediated paracrine T cell regulation by the receptor NKG2D in tumor immunity. *Nature Immunology* **7,** 755–762 (2006).

136. Groh, V., Steinle, A., Bauer, S. & Spies, T. Recognition of Stress-Induced MHC Molecules by Intestinal Epithelial T Cells. *Science* **279,** 1737–1740 (1998).

137. Groh, V., Wu, J., Yee, C. & Spies, T. Tumour-derived soluble MIC ligands impair expression of NKG2D and T-cell activation. *Nature* **419,** 734–738 (2002).

138. Gronke, K. *et al.* Interleukin-22 protects intestinal stem cells against genotoxic stress. *Nature* **566,** 249–253 (2019).

139. Guerra, N. *et al.* A selective role of NKG2D in inflammatory and autoimmune diseases. *Clinical Immunology* **149,** 432–439 (2013).

140. Guerra, N. *et al.* NKG2D-deficient mice are defective in tumor surveillance in models of spontaneous malignancy. *Immunity* **28,** 571–580 (2008).

141. Guinney, J. *et al.* The consensus molecular subtypes of colorectal cancer. *Nature Medicine* **21,** 1350–1356 (2015).

142. Guo, M., Xu, E. & Ai, D. Inferring Bacterial Infiltration in Primary Colorectal Tumors From Host Whole Genome Sequencing Data. *Frontiers in Genetics* **10,** 213 (2019).

143. Guo, X. *et al.* Innate Lymphoid Cells Control Early Colonization Resistance against Intestinal Pathogens through ID2-Dependent Regulation of the Microbiota. *Immunity* **42,** 731–743 (2015).

144. Gur, C. *et al.* Binding of the Fap2 protein of Fusobacterium nucleatum to human inhibitory receptor TIGIT protects tumors from immune cell attack. *Immunity* **42,** 344–55 (2015).

145. Hadis, U. *et al.* Intestinal tolerance requires gut homing and expansion of FoxP3+ regulatory T cells in the lamina propria. *Immunity* **34,** 237–246 (2011).

146. Hale, V. L. *et al.* Shifts in the Fecal Microbiota Associated with Adenomatous Polyps. *Cancer Epidemiology Biomarkers & Prevention* **26,** 85–94 (2016).

147. Hall, L. J. *et al.* Natural killer cells protect mice from DSS-induced colitis by regulating neutrophil function via the NKG2A receptor. *Mucosal Immunology* **6,** 1016–1026 (2013).

148. Hall, L. J. *et al.* Natural killer cells protect against mucosal and systemic infection with the enteric pathogen Citrobacter rodentium. *Infection and Immunity* **81** (ed McCormick, B. A.) 460–469 (2013).

149. Hamerman, J. A., Ogasawara, K. & Lanier, L. L. Cutting edge: Toll-like receptor signaling in macrophages induces ligands for the NKG2D receptor. *The Journal of Immunology* **172,** 2001 2005 (2004).

150. Han, S. *et al.* Astilbin promotes the induction of regulatory NK1.1- CD4+ NKG2D+ T cells through the PI3K, STAT3, and MAPK signaling pathways. *International Immunopharmacology* **81,** 106143 (2020).

151. Hanada, T. *et al.* IFNgamma-dependent, spontaneous development of colorectal carcinomas in SOCS1-deficient mice. *The Journal of Experimental Medicine* **203,** 1391–1397 (2006).

152. Hanahan, D. & Weinberg, R. A. Hallmarks of Cancer: The Next Generation. *Cell* **144,** 646–674 (2011).

153. Hansen, C. H. F. *et al.* Gut microbiota regulates NKG2D ligand expression on intestinal epithelial cells. *European Journal of Immunology* **43,** 447–457 (2013).

154. Hart, A. L. *et al.* Characteristics of intestinal dendritic cells in inflammatory bowel diseases. *Gastroenterology* **129,** 50–65 (2005).

155. Hedin, C. R. *et al.* Altered intestinal microbiota and blood T cell phenotype are shared by patients with Crohn's disease and their unaffected siblings. *Gut* **63,** 1578–86 (2014).

156. Heller, F. *et al.* Interleukin-13 is the key effector Th2 cytokine in ulcerative colitis that affects epithelial tight junctions, apoptosis, and cell restitution. *Gastroenterology* **129,** 550–564 (2005).

157. Helmink, B. A., Khan, M. A. W., Hermann, A., Gopalakrishnan, V. & Wargo, J. A. The microbiome, cancer, and cancer therapy. *Nature Medicine* **25,** 377–388 (2019).

158. Hepworth, M. R. *et al.* Innate lymphoid cells regulate CD4+ T-cell responses to intestinal commensal bacteria. *Nature* **498,** 113–7 (May 2013).

159. Higgins, L. M., Frankel, G., Douce, G., Dougan, G. & MacDonald, T. T. Citrobacter rodentium infection in mice elicits a mucosal Th1 cytokine response and lesions similar to those in murine inflammatory bowel disease. *Infection and Immunity* **67,** 3031–3039 (1999).

160. Hix, L. M. *et al.* Tumor STAT1 transcription factor activity enhances breast tumor growth and immune suppression mediated by myeloid-derived suppressor cells. *The Journal of Biological Chemistry* **288,** 11676–88 (2013).

161. Hongo, T. *et al.* Functional Expression of Fas and Fas Ligand on Human Colonic Intraepithelial T Lymphocytes. *Journal of International Medical Research* **28,** 132–142 (2000).

162. Hooper, L. V. & Macpherson, A. J. Immune adaptations that maintain homeostasis with the intestinal microbiota. *Nature Reviews Immunology* **10,** 159–169 (2010).

163. Hopkins, E. G. D., Roumeliotis, T. I., Mullineaux-Sanders, C., Choudhary, J. S. & Frankel, G. Intestinal Epithelial Cells and the Microbiome Undergo Swift Reprogramming at the Inception of Colonic Citrobacter rodentium Infection. *mBio* **10,** 333 (2019).

164. Hosomi, S. *et al.* Intestinal epithelial cell endoplasmic reticulum stress promotes MULT1 up-regulation and NKG2D-mediated inflammation. *The Journal of Experimental Medicine* **214,** jem.20162041 (2017).

165. Huang, G. *et al.* Ginsenosides Rb3 and Rd reduce polyps formation while reinstate the dysbiotic gut microbiota and the intestinal microenvironment in Apc(Min/+) mice. *Scientific Reports* **7,** 12552 (2017).

166. Hugot, J. P. *et al.* Association of NOD2 leucine-rich repeat variants with susceptibility to Crohn's disease. *Nature* **411,** 599–603 (2001).

167. Hutchings, A. B. *et al.* Secretory Immunoglobulin A Antibodies against the σ1 Outer Capsid Protein of Reovirus Type 1 Lang Prevent Infection of Mouse Peyer's Patches. *Journal of Virology* **78,** 947–957 (2004).

168. Idos, G. E. *et al.* The Prognostic Implications of Tumor Infiltrating Lymphocytes in Colorectal Cancer: A Systematic Review and Meta-Analysis. *Scientific Reports* **10,** 3360 (2020).

169. Iida, N. *et al.* Commensal bacteria control cancer response to therapy by modulating the tumor microenvironment. *Science* **342,** 967–70 (2013).

170. Ishigame, H. *et al.* Differential roles of interleukin-17A and -17F in host defense against mucoepithelial bacterial infection and allergic responses. *Immunity* **30,** 108–119 (2009).

171. Ismail, A. S. *et al.* Gammadelta intraepithelial lymphocytes are essential mediators of host-microbial homeostasis at the intestinal mucosal surface. *Proceedings of the National Academy of Sciences of the United States of America* **108,** 8743–8 (2011).

172. Ito, R. *et al.* Interferon-gamma is causatively involved in experimental inflammatory bowel disease in mice. *Clinical and Experimental Immunology* **146,** 330–338 (2006).

173. Ito, R. *et al.* Involvement of IL-17A in the pathogenesis of DSS-induced colitis in mice. *Biochemical and Biophysical Research Communications* **377,** 12–16 (2008).

174. Ito, Y. *et al.* Blockade of NKG2D signaling prevents the development of murine CD4+ T cell-mediated colitis. *AJP: Gastrointestinal and Liver Physiology* **294,** G199–G207 (2007).

175. James, O. J., Vandereyken, M. & Swamy, M. Isolation, Characterization, and Culture of Intestinal Intraepithelial Lymphocytes. *Methods in Molecular Biology* **2121,** 141–152 (2020).

176. Jarry, A., Cerf-bensussan, N., Brousse, N., Selz, F. & Guy-grand, D. Subsets of CD3+ (T cell receptor α/β or γ/δ) and CD3- lymphocytes isolated from normal human gut epithelium display phenotypical features different from their counterparts in peripheral blood. *European Journal of Immunology* **20,** 1097–1103 (1990).

177. Jiang, Y., Li, Y. & Zhu, B. T-cell exhaustion in the tumor microenvironment. *Cell Death & Disease* **6,** e1792 (2015).

178. Jiao, Y., Huntington, N. D., Belz, G. T. & Seillet, C. Type 1 Innate Lymphoid Cell Biology: Lessons Learnt from Natural Killer Cells. *Frontiers in Immunology* **7,** 426 (2016).

179. Jin, C. *et al.* Commensal Microbiota Promote Lung Cancer Development via γδ T Cells. *Cell* **176,** 998–1013.e16 (2019).

180. Joeris, T., Müller-Luda, K., Agace, W. W. & Mowat, A. M. Diversity and functions of intestinal mononuclear phagocytes. *Mucosal Immunology* **10,** 845–864 (2017).

181. Jones, G.-R. *et al.* Dynamics of Colon Monocyte and Macrophage Activation During Colitis. *Frontiers in Immunology* **9,** 935 (2018).

182. Kamada, N. *et al.* Unique CD14 intestinal macrophages contribute to the pathogenesis of Crohn disease via IL-23/IFN-gamma axis. *The Journal of Clinical Investigation* **118,** 2269–80 (2008).

183. Kang, J.-C., Chen, J.-S., Lee, C.-H., Chang, J.-J. & Shieh, Y.-S. Intratumoral macrophage counts correlate with tumor progression in colorectal cancer. *Journal of Surgical Oncology* **102,** 242–248 (2010).

184. Kang, T. H. *et al.* Tumor-targeted delivery of IL-2 by NKG2D leads to accumulation of antigen-specific CD8+ T cells in the tumor loci and enhanced anti-tumor effects. *PLoS ONE* **7,** e35141 (2012).

185. Karachaliou, N. *et al.* Interferon-gamma (INFG), an important marker of response to immune checkpoint blockade (ICB) in non-small cell lung cancer (NSCLC) and melanoma patients. *Journal of Clinical Oncology* **35,** 11504–11504 (2017).

186. Kaur, K. *et al.* Antibiotic-mediated bacteriome depletion in ApcMin/+ mice is associated with reduction in mucus-producing goblet cells and increased colorectal cancer progression. *Cancer Medicine* **7,** 2003–2012 (2018).

187. Kazemi-Shirazi, L. *et al.* IgA autoreactivity: a feature common to inflammatory bowel and connective tissue diseases. *Clinical & Experimental Immunology* **128,** 102–109 (2002).

188. Kett, K. & Brandtzaeg, P. Local IgA subclass alterations in ulcerative colitis and Crohn's disease of the colon. *Gut* **28,** 1013–1021 (1987).

189. Kim, T. W. *et al.* Involvement of lymphocytes in dextran sulfate sodium-induced experimental colitis. *World Journal of Gastroenterology* **12,** 302–305 (2006).

190. Kjellev, S. *et al.* Inhibition of NKG2D receptor function by antibody therapy attenuates transfer-induced colitis in SCID mice. *European Journal of Immunology* **37,** 1397–1406 (2007).

191. Klein, R. S. *et al.* Association of Streptococcus bovis with Carcinoma of the Colon. *New England Journal of Medicine* **297,** 800–802 (1977).

192. Kloor, M. & Doeberitz, M. v. K. The Immune Biology of Microsatellite-Unstable Cancer. *Trends in Cancer* **2,** 121–133 (2016).

193. Klose, C. S. N. *et al.* Differentiation of type 1 ILCs from a common progenitor to all helper-like innate lymphoid cell lineages. *Cell* **157,** 340–356 (2014).

194. Koelzer, V. H. *et al.* Phenotyping of tumor-associated macrophages in colorectal cancer: Impact on single cell invasion (tumor budding) and clinicopathological outcome. *OncoImmunology* **5,** e1106677 (2015).

195. Konijnenburg, D. P. H. v. *et al.* Intestinal Epithelial and Intraepithelial T Cell Crosstalk Mediates a Dynamic Response to Infection. *Cell* **171,** 783–794.e13 (2017).

196. Koopman, M. *et al.* Deficient mismatch repair system in patients with sporadic advanced colorectal cancer. *British Journal of Cancer* **100,** 266–73 (2009).

197. Koroleva, E. P. *et al.* Citrobacter rodentium-induced colitis: A robust model to study mucosal immune responses in the gut. *Journal of Immunological Methods* **421,** 61–72 (2015).

198. Kostic, A. D. *et al.* Fusobacterium nucleatum Potentiates Intestinal Tumorigenesis and Modulates the Tumor-Immune Microenvironment. *Cell Host and Microbe* **14,** 207–215 (2013).

199. Kristensen, N. N. *et al.* CXC chemokine receptor 3 expression increases the disease-inducing potential of CD4+ CD25- T cells in adoptive transfer colitis. *Inflammatory Bowel Diseases* **12,** 374–381 (2006).

200. Kuang, D.-M. *et al.* Peritumoral neutrophils link inflammatory response to disease progression by fostering angiogenesis in hepatocellular carcinoma. *Journal of Hepatology* **54,** 948–55 (2010).

201. Kühn, R., Löhler, J., Rennick, D., Rajewsky, K. & Müller, W. Interleukin-10-deficient mice develop chronic enterocolitis. *Cell* **75,** 263 274 (1993).

202. Kurts, C. Th17 cells: a third subset of CD4+ T effector cells involved in organ-specific autoimmunity. *Nephrology, Dialysis, Transplantation* **23,** 816–819 (2008).

203. Kusmartsev, S., Nefedova, Y., Yoder, D. & Gabrilovich, D. I. Antigen-Specific Inhibition of CD8 + T Cell Response by Immature Myeloid Cells in Cancer Is Mediated by Reactive Oxygen Species. *The Journal of Immunology* **172,** 989–999 (2004).

204. Lal, N. *et al.* KRAS mutation and Consensus Molecular Subtypes 2 and 3 are independently associated with reduced immune infiltration and reactivity in colorectal cancer. *Clinical Cancer Research* **24,** clincanres.1090.2017 (2017).

205. Lanier, L. L. DAP10- and DAP12-associated receptors in innate immunity. *Immunological Reviews* **227,** 150–160 (2009).

206. Laqueur, G. L., McDaniel, E. G. & Matsumoto, H. Tumor induction in germfree rats with methylazoxymethanol (MAM) and synthetic MAM acetate. *Journal of the National Cancer Institute* **39,** 355–71 (1967).

207. Lau, T. *et al.* A novel tankyrase small-molecule inhibitor suppresses APC mutation-driven colorectal tumor growth. *Cancer Research* **73,** 3132–44 (2013).

208. Le, D. T. *et al.* Mismatch repair deficiency predicts response of solid tumors to PD-1 blockade. *Science* **357,** 409–413 (2017).

209. Le, D. T. *et al.* PD-1 Blockade in Tumors with Mismatch-Repair Deficiency. *The New England Journal of Medicine* **372,** 2509–2520 (2015).

210. Lee, J.-S. *et al.* Application of comparative functional genomics to identify best-fit mouse models to study human cancer. *Nature Genetics* **36,** 1306–1311 (2004).

211. Lee, W.-J. & Hase, K. Gut microbiota-generated metabolites in animal health and disease. *Nature Chemical Biology* **10,** 416–24 (2014).

212. Legroux, L. *et al.* NKG2D and Its Ligand MULT1 Contribute to Disease Progression in a Mouse Model of Multiple Sclerosis. *Frontiers in Immunology* **10,** 154 (2019).

213. Lenartić, M. *et al.* NKG2D Promotes B1a Cell Development and Protection against Bacterial Infection. *Journal of Immunology* **198,** 1531–1542 (2017).

214. Lenz, H.-J. *et al.* Impact of Consensus Molecular Subtype on Survival in Patients With Metastatic Colorectal Cancer: Results From CALGB/SWOG 80405 (Alliance). *Journal of Clinical Oncology* **37,** 1876–1885 (2019).

215. Levy, M., Kolodziejczyk, A. A., Thaiss, C. A. & Elinav, E. Dysbiosis and the immune system. *Nature Reviews Immunology* **17,** 1–14 (2017).

216. Li, Y. *et al.* TLR9 Regulates the NF-κB-NLRP3-IL-1β Pathway Negatively in Salmonella-Induced NKG2D-Mediated Intestinal Inflammation. *Journal of Immunology* **199,** 761–773 (2017).

217. Li, Z. *et al.* Experimental treatment of colorectal cancer in mice with human T cells electroporated with NKG2D RNA CAR. *Immunotherapy* **0** (2020).

218. Li, Z. *et al.* Small intestinal intraepithelial lymphocytes expressing CD8 and T cell receptor γδ are involved in bacterial clearance during Salmonella enterica serovar Typhimurium infection. *Infection and Immunity* **80,** 565–74 (2011).

219. Lin, Y.-D., Arora, J., Diehl, K., Bora, S. A. & Cantorna, M. T. Vitamin D Is Required for ILC3 Derived IL-22 and Protection From Citrobacter rodentium Infection. *Frontiers in Immunology* **10,** 1 (2019).

220. Lonez, C. *et al.* Celyad's novel CAR T-cell therapy for solid malignancies. *Current Research in Translational Medicine* (2018).

221. Longman, R. S. *et al.* CX_3CR1^+ mononuclear phagocytes support colitis-associated innate lymphoid cell production of IL-22. *The Journal of Experimental Medicine* **211,** 1571–1583 (2014).

222. Lu, S. *et al.* Nonblocking Monoclonal Antibody Targeting Soluble MIC Revamps Endogenous Innate and Adaptive Antitumor Responses and Eliminates Primary and Metastatic Tumors. *Clinical Cancer Research* **21,** 4819–30 (2015).

223. Lutter, L., Konijnenburg, D. P. H. v., Brand, E. C., Oldenburg, B. & Wijk, F. v. The elusive case of human intraepithelial T cells in gut homeostasis and inflammation. *Nature Reviews Gastroenterology & Hepatology* **15,** 637–649 (2018).

224. Ma, H., Tao, W. & Zhu, S. T lymphocytes in the intestinal mucosa: defense and tolerance. *Cellular & Molecular Immunology* **100,** 813 (2019).

225. Mager, L. F. *et al.* Microbiome-derived inosine modulates response to checkpoint inhibitor immunotherapy. *Science,* 1481–1489 (2020).

226. Manichanh, C. *et al.* Reduced diversity of faecal microbiota in Crohn's disease revealed by a metagenomic approach. *Gut* **55,** 205–211 (2006).

227. Mantis, N. J. & Forbes, S. J. Secretory IgA: arresting microbial pathogens at epithelial borders. *Immunological Investigations* **39,** 383–406 (2010).

228. Mantovani, A., Sozaani, S., Locati, M., Allavena, P. & Sica, A. Macrophage polarization: tumor-associated macrophages as a paradigm for polarized M2 mononuclear phagocytes. *Trends in Immunology* **23,** 549–555 (2002).

229. Marcenaro, E., Notarangelo, L. D., Orange, J. S. & Vivier, E. Editorial: NK Cell Subsets in Health and Disease: New Developments. *Frontiers in Immunology* **8,** 1363 (2017).

230. Mariathasan, S. *et al.* TGFβ attenuates tumour response to PD-L1 blockade by contributing to exclusion of T cells. *Nature* **554,** 544–548 (2018).

231. Marsh, L., Coletta, P. L., Hull, M. A., Selby, P. J. & Carding, S. R. Altered intestinal epithelium-associated lymphocyte repertoires and function in ApcMin/+ mice. *International Journal of Oncology* **40,** 243–250 (2012).

232. Martin, H. M. *et al.* Enhanced Escherichia coli adherence and invasion in Crohn's disease and colon cancer. *Gastroenterology* **127,** 80–93 (2004).

233. Maruvada, P., Leone, V., Kaplan, L. M. & Chang, E. B. The Human Microbiome and Obesity: Moving beyond Associations. *Cell Host & Microbe* **22,** 589–599 (2017).

234. Masopust, D., Jiang, J., Shen, H. & Lefrançois, L. Direct Analysis of the Dynamics of the Intestinal Mucosa CD8 T Cell Response to Systemic Virus Infection. *The Journal of Immunology* **166,** 2348–2356 (2001).

235. McGilvray, R. W. *et al.* NKG2D ligand expression in human colorectal cancer reveals associations with prognosis and evidence for immunoediting. *Clinical Cancer Research* **15,** 6993–7002 (2009).

236. McMurdie, P. J. & Holmes, S. phyloseq: An R Package for Reproducible Interactive Analysis and Graphics of Microbiome Census Data. *PLoS ONE* **8,** e61217 (2013).

237. Meckawy, G. R. *et al.* Natural killer NKG2A and NKG2D in patients with colorectal cancer. *Journal of Gastrointestinal Oncology* **10,** 218–225 (2019).

238. Melo-Gonzalez, F. *et al.* Antigen-presenting ILC3 regulate T cell–dependent IgA responses to colonic mucosal bacteria. *The Journal of Experimental Medicine* **216,** 728–742 (2019).

239. Menon, M. *et al.* A novel tankyrase inhibitor, MSC2504877, enhances the effects of clinical CDK4/6 inhibitors. *Scientific Reports* **9,** 201 (2019).

240. Meresse, B. *et al.* Coordinated induction by IL15 of a TCR-independent NKG2D signaling pathway converts CTL into lymphokine-activated killer cells in celiac disease. *Immunity* **21,** 357–366 (2004).

241. Mielke, L. A. *et al.* Retinoic acid expression associates with enhanced IL-22 production by γδ T cells and innate lymphoid cells and attenuation of intestinal inflammation. *The Journal of Experimental Medicine* **210,** 1117–1124 (2013).

242. Miller, B. C. *et al.* Subsets of exhausted CD8+ T cells differentially mediate tumor control and respond to checkpoint blockade. *Nature Immunology* **20,** 326–336 (2019).

243. Molfetta, R. *et al.* c-Cbl regulates MICA- but not ULBP2-induced NKG2D down-modulation in human NK cells: Molecular immunology. *European Journal of Immunology* **44,** 2761–2770 (2014).

244. Momburg, F. *et al.* Loss of HLA-A,B,C andde novo expression of HLA-D in colorectal cancer. *International Journal of Cancer* **37,** 179–184 (1986).

245. Morgan, X. C. *et al.* Dysfunction of the intestinal microbiome in inflammatory bowel disease and treatment. *Genome Biology* **13,** R79 (2012).

246. Morhardt, T. L. *et al.* IL-10 produced by macrophages regulates epithelial integrity in the small intestine. *Scientific Reports* **9,** 1223 (2019).

247. Morris, G. P. *et al.* Hapten-induced model of chronic inflammation and ulceration in the rat colon. *Gastroenterology* **96,** 795–803 (1989).

248. Mortha, A. *et al.* Microbiota-dependent crosstalk between macrophages and ILC3 promotes intestinal homeostasis. *Science* **343,** 1249288–1249288 (2014).

249. Moser, A. *et al.* ApcMin: A mouse model for intestinal and mammary tumorigenesis. *European Journal of Cancer* **31,** 1061–1064 (1995).

250. Mowat, A. M. & Agace, W. W. Regional specialization within the intestinal immune system. *Nature Reviews Immunology* **14,** 667–85 (2014).

251. Müller-Hermelink, N. *et al.* TNFR1 signaling and IFN-gamma signaling determine whether T cells induce tumor dormancy or promote multistage carcinogenesis. *Cancer Cell* **13,** 507–18 (2008).

252. Murad, J. M. *et al.* Manufacturing development and clinical production of NKG2D chimeric antigen receptor–expressing T cells for autologous adoptive cell therapy. *Cytotherapy* **20,** 952–963 (2018).

253. Murai, M. *et al.* Interleukin 10 acts on regulatory T cells to maintain expression of the transcription factor Foxp3 and suppressive function in mice with colitis. *Nature Immunology* **10,** 1178–84 (2009).

254. Muzny, D. M. *et al.* Comprehensive molecular characterization of human colon and rectal cancer. *Nature* **487,** 330–7 (2012).

255. Nagaraj, S. *et al.* Altered recognition of antigen is a mechanism of CD8+ T cell tolerance in cancer. *Nature Medicine* **13,** 828–835 (2007).

256. Nagashima, R., Maeda, K., Imai, Y. & Takahashi, T. Lamina propria macrophages in the human gastrointestinal mucosa: their distribution, immunohistological phenotype, and function. *Journal of Histochemistry & Cytochemistry* **44,** 721–731 (1996).

257. Nausch, N., Galani, I. E., Schlecker, E. & Cerwenka, A. Mononuclear myeloid-derived "suppressor" cells express RAE-1 and activate natural killer cells. *Blood* **112,** 4080–4089 (2008).

258. Ng, S. C. *et al.* Worldwide incidence and prevalence of inflammatory bowel disease in the 21st century: a systematic review of population-based studies. *Lancet (London, England)* **390,** 2769–2778 (2018).

259. Noguchi, T., Ritter, G. & Nishikawa, H. Antibody-based therapy in colorectal cancer. *Immunotherapy* **5,** 533–45 (2013).

260. Nolan, J. P. & Condello, D. Spectral flow cytometry. *Current Protocols in Cytometry* **Chapter 1,** Unit1.27 (2013).

261. Noman, M. Z. *et al.* PD-L1 is a novel direct target of HIF-1α, and its blockade under hypoxia enhanced MDSC-mediated T cell activation. *The Journal of Experimental Medicine* **211,** 781–90 (2014).

262. Noronha, A. M. *et al.* Hyperactivated B cells in human inflammatory bowel disease. *Journal of Leukocyte Biology* **86,** 1007–16 (2009).

263. O'Callaghan, C. A., Cerwenka, A., Willcox, B. E., Lanier, L. L. & Bjorkman, P. J. Molecular Competition for NKG2D. *Immunity* **15,** 201–211 (2001).

264. Obermeier *et al.* Interferon-gamma (IFN-γ)- and tumour necrosis factor (TNF)-induced nitric oxide as toxic effector molecule in chronic dextran sulphate sodium (DSS)-induced colitis in mice. *Clinical & Experimental Immunology* **116,** 238–245 (1999).

265. Ogasawara, K. *et al.* NKG2D blockade prevents autoimmune diabetes in NOD mice. *Immunity* **20,** 757–767 (2004).

266. Ogura, Y. *et al.* A frameshift mutation in NOD2 associated with susceptibility to Crohn's disease. *Nature* **411,** 603–606 (2001).

267. Okayasu, I. *et al.* A novel method in the induction of reliable experimental acute and chronic ulcerative colitis in mice. *Gastroenterology* **98,** 694–702 (1990).

268. Okayasu, I. *et al.* A novel method in the induction of reliable experimental acute and chronic ulcerative colitis in mice. *Gastroenterology* **98,** 694–702 (1990).

269. Omenetti, S. *et al.* The Intestine Harbors Functionally Distinct Homeostatic Tissue-Resident and Inflammatory Th17 Cells. *Immunity* **51,** 77–89.e6 (2019).

270. Ondov, B. D., Bergman, N. H. & Phillippy, A. M. Interactive metagenomic visualization in a Web browser. *BMC Bioinformatics* **12,** 385 (2011).

271. Oppenheim, D. E. *et al.* Sustained localized expression of ligand for the activating NKG2D receptor impairs natural cytotoxicity in vivo and reduces tumor immunosurveillance. *Nature Immunology* **6,** 928–937 (2005).

272. OuYang, L.-Y. *et al.* Tumor-induced myeloid-derived suppressor cells promote tumor progression through oxidative metabolism in human colorectal cancer. *Journal of Translational Medicine* **13,** 47 (2015).

273. Overman, M. J. *et al.* Durable Clinical Benefit With Nivolumab Plus Ipilimumab in DNA Mismatch Repair–Deficient/Microsatellite Instability–High Metastatic Colorectal Cancer. *Journal of Clinical Oncology* **36,** 773–779 (2018).

274. Pabst, O. New concepts in the generation and functions of IgA. *Nature Reviews Immunology* **12,** 821–32 (2012).

275. Paczulla, A. M. *et al.* Absence of NKG2D ligands defines leukaemia stem cells and mediates their immune evasion. *Nature* **381,** 484 (2019).

276. Palm, N. W. *et al.* Immunoglobulin A coating identifies colitogenic bacteria in inflammatory bowel disease. *Cell* **158,** 1000–10 (2014).

277. Papadakis, K. A. *et al.* Expression and Regulation of the Chemokine Receptor CXCR3 on Lymphocytes from Normal and Inflammatory Bowel Disease Mucosa. *Inflammatory Bowel Diseases* **10,** 778–788 (2004).

278. Papotto, P. H., Ribot, J. C. & Silva-Santos, B. IL-17+ γδ T cells as kick-starters of inflammation. *Nature Immunology* **18,** 604–611 (2017).

279. Pardoll, D. M. The blockade of immune checkpoints in cancer immunotherapy. *Nature Reviews Cancer* **12,** 252–64 (2012).

280. Pariente, B. *et al.* Activation of the receptor NKG2D leads to production of Th17 cytokines in CD4+ T cells of patients with Crohn's disease. *Gastroenterology* **141,** 217 –26-226.e1-2 (2011).

281. Park, J. *et al.* Cancer cells induce metastasis-supporting neutrophil extracellular DNA traps. *Science Translational Medicine* **8,** 361ra138 (2016).

282. Paschen, A. *et al.* Differential clinical significance of individual NKG2D ligands in melanoma: soluble ULBP2 as an indicator of poor prognosis superior to S100B. *Clinical Cancer Research* **15,** 5208–15 (2009).

283. Pearson, C. *et al.* ILC3 GM-CSF production and mobilisation orchestrate acute intestinal inflammation. *eLife* **5,** e10066 (2016).

284. Perše, M. & Cerar, A. Dextran Sodium Sulphate Colitis Mouse Model: Traps and Tricks. *Journal of Biomedicine and Biotechnology* **2012,** 718617 (2012).

285. Petersen, R. P. *et al.* Tumor infiltrating Foxp3+ regulatory T-cells are associated with recurrence in pathologic stage I NSCLC patients. *Cancer* **107,** 2866–2872 (2006).

286. Poore, G. D. *et al.* Microbiome analyses of blood and tissues suggest cancer diagnostic approach. *Nature* **579,** 567–574 (2020).

287. Probert, C. S. J., Saubermann, L. J., Balk, S. & Blumberg, R. S. Repertoire of the αβ T-cell receptor in the intestine. *Immunological Reviews* **215,** 215–225 (2007).

288. Pull, S. L., Doherty, J. M., Mills, J. C., Gordon, J. I. & Stappenbeck, T. S. Activated macrophages are an adaptive element of the colonic epithelial progenitor niche necessary for regenerative responses to injury. *Proceedings of the National Academy of Sciences* **102,** 99–104 (2004).

289. Purcell, R. V., Visnovska, M., Biggs, P. J., Schmeier, S. & Frizelle, F. A. Distinct gut microbiome patterns associate with consensus molecular subtypes of colorectal cancer. *Scientific Reports* **7,** 11590 (2017).

290. Pushalkar, S. *et al.* The Pancreatic Cancer Microbiome Promotes Oncogenesis by Induction of Innate and Adaptive Immune Suppression. *Cancer Discovery* **8,** 403–416 (2018).

291. Qi, X. *et al.* Brg1 restrains the pro-inflammatory properties of ILC3s and modulates intestinal immunity. *Mucosal Immunology,* 1–15 (2020).

292. Qian, X. *et al.* NK1.1- CD4+ NKG2D+ T cells suppress DSS-induced colitis in mice through production of TGF-β. *Journal of Cellular and Molecular Medicine* **21,** 1431–1444 (2017).

293. Qu, P., Yan, C. & Du, H. Matrix metalloproteinase 12 overexpression in myeloid lineage cells plays a key role in modulating myelopoiesis, immune suppression, and lung tumorigenesis. *Blood* **117,** 4476–89 (2011).

294. Qualls, J. E., Kaplan, A. M., Rooijen, N. v. & Cohen, D. A. Suppression of experimental colitis by intestinal mononuclear phagocytes. *Journal of Leukocyte Biology* **80,** 802–815 (2006).

295. Qualls, J. E., Tuna, H., Kaplan, A. M. & Cohen, D. A. Suppression of experimental colitis in mice by CD11c+ dendritic cells. *Inflammatory Bowel Diseases* **15,** 236–247 (2009).

296. Raab, S. *et al.* Fc-Optimized NKG2D–Fc Constructs Induce NK Cell Antibody-Dependent Cellular Cytotoxicity against Breast Cancer Cells Independently of HER2/neu Expression Status. *The Journal of Immunology* **193,** 4261–4272 (2014).

297. Raber, P., Ochoa, A. C. & Rodríguez, P. C. Metabolism of L-arginine by myeloid-derived suppressor cells in cancer: mechanisms of T cell suppression and therapeutic perspectives. *Immunological Investigations* **41,** 614–34 (2012).

298. Rakoff-Nahoum, S. & Medzhitov, R. Regulation of spontaneous intestinal tumorigenesis through the adaptor protein MyD88. *Science* **317,** 124–127 (2007).

299. Rao, H.-L. *et al.* Increased intratumoral neutrophil in colorectal carcinomas correlates closely with malignant phenotype and predicts patients' adverse prognosis. *PLoS ONE* **7,** e30806 (2012).

300. Raulet, D. H. Roles of the NKG2D immunoreceptor and its ligands. *Nature Reviews Immunology* **3,** 781–790 (2003).

301. Raulet, D. H., Gasser, S., Gowen, B. G., Deng, W. & Jung, H. Regulation of ligands for the NKG2D activating receptor. *Annual Review of Immunology* **31,** 413–441 (2013).

302. Rausch, A. *et al.* Interleukin-15 mediates protection against experimental tuberculosis: a role for NKG2D-dependent effector mechanisms of CD8+ T cells. *European Journal of Immunology* **36,** 1156–1167 (2006).

303. Reid-Yu, S. A., Small, C.-L. N. & Coombes, B. K. $CD3^{-}NK1.1^{+}$ cells aid in the early induction of a Th1 response to an attaching and effacing enteric pathogen. *European Journal of Immunology* **43,** 2638–2649 (2013).

304. Reinisch, W. *et al.* A dose escalating, placebo controlled, double blind, single dose and multidose, safety and tolerability study of fontolizumab, a humanised anti-interferon gamma antibody, in patients with moderate to severe Crohn's disease. *Gut* **55,** 1138–1144 (2006).

305. Robinette, M. L. *et al.* IL-15 sustains IL-7R-independent ILC2 and ILC3 development. *Nature Communications* **8,** 14601 (2017).

306. Rocca, Y. S. *et al.* Altered phenotype in peripheral blood and tumor-associated NK cells from colorectal cancer patients. *Innate Immunity* **19,** 76–85 (2012).

307. Rooks, M. G. & Garrett, W. S. Gut microbiota, metabolites and host immunity. *Nature Reviews Immunology* **16,** 341–52 (2016).

308. Rosen, D. B. *et al.* A Structural basis for the association of DAP12 with mouse, but not human, NKG2D. *The Journal of Immunology* **173,** 2470–2478 (2004).

309. Round, J. L. & Mazmanian, S. K. Inducible Foxp3+ regulatory T-cell development by a commensal bacterium of the intestinal microbiota. *Proceedings of the National Academy of Sciences of the United States of America* **107,** 12204–9 (2010).

310. Rubinstein, M. R. *et al.* Fusobacterium nucleatum promotes colorectal carcinogenesis by modulating E-cadherin/β-catenin signaling via its FadA adhesin. *Cell Host & Microbe* **14,** 195–206 (2013).

311. Sagebiel, A. F. *et al.* Tissue-resident Eomes+ NK cells are the major innate lymphoid cell population in human infant intestine. *Nature Communications* **10,** 975 (2019).

312. Sakaguchi, S. N aturally A rising CD4 + R egulatory T C ells for I mmunologic S elf -T olerance and N egative C ontrol of I mmune R esponses. *Annual Review of Immunology* **22,** 531–562 (2004).

313. Sakai, H. *et al.* Genetic ablation of Tnfα demonstrates no detectable suppressive effect on inflammation-related mouse colon tumorigenesis. *Chemico-Biological Interactions* **184,** 423–430 (2010).

314. Salih, H. R., Rammensee, H.-G. & Steinle, A. Cutting Edge: Down-Regulation of MICA on Human Tumors by Proteolytic Shedding. *The Journal of Immunology* **169,** 4098–4102 (2002).

315. Sandel, M. H. *et al.* Prognostic Value of Tumor-Infiltrating Dendritic Cells in Colorectal Cancer: Role of Maturation Status and Intratumoral Localization. *Clinical Cancer Research* **11,** 2576–2582 (2005).

316. Sanos, S. L. & Diefenbach, A. Isolation of NK cells and NK-like cells from the intestinal lamina propria. *Methods in Molecular Biology* **612,** 505–517 (2009).

317. Satoh-Takayama, N. *et al.* Microbial flora drives interleukin 22 production in intestinal NKp46+ cells that provide innate mucosal immune defense. *Immunity* **29,** 958–970 (2008).

318. Satoh-Takayama, N. *et al.* The natural cytotoxicity receptor NKp46 is dispensable for IL-22-mediated innate intestinal immune defense against Citrobacter rodentium. *Journal of Immunology* **183,** 6579–6587 (2009).

319. Sawa, S. *et al.* RORγt+ innate lymphoid cells regulate intestinal homeostasis by integrating negative signals from the symbiotic microbiota. *Nature Immunology* **12,** 320–326 (2011).

320. Scaleia, R. L. *et al.* NKG2D/Ligand dysregulation and functional alteration of innate immunity cell populations in pediatric IBD. *Inflammatory Bowel Diseases* **18,** 1910–22 (2012).

321. Schepers, A. & Clevers, H. Wnt signaling, stem cells, and cancer of the gastrointestinal tract. *Cold Spring Harbor Perspectives in Biology* **4,** a007989 (2012).

322. Schultsz, C., Berg, F. M. v. d., Kate, F. W. t., Tytgat, G. N. J. & Dankert, J. The intestinal mucus layer from patients with inflammatory bowel disease harbors high numbers of bacteria compared with controls. *Gastroenterology* **117,** 1089–1097 (1999).

323. Sconocchia, G. *et al.* NK cells and T cells cooperate during the clinical course of colorectal cancer. *OncoImmunology* **3,** e952197 (2014).

324. Sender, R., Fuchs, S. & Milo, R. Revised Estimates for the Number of Human and Bacteria Cells in the Body. *PLoS Biology* **14,** e1002533 (2016).

325. Sharon, G., Sampson, T. R., Geschwind, D. H. & Mazmanian, S. K. The Central Nervous System and the Gut Microbiome. *Cell* **167,** 915–932 (2016).

326. Shen, Y. *et al.* Possible association of decreased NKG2D expression levels and suppression of the activity of natural killer cells in patients with colorectal cancer. *International Journal of Oncology* **40,** 1285–90 (2011).

327. Sheppard, S., Ferry, A., Guedes, J. & Guerra, N. The Paradoxical Role of NKG2D in Cancer Immunity. *Frontiers in Immunology* **9,** 1808 (2018).

328. Sheppard, S. *et al.* Characterization of a novel NKG2D and NKp46 double-mutant mouse reveals subtle variations in the NK cell repertoire. *Blood* **121,** 5025–5033 (2013).

329. Sheppard, S. *et al.* The immunoreceptor NKG2D promotes tumour growth in a model of hepatocellular carcinoma. *Nature Communications* **8,** 13930 (2017).

330. Shibutani, M. *et al.* The Prognostic Significance of the Tumor-infiltrating Programmed Cell Death-1+ to CD8+ Lymphocyte Ratio in Patients with Colorectal Cancer. *Anticancer Research* **37,** 4165–4172 (2017).

331. Shiomi, H. *et al.* Gamma interferon produced by antigen-specific CD4+ T cells regulates the mucosal immune responses to Citrobacter rodentium infection. *Infection and Immunity* **78,** 2653–2666 (2010).

332. Shires, J., Theodoridis, E. & Hayday, A. C. Biological Insights into TCRγδ+ and TCRαβ+ Intraepithelial Lymphocytes Provided by Serial Analysis of Gene Expression (SAGE). *Immunity* **15,** 419–434 (2001).

333. Simmons, C. P. *et al.* Impaired Resistance and Enhanced Pathology During Infection with a Noninvasive, Attaching-Effacing Enteric Bacterial Pathogen, Citrobacter rodentium, in Mice Lacking IL-12 or IFN-γ. *The Journal of Immunology* **168,** 1804–1812 (2002).

334. Skinn, A. C. *et al.* Citrobacter rodentium infection causes iNOS-independent intestinal epithelial dysfunction in mice. *Canadian Journal of Physiology and Pharmacology* **84,** 1301–1312 (2006).

335. Smythies, L. E. *et al.* Human intestinal macrophages display profound inflammatory anergy despite avid phagocytic and bacteriocidal activity. *Journal of Clinical Investigation* **115,** 66–75 (2005).

336. Smythies, L. E. *et al.* Inflammation anergy in human intestinal macrophages is due to Smad-induced IkappaBalpha expression and NF-kappaB inactivation. *The Journal of Biological Chemistry* **285,** 19593–604 (2010).

337. Son, J. S. *et al.* Altered Interactions between the Gut Microbiome and Colonic Mucosa Precede Polyposis in APCMin/+ Mice. *PLoS ONE* **10,** e0127985 (2015).

338. Sonnenberg, G. F. *et al.* Innate Lymphoid Cells Promote Anatomical Containment of Lymphoid-Resident Commensal Bacteria. *Science* **336,** 1321–1325 (2012).

339. Spits, H., Bernink, J. H. & Lanier, L. NK cells and type 1 innate lymphoid cells: partners in host defense. *Nature Immunology* **17,** 758–764 (2016).

340. Steel, A. W., Mela, C. M., Lindsay, J. O., Gazzard, B. G. & Goodier, M. R. Increased proportion of CD16(+) NK cells in the colonic lamina propria of inflammatory bowel disease patients, but not after azathioprine treatment. *Alimentary Pharmacology & Therapeutics* **33,** 115–126 (2011).

341. Steinbacher, J. *et al.* An Fc-optimized NKG2D-immunoglobulin G fusion protein for induction of natural killer cell reactivity against leukemia: NKG2D-Ig for Treatment of Leukemia. *International Journal of Cancer* **136,** 1073–1084 (2014).

342. Stephens, M. & Weid, P.-Y. v. d. Lipopolysaccharides modulate intestinal epithelial permeability and inflammation in a species-specific manner. *Gut Microbes,* 1–12 (2019).

343. Stojanovic, A., Correia, M. P. & Cerwenka, A. The NKG2D/NKG2DL Axis in the Crosstalk Between Lymphoid and Myeloid Cells in Health and Disease. *Frontiers in Immunology* **9,** 730 (2018).

344. Strober, W. & Fuss, I. J. Proinflammatory Cytokines in the Pathogenesis of Inflammatory Bowel Diseases. *Gastroenterology* **140,** 1756–1767.e1 (2011).

345. Sugahara *et al.* Extrathymic derivation of gut lymphocytes in parabiotic mice. *Immunology* **96,** 57–65 (1999).

346. Sui, H. *et al.* YYFZBJS ameliorates colorectal cancer progression in ApcMin/+ mice by remodeling gut microbiota and inhibiting regulatory T-cell generation. *Cell Communication and Signaling* **18,** 113 (2020).

347. Swann, J. B. *et al.* Demonstration of inflammation-induced cancer and cancer immunoediting during primary tumorigenesis. *Proceedings of the National Academy of Sciences* **105,** 652–656 (2008).

348. Tabernero, J. The Role of VEGF and EGFR Inhibition: Implications for Combining Anti-VEGF and Anti-EGFR Agents. *Molecular Cancer Research* **5,** 203–220 (2007).

349. Takagi, T. *et al.* Elevated ER stress exacerbates dextran sulfate sodium-induced colitis in PRDX4-knockout mice. *Free Radical Biology and Medicine* **134,** 153–164 (2018).

350. Takashima, S. *et al.* T cell-derived interferon-γ programs stem cell death in immune-mediated intestinal damage. *Science Immunology* **4,** eaay8556 (2019).

351. Takayama, T. *et al.* Imbalance of NKp44(+)NKp46(-) and NKp44(-)NKp46(+) natural killer cells in the intestinal mucosa of patients with Crohn's disease. *Gastroenterology* **139,** 882 –92- 892.e1-3 (2010).

352. Takeda, K. *et al.* IFN-γ is required for cytotoxic T cell-dependent cancer genome immunoediting. *Nature Communications* **8,** 14607 (2017).

353. Tan, L. *et al.* Single-Cell Transcriptomics Identifies the Adaptation of Scart1+ Vγ6+ T Cells to Skin Residency as Activated Effector Cells. *Cell Reports* **27,** 3657–3671.e4 (2019).

354. Tan, L. *et al.* Chitosan nanoparticle-based delivery of fused NKG2D-IL-21 gene suppresses colon cancer growth in mice. *International Journal of Nanomedicine* **12,** 3095–3107 (2017).

355. Thibodeau, S., Bren, G. & Schaid, D. Microsatellite instability in cancer of the proximal colon. *Science* **260,** 816–819 (1993).

356. Tieng, V. *et al.* Binding of Escherichia coli adhesin AfaE to CD55 triggers cell-surface expression of the MHC class I-related molecule MICA. *Proceedings of the National Academy of Sciences* **99,** 2977–2982 (2002).

357. Tietje, A., Yang, X., Yu, X. & Wei, Y. MICA/IL-12: A novel bifunctional protein for killer cell activation. *Oncology Reports* **37,** 1889–1895 (2017).

358. Tjalsma, H., Boleij, A., Marchesi, J. R. & Dutilh, B. E. A bacterial driver–passenger model for colorectal cancer: beyond the usual suspects. *Nature Reviews Microbiology* **10,** 575–582 (2012).

359. Tomkovich, S. *et al.* Locoregional Effects of Microbiota in a Preclinical Model of Colon Carcinogenesis. *Cancer Research* **77,** 2620–2632 (2017).

360. Tosolini, M. *et al.* Clinical Impact of Different Classes of Infiltrating T Cytotoxic and Helper Cells (Th1, Th2, Treg, Th17) in Patients with Colorectal Cancer. *Cancer Research* **71,** 1263–71 (2011).

361. Triantafillidis, J. K., Nasioulas, G. & Kosmidis, P. A. Colorectal cancer and inflammatory bowel disease: epidemiology, risk factors, mechanisms of carcinogenesis and prevention strategies. *Anticancer Research* **29,** 2727–2737 (2009).

362. Turnbaugh, P. J. *et al.* The Human Microbiome Project. *Nature* **449,** 804–810 (2007).

363. Uhlig, H. H. & Powrie, F. Translating Immunology into Therapeutic Concepts for Inflammatory Bowel Disease. *Annual Review of Immunology* **36,** 755–781 (2018).

364. Urbaniak, C. *et al.* Microbiota of Human Breast Tissue. *Applied and Environmental Microbiology* **80,** 3007–3014 (2014).

365. Vadstrup, K. & Bendtsen, F. Anti-NKG2D mAb: A New Treatment for Crohn's Disease? *International Journal of Molecular Sciences* **18,** 1997 (2017).

366. Vadstrup, K. *et al.* NKG2D ligand expression in Crohn's disease and NKG2D-dependent stimulation of CD8+ T cell migration. *Experimental and Molecular Pathology* **103,** 56–70 (2017).

367. Vancamelbeke, M. & Vermeire, S. The intestinal barrier: a fundamental role in health and disease. *Expert Review of Gastroenterology & Hepatology* **11,** 821–834 (2017).

368. Vandereyken, M., James, O. J. & Swamy, M. Mechanisms of activation of innate-like intraepithelial T lymphocytes. *Mucosal Immunology,* 1–11 (2020).

369. Vermeiren, J. *et al.* Decreased colonization of fecal Clostridium coccoides/Eubacterium rectale species from ulcerative colitis patients in an in vitro dynamic gut model with mucin environment. *FEMS Microbiology Ecology* **79,** 685–696 (2011).

370. Vernocchi, P., Chierico, F. D. & Putignani, L. Gut Microbiota Profiling: Metabolomics Based Approach to Unravel Compounds Affecting Human Health. *Frontiers in Microbiology* **7,** 1144 (2016).

371. Vétizou, M. *et al.* Anticancer immunotherapy by CTLA-4 blockade relies on the gut microbiota. *Science* **350,** 1079–84 (2015).

372. Vincent, J. *et al.* 5-Fluorouracil Selectively Kills Tumor-Associated Myeloid-Derived Suppressor Cells Resulting in Enhanced T Cell-Dependent Antitumor Immunity. *Cancer Research* **70,** 3052–3061 (2010).

373. Vivier, E. *et al.* Innate Lymphoid Cells: 10 Years On. *Cell* **174,** 1054–1066 (2018).

374. Vonarbourg, C. *et al.* Regulated expression of nuclear receptor RORγt confers distinct functional fates to NK cell receptor-expressing RORγt(+) innate lymphocytes. *Immunity* **33,** 736–751 (2010).

375. Vries, N. L. d. *et al.* High-dimensional cytometric analysis of colorectal cancer reveals novel mediators of antitumour immunity. *Gut* **69,** 691–703 (2019).

376. Waaij, L. A. v. d., Limburg, P. C., Mesander, G. & Waaij, D. v. d. In vivo IgA coating of anaerobic bacteria in human faeces. *Gut* **38,** 348–354 (1996).

377. Walker, A. W., Duncan, S. H., Louis, P. & Flint, H. J. Phylogeny, culturing, and metagenomics of the human gut microbiota. *Trends in Microbiology* **22,** 267–74 (2014).

378. Walker, A. W. *et al.* High-throughput clone library analysis of the mucosa-associated microbiota reveals dysbiosis and differences between inflamed and non-inflamed regions of the intestine in inflammatory bowel disease. *BMC microbiology* **11,** 7 (2011).

379. Wang, F. *et al.* Regulatory role of NKG2D+ NK cells in intestinal lamina propria by secreting double-edged Th1 cytokines in ulcerative colitis. *Oncotarget* **5,** 1–8 (2017).

380. Wang, L., Wang, Y., Song, Z., Chu, J. & Qu, X. Deficiency of interferon-gamma or its receptor promotes colorectal cancer development. *Journal of Interferon & Cytokine Research* **35,** 273–280 (2015).

381. Wang, L. & Zhang, Q. Application of the Apc(Min/+) mouse model for studying inflammation-associated intestinal tumor. *Biomedicine & pharmacotherapy = Biomedecine & pharmacotherapie* **71,** 216–221 (2015).

382. Wang, Y. *et al.* Unique invariant natural killer T cells promote intestinal polyps by suppressing TH1 immunity and promoting regulatory T cells. *Mucosal Immunology* **11,** 131–143 (2018).

383. Watchmaker, P. B. *et al.* Comparative transcriptional and functional profiling defines conserved programs of intestinal DC differentiation in humans and mice. *Nature Immunology* **15,** 98–108 (2013).

384. Watson, N. F. S. *et al.* Expression of the stress-related MHC class I chain-related protein MICA is an indicator of good prognosis in colorectal cancer patients. *International Journal of Cancer* **118,** 1445–1452 (2006).

385. Weichselbaum, R. R. *et al.* An interferon-related gene signature for DNA damage resistance is a predictive marker for chemotherapy and radiation for breast cancer. *Proceedings of the National Academy of Sciences of the United States of America* **105,** 18490–5 (2008).

386. Wensveen, F. M., Jelenčić, V. & Polic, B. NKG2D: A Master Regulator of Immune Cell Responsiveness. *Frontiers in Immunology* **9,** 441 (2018).

387. Wesselkamper, S. C. *et al.* NKG2D Is Critical for NK Cell Activation in Host Defense against Pseudomonas aeruginosa Respiratory Infection. *The Journal of Immunology* **181,** 5481–5489 (2008).

388. Wijk, F. v. & Cheroutre, H. Mucosal T cells in gut homeostasis and inflammation. *Expert Review of Clinical Immunology* **6,** 559–66 (2010).

389. Wikberg, M. L. *et al.* Neutrophil infiltration is a favorable prognostic factor in early stages of colon cancer. *Human Pathology* **68,** 193–202 (2017).

390. Wiltrout, R. H. *et al.* Reactivity of anti-asialo GM1 serum with tumoricidal and non-tumoricidal mouse macrophages. *Journal of Leukocyte Biology* **37,** 597–614 (1985).

391. Wine, E. *et al.* Osteopontin mediates Citrobacter rodentium-induced colonic epithelial cell hyperplasia and attaching-effacing lesions. *The American Journal of Pathology* **177,** 1320–1332 (2010).

392. Wolk, K. *et al.* IL-22 Increases the Innate Immunity of Tissues. *Immunity* **21,** 241–254 (2004).

393. Wright, E. K. *et al.* Recent advances in characterizing the gastrointestinal microbiome in Crohn's disease: a systematic review. *Inflammatory Bowel Diseases* **21,** 1219–28 (2015).

394. Wu, P. *et al.* γδT17 cells promote the accumulation and expansion of myeloid-derived suppressor cells in human colorectal cancer. *Immunity* **40,** 785–800 (2014).

395. Wu, S., Morin, P. J., Maouyo, D. & Sears, C. L. Bacteroides fragilis enterotoxin induces c-Myc expression and cellular proliferation. *Gastroenterology* **124,** 392–400 (2003).

396. Wu, X., Zhang, Y., Li, Y. & Schmidt-Wolf, I. G. H. Increase of Antitumoral Effects of Cytokine-Induced Killer Cells by Antibody-Mediated Inhibition of MICA Shedding. *Cancers* **12,** 1818 (2020).

397. Xia, M. *et al.* Immune activation resulting from NKG2D/ligand interaction promotes atherosclerosis. *Circulation* **124,** 2933–2943 (2011).

398. Xiao, L. *et al.* Adoptive Transfer of NKG2D CAR mRNA-Engineered Natural Killer Cells in Colorectal Cancer Patients. *Molecular Therapy* (2019).

399. Xiao, Y.-T., Yan, W.-H., Cao, Y., Yan, J.-K. & Cai, W. Neutralization of IL-6 and TNF-α ameliorates intestinal permeability in DSS-induced colitis. *Cytokine* **83,** 189–192 (2016).

400. Xu, L. *et al.* NGS Evaluation of Colorectal Cancer Reveals Interferon Gamma Dependent Expression of Immune Checkpoint Genes and Identification of Novel IFNγ Induced Genes. *Frontiers in Immunology* **11,** 224 (2020).

401. Yamada, Y. & Mori, H. Multistep carcinogenesis of the colon in ApcMin/+ mouse. *Cancer Science* **98,** 6–10 (2007).

402. Yang, F. *et al.* Th1/Th2 Balance and Th17/Treg-Mediated Immunity in relation to Murine Resistance to Dextran Sulfate-Induced Colitis. *Journal of Immunology Research* **2017,** 7047201–11 (2017).

403. Yang, L., Pang, Y. & Moses, H. L. TGF-beta and immune cells: an important regulatory axis in the tumor microenvironment and progression. *Trends in Immunology* **31,** 220–7 (2010).

404. Yang, L. *et al.* DNA of neutrophil extracellular traps promotes cancer metastasis via CCDC25. *Nature,* 1–6 (2020).

405. Yang, X.-P. *et al.* Opposing regulation of the locus encoding IL-17 through direct, reciprocal actions of STAT3 and STAT5. *Nature Immunology* **12,** 247–54 (2011).

406. Yang, X. O. *et al.* Regulation of inflammatory responses by IL-17F. *The Journal of Experimental Medicine* **205,** 1063–1075 (2008).

407. Yen, D. *et al.* IL-23 is essential for T cell–mediated colitis and promotes inflammation via IL-17 and IL-6. *Journal of Clinical Investigation* **116,** 1310–1316 (2006).

408. Yoshida, S. *et al.* Involvement of an NKG2D Ligand H60c in Epidermal Dendritic T Cell-Mediated Wound Repair. *The Journal of Immunology* **188,** 3972–3979 (2012).

409. Zafirova, B. *et al.* Altered NK Cell Development and Enhanced NK Cell-Mediated Resistance to Mouse Cytomegalovirus in NKG2D-Deficient Mice. *Immunity* **31,** 270–282 (2009).

410. Zenewicz, L. A. *et al.* IL-22 deficiency alters colonic microbiota to be transmissible and colitogenic. *Journal of Immunology* **190,** 5306–12 (2013).

411. Zenewicz, L. A. *et al.* Innate and adaptive interleukin-22 protects mice from inflammatory bowel disease. *Immunity* **29,** 947–957 (2008).

412. Zhang, J. *et al.* Antibody targeting tumor-derived soluble NKG2D ligand sMIC provides dual co-stimulation of CD8 T cells and enables sMIC+ tumors respond to PD1/PD-L1 blockade therapy. *Journal for Immunotherapy of Cancer* **7,** 223 (2019).

413. Zhang, Q.-Q. *et al.* CD11b deficiency suppresses intestinal tumor growth by reducing myeloid cell recruitment. *Scientific Reports* **5,** 15948 (2015).

414. Zheng, Y. *et al.* Interleukin-22 mediates early host defense against attaching and effacing bacterial pathogens. *Nature Medicine* **14,** 282–289 (2008).

415. Zuo, T. & Ng, S. C. The Gut Microbiota in the Pathogenesis and Therapeutics of Inflammatory Bowel Disease. *Frontiers in Microbiology* **9,** 2247 (2018).

Appendix

NKG2D signaling sustains IL-17-producing T cells to promote cancer progression in mucosal tissues

Sophie Curio[1], Sarah C. Edwards[2,3], Toshiyasu Suzuki[2,3], Jenny McGovern[1], Chiara Triulzi[1], Nagisa Yoshida[1], Gustav Jonsson[1], Teresa Glauner[2,3], Damiano Rami[2,3], Rachel Violet Purcell[4], Seth B. Coffelt[2,3] and Nadia Guerra[1*]

[1] Department of Life Sciences, Imperial College London, London, UK

[2] Institute of Cancer Sciences, University of Glasgow, Glasgow, UK

[3] Cancer Research UK Beatson Institute, Glasgow, UK

[4] Department of Surgery, University of Otago, Christchurch, New Zealand

* Corresponding author: n.guerra@imperial.ac.uk

Abstract

NKG2D is an activating immune receptor associated with both beneficial and detrimental effects in disease pathology. NKG2D is directly involved in anti-tumor immunity, yet, it can also drive a pro-tumor response in inflammation-driven liver cancer. This opposing function is poorly understood and whether NKG2D promotes tumor growth in other cancer types is unknown. Here, we demonstrate that NKG2D signaling promotes cancer progression in models of primary intestinal cancer and metastatic breast cancer. Genetic deletion or antibody-mediated blocking of NKG2D adversely affects NKG2D-expressing pro-tumorigenic IL-17A-producing γδT cells, whereas homeostatic levels of IL-17A-producing γδT cells are unaffected by genetic loss of NKG2D. Our findings indicate that activation of IL-17A-producing γδT cells by NKG2D is specific to the disease setting, where NKG2D favors a pro-inflammatory environment that fosters tumor growth in mucosal tissues. These data underscore the importance of understanding the consequences of NKG2D-mediated immunity for therapeutic purposes.

Introduction

NKG2D is an activating immune receptor expressed on both innate and adaptive immune cells, including NK cells and Type 1 innate lymphoid cells (ILC1s), as well as a number of T cell subsets[1,2]. Human resting $CD8^+$ T cells express NKG2D constitutively, while mouse NKG2D expression is restricted to effector memory $CD8^+$ T cells[3]. In addition, a subset of $CD4^+$ T cells, γδT cells, and invariant (i)-NKT cells express NKG2D in humans and mice[1]. Ligands for NKG2D resemble major histocompatibility (MHC) class-I molecules and are typically absent from healthy tissue; these ligands are mainly expressed on rapidly proliferating, transformed, or stressed cells[4]. Upon binding to its ligands, NKG2D elicits a strong immune response, resulting in the secretion of cytokines and cytotoxic molecules from NK cells and T cells to induce target cell apoptosis. The presence of NKG2D ligands on tumor tissue identified NKG2D as an important player in anti-tumor immunity, which has been confirmed in various *in vitro* killing assays and mouse models of cancer[4–6]. Several clinical trials are exploring NKG2D as a potential therapeutic candidate, with the goal to harness the anti-tumor activity of NKG2D-expressing cells[7,8]. A major concern with targeting the NKG2D/NKG2D-ligand axis is the risk of toxicity against healthy tissues. Indeed, the contribution of NKG2D to local chronic inflammation and associated disorders has been evidenced in a number of clinical and translational studies of intestinal disorders[9,10], atherosclerosis[11], diabetes[12], asthma[13] and experimental autoimmune encephalitis[14,15].

Chronic inflammation is one of the hallmarks of cancer. We previously tested the hypothesis that NKG2D-expressing cells can ultimately lead to cancer progression through their ability to sustain tissue inflammation and cause tissue damage. This was evidenced in a model of chemically-induced hepatocellular carcinoma where NKG2D ligands are highly expressed in both tumor and non-tumor adjacent liver tissues[16,17]. Germline deletion of *Klrk1,* encoding NKG2D, reduced tissue damage and improved mice survival compared to wild-type littermates. Reduced tumor growth was associated with reduced T cell infiltration, as well as diminished accumulation of pro-inflammatory cytokines. These findings have uncovered a novel link between NKG2D-driven inflammation and tumorigenesis; however, the molecular and cellular interplay accounting for a pro-tumor versus anti-tumor effect remain elusive.

To gain further insight into the mechanisms underlying the noncanonical pro-tumor effect of the NKG2D pathway and further appreciate its extent, we studied NKG2D function in two major mucosal tissues, the intestine and the lung, where NKG2D-expressing cells are highly represented. We provide an in-depth characterization of the cells expressing NKG2D in the intestine and the lung and demonstrate that NKG2D-deficient mice develop normally and show no defects in the composition or functionality of the mucosal immune system. We demonstrate that the loss of NKG2D function via germline deletion or antibody blockade delays cancer progression and disease severity in a model of primary intestinal cancer and pre-metastatic mammary cancer. This delay in cancer progression is mainly associated with reduced accumulation of the pro-tumorigenic γδT cell subset in the mucosal tissues, reducing the amount of IL-17A present in the tumor microenvironment (TME). These data advance our understanding of the nature and the source of the pro-inflammatory milieu associated with NKG2D-dependent tumor growth.

Results

High proportions of NKG2D-expressing cells are detected in mucosal tissues of naïve mice

NKG2D ligands are constitutively expressed on human intestinal epithelium[18], and the NKG2D/NKG2D ligand axis is implicated in a number of human intestinal disorders[9,10] and mouse models of gut inflammation[19]. Yet, the distribution and function of NKG2D-expressing cells in the healthy mucosal tissue and whether constitutive ligand expression leads to immune activation is unknown. We explored the expression pattern of NKG2D under homeostatic conditions in the intestine of naïve (NKG2D-sufficient) mice by determining frequencies of NKG2D-expressing cells in the colonic and small intestinal (SI) lamina propria (LP) and mesenteric lymph nodes (MLN). NKG2D is expressed on NK cells and T cell subsets to various extents. The highest amount of NKG2D is found within the NK cell population in all tissues studied (Figure 1a,b). Among T cells, the frequency of NKG2D-expressing cells is highest on γδT cells, with greater expression on cells from MLNs and colon compared to the SI (Figure 1a,b). In contrast to NK cells, the proportions of NKG2D-expressing $CD4^+$ and $CD8^+$ T cells are scarce with less than 1% in the MLN and fewer than 5% in the colon and SI (Figure 1a,b). Overall, the frequencies of NKG2D-expressing cells are significantly higher in the colon compared to the MLN, suggesting a potential role for NKG2D in the intestinal mucosa.

We determined the expression pattern of NKG2D in the lung, a mucosal tissue that is, like the intestine, regularly exposed to foreign and microbial antigens. We found that while less than 1% of $CD4^+$ and $CD8^+$ T cells express NKG2D in naïve mice, up to 58% of lung NK cells do, which is comparable to the frequencies detected in the intestine (Figure 1c,d). Strikingly, a third of γδT cells express NKG2D, suggesting that among T cells in the lung, γδT cells play a major role in sensing stress signals through NKG2D. Using the CD27 marker to distinguish IFNγ-producing $CD27^+$ from IL-17A-producing $CD27^-$ γδT cells[20], we discovered that half of $CD27^-$ γδT cells express NKG2D whereas only ~12% of $CD27^+$ γδT cells were $NKG2D^+$ (Supplementary Figure 1a). NKG2D expression on $CD27^-$ γδT cells is dependent on the age of the mouse with almost all $CD27^-$ γδT cells isolated from the lung of neonates being $NKG2D^-$ and a significant increase over time to a maximum of 60% in adult mice (Figure 1e). By comparison, NK cells express significant levels of NKG2D from birth, pointing to a γδT cell-specific

role in host-environment interactions (Supplementary Figure 1b). Among NKG2D$^+$ CD27$^-$ γδT cells in the lung, the majority of γδT cells are Vγ1$^-$ and Vγ4$^-$, indicating they are Vγ6$^+$ cells - the most abundant γδT cell subset in the lung (Supplementary Figure 1c).

To assess whether the lack of NKG2D has an impact on the development of mucosal immune compartments, we quantified the frequencies of leukocytes from the intestine and the lung of NKG2D wild-type mice (*Klrk1*$^{+/+}$) and NKG2D-deficient mice (*Klrk1*$^{-/-}$). We found no major differences in the frequencies of B cells, myeloid cells or T cells in the colon (Figure 1f), SI (data not shown) or lung tissues (Figure 1f) isolated from each cohort. CD4$^+$ T cells are reduced in the colon, but not in the lung (data not shown) of *Klrk1*$^{-/-}$ mice compared to *Klrk1*$^{+/+}$ mice while frequencies of CD8$^+$ T cells, γδT cells, and NK cells are comparable (Supplementary Figure 1d,e). Likewise, frequencies of IL-17A-producing T cells in the colon are similar in *Klrk1*$^{-/-}$ compared to *Klrk1*$^{+/+}$ mice, suggesting that the lack of NKG2D is dispensable for the development of mucosal immunity (Supplementary Figure 1f).

NKG2D contributes to disease progression in a model of intestinal cancer

NKG2D ligands are expressed on various tumor types, including intestinal tumors[21]. With inflammation being a main risk factor for the development of intestinal tumors and colorectal cancer[22], we hypothesized that NKG2D exacerbates intestinal inflammation and subsequently tumorigenesis. This was tested in the *Apc*$^{min/+}$ mouse model that harbors a point mutation in the *Apc* gene resulting in the development of multiple intestinal neoplasia and colon carcinoma. Tumor development in this model is comparable to human familial adenomatous polyposis and due to its chronicity and inflammatory properties, it constitutes a good model to study chronic inflammatory disease leading to tumorigenesis[23]. Moreover, IL-17A and γδT cells – which express considerable levels of NKG2D in intestinal tissues (Figure 1a,b) – drive cancer progression in this model[24,25].

Apc$^{min/+}$ mice intercrossed with *Klrk1*$^{+/-}$ mice generated cohorts of NKG2D-sufficient (*Apc*$^{min/+}$*;Klrk1*$^{+/+}$) and NKG2D-deficient (*Apc*$^{min/+}$*;Klrk1*$^{-/-}$) mice that were assessed for survival and studied for the development of spontaneous intestinal tumors. Supporting our hypothesis, *Apc*$^{min/+}$*;Klrk1*$^{-/-}$ mice display significantly increased survival rates compared to *Apc*$^{min/+}$*;Klrk1*$^{+/+}$

littermates (Figure 2a), as well as a two-fold decrease in colon tumors (Figure 2b). Hematocrit (HCT) was measured as an additional read-out of disease severity, as *Apc*$^{min/+}$ mice are known to develop severe anemia. Blood collected at disease endpoint show higher HCT in *Apc*$^{min/+}$*;Klrk1*$^{+/+}$ mice compared to *Apc*$^{min/+}$*;Klrk1*$^{-/-}$ mice (Figure 2c), further supporting the observations that tumor progression is indeed advanced in *Apc*$^{min/+}$*;Klrk1*$^{+/+}$ mice compared to NKG2D-deficient littermates.

Anemia is a consequence of the high number of multiple intestinal polyps in the SI, which can exceed 100 tumors per mouse and leads to significant blood loss. We assessed the number of SI tumors at several time points including early stages (10-12 weeks), intermediate stages (18-20 weeks), and disease endpoint (exceeding 18 weeks and averaging at 22 weeks). *Apc*$^{min/+}$*;Klrk1*$^{+/+}$ mice show a 2.8-fold increase in tumor number at 10-12 weeks compared to *Apc*$^{min/+}$*;Klrk1*$^{-/-}$ mice and mild differences at later stages (Figure 2d). We observed an inverse correlation between the number of SI polyps at disease endpoint and mouse survival, in both *Apc*$^{min/+}$*;Klrk1*$^{+/+}$ mice and *Apc*$^{min/+}$*;Klrk1*$^{-/-}$ mice (Figure 2e). Interestingly, more *Apc*$^{min/+}$*;Klrk1*$^{+/+}$ mice develop large numbers of tumors before 25 weeks (dotted line), while most *Apc*$^{min/+}$*;Klrk1*$^{-/-}$ mice develop fewer tumors resulting in prolonged survival.

We examined the level of expression of NKG2D on tumor-infiltrating lymphocytes (TIL) in *Apc*$^{min/+}$ mice. NKG2D median fluorescent intensity (MFI) is increased in all subsets of NKG2D-expressing TILs compared to intraepithelial lymphocytes (IEL) and lamina propria lymphocytes (LPL) from healthy mice (Figure 2f and Supplementary Figure 2a,b). Notably, a five-fold increase in NKG2D MFI was observed on tumor-associated γδT cells and a two-fold increase on NK cells and CD8$^+$ T cells compared to the same cell populations from non-tumor gut tissue in naïve mice (Figure 2f).

Together, our findings demonstrate that the presence of NKG2D promotes tumor growth in this model, supporting the conclusion that NKG2D contributes to establishing a microenvironment that favors the development of intestinal tumors.

NKG2D promotes CD8$^+$ T cell enrichment and IFNγ production at advanced stages of the disease

To assess how and to what extent the presence of NKG2D influences immune cell infiltration into intestinal tumors, we compared the frequencies of tumor-infiltrating immune cell subsets in *Apc*$^{min/+}$*;Klrk1*$^{+/+}$ and *Apc*$^{min/+}$*;Klrk1*$^{-/-}$ mice. This was done at 18-20 weeks - the earliest time point

when tumors are numerous enough in the majority of mice to yield sufficient number of lymphocytes for *ex vivo* analysis - as well as at disease endpoint. B and T cells constitute the largest proportion of TILs at 18-20 weeks, while only few NK cells are present, and no differences in the incidence of the various immune cell subsets between the cohorts were observed at this time point (Figure 3a). Interestingly, the composition of immune cells evolved during tumor growth. When comparing TILs at 18-20 weeks (Figure 3a) versus disease endpoint (Figure 3b), we measured a proportional decrease in B cells and an increase in myeloid cells and in NK cells. At endpoint, the frequency of T cells is significantly higher in tumors from *Apc*$^{min/+}$*;Klrk1*$^{+/+}$ mice than from *Apc*$^{min/+}$*;Klrk1*$^{-/-}$ mice, suggesting that NKG2D signaling influences T cell infiltration and/or accumulation at late stages of the disease (Figure 3b). Further characterization of the T cell subsets revealed that CD8^{+} T cells are significantly increased in tumor-bearing NKG2D-sufficient mice (Figure 3c,d) indicating an NKG2D-dependent infiltration of the tumor.

Next, we assessed the functionality of TILs by means of IFNγ production – an inflammatory cytokine associated with both pro- and anti-tumorigenic properties[26–28] . Frequencies of IFNγ-producing T and NK cells are low at 18-20 weeks, but increased as the disease progressed (Figure 3e,f). The most striking increase in the frequency of IFNγ-producing cells was observed among CD8^{+} T cells, with a five-fold difference between 18-20 weeks and disease endpoint (Figure 3f).

We divided the ability of T cells to produce IFNγ into three categories: 'high' (>20% positive cells), 'medium' (10-20% positive cells) and 'low' (<10% positive cells) (Figure 3g,h). When comparing *Apc*$^{min/+}$*;Klrk1*$^{+/+}$ to *Apc*$^{min/}$*; Klrk1*$^{-/-}$, we observed a higher fraction of IFNγ-high producing CD8^{+} T cells from *Apc*$^{min/+}$*;Klrk1*$^{+/+}$ mice than *Apc*$^{min/+}$*;Klrk1*$^{-/-}$ (Figure 3g,h). Mice falling into the 'low' category were evenly distributed among genotypes (7 *Apc*$^{min/+}$*;Klrk1*$^{+/+}$ and 7 *Apc*$^{min/+}$*;Klrk1*$^{-/-}$), 4 *Apc*$^{min/+}$*;Klrk1*$^{+/+}$ mice were classified as 'medium' and 9 as 'high'. Conversely, 10 *Apc*$^{min/+}$*;Klrk1*$^{-/-}$, mice had a 'medium' frequency of IFNγ^{+} CD8^{+} T cells and only 1 'high' (Figure 3h). The higher proportion of IFNγ^{+} CD8^{+} T cells in NKG2D-sufficient versus -deficient mice implies an accumulation of IFNγ in the TME in an NKG2D-dependent manner. PD-1, a marker associated with T cell activation and exhaustion, is expressed by 40% of CD8^{+} T cells at disease endpoint, but not earlier stages (< 10%)

(Supplementary Figure 3a), indicating that strong activating signals drive the upregulation of inhibitory checkpoints as the disease progresses.

NKG2D signaling regulates tumor-associated IL-17A-producing γδT cells

It has been previously shown that γδT cells drive cancer progression in the *Apc*$^{min/+}$ model[25]. The presence of a significant fraction of NKG2D^{+} γδT cells at the mucosal barrier in naïve mice (Figure 1a,b) and high amount of NKG2D displayed on tumor-infiltrating γδT cells (Figure 2f) prompted further investigations of γδT cell phenotypes and functions in NKG2D-deficient mice. Firstly, we found that γδT cells are less abundant in the TME of *Apc*$^{min/+}$*;Klrk1*$^{-/-}$ compared to *Apc*$^{min/+}$*;Klrk1*$^{+/+}$ mice (Figure 4a,b). Recent in-depth analysis of cutaneous γδT cell subsets revealed that a proportion of skin tissue-resident cells express the Vγ6 T cell receptor chain and are capable of producing IL-17A. These cells were shown to express high levels of PD-1, which is a unique feature of this γδT cell subset[29]. We found that in the lung, PD-1 was constitutively expressed on NKG2D^{+} and NKG2D^{-} Vγ6 T cells (Supplementary Figure 4a) and was therefore used as a surrogate marker for Vγ6 cells. The frequency of PD-1^{+} γδT cells was measured at 18-20 weeks and endpoint and revealed that tumor-infiltrating PD-1^{+} γδT cells increase by eight-fold from early to end stage tumors in *Apc*$^{min/+}$*;Klrk1*$^{+/+}$ mice (Figure 4c,d). However, this increase is blunted in tumors from NKG2D-deficient mice at disease endpoint (Figure 4c,d), indicating that infiltration of PD-1^{+} γδT cells is partially regulated by NKG2D signaling. IL-17A, a pro-inflammatory cytokine known to drive intestinal tumorigenesis in the *Apc*$^{min/+}$ mouse model[24], is produced by certain subsets of γδT cells, including skin- and lung-resident PD-1^{+}Vγ6^{+} cells[29]. Therefore, we determined frequencies of IL-17A-producing cells infiltrating intestinal tumors and found that, similar to IFNγ-expressing CD8^{+} T cells (Figure 3f), IL-17A-producing γδT cells are more represented in the TME at disease endpoint than at 18-20 weeks of age (Figure 4e). The same observation was made for CD4^{+} and CD8^{+} T cells. Main producers of IL-17A are CD4^{+} T cells and γδT cells (Figure 4e) and are similarly represented in NKG2D-deficient and -sufficient mice (Figure 4f). Nonetheless, we presume that the cumulative amount of IL-17A being produced in the TME of NKG2D-deficient mice is reduced as a consequence of the reduced accumulation of γδT cells observed in the

absence of NKG2D (Figure 4b). This is further supported by the fact that the median fluorescence intensity (MFI) of IL-17A produced by NKG2D$^+$ γδT cells localized in the MLN of tumor bearing, but not healthy mice, is higher than the MFI measured in NKG2D$^-$ γδT cells (Figure 4g). Together, these data indicate that NKG2D signaling regulates both accumulation of PD-1$^+$ γδT cells into tumors and their ability to produce IL-17A.

To further address the importance of IL-17A-producing γδT cells in intestinal tumorigenesis, we used another model driven by the complete loss of the *Apc* gene: the *Villin-Cre^{ERT2};Apc$^{F/+}$* model. In this inducible mouse model, one copy of *Apc* is deleted specifically in enterocytes upon administration of tamoxifen and the other copy of *Apc* is stochastically lost over time. Mice develop adenomas in the SI and colon, and they succumb to disease burden after about 30 weeks. We analyzed IL-17A production by T cells at disease endpoint and observed higher proportion of IL-17A-producing γδT cells in the SI of the *Villin-Cre^{ERT2};Apc$^{F/+}$* mice than of tumor-free mice (Figure 4h). This observation is specific to γδT cells, as IL-17A expression levels by CD4$^+$ T cells remain unchanged and CD8$^+$ T cells expressed no IL-17A in tumor-bearing mice (Figure 4h). We crossed *Villin-Cre^{ERT2};Apc$^{F/+}$* mice with mice carrying a germline deletion of the *Tcrd* gene, resulting in the complete loss of γδT cells. Tumor-bearing mice lacking γδT cells survive longer than the *Tcrd$^{+/+}$* mice, confirming a pro-tumorigenic role for IL-17A-producing γδT cells in *Apc*-deficient intestinal tumors (Figure 4i). These data corroborate the pathogenic role of IL-17A-producing γδT cells in the *Apc$^{min/+}$* model[24,25].

Tumor progression is associated with sustained expression of NKG2D ligands and minor changes in the microbiota

NKG2D ligands have been detected on healthy tissues including human epithelium[18]. In accordance with these observations, we detected RAE-1, one of the mouse NKG2D ligands, in the healthy SI (Figure 5a white bar, b) and colon (data not shown) on the majority of epithelial cells in mice aged 10-12 weeks. RAE-1 expression on normal intestinal tissue is decreased in older mice (>20 weeks) from both the *Apc$^{min/+}$* and wild-type backgrounds (control *Klrk1$^{+/+}$* mice). This reduction is independent of NKG2D

expression and *Apc*$^{min/+}$*;Klrk1*$^{+/+}$ and *Apc*$^{min/+}$*;Klrk1*$^{-/-}$ mice express similar RAE-1 levels, ruling out immunoediting (Figure 5a,b).

NKG2D ligands can be regulated by the microbiota[30] and changes in microbial composition play a role in tumorigenesis[31]. Yet, the impact of the NKG2D/NKG2D ligand axis on the microbiome and on the integrity of the mucosal barrier is not known. Hence, we investigated changes in the microbiota during disease development by performing 16s rRNA gene microbial sequencing of fecal samples and tumor tissues. At 18 weeks, *Bacteroidetes* and *Firmicutes* are the most abundant phylum in healthy controls and *Apc*$^{min/+}$ mice, together making up more than 90% of the identified bacteria (Figure 5c left and middle). *Proteobacteria* are highly represented in tumors, but not fecal samples (Figure 5c right).

Analysis of alterations in the microbiota over time revealed no changes in Shannon diversity in fecal samples of 3, 10, or 18-week old *Apc*$^{min/+}$*;Klrk1*$^{+/+}$ mice compared to 18-week old *Klrk1*$^{+/+}$ controls (Figure 5d). The relative abundance of *Firmicutes* decreases over time (Figure 5e left), while the relative abundance of *Bacteroidetes* increasing (Figure 5e right). Krona plots reveal changes in the composition of *Firmicutes* over time: at 3 weeks, the ratio of *Clostridia* to *Bacilli* is 0.5, while *Clostridia* are more abundant than *Bacilli* at 18 weeks (ratio 0.75, Figure 5f). This demonstrates that the microbiota of healthy control mice is comparable to young *Apc*$^{min/+}$ mice and that changes in the microbial composition occur over time in parallel to disease progression.

Principal component analysis of fecal and tumor tissue from NKG2D-sufficient and NKG2D-deficient mice revealed no major differences between genotypes (Figure 5g and Supplementary Figure 5a) beyond a trend towards a higher *Bacteroidetes* to *Firmicutes* ratio in *Apc*$^{min/+}$*;Klrk1*$^{+/+}$ mice compared to *Apc*$^{min/+}$*;Klrk1*$^{-/-}$ littermates (Figure 5h). The composition of tumor-associated bacteria is similar in both genotype (Figure 5i). Our data show that the microbial composition evolves as the disease progresses. Thus, the presence of intestinal NKG2D^{+} effector cells does not regulate NKG2D ligand expression and does not significantly impact the microbial composition in this model.

NKG2D signaling stimulates pro-tumorigenic IL-17A-producing T cells

Having established a role for NKG2D on intestinal tumor-associated IL-17A-producing γδT cells, we asked whether the relationship between NKG2D and these cells is important in other cancer contexts. IL-17A-producing γδT cells in the lung play a critical role in supporting metastasis of p53-deficient mammary tumors[32,33]. We found that these cells express high levels of NKG2D (Figure 1c,d) and questioned whether NKG2D signaling could impact IL-17A expression by lung γδT cells in a mouse model of breast cancer. Using mammary tumor-bearing *K14-Cre;Brca1$^{F/F}$;Trp53$^{F/F}$* (KB1P) mice[34] with lung metastasis, we first profiled NKG2D expression in CD27^{-} and CD27^{+} γδT cells, CD4^{+} and CD8^{+} T cells, as well as NK cells extracted from the lungs. NKG2D expression remained constant between tumor-free, wild-type mice, and KB1P tumor-bearing mice across all lymphocyte populations (Supplementary Figure 6a). We employed an orthotopic transplant model using mammary tumors from KB1P mice[35]. Mice bearing KB1P tumor transplants were treated with IgG control antibodies or anti-NKG2D blocking antibodies and cytokine expression by γδT cells and other lymphocytes in the pre-metastatic lung was measured. Blocking NKG2D results in reduced IL-17A expression by γδT cells when compared with controls (Figure 6 a,b), indicating that NKG2D signaling positively regulates pro-metastatic IL-17A-producing γδT cells in the lung. The expression of IL-17A is further decreased in lung CD4^{+} T cells following treatment of KB1P tumor-bearing mice with anti-NKG2D antibodies (Figure 6a,b). These data accord well with a recent study reporting that NKG2D supports IL-17A and expression of other cytokines in T_H17 cells[15]. In this model, GzB production in NK cells is reduced following NKG2D blockade, indicating that antibody treatment also impacts NK cells (Supplementary Figure 6b). However, blocking NKG2D signaling does not affect the frequency of mature NK cells (Supplementary Figure 6c) or IFNγ production by NK cells, γδT cells, CD8^{+} and CD4^{+} T cells (Supplementary Figure 6d). These data indicate that NKG2D activates IL-17A-producing γδT cells and T_H17 cells in the lung, without affecting IFNγ-producing cells in this model. These findings demonstrate that the relationship between NKG2D and γδT cells is not restricted to the intestine.

To gain further insight into the regulation of γδT cells by the NKG2D receptor, we performed co-cultured experiments to stimulate T cells from the lungs of naïve mice with the NKG2D ligand-expressing lymphoma cell line, YAC-1. In this assay, the proportion of γδT cells (Figure 6c,d), but not

other T cells (Supplementary Figure 6e), increased after interaction with YAC-1 cells. This is specifically due to an increase in CD27^{-} γδT cells (Figure 6c,d). We examined T cells from the lungs of *Rorc-Cre;Klrk1*$^{F/F}$ mice, whose IL-17A-producing cells lack expression of NKG2D. In contrast to NKG2D-proficient cells (Figure 6d), the proportions of γδT cells and NKG2D-deficient CD27^{-} γδT cells failed to increase after co-culture with YAC-1 cells (Figure 6e). These data indicate that NKG2D engagement via RAE-1 supports the survival of NKG2D^{+}CD27^{-} γδT cells.

Discussion

We recently evidenced that NKG2D can promote cancer growth in a model of liver cancer[16,17]. The present study further supports these findings in a model of intestinal cancer and provides mechanistic insights into the immune components involved in regulating chronic tissue inflammation. First, we demonstrate that germline deletion of NKG2D in the *Apc*$^{min/+}$ model of intestinal and colon cancer results in a reduction in tumor burden and increased survival rates. This is associated with a reduced accumulation of pro-tumorigenic γδT cells and CD8$^+$ T cells producing high levels of IFNγ in intestinal tumors. The accumulation of IFNγ-high CD8$^+$ T cells in the TME is intriguing and could be the result of overtly activated clones specific for tumor antigens that no longer efficiently eliminate tumors yet contribute to feeding IFNγ to the inflammatory milieu.

Furthermore, we defined a specific pro-tumor role for the CD27$^-$ γδT subset expressing IL-17A as opposed to CD27$^+$ γδT cells producing IFNγ that typically exhibit anti-tumor activities. This supports observations made in a variety of cancers, such as hepatocellular carcinoma, colon, lung, and ovarian cancer[36–41]. In an orthotopic transplant model of breast cancer, we demonstrate that NKG2D blockade significantly reduces IL-17-secretion by γδT and CD4$^+$ T cells in the pre-metastatic lungs of tumor-bearing mice. A direct link between NKG2D and IL-17A was recently evidenced when Babic *et al*., who showed that NKG2D regulates T_H17 effector cell function and that lack of NKG2D on T cells ameliorates IL-17A-driven pathology[15]. In the context of tumor immunity, antibody blockade of NKG2D has previously been shown to partially reduced IL-17A production by γδT cells[42,43].

Our data from *in vitro* co-culture systems demonstrate that lung NKG2D$^+$CD27$^-$ γδT cells selectively expand over CD27$^+$ γδT cells and other T cells when cultured with RAE-1-expressing YAC-1 cells, suggesting that engagement of NKG2D promotes the survival of these cells to some extent. Collectively, these data evidence that NKG2D supports tumor development in contributing to chronic tissue inflammation.

Here, we demonstrate a direct role for NKG2D in shaping the microenvironment of mucosal tumors, favoring the accumulation of the pro-tumorigenic NKG2D$^+$IL17-A$^+$ γδT cell subset.

Our findings are important in the light of recent clinical studies using NKG2D-based approaches in immunotherapy[44–47]. While NKG2D has the potential to recognize tumor cells and initiate an anti-tumor response, we provide further evidence for a pro-tumorigenic role, specifically in slowly arising, inflammation-driven cancers. These findings underline the need to better understand the function of tumor-infiltrating NKG2D$^+$ cells and raise the question of whether reactivation of NKG2D-expressing cells through immune checkpoint blockade therapy will unleash a pro-inflammatory and tumor-promoting immune response or whether it would reactivate tumor antigen-experienced NKG2D$^+$ T cells to specifically kill NKG2D ligand-expressing tumors. Current studies using anti-NKG2D antibodies to treat Crohn's Disease patients, as well as ongoing trials on NKG2D CAR-T cells in colorectal cancer patients (Celyad, NCT03310008), will provide crucial information on the function of NKG2D in advanced disease. Together, we unravel a novel role of NKG2D in mucosal immunity and tumorigenesis and confirm a paradoxical role of NKG2D in cancer. These data highlight the need to better understand the function of NKG2D$^+$ cells and NKG2D ligand expression in the TME at various stages of the disease especially tissue-specific immune responses.

Methods

Mice

NKG2D-heterozygous ($Klrk1^{+/-}$)[5] mice were crossed with $Apc^{min/+}$ mice to generate $Klrk1^{+/+};Apc^{min/+}$, $Klrk1^{-/-};Apc^{min/+}$, $Klrk1^{+/+};Apc^{+/+}$ and $Klrk1^{-/-};Apc^{+/+}$ mice and to study the impact of NKG2D-deficiency in the intestine. Studies on the lung were performed on $Klrk1^{+/-}$ mice provided by Dr. Bojan Polic (University of Rijeka School of Medicine, Croatia). *Villin-*Cre^{ERT2}; $Apc^{F/+}$; $Tcrd^{-/-}$ mice were generated by crossing *Villin-*Cre^{ERT2}; $Apc^{F/+}$ with $Tcrd^{-/-}$. The alleles used were as follows: *Villin-*Cre^{ERT2} [48], Apc^{F} [49] and $Tcrd^{-}$ [50]. *Villin-*Cre^{ERT2} experiments were performed on a mixed background (N8 for C57BL/6J). Recombination by *Villin-*Cre^{ERT2} was induced with one intraperitoneal (i.p.) injection of 80 mg/kg tamoxifen when mice reached 20 g. The health status of $Apc^{min/+}$ and *Villin-*Cre^{ERT2}; $Apc^{F/+}$ mice was checked and evaluated frequently. Disease severity was assessed using a scoring scheme that included parameters such as appearance, natural behavior, provoked behavior, body condition, and tumor score. For hematocrit measurement, blood was collected from the tail vein of live mice into Eppendorf tubes containing 100 µl 0.5 M to prevent clotting. Blood parameters, including hematocrit. were measured using the XN-350 (Sysmex). Mice were humanely euthanized when they had reached the experimental endpoint.

$Klrk1^{F/F}$ mice were provided by Dr. Bojan Polic (University of Rijeka School of Medicine, Croatia) and crossed with *Rorc-Cre* mice (JAX) to generate *Rorc-Cre;*$Klrk1^{F/F}$ mice.

K14-Cre;$Brca1^{F/F}$*;*$Trp53^{F/F}$ (KB1P) mice were a gift from Dr. Jos Jonkers (Netherlands Cancer Institute). KB1P mice were maintained on FVB background and generation of this strain has previously been described, where a human K14 gene promoter drives *Cre* recombinase transgene expression, resulting in LoxP *Trp53* and *Brca1* specific deletion in the mammary epithelium (Liu, Holstege *et al*., 2007). This genetically engineered mouse model resembles human triple negative breast cancer and mice develop single mammary tumors at approximately

25-30 weeks of age. *Cre* recombinase negative (Cre^{-}) littermates were used as wild-type (WT) controls. Female FVB mice (8-10 weeks of age) were obtained from Charles River. Mice were palpated twice per week from 12 weeks of age for mammary tumors and perpendicular tumor diameters were measured with a caliper. Mice were sacrificed once a tumor reached >1 cm in any direction.

Mice were bred and maintained in the animal facility at Imperial College London or the Beatson Institute (University of Glasgow) in a specific pathogen-free environment. Work was carried out in compliance with the British Home Office Animals Scientific Procedures Act 1986 and the EU Directive 2010, and sanctioned by Local Ethical Review Process (PPL 70/8606 and 70/8645).

Blockade of NKG2D in vivo

WT mice were orthotopically transplanted in their mammary fat pat with 1x1 mm tumor pieces of syngeneic *K14-Cre;Brca1*$^{F/F}$*;Trp53*$^{F/F}$ (KB1P) mice. Once tumors reached 1cm, animals were injected intraperitoneally with a single dose of 200 μg anti-NKG2D (Clone HMG2D, Bio X Cell) on day 1 followed by individual injections of 100 μg on two consecutive days. Control mice followed the same dosage regime with Armenian hamster IgG isotype control (Clone Polyclonal, Bio X Cell). Tumor growth was measured by calipers and mice were euthanized one day after final antibody injection.

Tissue processing

Tumors isolated from KB1P mice were collected in PBS, cut into small pieces, and resuspended in Dulbecco's Modified Eagle Medium F12 (DMEM) containing 30% fetal calf serum (FCS) and 10% dimethyl sulfoxide and stored at -150 °C. Lungs, lymph nodes (LN) (axillary, brachial, mesenteric), and/or the spleen were isolated in ice-cold phosphate-buffered saline (PBS). Lungs

were mechanically dissociated by using a scalpel and transferred to collagenase solution consisting of DMEM supplemented with collagenase D (Roche, 1 mg/ml) and DNase1 (ThermoFisher, 25 µg/ml). Enzymatic dissociation was assisted by heat and mechanical tissue dissociation, using the gentleMACS Octo Dissociator (Miltenyi Biotec) (run name: 37C_m_LDK), according to the manufacturer's dissociation protocol. The lung cell suspension was filtered through a 70 µm cell strainer using a syringe plunger and enzyme activity was stopped by addition of 2 ml of FCS followed by 5 ml DMEM medium supplemented with 10% FCS, L-glutamine (2 mM, ThermoFisher) and penicillin (10000 U/ml) / streptomycin (10000 µg/ml, ThermoFisher). Spleen and LN were processed and filtered through a 70 µm cell strainer using a syringe plunger, and the tissue was flushed through with PBS containing 0.5% Bovine Serum Albumin (BSA). Cell suspension were centrifuged at 201 x g for 5 min, and supernatant was discarded. Cells were resuspended in PBS containing 0.5% BSA and cell number was determined using a hemocytometer.

The small intestine (SI) and tumor from control mice (age-matched *Villin-Cre^{ERT2}* negative; *Apc$^{F/+}$* mice) and *Villin-Cre^{ERT2}*; *Apc$^{F/+}$* mice were collected in PBS, cut into small pieces using a Mcilwain tissue chopper (Campden Instruments Ltd), and digested by heat and mechanical tissue dissociation using the gentleMACS Octo Dissociator (Miltenyi Biotec) (run name: 37C_m_TDK_1), according to the manufacturer's dissociation protocol. Cells were resuspended in PBS containing 0.5% BSA.

Small intestine and colon were harvested from healthy *Klrk1$^{+/+}$, Klrk1$^{-/-}$,* and *Apc$^{min/+}$*mice. Once the caecum was removed, the small intestine was separated into duodenum, jejunum, and ileum. Data presented in this study relate to tumors isolated from the ileum unless otherwise stated. Remaining fat, as well as the gut content, was removed from the intestine before it was

flushed with PBS. For tumor cell isolation, the tumor was carefully excised avoiding cutting through tumors. Mucus was removed, and tumor cells were counted before they were carefully removed from the intestinal tissue and minced using a scalpel. Tissue was transferred to a 1.5 ml tube and 1 ml of RPMI-1640 containing 5% FCS, 25 mM HEPES, 150 U/ml collagenase IV (Sigma Aldrich), and 50 U/ml DNase (Roche) were added. Tubes were shaken in a horizontal position on an incubator shaker (37° C, 200 rpm, 30 minutes). Dissociated tissue was transferred to a 50 ml tube through a 100 µm cell strainer. To further dissociate the tissue, it was pushed through the filter using the plunger of a 2 ml syringe. To inhibit enzyme activity, 1 ml of PBS containing 10% FCS and 5 mM EDTA was added to the 1.5 ml tube and then transferred to the 50 ml tube. Cells were centrifuged for 10 minutes at 500 x g and resuspended in RPMI-1640 containing 5% FCS.

To isolate lamina propria lymphocytes, the tissue was cut into small pieces and transferred to a 15 ml tube containing 10 ml of HBSS containing 1 mM DTT, 2% FCS, 100 U/ml penicillin and 100 µg/ml streptomycin. Tubes were vortexed for 30 s and the solution was replaced. Tubes were shaken in a horizontal position on an incubator shaker (37° C, 200 rpm, 20 minutes), which resulted in the removal of the mucus layer. Using a 100 µm cell strainer, the tissue was then transferred to a new 15 ml tube containing 10 ml of HBSS containing 1 mM EDTA, 2% FCS, 100 U/ml penicillin, and 100 µg/ml streptomycin. It was again shaken in a horizontal position (37° C, 200 rpm, 15 minutes), before it was filtered through a 100 µm strainer. The liquid was taken up and the tissue transferred back to the 15 ml tube and 10 ml of fresh solution was added. This step was repeated two or three times for large and small intestine, respectively, and resulted in the removal of all epithelial cells. The tissue was then transferred to a 6 well plate and minced into small pieces using a pair of scissors. Seven ml of RPMI-1640 containing 100 U/ml collagenase VIII (Sigma Aldrich) and 50 U/ml DNase (Roche), as well as 5% FCS,

100 U/ml penicillin and 100 µg/ml streptomycin was added to each well. Tissue was incubated on an orbital shaker at 100 rpm for 45 minutes at 37° C. To dissociate the cells further, the tissue was mixed every 15 minutes using tweezers. The digested tissue was then taken up into 10 ml stripettes and filtered through 100 µm cell filters into 50 ml tubes. This resulted in a single cell suspension, which was then centrifuged for 10 minutes at 500 x g and resuspended in RPMI-1640 containing 5% FCS.

Magnetic-activated cell sorting to isolate T cells

To isolate T cells from lung, LN and spleen, single cell suspensions were obtained as previously described. $CD3^+$ enrichment was achieved by MojoSort negative selection using MojoSort mouse $CD3^+$ T-cell Isolation Kit (BioLegend) according to manufacturer's instructions. In brief, $1x10^7$ cells were resuspended in 100 µL MojoSort buffer and cells were incubated with 10 µL of the biotin-antibody cocktail in a 5 ml polypropylene tube and incubated for 15 min on ice. Ten µL of streptavidin nanobeads were added and mixed and incubated on ice for further 15 min. Two and a half ml of MojoSort buffer was added and the tube placed in the magnet for 5 min to allow magnetically labelled cells to bind to the tube and magnetic separator. The untouched $CD3^+$ cells were collected by decanting the liquid into a new tube. Cells after enrichment were counted with a hemocytometer and plated at a density of $1x10^6$ cells/ml in round bottom 96-well plates.

Cell culture

YAC-1 lymphoma cells were maintained in RPMI-1640 medium supplemented with 10% FCS, 100 U/ml penicillin and streptomycin and 2 mM glutamine and kept in incubators at 37°C under normoxic conditions. Freshly isolated T cells were added at an effector : target (E:T) ratio of 10:1 to YAC-1 cells. Co-cultures were incubated in normoxia at 20% O_2, 5% CO_2, and 37°C

for 48 h in complete IMDM medium (supplemented with 10% FCS, L-glutamine (2 mM) and penicillin (10000 U/ml) and streptomycin (10000 µg/ml) and 50 µM β-mercaptoethanol).

Flow cytometry

Prior to antibody staining, cells were stimulated with PMA (final concentration 600 ng/ml), ionomycin (final concentration 100 ng/ml) and Brefeldin A (final concentration 10 µg/ml) in RPMI-1640 containing 5% FCS, 100 U/ml penicillin and 100 µg/ml streptomycin to enhance cytokine production. Unspecific binding by the Fc receptor was prevented by incubation of anti-mouse CD16+CD32 (BD) for 20 minutes. Dead cells were stained using the LIVE/DEAD Fixable Aqua Dead Cell Stain kit (ThermoFisher) or the Zombie NIR Fixable Viability Dye (BioLegend) before antibodies were added and incubated for 30 minutes. Before staining of intracellular cytokines and transcription factors, cells were permeabilized using the Transcription Factor Fixation/Permeabilization kit (eBioscience). Antibodies to detect intracellular antibens were added and incubated for 30 minutes before cells were washed and transferred to round-bottom polystyrene 5ml tubes through a filter mesh. Samples were acquired on a BD LSR Fortessa and analyzed using FlowJo software. All antibodies used in this study are listed in Supplementary Table 1.

Immunohistochemistry

Swiss rolls of intestines were prepared according to published protocols [51]. Tissues were fixed in 10% formalin in water overnight and then transferred to 70% ethanol in where where it was kept until paraffin embedding. Paraffin blocks were cut into 4 µm sections using a microtome (Leica), placed in a 40° C water bath, and affixed onto Superfrost Plus Microscope Slides (Thermo Scientific). Prior to staining, slides were deparaffinized and rehydrated. After heat-induced epitope retrieval (HIER), several blocking steps were performed to prevent non-

specific binding of antibodies. Primary antibody (Anti-mouse Rae1 pan-specific antibody, recognizing Rae-1α, β, δ, γ and ε (R&D Systems, Catalogue Number AF1136) or an appropriate isotype-matched control (polyclonal goat isotype IgG, NEB) was added at a final concentration of 10 µg/ml and incubated overnight. After several washing steps, the secondary antibody (10 µg/ml of biotinylatd rabbit anti-goat, Vectorlabs) was added and incubated for 30 minutes. The antigen was revealed using ABC (Vectorlabs) and DAB reagents (Abcam). Slides were counterstained by immersion in Harris Haematoxylin and dehydrated before coverslips were mounted using HistoMount mounting medium (ThermoFisher). Slides were scanned using an AxioScan.Z1 slide scanner (Zeiss). For image analysis, tumors and surrounding tissue were identified and marked using Fiji software (ImageJ). Percentage of positive cells was determined using a macro by comparing specific stained samples to isotype-matched Ig control samples.

Sample collection and extraction for 16s sequencing

Fecal samples were collected at 3, 10, and 18 weeks of age and stored at -80° C until extraction. Tumor samples were collected at 18 weeks and stored in RNAlater Stabilization Solution (ThermoFisher) at -80° C until extraction. For DNA extraction, samples were thawed and processed using the FastDNA™ SPIN Kit for Soil (MP Biomedicals), following the manufacturers recommendations. Concentration and purity were determined using a NanoDrop (Thermo Scientific). Samples with a low 260/230 ratio (< 1.8) were purified further. For this, 30 µl of NaCl was added, samples were vortexed and centrifuged at 4° C, 14000 x g for 5 minutes. Supernatant was transferred to a new tube and 100 µl of 96% ethanol in water was added. Samples were vortexed and kept at -20° C for 20 minutes. Samples were centrifuged as before, 100 µl of 70% ethanol in water was added and supernatant discarded after another centrifugation step. The tubes were left to dry upside down at room temperature for

approximately 10 minutes. To elute the DNA, 50 - 100 µl of Tris-EDTA (TE) buffer was added and heated up to 50° C for 20 minutes. Samples were stored in -80° C until further use.

16s sequencing and analysis

16s sequencing was performed by LC Sciences. After QC, the 16s rRNA gene V4 variable region was amplified using the 515F: 5'-GTGYCAGCMGCCGCGGTAA-3' and 806R: 5'-GGACTACHVGGGTWTCTAAT-3' primers. The Illumina Sequencing Library was prepared using adapters and barcodes for sample identification. Before sequencing, the PCR AxyPrep™ Mag PCR Normalizer kit was used for DNA quantitation and concentration normalization. Samples were then sequenced using the Illumina MiSeq following the manufacturer's guidelines.

Paired-end sequences were demultiplexed and primers were removed using Quantitative Insights into Microbial Ecology (QIIME) 2[52]. Using DADA2[53], Illumina-sequenced amplicon errors were corrected, forward reads were truncated at position 220 bp, and reverse reads at 200 bp and 10 bp were trimmed left and right. Taxonomy was assigned using SILVA132. Sequence variants were analyzed using the R package phyloseq. Differences between groups were visualized using Weighted UniFrac PCoA and statistical differences were determined using PERMANOVA. Pie charts were created using KronaTools[54].

Statistical analysis

Unless stated otherwise, statistical analysis was performed using Python, Pandas, or GraphPad Prism. Shapiro-Wilk tests were performed to test for normality and significance was determined using Mann-Whitey U or unpaired t tests unless stated otherwise. Data visualization was performed using GraphPad Prism (version 8.4.2).

Acknowledgements

We thank L. Lanier, S. Sheppard and G. Gorkiewicz for critical reading of the manuscript, B. Polić for providing reagents and insightful discussion, J. Srivastava and J. Rowley from the Imperial College Flow Facility, L. Lawrence from the Imperial College Research Histology Facility and the Blizard Core Pathology Facility for technical support. We thank the Core Services and Advanced Technologies at the Cancer Research UK Beatson Institute (C596/A17196), with particular thanks to the Biological Services and Flow Cytometry Facilities.

This work was supported by the Wellcome Trust RCDF (RCDF088381/Z/09/Z to N.G.), a Wellcome Trust PhD studentship (203948/Z/16A to S.C.), the Stevenson Fund to S.C., Breast Cancer Now (2018JulPR1101 to S.B.C.), Cancer Research UK Glasgow Centre (A25142 to S.B.C.), Wellcome Trust (208990/Z/17/Z to S.B.C.), Marie Curie European Fellowship (GDCOLCA 800112 to T.S.) and Naito Foundation Grant for Research Abroad to T.S.

Author contributions

S.C. designed and performed experiments, analyzed data and wrote the manuscript. S.C.E and T.S. designed and performed experiments, analyzed data and reviewed the manuscript. J.M., C.T. and N.Y. performed experiments and analyzed data. G.J., T.G. and D.R. contributed to some of the experiments. R.P. supervised the microbiota study. N.G. and S.B.C. designed and supervised the studies, analyzed the data and wrote the manuscript.

References

1. Lanier, L. L. NKG2D Receptor and Its Ligands in Host Defense. *Cancer Immunol Res* **3**, 575–582 (2015).

2. Spits, H., Bernink, J. H. & Lanier, L. NK cells and type 1 innate lymphoid cells: partners in host defense. *Nat Immunol* **17**, 758–764 (2016).

3. Bauer, S. *et al.* Activation of NK cells and T cells by NKG2D, a receptor for stress-inducible MICA. *Science* **285**, 727–729 (1999).

4. Diefenbach, A., Jensen, E. R., Jamieson, A. M. & Raulet, D. H. Rae1 and H60 ligands of the NKG2D receptor stimulate tumour immunity. *Nature* **413**, 165–171 (2001).

5. Guerra, N. *et al.* NKG2D-deficient mice are defective in tumor surveillance in models of spontaneous malignancy. *Immunity* **28**, 571–580 (2008).

6. Cerwenka, A., Baron, J. L. & Lanier, L. L. Ectopic expression of retinoic acid early inducible-1 gene (RAE-1) permits natural killer cell-mediated rejection of a MHC class I-bearing tumor in vivo. *Proc National Acad Sci* **98**, 11521–11526 (2001).

7. Baumeister, S. H. *et al.* Phase 1 Trial of Autologous CAR T Cells Targeting NKG2D Ligands in Patients with AML/MDS and Multiple Myeloma. *Cancer Immunol Res* canimm.0307.2018 (2018).

8. Xiao, L. *et al.* Adoptive Transfer of NKG2D CAR mRNA-Engineered Natural Killer Cells in Colorectal Cancer Patients. *Molecular Therapy* (2019).

9. Allez, M. *et al.* CD4+NKG2D+ T Cells in Crohn's Disease Mediate Inflammatory and Cytotoxic Responses Through MICA Interactions. *Gastroenterology* **132**, 2346–2358 (2007).

10. Meresse, B. *et al.* Coordinated induction by IL15 of a TCR-independent NKG2D signaling pathway converts CTL into lymphokine-activated killer cells in celiac disease. *Immunity* **21**, 357–366 (2004).

11. Xia, M. *et al.* Immune activation resulting from NKG2D/ligand interaction promotes atherosclerosis. *Circulation* **124**, 2933–2943 (2011).

12. Ogasawara, K. *et al.* NKG2D blockade prevents autoimmune diabetes in NOD mice. *Immunity* **20**, 757–767 (2004).

13. Farhadi, N. *et al.* Natural killer cell NKG2D and granzyme B are critical for allergic pulmonary inflammation. *J Allergy Clin Immun* **133**, 827-835.e3 (2014).

14. Guerra, N. *et al.* A selective role of NKG2D in inflammatory and autoimmune diseases. *Clin Immunol* **149**, 432–439 (2013).

15. Babic, M. *et al.* NK cell receptor NKG2D enforces proinflammatory features and pathogenicity of Th1 and Th17 cells. *J Exp Medicine* **217**, (2020).

16. Sheppard, S. *et al.* The immunoreceptor NKG2D promotes tumour growth in a model of hepatocellular carcinoma. *Nat Commun* **8**, 13930 (2017).

17. Sheppard, S., Ferry, A., Guedes, J. & Guerra, N. The Paradoxical Role of NKG2D in Cancer Immunity. *Front Immunol* **9**, 1808 (2018).

18. Groh, V. *et al.* Cell stress-regulated human major histocompatibility complex class I gene expressed in gastrointestinal epithelium. *Proc National Acad Sci* **93**, 12445–12450 (1996).

19. Ito, Y. *et al.* Blockade of NKG2D signaling prevents the development of murine CD4+ T cell-mediated colitis. *Am J Physiol Gastrointest Liver Physiol* **294**, G199–G207 (2007).

20. Ribot, J. C. *et al.* CD27 is a thymic determinant of the balance between interferon-γ- and interleukin 17–producing γδ T cell subsets. *Nat Immunol* **10**, 427–436 (2009).

21. McGilvray, R. W. *et al.* NKG2D ligand expression in human colorectal cancer reveals associations with prognosis and evidence for immunoediting. *Clin Cancer Res* **15**, 6993–7002 (2009).

22. Long, A. G., Lundsmith, E. T. & Hamilton, K. E. Inflammation and Colorectal Cancer. *Curr Colorectal Cancer Reports* **13**, 341–351 (2017).

23. Moser, A. R. *et al.* ApcMin: A mouse model for intestinal and mammary tumorigenesis. *Eur J Cancer* **31**, 1061–1064 (1995).

24. Chae, W.-J. *et al.* Ablation of IL-17A abrogates progression of spontaneous intestinal tumorigenesis. *Proc National Acad Sci* **107**, 5540–5544 (2010).

25. Marsh, L., Coletta, P. L., Hull, M. A., Selby, P. J. & Carding, S. R. Altered intestinal epithelium-associated lymphocyte repertoires and function in ApcMin/+ mice. *International Journal of Oncology* **40**, 243–250 (2012).

26. Wang, L., Wang, Y., Song, Z., Chu, J. & Qu, X. Deficiency of interferon-gamma or its receptor promotes colorectal cancer development. *J Interf Cytokine Res* **35**, 273–280 (2015).

27. Hanada, T. *et al.* IFNgamma-dependent, spontaneous development of colorectal carcinomas in SOCS1-deficient mice. *The Journal of experimental medicine* **203**, 1391–1397 (2006).

28. Zhang, C. *et al.* Lack of interferon-γ receptor results in a microenvironment favorable for intestinal tumorigenesis. *Oncotarget* **7**, 42099–42109 (2016).

29. Tan, L. *et al.* Single-Cell Transcriptomics Identifies the Adaptation of Scart1+ Vγ6+ T Cells to Skin Residency as Activated Effector Cells. *Cell Reports* **27**, 3657-3671.e4 (2019).

30. Hansen, C. H. F. *et al.* Gut microbiota regulates NKG2D ligand expression on intestinal epithelial cells. *Eur J Immunol* **43**, 447–457 (2013).

31. Hale, V. L. *et al.* Shifts in the Fecal Microbiota Associated with Adenomatous Polyps. *Cancer Epidem Biomar* **26**, 85–94 (2016).

32. Coffelt, S. B. *et al.* IL-17-producing γδ T cells and neutrophils conspire to promote breast cancer metastasis. *Nature* **522**, 345–348 (2015).

33. Wellenstein, M. D. *et al.* Loss of p53 triggers WNT-dependent systemic inflammation to drive breast cancer metastasis. *Nature* **572**, 538–542 (2019).

34. Liu, X. *et al.* Somatic loss of BRCA1 and p53 in mice induces mammary tumors with features of human BRCA1-mutated basal-like breast cancer. *Proc National Acad Sci* **104**, 12111–12116 (2007).

35. Doornebal, C. W. *et al.* A Preclinical Mouse Model of Invasive Lobular Breast Cancer Metastasis. *Cancer Res* **73**, 353–363 (2013).

36. Haas, J. D. *et al.* CCR6 and NK1.1 distinguish between IL-17A and IFN-γ-producing γδ effector T cells. *Eur J Immunol* **39**, 3488–3497 (2009).

37. Gao, Y. *et al.* γδ T Cells Provide an Early Source of Interferon γ in Tumor Immunity. *J Exp Medicine* **198**, 433–442 (2003).

38. Wu, P. *et al.* γδT17 cells promote the accumulation and expansion of myeloid-derived suppressor cells in human colorectal cancer. *Immunity* **40**, 785–800 (2014).

39. Rei, M. *et al.* Murine CD27(−) Vγ6(+) γδ T cells producing IL-17A promote ovarian cancer growth via mobilization of protumor small peritoneal macrophages. *Proc National Acad Sci* **111**, E3562–E3570 (2014).

40. Ma, S. *et al.* IL-17A Produced by γδ T Cells Promotes Tumor Growth in Hepatocellular Carcinoma. *Cancer Res* **74**, 1969–1982 (2014).

41. Jin, C. *et al.* Commensal Microbiota Promote Lung Cancer Development via γδ T Cells. *Cell* **176**, 998-1013.e16 (2019).

42. Wakita, D. *et al.* Tumor-infiltrating IL-17-producing γδ T cells support the progression of tumor by promoting angiogenesis. *Eur J Immunol* **40**, 1927–1937 (2010).

43. Tang, Q. *et al.* Hmgb1-IL-23-IL-17-IL-6-Stat3 Axis Promotes Tumor Growth in Murine Models of Melanoma. *Mediat Inflamm* **2013**, 1–13 (2013).

44. Lonez, C. *et al.* Celyad's novel CAR T-cell therapy for solid malignancies. *Curr Res Transl Medicine* (2018).

45. Murad, J. M. *et al.* Manufacturing development and clinical production of NKG2D chimeric antigen receptor–expressing T cells for autologous adoptive cell therapy. *Cytotherapy* **20**, 952–963 (2018).

46. Lu, S. *et al.* Nonblocking Monoclonal Antibody Targeting Soluble MIC Revamps Endogenous Innate and Adaptive Antitumor Responses and Eliminates Primary and Metastatic Tumors. *Clin Cancer Res Official J Am Assoc Cancer Res* **21**, 4819–30 (2015).

47. Andrade, L. F. de *et al.* Antibody-mediated inhibition of MICA and MICB shedding promotes NK cell-driven tumor immunity. *Cancer immunity* 1–7 (2018).

48. Marjou, F. E. *et al.* Tissue-specific and inducible Cre-mediated recombination in the gut epithelium. *Genesis* **39**, 186–193 (2004).

49. Shibata, H. *et al.* Rapid Colorectal Adenoma Formation Initiated by Conditional Targeting of the *Apc* Gene. *Science* **278**, 120–123 (1997).

50. Itohara, S. *et al.* T cell receptor δ gene mutant mice: Independent generation of αβ T cells and programmed rearrangements of γδ TCR genes. *Cell* **72**, 337–348 (1993).

51. Bialkowska, A. B., Ghaleb, A. M., Nandan, M. O. & Yang, V. W. Improved Swiss-rolling Technique for Intestinal Tissue Preparation for Immunohistochemical and Immunofluorescent Analyses. *J Vis Exp* e54161–e54161 (2016).

52. Bolyen, E. *et al.* Reproducible, interactive, scalable and extensible microbiome data science using QIIME 2. *Nat Biotechnol* **37**, 852–857 (2019).

53. Callahan, B. J. *et al.* DADA2: High-resolution sample inference from Illumina amplicon data. *Nat Methods* **13**, 581–583 (2016).

54. Ondov, B. D., Bergman, N. H. & Phillippy, A. M. Interactive metagenomic visualization in a Web browser. *Bmc Bioinformatics* **12**, 385 (2011).

55. Hatano, S. et al. Development of a new monoclonal antibody specific to mouse Vγ6 chain. *Life Sci Alliance* 2, e201900363 (2019)..

Figure legends

Figure 1. Mucosal tissues of naïve *Klrk1*+/+ mice harbor high frequencies of NKG2D-expressing T cells | a. Representative flow cytometry dot plots depicting NKG2D-expressing cells in the colon and MLN from *Klrk1*$^{+/+}$ mice b. Average frequencies of NKG2D-expressing cells among T cells and NK cells in the MLN (n = 15), SI (n = 6) and colon (n = 14-16) isolated from *Klrk1*$^{+/+}$ mice. c. Representative flow cytometry dot plots depicting NKG2D-expressing cells in the lung. d. Average frequencies of NKG2D-expressing cells among T cells and NK cells in the lung (n = 3). e. Average frequencies of NKG2D-expressing CD27^{-} γδT cells in the aging lung (n = 5-9) of *Klrk1*$^{+/+}$ mice. f. Average frequencies of colonic (left) and lung (right) lymphocyte subsets in *Klrk1*$^{+/+}$ and *Klrk1*$^{-/-}$ mice. n ≥ 6 for *Klrk*$^{-/-}$ and n = 17 for *Klrk1*$^{+/+}$ (colon) and n = 3-4 (lung). SI = small intestine, MLN = mesenteric lymph nodes. Bars represent mean ± SEM. Significance in b was determined using Mann-Whitney U or unpaired t-test following Shapiro-Wilk normality test. Significance in e was determined using Kruksal-Wallis test. * $p \leq 0.05$, ** $p \leq 0.01$, *** $p \leq 0.001$ and **** $p \leq 0.0001$.

Figure 2. NKG2D signaling promotes cancer progression in *Apc*$^{min/+}$ mice. | a. Kaplan-Meier representation of *Apc*$^{min/+}$;*Klrk1*$^{+/+}$ (n = 40) and *Apc*$^{min/+}$;*Klrk1*$^{-/-}$ (n = 35) mice. b. Number of tumors in the colon of *Apc*$^{min/+}$;*Klrk1*$^{+/+}$ (n = 40) and *Apc*$^{min/+}$;*Klrk1*$^{-/-}$ mice (n = 35) at disease endpoint. c. Hematocrit measures from the blood of healthy *Klrk1*$^{+/+}$ control mice (n = 8), *Apc*$^{min/+}$;*Klrk1*$^{+/+}$ (n = 18) and *Apc*$^{min/+}$;*Klrk1*$^{-/-}$ (n = 15) mice at disease endpoint. Data points represent individual mice. d. Average frequencies of SI tumors at 10-12 weeks (n = 12-14), 18-20 weeks (n = 12-19) and disease endpoint (n = 32-37) of *Apc*$^{min/+}$;*Klrk1*$^{+/+}$ and *Apc*$^{min/+}$;*Klrk1*$^{-/-}$ mice. e. Correlation between number of SI tumors and survival in *Apc*$^{min/+}$;*Klrk1*$^{+/+}$ (top, red) and *Apc*$^{min/+}$;*Klrk1*$^{-/-}$ (bottom, blue) mice at disease endpoint. Data points represent individual mice. f. MFI of NKG2D on TIL (n = 8-15) compared to healthy IEL (n = 6) in *Apc*$^{min/+}$ *Klrk1*$^{+/+}$ mice at 18-20 weeks. wk = week, SI = small intestine, HCT = hematocrit, IEL = intraepithelial lymphocytes, MFI = median fluorescent intensity. Bars represent mean ± SEM. Significance was determined using Log-rank (Mantel-Cox) test (a), Mann-Whitney U or

unpaired t-test following Shapiro-Wilk normality test (b-d and f) and linear regression (e). * $p \leq 0.05$, ** $p \leq 0.01$, *** $p \leq 0.001$ and **** $p \leq 0.0001$.

Figure 3. Loss of NKG2D reduces accumulation of IFNγ-expressing CD8$^+$ T cells in *Apc$^{min/+}$* tumors. | a. Average frequencies of T cells (CD3$^+$), B cells (CD19$^+$), myeloid cells (CD11b$^+$) and NK cells (CD3$^-$NK1.1$^+$) in the TME of SI tumors of *Apc$^{min/+}$;Klrk1$^{+/+}$* (n = 11) compared to *Apc$^{min/+}$;Klrk1$^{-/-}$* mice (n = 7) at 18-20 weeks. b. Average frequencies T cells (CD3$^+$), B cells (CD19$^+$), myeloid cells (CD11b$^+$) and NK cells (CD3$^-$NK1.1$^+$) in the TME SI tumors of *Apc$^{min/+}$;Klrk1$^{+/+}$* (n = 41-47) compared to *Apc$^{min/+}$;Klrk1$^{-/-}$* mice (n = 29-33) at disease endpoint. c. Representative flow cytometry dot plots depicting CD8$^+$ T cells, gated on live CD3$^+$ lymphocytes, in the SI TME of *Apc$^{min/+}$;Klrk1$^{+/+}$* (top) and *Apc$^{min/+}$;Klrk1$^{-/-}$* mice (bottom) at disease endpoint. d. Average frequencies of CD8$^+$ T cells (gated on CD3$^+$ lymphocytes) in the SI TME at disease endpoint in *Apc$^{min/+}$;Klrk1$^{+/+}$*(n = 46) compared to *Apc$^{min/+}$;Klrk1$^{-/-}$* mice (n = 31). Data points represent individual mice. e. Representative flow cytometry dot plots depicting IFNγ-expressing T cells (gated on CD8, CD4 or γδTCR following selection of CD3$^+$ lymphocytes) and NK cells (CD3$^-$NK1.1$^+$) in the SI TME at disease endpoint. f. Average frequencies of IFNγ-producing T cells (gated on CD8, CD4 or γδTCR following selection of CD3$^+$ lymphocytes) and NK cells (CD3$^-$NK1.1$^+$) in the SI TME of *Apc$^{min/+}$;Klrk1$^{+/+}$* mice at 18-20 weeks (n = 3-7) compared to endpoint (n = 20-26). g. Average frequencies of IFNγ$^+$ CD8$^+$ T cells (gated on CD3$^+$ lymphocytes) in the TME of SI tumors of *Apc$^{min/+}$;Klrk1$^{+/+}$* (n = 20) compared to *Apc$^{min/+}$;Klrk1$^{-/-}$* (n = 18) mice at disease endpoint. Data points represent individual mice. h. Categories of IFNγ levels in *Apc$^{min/+}$;Klrk1$^{+/+}$* compared to *Apc$^{min/+}$;Klrk1$^{-/-}$* mice in the SI TME at disease endpoint. TME = tumor microenvironment, SI = small intestine. Significance was determined using Mann-Whitney U or unpaired t-test following Shapiro-Wilk normality test (b, d and f) and Chi-Squared test (h). Bars represent mean ± SEM. * $p \leq 0.05$.

Figure 4. NKG2D regulates γδT cell accumulation and IL-17A expression in intestinal tumors. | a. Representative flow cytometry dot plots depicting γδT cells, gated on live CD3$^+$ lymphocytes in the SI TME of *Apc$^{min/+}$;Klrk1$^{+/+}$* (top) and *Apc$^{min/+}$;Klrk1$^{-/-}$* mice (bottom) at disease endpoint. b. Average frequencies of γδT cells at disease endpoint in *Apc$^{min/+}$;Klrk1$^{+/+}$* (n = 44) compared to *Apc$^{min/+}$;Klrk1$^{-/-}$*

(n = 30) mice. Data points represent individual mice. c. Representative flow cytometry dot plots depicting PD-1 expression on γδT cells in the SI TME of *Apc*$^{min/+}$;*Klrk1*$^{+/+}$ (left) and *Apc*$^{min/+}$;*Klrk1*$^{-/-}$ mice (right) at 18-20 weeks (top) and disease endpoint (bottom). d. Average frequencies of PD-1 expressing γδT cells in the SI TME of *Apc*$^{min/+}$;*Klrk1*$^{+/+}$ and *Apc*$^{min/+}$;*Klrk1*$^{-/-}$ mice at 18-20 weeks (n = 11) compared to endpoint (n = 3-4). e. Average frequencies of IL-17A^{+} T cells in the SI TME of *Apc*$^{min/+}$;*Klrk1*$^{+/+}$ mice at 18-20 weeks (n = 4-7) compared to endpoint (n = 22-24). f. Average frequencies of IL-17A^{+} T cells in the SI TME of *Apc*$^{min/+}$;*Klrk1*$^{+/+}$ (n = 22-24) compared to *Apc*$^{min/+}$;*Klrk1*$^{-/-}$ (n = 17) mice at disease endpoint. g. Direct comparison of IL-17A MFI in NKG2D^{+} and NKG2D^{-} γδT cells, gated on live CD3^{+} lymphocytes, isolated from the MLN of *Klrk1*$^{+/+}$ (n = 6) and *Apc*$^{min/+}$;*Klrk1*$^{+/+}$ mice at 18-20 weeks (n = 10). h. Frequencies of IL-17A producing T cells (gated γδTCR^{-}CD4^{+}, γδTCR^{-}CD8^{+} or CD4^{-}CD8^{-}γδTCR^{+} following gating on live CD3^{+} lymphocytes) in the *Villin-Cre*^{ERT2};*Apc*$^{F/+}$ mouse model of intestinal cancer at disease endpoint compared to healthy control mice (n = 4). i. Survival of *Villin-Cre*^{ERT2};*Apc*$^{F/+}$ compared to *Villin-Cre*^{ERT2}; *Apc*$^{F/+}$ *Tcrd*$^{-/-}$ mice. SI = small intestine, TME = tumor microenvironment, MLN = mesenteric lymph nodes. Bars represent mean ± SEM. Significance was determined using Mann-Whitney U or unpaired t-test following Shapiro-Wilk normality test (b, d and e), paired t-test (g) and Log-rank (Mantel-Cox) test (i). * $p \leq 0.05$, ** $p \leq 0.01$, *** $p \leq 0.001$.

Figure 5. NKG2D ligand expression and microbial composition is independent of NKG2D expression in intestinal tumors. | a. Average RAE-1^{+} area at different timepoints in surrounding tissue and tumor tissue of *Apc*$^{min/+}$;*Klrk1*$^{+/+}$, *Apc*$^{min/+}$;*Klrk1*$^{+/+}$ and non-*Apc* *Klrk1*$^{+/+}$ mice determined by immunohistochemistry. (n = 6 for 10-12 weeks, n = 8-10 for endpoint, surrounding, except non-*Apc* *Klrk1*$^{+/+}$ where n = 2, n = 9-10 for endpoint, tumor tissue). b. Representative staining of RAE-1 on healthy mice (top) and *Apc*$^{min/+}$*Klrk1*$^{+/+}$ mice (bottom). Scale bar = 500 μm. c. Relative abundance of bacteria at the rank of phylum in fecal samples of individual 18 week old *Klrk1*$^{+/+}$ (left) and fecal (middle) and tumor (right) samples of 18 week old *Apc*$^{min/+}$;*Klrk1*$^{+/+}$ mice. Each bar represents one sample. d. Shannon diversity index of *Apc*$^{min/+}$;*Klrk1*$^{+/+}$ mice (n = 6) over time compared to 18 week old *Klrk1*$^{+/+}$ mice (n = 4). e. Relative abundance of *Firmicutes* (left) and *Bacteroidetes* (right) of

Apc$^{min/+}$*Klrk1*$^{+/+}$ mice (n = 6) over time compared to 18 week old *Klrk1*$^{+/+}$ mice (n = 4). f. Krona plots showing relative abundance of bacterial taxa in fecal samples of *Apc*$^{min/+}$*;Klrk1*$^{+/+}$ mice collected at 3 weeks (left), 10 weeks (middle) and 18 weeks of age (right) (n = 6). g. Weighted UniFrac PCoA of fecal bacteria and tumor tissue. h. Relative abundance of *Firmicutes* (left) and *Bacteroidetes* (right) in *Apc*$^{min/+}$*;Klrk1*$^{+/+}$ (n = 7) and *Apc*$^{min/+}$*;Klrk1*$^{-/-}$ (n = 8) compared to non-*Apc Klrk1*$^{+/+}$ control (n = 4) mice. i. Relative abundances of tumor-associated bacteria at phylum level of *Apc*$^{min/+}$*;Klrk1*$^{+/+}$ (n = 5) compared to *Apc*$^{min/+}$*; Klrk1*$^{-/-}$ mice (n = 6) at 18-20 weeks.. PCoA = Principal Component Analysis, wks = weeks. Bars represent mean ± SEM. Significance was determined using Mann-Whitney U or unpaired t-test following Shapiro-Wilk normality test. ** $p \leq 0.01$.

Figure 6. NKG2D signaling regulates IL-17A-producing T cells | a. Representative flow cytometry dot plots depicting IL-17A staining on γδT cells (top) and CD4$^+$ T cells (bottom) in in mice bearing KB1P tumor transplants treated with isotype control IgG antibody or anti-NKG2D antibody. b. Average frequencies of IL-17A-producing CD4$^+$, gated on live CD3$^+$ T cells (top) and γδT cells, gated on live CD3$^+$ T cells (bottom) in in mice bearing KB1P tumor transplants treated with the isotype control IgG (n = 5) antibody or anti-NKG2D (n = 7) antibody. c. Representative flow cytometry dot plots of γδTCR (top, gated on CD3$^+$ live lymphocytes) and CD27 expression (bottom, gated on γδTCR$^+$CD3$^+$ live lymphocytes) before and after co-culture of T cells isolated from the lung with NKG2D ligand-expressing YAC cells. d. Average frequencies of wild-type γδT cells (top) and CD27$^-$ γδT cells (bottom) before and after co-culture of T cells isolated from the lung with YAC cells (n = 8). Each line represents one individual mouse. e. Frequencies of *Rorc-Cre;Klrk1*$^{F/F}$ γδT cells (top) and CD27$^-$ γδT cells (bottom) before and after co-culture of T cells isolated from the lung with YAC cells (n = 3). Each line represents one individual mouse. Bars represent mean ± SEM. Significance was determined using Mann-Whitney U or unpaired t-test following Shapiro-Wilk normality test (b) or paired t-test (d). * $p \leq 0.05$, ** $p \leq 0.01$.

Supplementary Figure 1 | a. Average frequencies of NKG2D-expressing CD27$^-$ and CD27$^+$ γδT cells in the lung isolated from *Klrk1*$^{+/+}$ mice (n = 3). b. Average frequencies of NKG2D-expressing NK cells in the developing lung of *Klrk1*$^{+/+}$ mice (n = 5-9). c. TCR Vγ expression pattern among NKG2D$^+$CD27$^-$

γδT cells in the lung isolated from *Klrk1*$^{+/+}$ mice (n = 3). d. Average frequencies of γδT cell subsets in the lung of *Klrk1*$^{+/+}$ and *Klrk1*$^{-/-}$ mice (n = 6). e. Average frequencies of colonic T cell subsets and NK cells in *Klrk1*$^{+/+}$ (n = 11) and *Klrk1*$^{-/-}$ (n= 17) mice. f. Average frequencies of colonic IL-17-producing T cell subsets in *Klrk1*$^{+/+}$ (n = 8) and *Klrk1*$^{-/-}$ (n = 10) mice. Bars represent mean ± SEM. Significance in b was determined using Kruksal-Wallis test. *** $p \leq 0.001$.

Supplementary Figure 2 | a. Average frequencies of NKG2D-expressing cells in healthy SI IEL (n = 6) and SI LPL (n = 6) compared to SI TIL (n = 8-15) in *Apc*$^{min/+}$;*Klrk1*$^{+/+}$ mice at 18-20 weeks. b. Average MFI of NKG2D on in healthy SI IEL(n = 6) and SI LPL (n = 6) compared to SI TIL (n = 8-15) in *Apc*$^{min/+}$;*Klrk1*$^{+/+}$ mice at 18-20 weeks.. SI = small intestine, LPL = lamina propria lymphocytes, IEL = intraepithelial lymphocytes, MFI = median fluorescent intensity. Bars represent mean ± SEM. Significance was determined using Mann-Whitney U or unpaired t-test following Shapiro-Wilk normality test. * $p \leq 0.05$, ** $p \leq 0.01$.

Supplementary Figure 3 | a. Average frequencies of PD-1-expressing CD8$^+$ (left) and CD4$^+$ (right) T cells, gated on live CD3$^+$ lymphocytes, in the SI TME of *Apc*$^{min/+}$;*Klrk1*$^{+/+}$ mice at 18-20 weeks (left) (n = 11) and disease endpoint (right) (n = 4 for *Apc*$^{min/+}$;*Klrk1*$^{+/+}$ and n = 8 for *Apc*$^{min/+}$;*Klrk1*$^{-/-}$). SI = small intestine, TME = tumor microenvironment. Bars represent mean ± SEM. Significance was determined using Mann-Whitney U or unpaired t-test following Shapiro-Wilk normality test. * $p \leq 0.05$, ** $p \leq 0.01$.

Supplementary Figure 4 | a. PD-1 staining on Vγ6 and NKG2D expressing γδT cells a. Representative flow cytometry dot plots depicting NKG2D- and Vγ6 TCR-expressing CD27$^-$ γδT cells isolated from the lung of *Klrk1*$^{+/+}$ mice. including negative controls for NKG2D (*Klrk1*$^{-/-}$, left) and Vγ6 (FMO, right) staining. b. Representative flow cytometry dot plots of PD-1 expression on NKG2D$^+$Vγ6$^-$, NKG2D$^+$Vγ6$^+$, NKG2D$^-$Vγ6$^+$ and NKG2D$^-$Vγ6$^-$ CD27$^-$ γδT cells. c. Frequencies of PD-1-expressing NKG2D$^+$Vγ6$^+$CD27$^-$ γδT cells (n=6). FMO = fluorescence minus one.

Supplementary Figure 5 | a. Relative abundance of Firmicutes (left) and Bacteroidetes (right) in healthy *Klrk1*$^{+/+}$ and *Klrk1*$^{-/-}$ mice. n ≥ 8. Bars represent mean ± SEM.

Supplementary Figure 6 | a. Average NKG2D expression on lung immune cells in WT (n = 7-9) and KB1P tumor-bearing mice (n = 5). b. Average frequencies of Granzyme B-producing NK cells in in mice bearing KB1P tumor transplants treated with the isotype control IgG antibody (n = 5) or anti-NKG2D antibody (n = 7). c. Average frequencies of NK cells (gated on CD3$^-$NKp46$^+$ cells) in KB1P mice treated with the isotype control IgG antibody (n = 5) or anti-NKG2D antibody (n = 7). n ≥ 5. d. Average frequencies of IFNγ producing NK cells, CD8$^+$ and CD4$^+$ T in in mice bearing KB1P tumor transplants treated with the isotype control IgG antibody (n = 5) or anti-NKG2D antibody (n = 7). e. Average frequencies of γδTCR$^-$ CD3$^+$ T cells before and after co-culture of T cells isolated from the lung with YAC cells (n = 4). Each line represents one individual mouse. WT = wild-type. Significance was determined using Mann-Whitney U test. Bars represent mean ± SEM. * p ≤ 0.05.

Tables

Table 1 | Antibodies used in this study.

Antigen	Conjugate	Clone	Source
B220	PE-Cy7	RA3-6B2	BioLegend
CD11b	APC-eFluor780	M1/70	eBioscience
CD11b	PE-CF594	M1/70	BD
CD11b	PerCp-Cy5.5	M1/70	eBioscience
CD19	APC-eFluor780	1D3	eBioscience
CD19	BV650	6D5	BioLegend
CD27	BV510	LG.3A10	BD
CD27	PE/Dazzle594	LG.3A10	BioLegend
CD3	BV650	17A2	BioLegend
CD3	V450	17A2	BD
CD3	PE-CF594	145-2C11	BD
CD3	BUV737	145-2C11	BD
CD4	APC-eFluor780	GK1.5	Invitrogen
CD4	BV605	GK1.5	BioLegend
CD4	APC-eFluor780	RM4-5	eBioscience
CD4	BV711	RM4-5	BioLegend
CD4	BUV495	GK1.5	BD
CD44	PerCP-Cy5.5	IM7	BioLegend
CD45	BV605	30-F11	BioLegend
CD45	AF700	30-F11	BioLegend
CD8α	BUV395	53-6.7	BD
CD8α	APC-eFluor780	53-6.7	Invitrogen
CD8α	PerCp-Cy5.5	53-6.7	BioLegend
CD8α	BV785	53-6.7	BioLegend
CD8α	BUV395	53-6.7	BD
EpCAM	APC-eFluor780	G8.8	eBioscience
Fixable Aqua Dead Cell Stain Kit	N/A	N/A	ThermoFisher
Granzyme B	AlexaFluor-647	GB11	BioLegend
IFN-γ	PE-Cy7	XMG1.2	eBioscience
IFN-γ	PE	XMG1.2	eBioscience
IL-17A	FITC	GL3	eBioscience
IL-17A	PE-Cy7	TC11-18H10.1	BioLegend

IL-17A	PE	eBio17B7	eBioscience
NK1.1	AlexaFluor-488	PK136	BioLegend
NK1.1	PE-Cy7	PK136	BioLegend
NKG2D	PE/Dazzle594	CX5	BioLegend
NKG2D	APC	CX5	BioLegend
NKG2D	PE	CX5	eBioscience
NKp46	BV421	29A1.4	BioLegend
PD-1	BV650	J43	BD
TCR Vγ1	PE	2.11	BioLegend
TCR Vγ4	APC	UC3-10A6	BioLegend
TCR Vγ4	PeCy7	UC3-10A6	eBioscience
TCR Vγ6	Pacific blue	1C10-1F7	Provided by Shinya Hatano and Yasunobu Yoshikai[55]
Zombie NIR	N/A	N/A	BioLegend
γδTCR	PerCp-eFluor 710	GL3	eBioscience
γδTCR	BV421	GL3	BD
γδTCR	APC	GL3	eBioscience
γδTCR	PE-Cy5	GL3	eBioscience
γδTCR	FITC	GL3	eBioscience

Figure 1

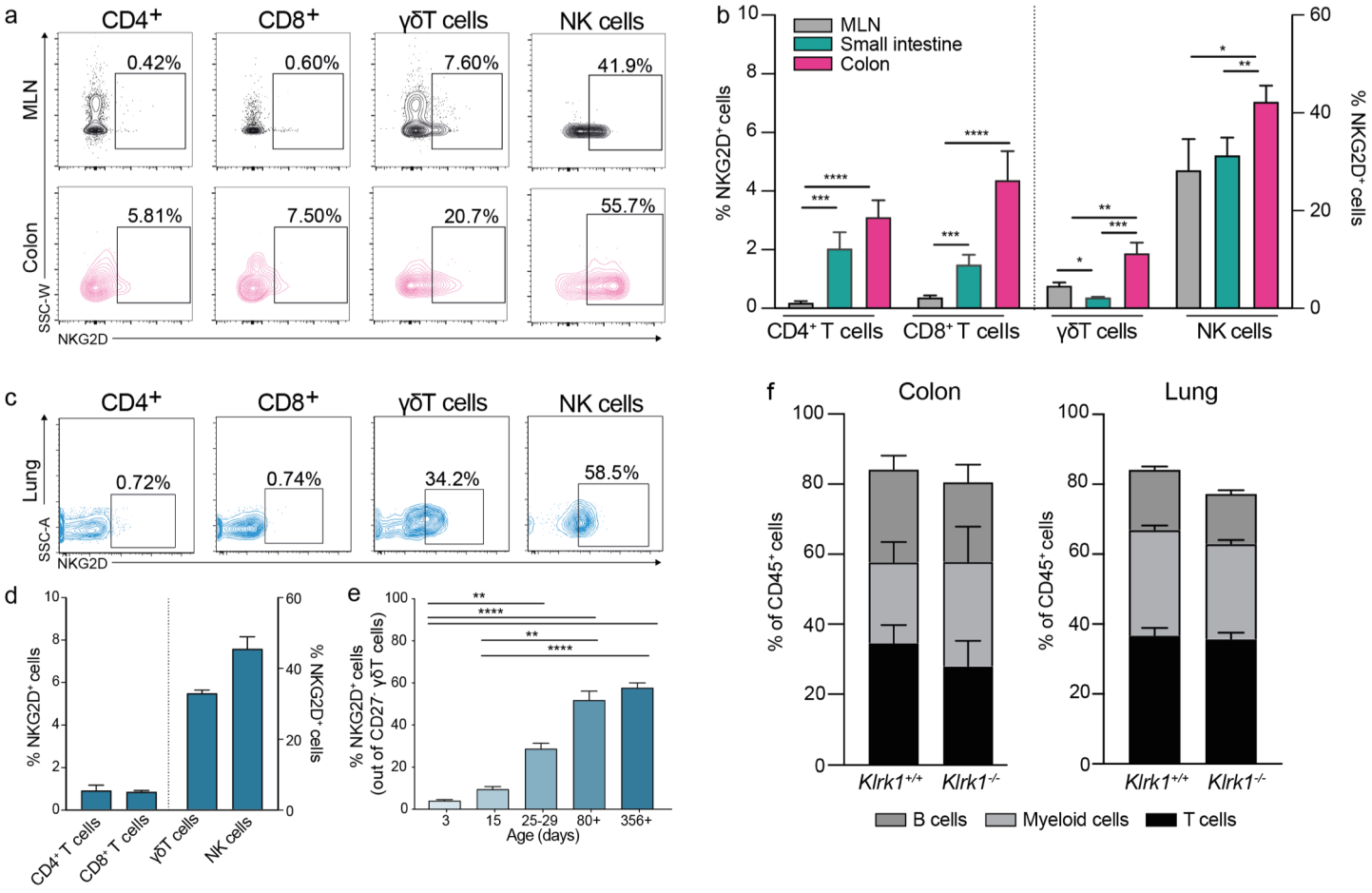

Figure 1. Mucosal tissues of naïve *Klrk1*+/+ mice harbor high frequencies of NKG2D-expressing T cells | a. Representative flow cytometry dot plots depicting NKG2D-expressing cells in the colon and MLN from *Klrk1*$^{+/+}$ mice b. Average frequencies of NKG2D-expressing cells among T cells and NK cells in the MLN (n = 15), SI (n = 6) and colon (n = 14-16) isolated from *Klrk1*$^{+/+}$ mice. c. Representative flow cytometry dot plots depicting NKG2D-expressing cells in the lung. d. Average frequencies of NKG2D-expressing cells among T cells and NK cells in the lung (n = 3). e. Average frequencies of NKG2D-expressing CD27^{-} γδT cells in the aging lung (n = 5-9) of *Klrk1*$^{+/+}$ mice. f. Average frequencies of colonic (left) and lung (right) lymphocyte subsets in *Klrk1*$^{+/+}$ and *Klrk1*$^{-/-}$ mice. n ≥ 6 for *Klrk*$^{-/-}$ and n = 17 for *Klrk1*$^{+/+}$ (colon) and n = 3-4 (lung). SI = small intestine, MLN = mesenteric lymph nodes. Bars represent mean ± SEM. Significance in b was determined using Mann-Whitney U or unpaired t-test following Shapiro-Wilk normality test. Significance in e was determined using Kruksal-Wallis test. * p ≤ 0.05, ** p ≤ 0.01, *** p ≤ 0.001 and **** p ≤ 0.0001.

Figure 2

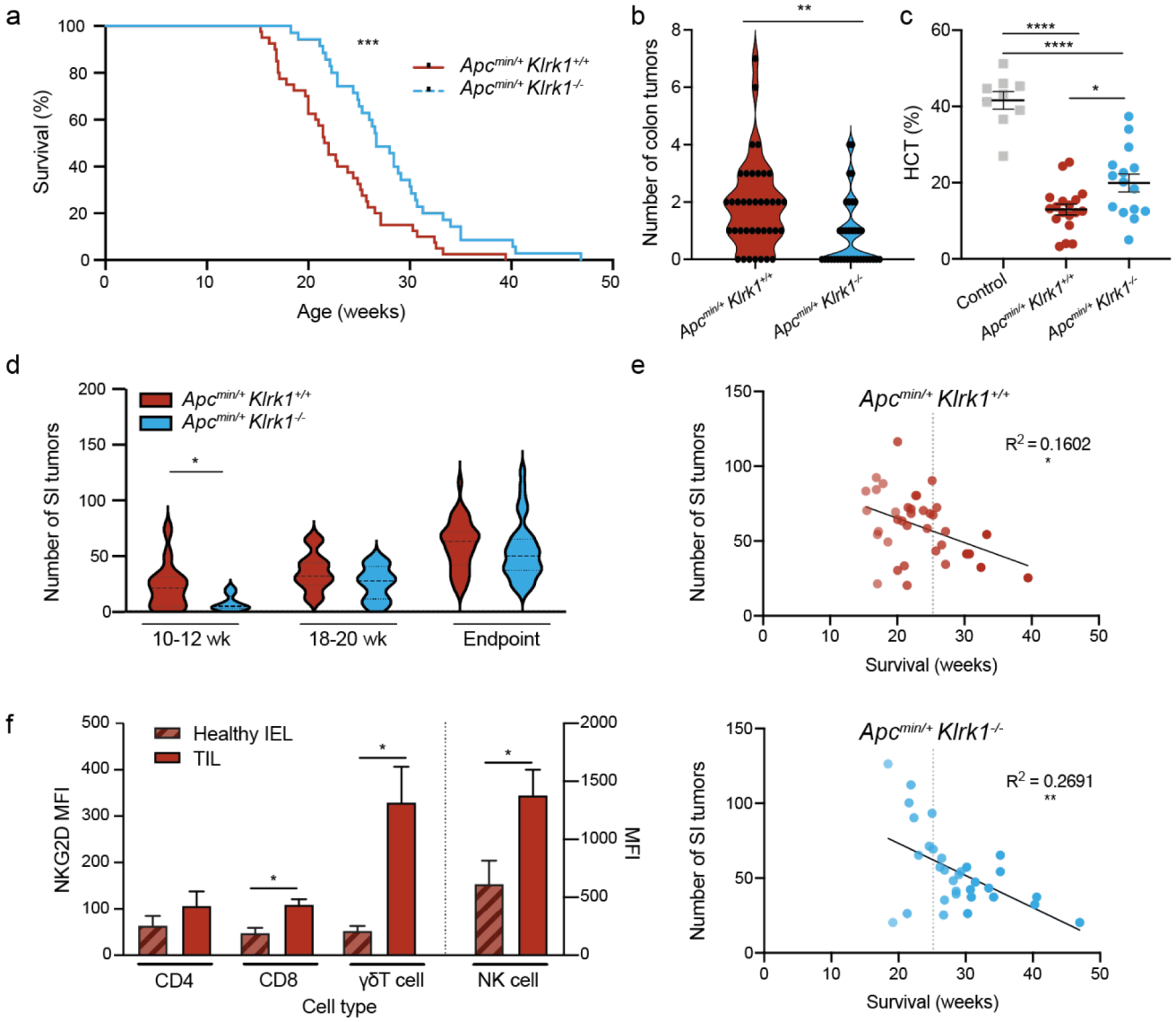

Figure 2. NKG2D signaling promotes cancer progression in *Apc*$^{min/+}$ mice. | a. Kaplan-Meier representation of *Apc*$^{min/+}$;*Klrk1*$^{+/+}$ (n = 40) and *Apc*$^{min/+}$;*Klrk1*$^{-/-}$ (n = 35) mice. b. Number of tumors in the colon of *Apc*$^{min/+}$;*Klrk1*$^{+/+}$ (n = 40) and *Apc*$^{min/+}$;*Klrk1*$^{-/-}$ mice (n = 35) at disease endpoint. c. Hematocrit measures from the blood of healthy *Klrk1*$^{+/+}$ control mice (n = 8), *Apc*$^{min/+}$;*Klrk1*$^{+/+}$ (n = 18) and *Apc*$^{min/+}$;*Klrk1*$^{-/-}$ (n = 15) mice at disease endpoint. Data points represent individual mice. d. Average frequencies of SI tumors at 10-12 weeks (n = 12-14), 18-20 weeks (n = 12-19) and disease endpoint (n = 32-37) of *Apc*$^{min/+}$;*Klrk1*$^{+/+}$ and *Apc*$^{min/+}$;*Klrk1*$^{-/-}$ mice. e. Correlation between number of SI tumors and survival in *Apc*$^{min/+}$;*Klrk1*$^{+/+}$ (top, red) and *Apc*$^{min/+}$;*Klrk1*$^{-/-}$ (bottom, blue) mice at disease endpoint. Data points represent individual mice. f. MFI of NKG2D on TIL (n = 8-15) compared to healthy IEL (n = 6) in *Apc*$^{min/+}$ *Klrk1*$^{+/+}$ mice at 18-20 weeks. wk = week, SI = small intestine, HCT = hematocrit, IEL = intraepithelial lymphocytes, MFI = median fluorescent intensity. Bars represent mean ± SEM. Significance was determined using Log-rank (Mantel-Cox) test (a), Mann-Whitney U or unpaired t-test following Shapiro-Wilk normality test (b-d and f) and linear regression (e). * $p \leq 0.05$, ** $p \leq 0.01$, *** $p \leq 0.001$ and **** $p \leq 0.0001$.

Figure 3

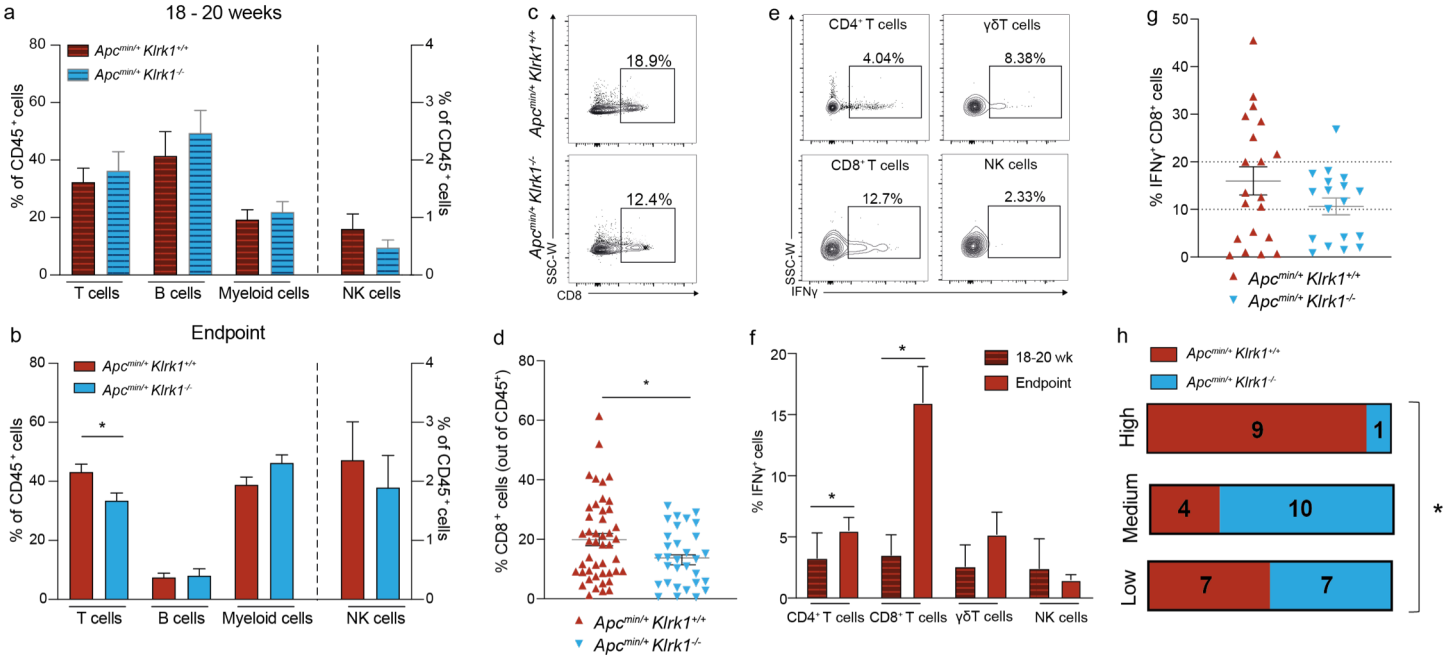

Figure 3. Loss of NKG2D reduces accumulation of IFNγ-expressing CD8⁺ T cells in *Apc*$^{min/+}$ tumors. | a. Average frequencies of T cells (CD3⁺), B cells (CD19⁺), myeloid cells (CD11b⁺) and NK cells (CD3⁻NK1.1⁺) in the TME of SI tumors of *Apc*$^{min/+}$;*Klrk1*$^{+/+}$ (n = 11) compared to *Apc*$^{min/+}$;*Klrk1*$^{-/-}$ mice (n = 7) at 18-20 weeks. b. Average frequencies T cells (CD3⁺), B cells (CD19⁺), myeloid cells (CD11b⁺) and NK cells (CD3⁻NK1.1⁺) in the TME SI tumors of *Apc*$^{min/+}$;*Klrk1*$^{+/+}$ (n = 41-47) compared to *Apc*$^{min/+}$;*Klrk1*$^{-/-}$ mice (n = 29-33) at disease endpoint. c. Representative flow cytometry dot plots depicting CD8⁺ T cells, gated on live CD3⁺ lymphocytes, in the SI TME of *Apc*$^{min/+}$;*Klrk1*$^{+/+}$ (top) and *Apc*$^{min/+}$;*Klrk1*$^{-/-}$ mice (bottom) at disease endpoint. d. Average frequencies of CD8⁺ T cells (gated on CD3⁺ lymphocytes) in the SI TME at disease endpoint in *Apc*$^{min/+}$;*Klrk1*$^{+/+}$(n = 46) compared to *Apc*$^{min/+}$;*Klrk1*$^{-/-}$ mice (n = 31). Data points represent individual mice. e. Representative flow cytometry dot plots depicting IFNγ-expressing T cells (gated on CD8, CD4 or γδTCR following selection of CD3⁺ lymphocytes) and NK cells (CD3⁻NK1.1⁺) in the SI TME at disease endpoint. f. Average frequencies of IFNγ-producing T cells (gated on CD8, CD4 or γδTCR following selection of CD3⁺ lymphocytes) and NK cells (CD3⁻NK1.1⁺) in the SI TME of *Apc*$^{min/+}$;*Klrk1*$^{+/+}$ mice at 18-20 weeks (n = 3-7) compared to endpoint (n = 20-26). g. Average frequencies of IFNγ⁺ CD8⁺ T cells (gated on CD3⁺ lymphocytes) in the TME of SI tumors of *Apc*$^{min/+}$;*Klrk1*$^{+/+}$ (n = 20) compared to *Apc*$^{min/+}$;*Klrk1*$^{-/-}$ (n = 18) mice at disease endpoint. Data points represent individual mice. h. Categories of IFNγ levels in *Apc*$^{min/+}$;*Klrk1*$^{+/+}$ compared to *Apc*$^{min/+}$;*Klrk1*$^{-/-}$ mice in the SI TME at disease endpoint. TME = tumor microenvironment, SI = small intestine. Significance was determined using Mann-Whitney U or unpaired t-test following Shapiro-Wilk normality test (b, d and f) and Chi-Squared test (h). Bars represent mean ± SEM. * p ≤ 0.05.

Figure 4

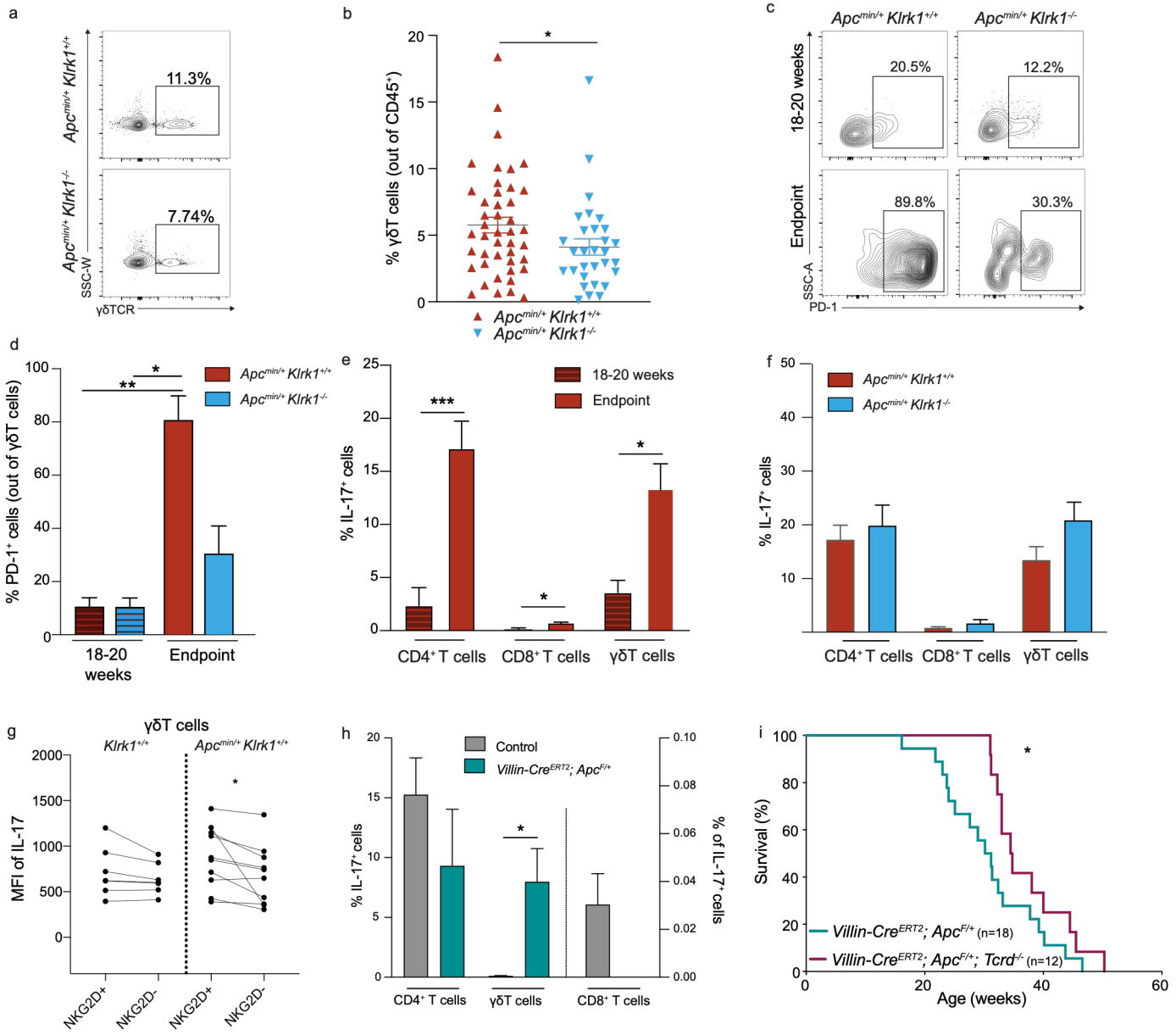

Figure 4. NKG2D regulates γδT cell accumulation and IL-17A expression in intestinal tumors. | a. Representative flow cytometry dot plots depicting γδT cells, gated on live CD3$^+$ lymphocytes in the SI TME of *Apc$^{min/+}$;Klrk1$^{+/+}$* (top) and *Apc$^{min/+}$;Klrk1$^{-/-}$* mice (bottom) at disease endpoint. b. Average frequencies of γδT cells at disease endpoint in *Apc$^{min/+}$;Klrk1$^{+/+}$* (n = 44) compared to *Apc$^{min/+}$;Klrk1$^{-/-}$* (n = 30) mice. Data points represent individual mice. c. Representative flow cytometry dot plots depicting PD-1 expression on γδT cells in the SI TME of *Apc$^{min/+}$;Klrk1$^{+/+}$* (left) and *Apc$^{min/+}$;Klrk1$^{-/-}$* mice (right) at 18-20 weeks (top) and disease endpoint (bottom). d. Average frequencies of PD-1 expressing γδT cells in the SI TME of *Apc$^{min/+}$;Klrk1$^{+/+}$* and *Apc$^{min/+}$;Klrk1$^{-/-}$* mice at 18-20 weeks (n = 11) compared to endpoint (n = 3-4). e. Average frequencies of IL-17A$^+$ T cells in the SI TME of *Apc$^{min/+}$;Klrk1$^{+/+}$* mice at 18-20 weeks (n = 4-7) compared to endpoint (n = 22-24). f. Average frequencies of IL-17A$^+$ T cells in the SI TME of *Apc$^{min/+}$;Klrk1$^{+/+}$* (n = 22-24) compared to *Apc$^{min/+}$;Klrk1$^{-/-}$* (n = 17) mice at disease endpoint. g. Direct comparison of IL-17A MFI in NKG2D$^+$ and NKG2D$^-$ γδT cells, gated on live CD3$^+$ lymphocytes, isolated from the MLN of *Klrk1$^{+/+}$* (n = 6) and *Apc$^{min/+}$;Klrk1$^{+/+}$* mice at 18-20 weeks (n = 10). h. Frequencies of IL-17A producing T cells (gated γδTCR$^-$CD4$^+$, γδTCR$^-$CD8$^+$ or CD4$^-$CD8$^-$γδTCR$^+$ following gating on live CD3$^+$ lymphocytes) in the *Villin-Cre^{ERT2};Apc$^{F/+}$* mouse model of intestinal cancer at disease endpoint compared to healthy control mice (n = 4). i. Survival of *Villin-Cre^{ERT2};Apc$^{F/+}$* compared to *Villin-Cre^{ERT2}; Apc$^{F/+}$ Tcrd$^{-/-}$* mice. SI = small intestine, TME = tumor microenvironment, MLN = mesenteric lymph nodes. Bars represent mean ± SEM. Significance was determined using Mann-Whitney U or unpaired t-test following Shapiro-Wilk normality test (b, d and e), paired t-test (g) and Log-rank (Mantel-Cox) test (i). * $p \leq 0.05$, ** $p \leq 0.01$, *** $p \leq 0.001$.

Figure 5

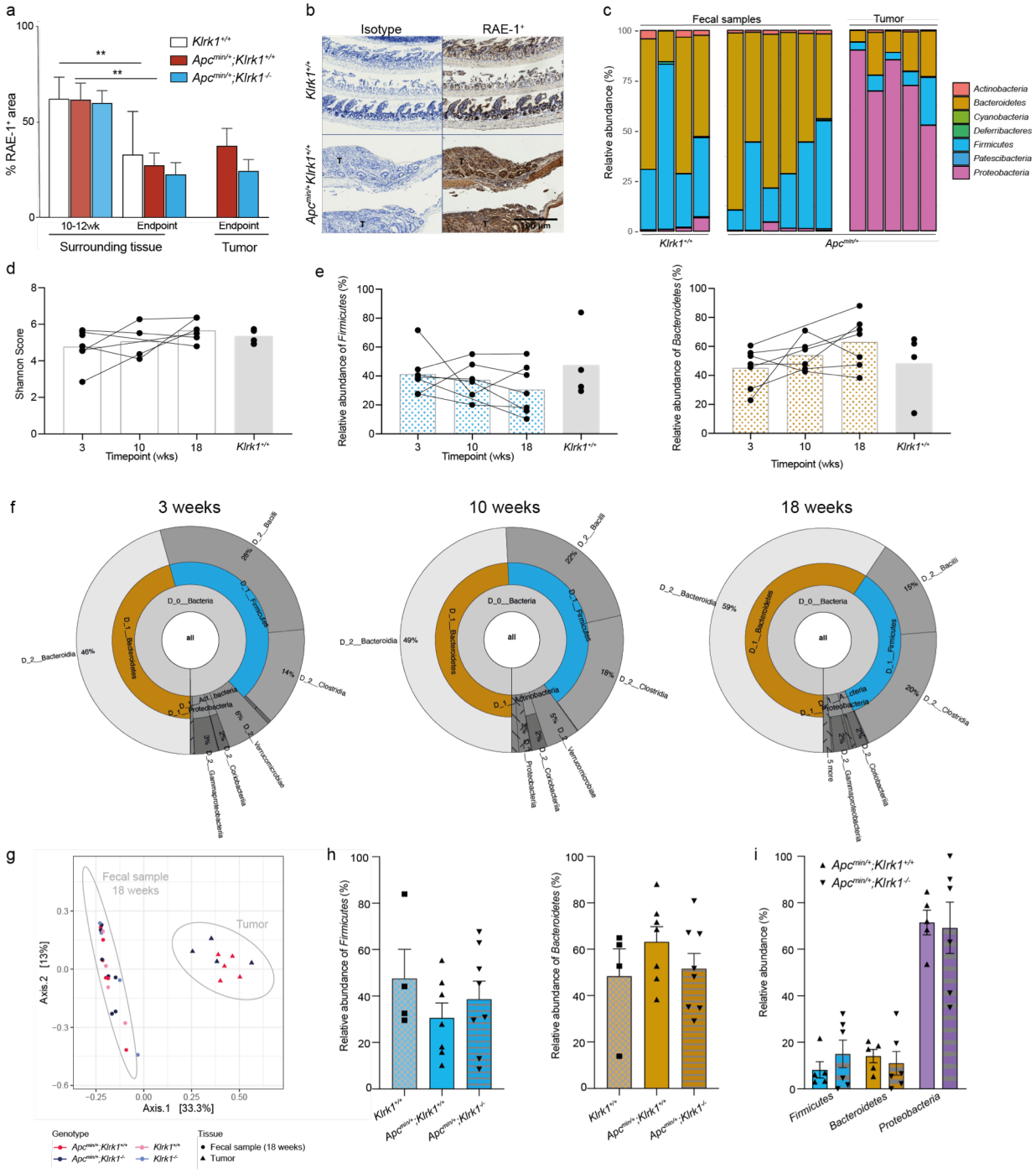

Figure 5. NKG2D ligand expression and microbial composition is independent of NKG2D expression in intestinal tumors. | a. Average RAE-1⁺ area at different timepoints in surrounding tissue and tumor tissue of *Apc*$^{min/+}$*;Klrk1*$^{+/+}$, *Apc*$^{min/+}$*;Klrk1*$^{+/+}$ and non-*Apc Klrk1*$^{+/+}$ mice determined by immunohistochemistry. (n = 6 for 10-12 weeks, n = 8-10 for endpoint, surrounding, except non-*Apc Klrk1*$^{+/+}$ where n = 2, n = 9-10 for endpoint, tumor tissue). b. Representative staining of RAE-1 on healthy mice (top) and *Apc*$^{min/+}$*Klrk1*$^{+/+}$ mice (bottom). Scale bar = 500 µm. c. Relative abundance of bacteria at the rank of phylum in fecal samples of individual 18 week old *Klrk1*$^{+/+}$ (left) and fecal (middle) and tumor (right) samples of 18 week old *Apc*$^{min/+}$*;Klrk1*$^{+/+}$ mice. Each bar represents one sample. d. Shannon diversity index of *Apc*$^{min/+}$*;Klrk1*$^{+/+}$ mice (n = 6) over time compared to 18 week old *Klrk1*$^{+/+}$ mice (n = 4). e. Relative abundance of *Firmicutes* (left) and *Bacteroidetes* (right) of *Apc*$^{min/+}$*Klrk1*$^{+/+}$ mice (n = 6) over time compared to 18 week old *Klrk1*$^{+/+}$ mice (n = 4). f. Krona plots showing relative abundance of bacterial taxa in fecal samples of *Apc*$^{min/+}$*;Klrk1*$^{+/+}$ mice collected at 3 weeks (left), 10 weeks (middle) and 18 weeks of age (right) (n = 6). g. Weighted UniFrac PCoA of fecal bacteria and tumor tissue. h. Relative abundance of *Firmicutes* (left) and *Bacteroidetes* (right) in *Apc*$^{min/+}$*;Klrk1*$^{+/+}$ (n = 7) and *Apc*$^{min/+}$*;Klrk1*$^{-/-}$ (n = 8) compared to non-*Apc Klrk1*$^{+/+}$ control (n = 4) mice. i. Relative abundances of tumor-associated bacteria at phylum level of *Apc*$^{min/+}$*;Klrk1*$^{+/+}$ (n = 5) compared to *Apc*$^{min/+}$*; Klrk1*$^{-/-}$ mice (n = 6) at 18-20 weeks.. PCoA = Principal Component Analysis, wks = weeks. Bars represent mean ± SEM. Significance was determined using Mann-Whitney U or unpaired t-test following Shapiro-Wilk normality test. ** p ≤ 0.01.

Figure 6

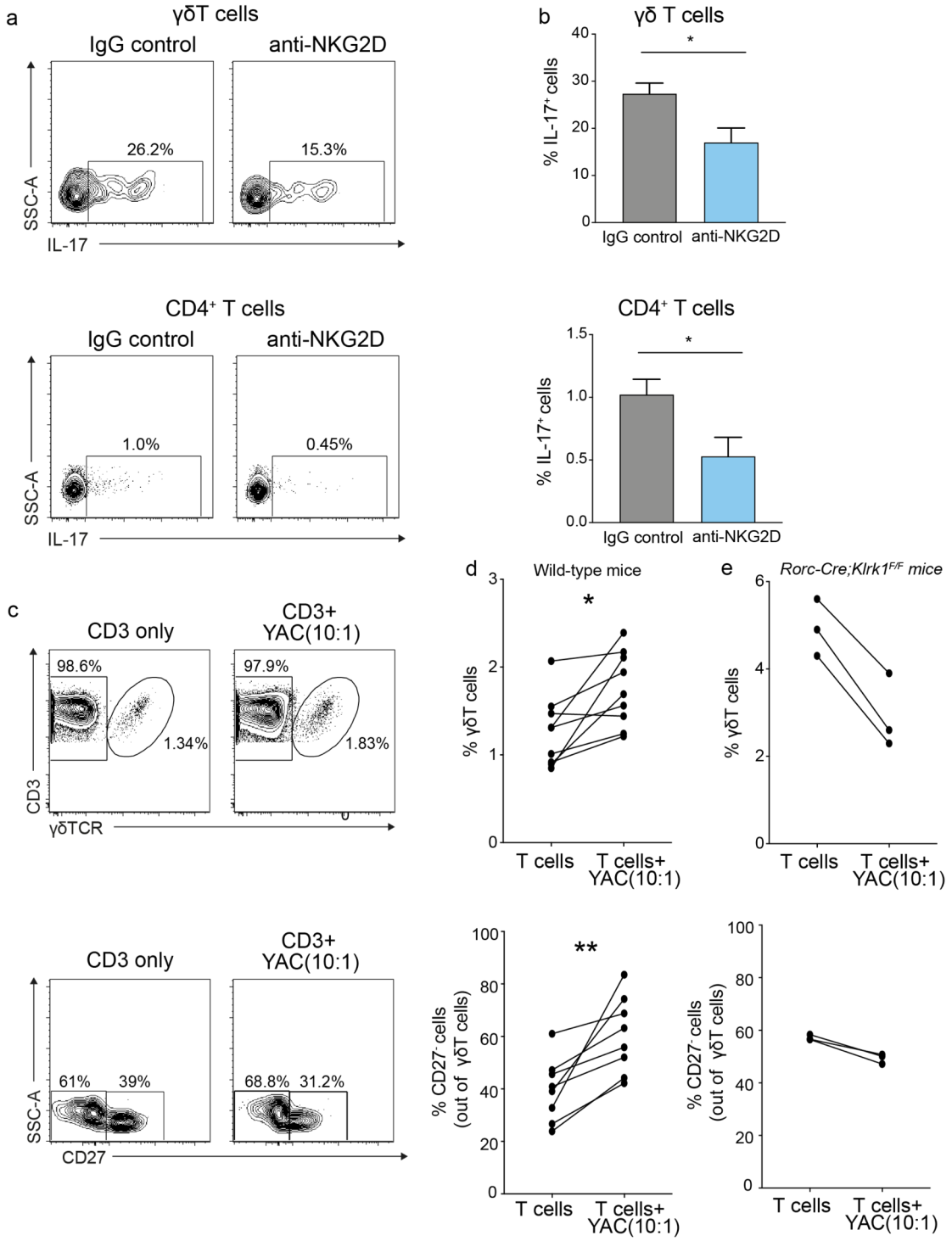

Figure 6. NKG2D signaling regulates IL-17A-producing T cells | a. Representative flow cytometry dot plots depicting IL-17A staining on γδT cells (top) and CD4+ T cells (bottom) in in mice bearing KB1P tumor transplants treated with isotype control IgG antibody or anti-NKG2D antibody. b. Average frequencies of IL-17A-producing CD4+, gated on live CD3+ T cells (top) and γδT cells, gated on live CD3+ T cells (bottom) in in mice bearing KB1P tumor transplants treated with the isotype control IgG (n = 5) antibody or anti-NKG2D (n = 7) antibody. c. Representative flow cytometry dot plots of γδTCR (top, gated on CD3+ live lymphocytes) and CD27 expression (bottom, gated on γδTCR+CD3+ live lymphocytes) before and after co-culture of T cells isolated from the lung with NKG2D ligand-expressing YAC cells. d. Average frequencies of wild-type γδT cells (top) and CD27− γδT cells (bottom) before and after co-culture of T cells isolated from the lung with YAC cells (n = 8). Each line represents one individual mouse. e. Frequencies of *Rorc-Cre;Klrk1F/F* γδT cells (top) and CD27− γδT cells (bottom) before and after co-culture of T cells isolated from the lung with YAC cells (n = 3). Each line represents one individual mouse. Bars represent mean ± SEM. Significance was determined using Mann-Whitney U or unpaired t-test following Shapiro-Wilk normality test (b) or paired t-test (d). * p ≤ 0.05, ** p ≤ 0.01.

Supplementary Figure 1

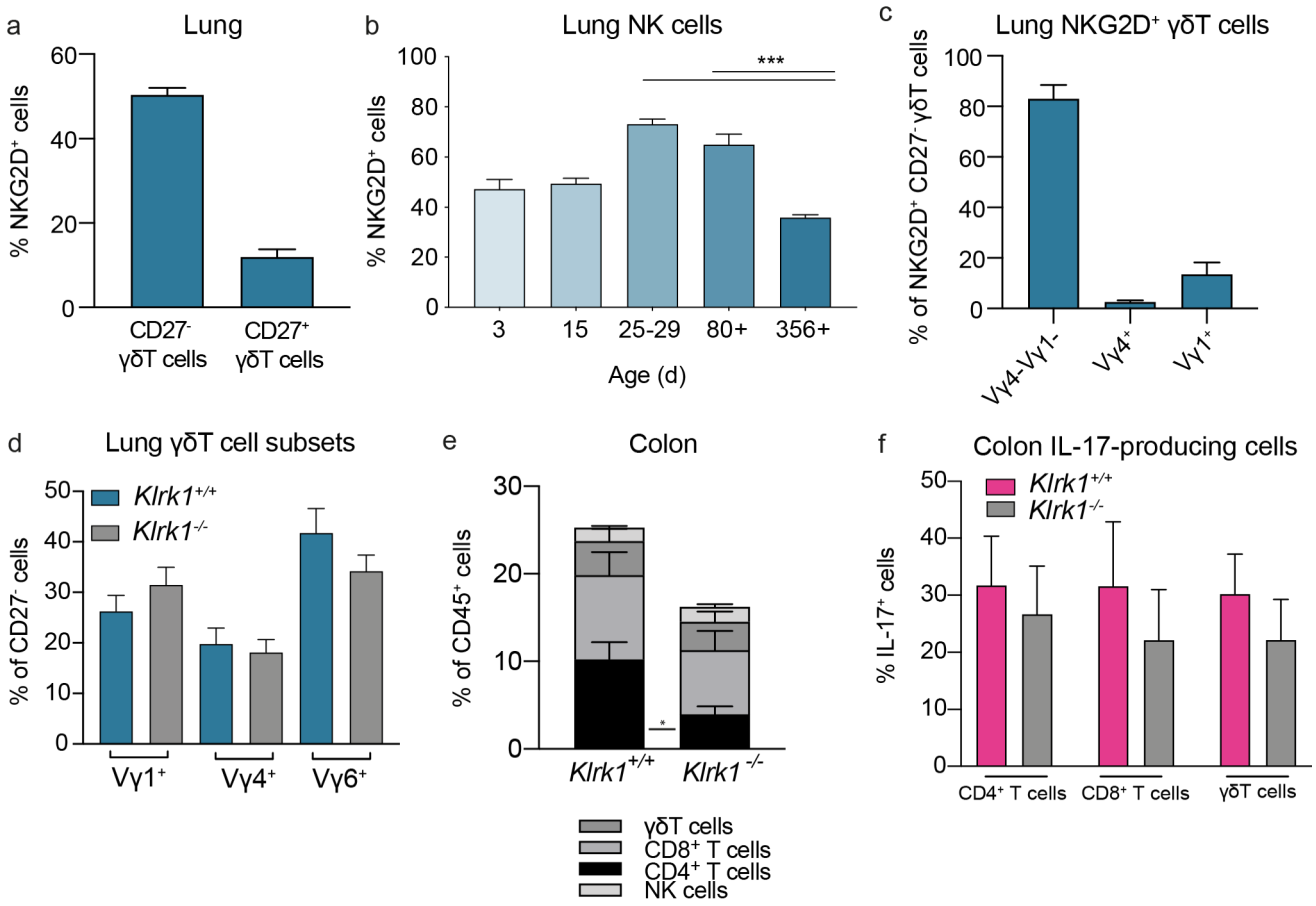

Supplementary Figure 1 | a. Average frequencies of NKG2D-expressing CD27⁻ and CD27⁺ γδT cells in the lung isolated from *Klrk1*$^{+/+}$ mice (n = 3). b. Average frequencies of NKG2D-expressing NK cells in the developing lung of *Klrk1*$^{+/+}$ mice (n = 5-9). c. TCR Vγ expression pattern among NKG2D^{+}CD27^{-} γδT cells in the lung isolated from *Klrk1*$^{+/+}$ mice (n = 3). d. Average frequencies of γδT cell subsets in the lung of *Klrk1*$^{+/+}$ and *Klrk1*$^{-/-}$ mice (n = 6). e. Average frequencies of colonic T cell subsets and NK cells in *Klrk1*$^{+/+}$ (n = 11) and *Klrk1*$^{-/-}$ (n= 17) mice. f. Average frequencies of colonic IL-17-producing T cell subsets in *Klrk1*$^{+/+}$ (n = 8) and *Klrk1*$^{-/-}$ (n = 10) mice. Bars represent mean ± SEM. Significance in b was determined using Kruksal-Wallis test. *** $p \leq 0.001$.

Supplementary Figure 2

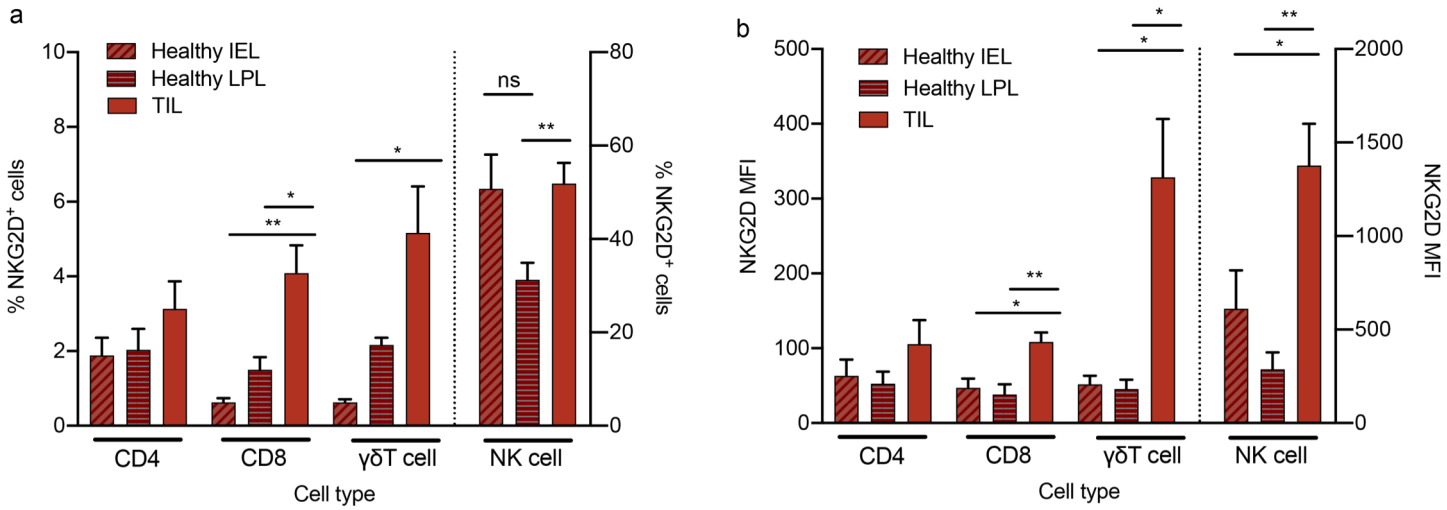

Supplementary Figure 2 | a. Average frequencies of NKG2D-expressing cells in healthy SI IEL (n = 6) and SI LPL (n = 6) compared to SI TIL (n = 8-15) in *Apc*$^{min/+}$;*Klrk1*$^{+/+}$ mice at 18-20 weeks. b. Average MFI of NKG2D on in healthy SI IEL(n = 6) and SI LPL (n = 6) compared to SI TIL (n = 8-15) in *Apc*$^{min/+}$;*Klrk1*$^{+/+}$ mice at 18-20 weeks.. SI = small intestine, LPL = lamina propria lymphocytes, IEL = intraepithelial lymphocytes, MFI = median fluorescent intensity. Bars represent mean ± SEM. Significance was determined using Mann-Whitney U or unpaired t-test following Shapiro-Wilk normality test. * $p \leq 0.05$, ** $p \leq 0.01$.

Supplementary Figure 3

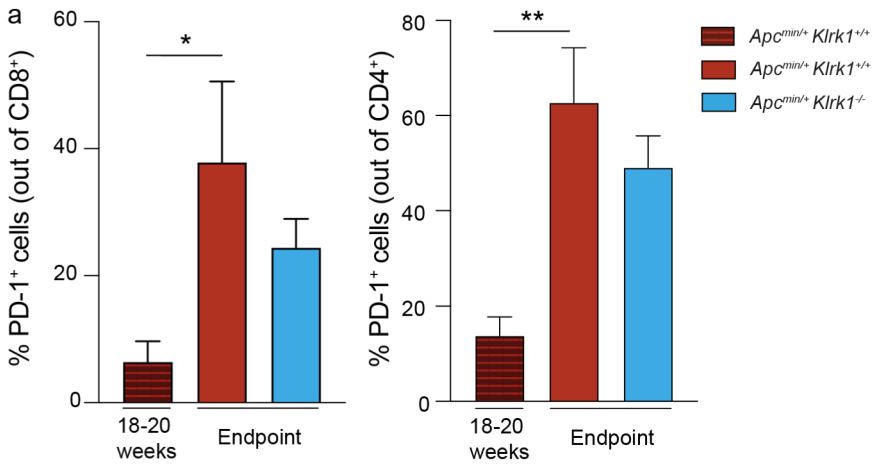

Supplementary Figure 3 | a. Average frequencies of PD-1-expressing CD8⁺ (left) and CD4⁺ (right) T cells, gated on live CD3⁺ lymphocytes, in the SI TME of *Apc*$^{min/+}$;*Klrk1*$^{+/+}$ mice at 18-20 weeks (left) (n = 11) and disease endpoint (right) (n = 4 for *Apc*$^{min/+}$;*Klrk1*$^{+/+}$ and n = 8 for *Apc*$^{min/+}$;*Klrk1*$^{-/-}$). SI = small intestine, TME = tumor microenvironment. Bars represent mean ± SEM. Significance was determined using Mann-Whitney U or unpaired t-test following Shapiro-Wilk normality test. * $p \leq 0.05$, ** $p \leq 0.01$.

Supplementary Figure 4

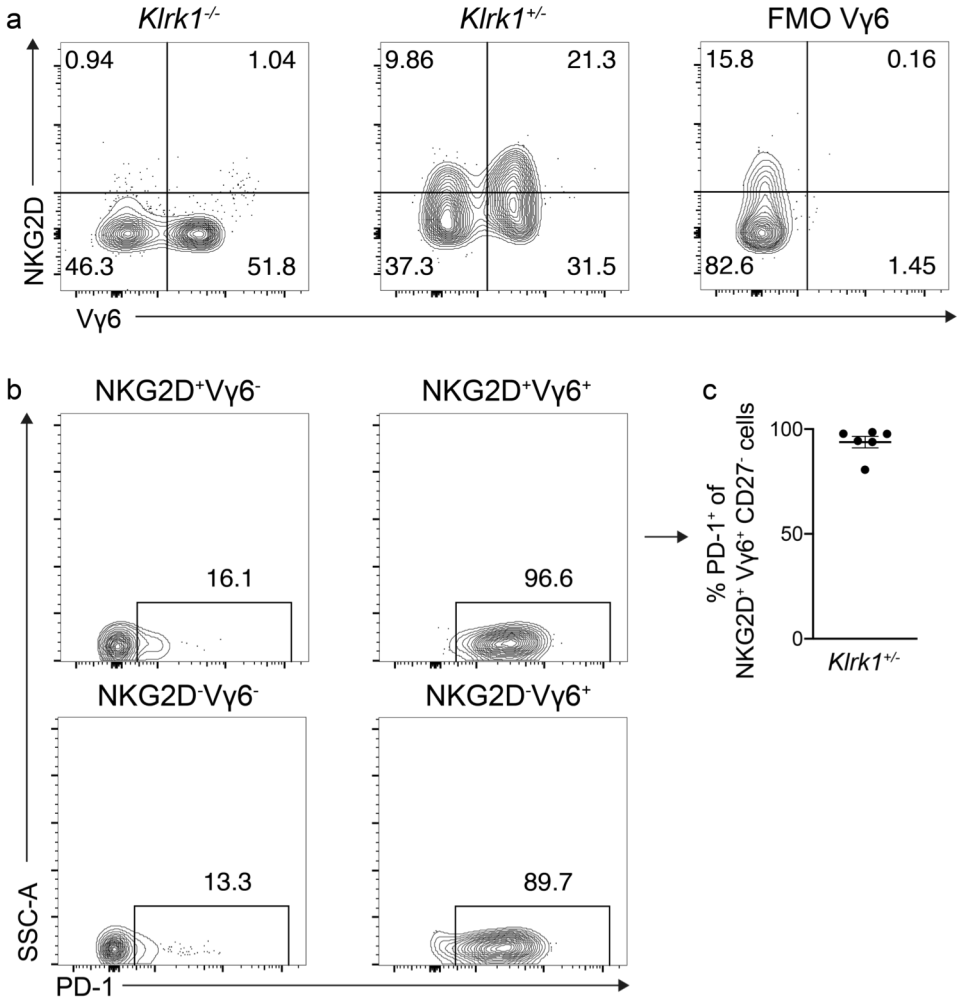

Supplementary Figure 4 | a. PD-1 staining on Vγ6 and NKG2D expressing γδT cells a. Representative flow cytometry dot plots depicting NKG2D- and Vγ6 TCR-expressing CD27^{-} γδT cells isolated from the lung of *Klrk1*$^{+/+}$ mice. including negative controls for NKG2D (*Klrk1*$^{-/-}$, left) and Vγ6 (FMO, right) staining. b. Representative flow cytometry dot plots of PD-1 expression on NKG2D^{+}Vγ6^{-}, NKG2D^{+}Vγ6^{+}, NKG2D^{-}Vγ6^{+} and NKG2D^{-}Vγ6^{-} CD27^{-} γδT cells. c. Frequencies of PD-1-expressing NKG2D^{+}Vγ6^{+}CD27^{-} γδT cells (n=6). FMO = fluorescence minus one.

Supplementary Figure 5

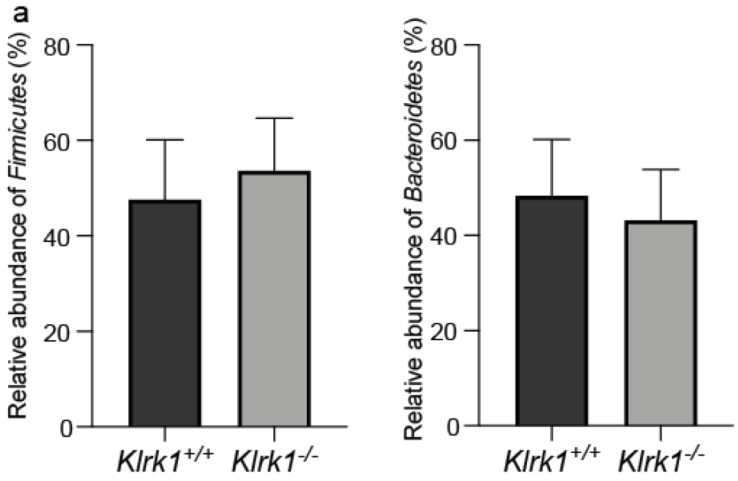

Supplementary Figure 5 | a. Relative abundance of Firmicutes (left) and Bacteroidetes (right) in healthy *Klrk1*$^{+/+}$ and *Klrk1*$^{-/-}$ mice. n ≥ 8. Bars represent mean ± SEM.

Supplementary Figure 6

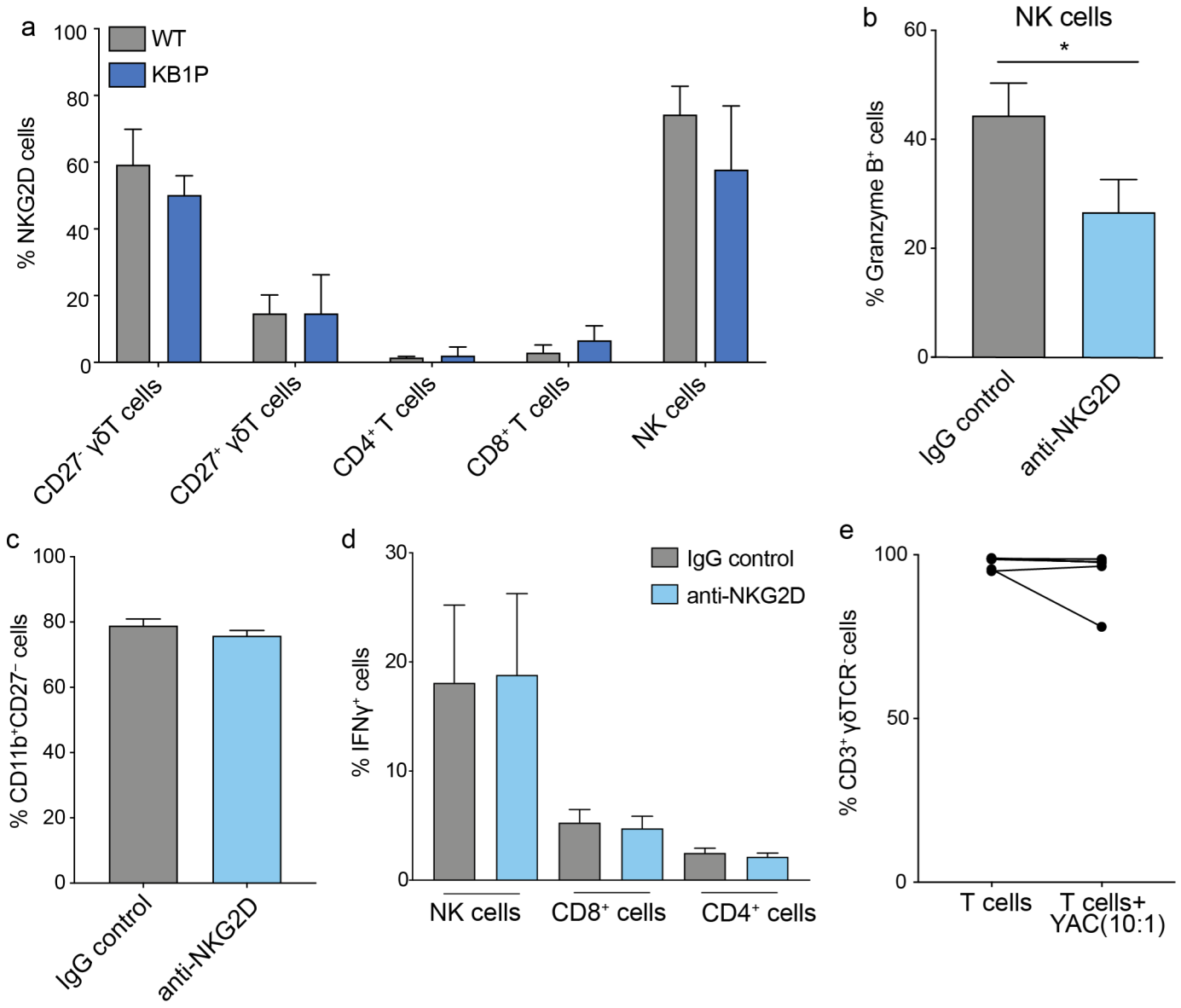

Supplementary Figure 6 | a. Average NKG2D expression on lung immune cells in WT (n = 7-9) and KB1P tumor-bearing mice (n = 5). b. Average frequencies of Granzyme B-producing NK cells in in mice bearing KB1P tumor transplants treated with the isotype control IgG antibody (n = 5) or anti-NKG2D antibody (n = 7). c. Average frequencies of NK cells (gated on $CD3^{-}NKp46^{+}$ cells) in KB1P mice treated with the isotype control IgG antibody (n = 5) or anti-NKG2D antibody (n = 7). n ≥ 5. d. Average frequencies of IFNγ producing NK cells, $CD8^{+}$ and $CD4^{+}$ T in in mice bearing KB1P tumor transplants treated with the isotype control IgG antibody (n = 5) or anti-NKG2D antibody (n = 7). e. Average frequencies of $\gamma\delta TCR^{-}$ $CD3^{+}$ T cells before and after co-culture of T cells isolated from the lung with YAC cells (n = 4). Each line represents one individual mouse. WT = wild-type. Significance was determined using Mann-Whitney U test. Bars represent mean ± SEM. * $p \leq 0.05$.